Experimental Investigation of Fluid Dynamics Effects on Scale Growth and Suppression in the Bayer Process

By
Prasanjit Das

A dissertation submitted in fulfilment of the requirement for the award of the degree of

Doctor of Philosophy

School of Engineering and Technology, Tertiary Education Division

Central Queensland University
Australia

April 2018

To my Parents (Ranu Das and Shishir Das)

for their unflinching support and inspiration.

ABSTRACT

Scale formation on the process equipment is a major problem in the mineral industry because it leads to reduced plant efficiency and additional operational cost. Scale formation in the Bayer process equipment is a natural consequence of supersaturated solutions that are generated throughout the process and the costs involved in the de-scaling process may be as much as one-quarter of operational costs of an alumina refinery. The scale formation in the Bayer process mainly occurs from crystallisation of Bayer liquor which is not well understood yet. A series of systematic experiments were done using laboratory-made potassium nitrate (KNO_3) aqueous solutions for safety reasons, since the real Bayer liquor requires high processing temperature and pressure and it has caustic property. The study provides a novel approach to elucidating the fluid dynamics effects on crystallisation scale growth and its suppression mechanism using for the first time a normal soluble salt to generate the crystallisation scale deposition in a newly fabricated lab-scale agitation tank that effectively replicates many industrial processes.

Firstly, the impact of impeller agitation rate on the scale growth and its suppression was examined. Tests were conducted with three different size impellers (86, 114 and 160 mm) at varying rotational speeds ranging from 100 to 700 rpm using the KNO_3 solutions of various supersaturation levels (4.5, 4.75 and 5.25 mol/dm^3) to investigate the hydrodynamic effects on scale growth and suppression in the agitation tank. It was found that higher agitation rates suppressed the scale deposition on the agitation tank wall and lower agitation rates enhanced the scale deposition. The wall scale growth rate decreased asymptotically with time ranging from 58.06% to 6.79% and the corresponding bottom settled scale increased ranging from 4.19% to 80.2% depending on the agitation rate, impeller size, solution concentration and tank conditions.

Secondly, the investigation of the impact of scale growth on heat transfer was conducted and observed that there was a significant variation of overall heat transfer coefficients (OHTC) and scaling thermal resistance (TR) coefficients due to crystallisation scale deposition. For a concentration of 4.50 mol/dm^3, OHTC decreases asymptotically with time ranging from 75% to 38%, 73% to 23% and 72% to 2.6% for impeller diameters of 86, 114 and 160 mm respectively, due to crystallisation scale deposition on the wall of the tank with inserted baffles. For the unbaffled tank, OHTC decreases asymptotically with time ranging from 70% to 0.6% which depends on agitation rate and impeller size. The TR appreciably decreases with the increase of impeller agitation rate ranging from 159.37 to 0.57 cm^{2}K/W. It is observed that the

lesser scale deposition occurs in unbaffled condition compared to the baffled condition, due to the former creating a swirl flow condition that is conducive to augmentation of OHTC and reduction of TR.

Finally, the effect of scale growth on different heat exchanger pipes material such as copper, aluminium, stainless steel, mild steel and polycarbonate (Cu, Al, SS316, MS, and Polycarbonate) during the convective heat transfer was investigated. The results show that crystallisation scale deposition increases with time and is augmented with an increase in thermal conductivity in the hierarchical order of copper (Cu) > aluminium (Al) > stainless steel (SS316) > mild steel (MS) > polycarbonate. The potential of a gum arabic additive to mitigate the crystalline deposition of normal soluble salt at convective heat transfer condition in the heat exchanger was also investigated, and a noticeable scale suppression was observed.

The outcomes of this study offer a new body of knowledge in elucidating the scale growth characteristics and provide design guidelines for agitation tanks and selection of suitable impeller blades which attract less or no scale deposition under hydrodynamics conditions.

Key Words: Scale growth, suppression, agitation tank, crystallisation, agitation speed, Bayer process, heat transfer coefficient, thermal resistance

DECLARATION OF AUTHORSHIP AND ORIGINALITY

I hereby declare the following research and discussion presented in this dissertation is original work performed by the author. No content of this thesis has been submitted or considered either in whole or in part or any materials for a degree, diploma or any other qualification of award at any university. I also declare that any material presented in this thesis performed by another person or institute has been referenced in the text.

……

(Prasanjit Das) April 2018

COPYRIGHT STATEMENT

……..

(Prasanjit Das) April 2018

TABLE OF CONTENTS

LIST OF FIGURES

LIST OF TABLES

LIST OF SYMBOLS

A Tank wetted surface area excluding the bottom or heat transfer area of the agitation tank[m^2]

A_i

Heat transfer surface area of process solution side [m^2]

A Heat transfer surface area of coolant side [m^2]

A_x Equivalent area of external coolant jacket [m]

C Bulk concentration of process solution [kg/m^3]

C_i

Concentration of process solution at solid-liquid interface [kg/m^3]

C_s

Saturation concentration of process solution [kg/m^3]

C_p Heat capacity of process solution [J/kg.K]

C_{Pc} Specific heat capacity of coolant [J/kg.K]

D or D_A Agitator or impeller diameter [m]

D_T Agitation tank diameter [m]

D_e Equivalent jacket diameter [m]

D_c Mean diameter of coolant jacket [m]

D_j Outside jacket diameter [m]

D_{ji} Inside jacket diameter [m]

ΔE Activation energy [J/mol]

ΔG	Overall excess energy [J/m^2]
ΔG_s	Surface excess free energy [J/m^2]

ΔG_V	Volume excess free energy [J/m^2]
i	Heat transfer coefficient of process solution side [W/m^2.K]
	Heat transfer coefficient of coolant side [W/m^2.K]
k	Thermal conductivity of tank wall material [W/m.K]
k_B	Boltzmann constant [J/K mol]
K_g^g	Crystal growth rate constant [m^4/kg.s]
k_{rm}	Proportionality constant for scale removal [m^3/ kg.s]
K_{rg}	Pre-exponential constant [m^4/kg.s]
K_s	Non-dimensional constant
k_s	Thermal conductivity of process solution [W/m.K]
k_c	Thermal conductivity of coolant [W/m.K]
L	Solution height inside the tank [m]
L_c	Coolant height in jacket [m]
$\dot{m}$	Scale mass [kg/m^2]
$\dot{m}_j$	Average coolant flow rate [kg/s]
$\dot{m}$	Scale mass deposited per unit area [kg/m^2]
$\dot{m}_r$	Scale mass removal per unit area [kg/m^2]
$\dot{m}_{ji}$	Mass flow rate at jacket inlet [kg/s]
$\dot{m}_j$	Mass flow rate at jacket outlet [kg/s]
	Order of reaction

N Impeller rotational speed [rev/s]

N_{Nu} Nusselt number [-]

N_{Re} Reynolds number [-]

N_{Pr} Prandlt number [-]

N_{μ} Viscosity number [-]

N_{Q} Impeller flow number [-]

P Agitator power [W]

P_{O} Power number [-]

Q
Impeller flow rate or Coolant flow rate through jacket [m^3/s]

$Q_{\mathbf{net}}$ Amount of heat content in the process solution [W]

$Q_{Overall}$ Overall heat flux [W/m^2]

$_{Coolant}$ Heat flux through the coolant [W/m^2]

$_{Wall}$ Heat flux through the wall [W/m^2]

$_{Solution}$ Heat flux through the solution [W/m^2]

R Gas constant [J/mol.K]

$R_{Coolant}$ Thermal resistance in coolant side [m^2.K/W]

R_{Wall} Thermal resistance of tank wall material [m^2.K/W]

$R_{Solution}$ Thermal resistance in solution side [m^2.K/W]

R_{Scale} Thermal resistance due to scale deposition [m^2.K/W]

$R_{Overall-Scale}$	Overall thermal resistance at scaled condition [m^2.K/W]
$R_{Overall}$	Overall thermal resistance at clean condition [m^2.K/W]
r	Radius [m]
r_i	Inner radius of tank [m]
r	Outer radius of tank [m]
	Degree of supersaturation [-]
T	Absolute temperature [K]
T_i	Temperature at the solid-liquid interface [°C]
T_B	Bulk temperature of process solution [°C]
T_{ref}	Reference temperature [°C]
T_J	Average coolant temperature [°C]
T_{ji}	Average inlet coolant temperature [°C]
T_j	Average outlet coolant temperature [°C]
T_B	Average bulk solution temperature [°C]
T_{WB}	Average tank wall temperature process solution side [°C]
T_J	Average coolant temperature [°C]
T_{WJ}	Average tank wall temperature coolant side [°C]
Δt_G	Temperature difference between the wall and bulk solution [°C]
t	Time [s]
U	Overall heat transfer coefficient [W/m^2.K]

U_{Scole}	Reduction of overall heat transfer due to scale formation [W/m^2.K]
$U_{Overall}$	Overall heat transfer coefficient at clean condition [W/m^2 .K]
$U_{O,,eral/-\&x,Je}$	Overall heat transfer coefficient at scaled condition **[W/m^2 .K]**
V	Velocity [mis]
$i,;,$	Volume of process solution [m^3]
$"V_{;}$	Volume of coolant flow through the jacket or Equivalent velocity of coolant through the jacket [m^3]
μ	Dynamic viscosity or crystalline solution [Pa.s]
μ_{rs}	Viscosity of process solution at bulk solution temperature [Pa.s]
μ_{ws}	Viscosity of process solution at wall temperature [Pa.s]
μ_{re}	Viscosity of cooling coolant at bulk coolant temperature [Pa.s]
μ_{wc}	Viscosity of cooling coolant at wall temperature [Pa.s]
P_C	Density of coolant [kg/m^3]
$R_{11:}$	Coefficient of volumetric expansion [-]

LIST OF GREEK SYMBOLS

μ	Chemical potential [J]
r	Surface energy [N/m^2]
$/J$	Mass transfer coefficient [mis]
$_{rs}$	Shear stress [N/m^2]
$_{O's}$	Shear strength [N/m^2]
	Scale deposit thickness [m]
p	Crystalline solution density [kg/m^3]
r	Shear rate [s^{-1}]

LIST OF ABBREVIATIONS

AR	Analytical reagents
CFD	Computational fluid dynamics
CSIRO	Commonwealth scientific and industrial research organisation
DSP	Desilication product
GNP	Gross national product
HTRI	Heat transfer research incorporated
homo	Homogeneous
hetero	Heterogeneous
J	Jacket
KNQ3	Potassium nitrate
OHTC	Overall heat transfer coefficient
QAL	Queensland alumina limited
Re	Reynolds number
RMS	Root mean square
SFT	Swirl flow technology
SIC	Standard industrial code
TEMA	Tubular exchange manufacturers association
TR	Thermal resistance

ACKNOWLEDGEMENTS

I would like to thank Almighty who gave me the patience and capability to complete my PhD dissertation. I gratefully acknowledge and thank the people who made this dissertation possible.

Firstly, my deepest and earnest gratitude is extended to my Principal Supervisor, Professor Masud Khan, for his endless support, encouragement, guidance and valuable suggestion during my research and study. His professional guidance and motivation facilitated to achieve my research objectives. I would also like to express my thanks to my Associate Supervisor, Associate Professor M G Rasul for his constructive comments and encouragement during my study. Heartfelt thanks go to my other Associate Supervisor Dr. Jie Wu, in CSIRO for his technical guidance and valuable comments.

I would like to express special thanks to Dr. Inju Youn, CSIRO, for his suggestion and technical guidance on the fabrication of laboratory scale mixing tank built for this project to investigate the scaling behaviour. Special thanks go to Randall Stock (Workshop Manager, Engineering, School of Engineering and Technology) and all other staffs of Central Queensland University for their assistance and technical support. I am also thankful to Dr. James Chapman and Vicky Caroll for their assistance in using the scanning electronic microscope (SEM).

I am grateful to Central Queensland University, Australia for providing me the financial support through the IPRS (International Postgraduate Research Scholarship) and UPRA (University Postgraduate Research Award) scholarship program. I acknowledge the administrative support from the Office of Research Services during my study.

I like to acknowledge the support and encouragement given by my parents throughout my study. Finally, I take this opportunity to thank my family, without whose support and encouragement this research would not have been possible.

ACKNOWLEDGEMENT OF PROFESSIONAL SERVICES

Professional editor, Jonathan Dyer, provided copyediting and proof-reading services, according to the guidelines laid out in the University-endorsed national 'Guidelines for Editing Research Theses'.

……..

(Prasanjit Das) April 2018

LIST OF PUBLICATIONS

The following articles were produced for publication during the course of my candidature. The authors' contributions in producing these papers are described below.

1. **Prasanjit Das**, Khan, M.M.K., Suvash C. Saha, M.G. Rasul, "CFD Simulation of Fluid Characteristics on Scale Growth Mechanism in a Concentric Reducer". *The 10th Australian Heat and Mass Transfer Conference, Brisbane, 14-15 July, 2016.*

2. **Prasanjit Das**, Khan, M.M.K., Suvash C. Saha, and M.G. Rasul, "Fluid Flow Characteristics on Scale Deposition in a Concentric Reducer Using CFD Approach". *11th International Conference on Heat Transfer, Fluid Mechanics and Thermodynamics* (HEFAT2015), 20 - 24 July 2015 in the Kruger National Park, South Africa. (**Awarded the outstanding paper of the session).**

3. **Prasanjit Das**, Khan, M.M.K., M.G. Rasul and Suvash C. Saha, "Study of Fluid Dynamics Approach to Scale Growth Mechanism and its Suppression Technique" *International Conference on Mechanical and Engineering and Renewable Energy 2015, 26-29 November, Chittagong, Bangladesh.* (Published in Journal of Mechanical Research, ISSN: 1990-5491).

Statement of Authors Contribution for papers 1, 2 and 3:

Prasanjit Das developed the numerical procedure, conducted numerical simulation and analysed the numerical results. Prasanjit also developed the content of the paper and drafted the manuscripts. Prof. M.M.K. Khan (principal supervisor) assisted in analysing data and results. Initially, Prof. Khan reviewed these manuscripts and provided guidance and valuable feedback for modification of the manuscripts. Then, A/Prof. Rasul and Dr. Saha reviewed the second draft of these manuscripts and made comments and suggestions for further improvement/development. These papers were finalised through further discussions between Prasanjit and the supervisory team.

4. **Prasanjit Das**, Khan, M.M.K., Suvash C. Saha, and M.G. Rasul, 2016. "Numerical study of flow through a reducer for scale growth suppression". Book chapter, Thermofluid Modeling for Energy Efficiency Applications. Editor: Khan et al., ISBN: 9780128023976. Elsevier Science Publishing Co. Inc., USA.

Statement of Authors Contribution for publication (Book chapter) 4:

Initially, Prasanjit Das and the supervisory team (M.M.K. Khan and M.G. Rasul) discussed the numerical procedure and content of the chapter. Prasanjit performed the numerical simulation, synthesised the data, analysed the results and drafted this manuscript. Prof. Khan (principal supervisor) assisted Prasanjit in analysing the data, the results and conclusion. Prof. Khan first reviewed this manuscript and provided important suggestions and feed back for modification and improvement. Then, Saha and Rasul reviewed the manuscript and made thoughtful comments and recommendations for further improvement.

5. **Prasanjit Das**, M.M.K. Khan, M.G. Rasul, Jie Wu, I. Youn, "Experimental investigation of hydrodynamic and heat transfer effects on scaling in an agitated tank. Accepted 17 April 2018, Chemical Engineering & Processing: Process Intensification.
6. **Prasanjit Das**, M.M.K. Khan, M.G. Rasul, Jie Wu, I. Youn, "Study of hydrodynamics effect on heat transfer and scale mitigation in the agitation tank" **(Submitted to Applied Thermal Engineering, Publisher: Elsevier, Year: 2017).**

Statement of Authors Contribution for papers 5 and 6:

Prasanjit designed and fabricated the new experimental setup, developed the methodology and experimental measurement procedures, conducted the experiments and measured the data, and analysed them. Prof. Khan (principal supervisor) and Dr. Jie Wu (associate supervisor, CSIRO) provided technical guidance for the experimental setup design and valuable comments on the overall project. Dr. Inju Youn (CSIRO) provided various suggestions and technical guidance during the design and fabrication of the laboratory scale agitation tank built for this project to investigate the scaling behaviour. Initially, Prof. Khan reviewed theses manuscripts and provided guidance and valuable feedback for modification of the manuscripts. Then, A/Prof. Rasul reviewed the second draft of these manuscripts and made comments and suggestions for further development. These papers were finalised though further discussion between Prasanjit

and the supervisory team. These papers were written based on the contents of chapter 5 and 6, respectively.

CHAPTER 1
INTRODUCTION

1.1 Motivationand Background

Scaling is a global problem and occurs in various process systems. The scale formation on processing equipment is an inherent chronic problem in most industries such as mineral processing, oil refineries, food processing, power generation, pulp and paper manufacturing and oil and gas. Scale formation in processing equipment (for example, heat exchanger, precipitation tank, condenser and crystalliser) of many industries is a natural consequence of supersaturated solutions that are generated throughout the processing. Numerous studies report that more than 90% of heat exchangers suffered from scale deposit (Müller-Steinhagen, 2010; Pritchard, 1988; Steinhagen et al., 1993). Scaling received more attention because of recent studies (from 1980s to early 1990s) which shows the cost incurred due to the formation of scaling is about 0.25% of the gross national product (GNP) of industrialised countries (Garrett - Price, 1985; Pritchard, 1988; Steinhagen et al., 1993). Due to global warming, all industrialised countries have an obligation to reduce their CO_2 emissions to which, according to the *Kyoto Protocol*, humans contributed to a significant part. Therefore, efficient energy management has a vital role in any endeavour to control CO_2 emissions. Heat transfer professionals have a great responsibility to design heat exchanger equipment to achieve effective utilisation of energy. The main contributor to lower heat transfer performance on heat exchanger surfaces is scaling or fouling and it has been stated that, "*scaling or fouling is the major unresolved problem in heat transfer"* (Taborek et al., 1972). Unfortunately, many bodies or organisations have overlooked the problem of scaling as part of tackling global warming. Most recently, the number of experts and researchers in universities and industries working in the field of scaling or fouling to identify or determine effective mitigation technology is increasing. Scaling research has two main objectives, firstly, to improve the design techniques that mitigate or reduce scaling deposits and secondly, to improve the technology to mitigate or suppress scaling on heat exchange surfaces or other equipment.

Scale formation is a more serious problem in the mineral industry than other process industries. Hence, focus of this study is on scale formation in alumina refineries as the most rapid scale formation occurs in the precipitation area, where alumina is chemically extracted from bauxite.

Deposition of scale in the Bayer plants occurs both in liquor and slurry streams. The main characteristic of scale deposit material is that it has low thermal conductivity which creates a major resistance to heat transfer, resulting in significantly reduced equipment performance. The accumulation of scale deposit reduces production efficiency and causes other problems such as flow blockage, probe malfunction, and significant operational costs involved in the de-scaling process. The immense cost for the mineral processing industry is evident through increased capital expenses and reduced plant capacity. It has been estimated that direct costs involved in removing scale may be as much as one-quarter of the operational costs of an alumina refinery (Nawrath et al., 2006).

There are many factors and parameters, which contribute to the scale formation and deposition. These are the quality of the bauxite ore (concentration of silica and other impurities in bauxite), the saturation level of caustic solution, the rheological properties (viscosity, temperature and density), the process equipment (material, surface finish and morphology), the turbulence and inertia of suspended particles, the velocity (stream-wise, cross-stream and circumferential velocity fluctuation components) of fluid particles, the particle size and shape and adhesive property of particles (Hoang et al., 2011; Nawrath et al., 2006). The scale development mechanism in the mixing process cycle is complex and still not well understood. Most of the above parameters are related to hydrodynamic characteristics of the process solution and play a critical role in scale deposition (Das et al., 2016). From a survey of literature it is clear that scaling is a physiochemical process which can be affected by process solution hydrodynamics and it has influences on the heat and mass transfer process. It is therefore important to understand the scale formation mechanism before attempting to optimise efforts to suppress scalegrowth.

Therefore, this study is focused on hydrodynamic interaction on scaling rather than on chemical or metallurgical effect as there is limited research dealing with hydrodynamics. The findings of this research will provide a fundamental and deeper understanding of hydrodynamic effects on scale formation and its suppression.

1.2 What is Scaling?

Scaling can refer to the formation of unwanted deposit layers on the heat exchange or transfer surfaces which lead to reduced efficiency of processing equipment. Scaling is the resultant effect of deposition and removal of scale deposits on the heat transfer surface. Kern and Seaton (1959) first described the scaling processes which involve two successive events as a net effect

of scaling on the heat transfer surface. The net scale deposition rate is the rate of scale deposition minus the rate of scale removal.

The mechanism of scale growth and the removal process for the typical system could be represented as shown in Figure 1.1. The particulate scaling could occur due to particle settling by gravity, whi on. The scaling and removal pr onditions such as level of sup l scale forming surface.

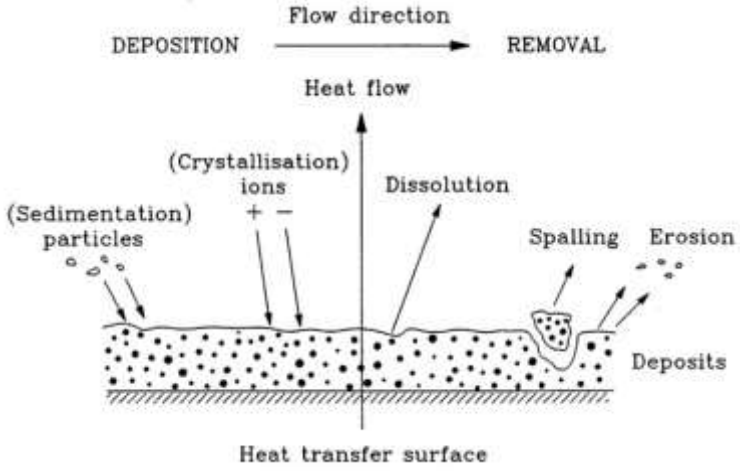

Figure 1.1: Various deposition and removal processes during scaling (Kazi, 2012)

It is convenient to classify the scaling on heat transfer surfaces based on the physical and chemical processes involved. The scaling can be categorised into the followings groups of Crystallisation or Precipitation scaling, Particulate or Sedimentation fouling, Chemical reaction fouling, Corrosion fouling and Biological fouling as summarised in Figure 1.2. The relative occurrence of the various scaling types is shown in Figure 1.3. As seen, from Figure 1.3, the maximum of 32% scaling occurs through crystallisation and minimum of 5% occurs via chemical scaling (Steinhagen et al. 1993).

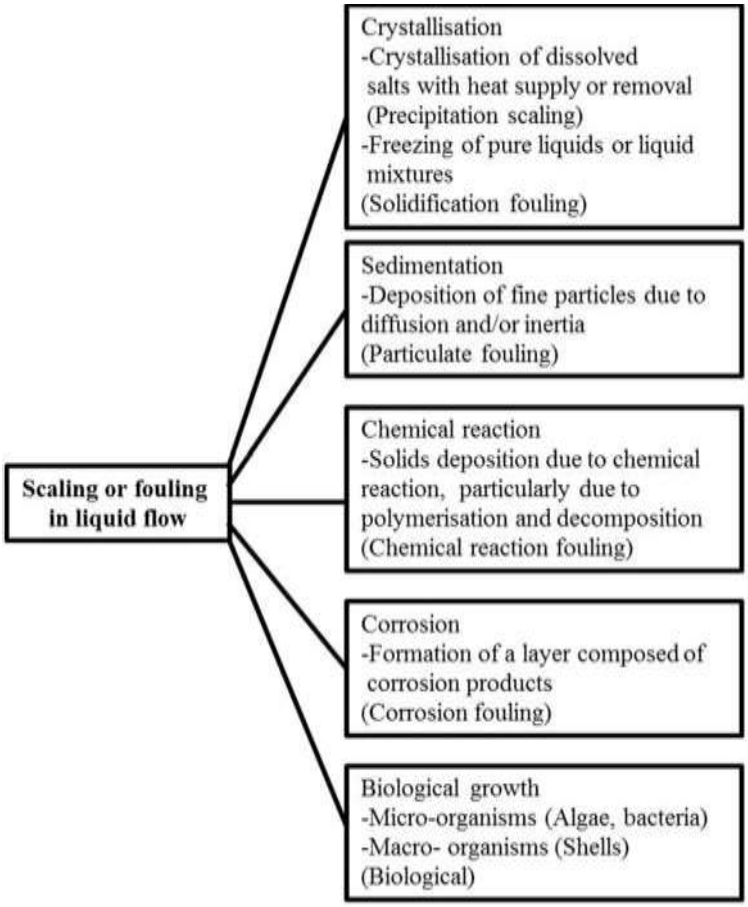

Figure 1.2: Different types of scaling or fouling in liquid flow (Mullin, 2001)

1.2.1 Crystallisation Scaling

Crystallisation scaling is one of most frequently occurring methods of scaling in industrial processing. In an aqueous system, the general term to describe crystallisation fouling is "scaling". Supersaturation is the main driving force for crystallisation scaling of normal or inverse soluble salts. Crystallisation scaling is formed by dissolved salts which precipitate out of the process solution on the heat transfer surface (cooled or heated) due to supersaturation. In general, for crystallisation scaling to occur, there is a requirement for the solubility limit for given conditions, particularly the prevailing temperature, to be exceeded (Bott, 1997). Freezing fouling or low temperature scaling refers to the phenomenon wherein a deposited layer is formed on the heat transfer surface which is colder than the bulk process solution via crystallisation of dissolved species or the solvent itself (Kern, 1966). Epstein (1983) further categorised fouling according to solubility behaviour as: *scaling* which is commonly observed in aqueous heating solutions associated with inverse solubility salts such as calcium carbonate,

gypsum and phosphate, and *freezing fouling* wherein scale deposit is formed on a sub-cooled surface via solidification related to normal solubility salts such as potassium nitrate, zinc sulfate and magnesium sulfate (Fernandez-Torres et al., 2001).

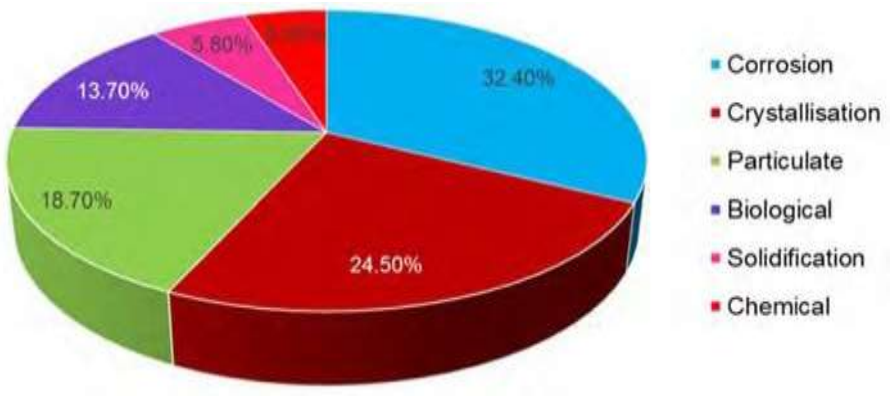

Figure 1.3: Mechanism of scaling (Steinhagen et al. 1993)

1.2.2 Particulate Fouling or Scaling

Particulate scaling occurs by the deposition of suspended particles in the process solution on the heat transfer surfaces due to gravity or deposition mechanisms (Mullin, 2001). Unburned fuels or soot particles, clay or mineral particles in river water, and deposition of salts in desalination process and so on, are examples of particulate scaling. The physical process of particulate scaling occurs in pipe flow as shown in Figure 1.4.

1.2.3 Chemical Reaction Fouling

In chemical reaction fouling, solids deposition occurs due to a chemical reaction between reactants contained in the process fluid in which the surface material itself is not a reactant or participant, particularly due to polymerisation and decomposition (Mullin, 2001). Examples of chemical fouling occur in oil refining, cooling of oil and gas, the polymerisation of process monomers, and so on.

1.2.4 Corrosion Fouling

Corrosion fouling occurs with some chemical or electrochemical reaction between the heat transfer surface itself and process solution, eventually causing product scale deposit on the surface to create resistance to heat transfer (Mullin, 2001). For example, the presence of sulfur in fuel can cause corrosion in gas and oil fired boilers.

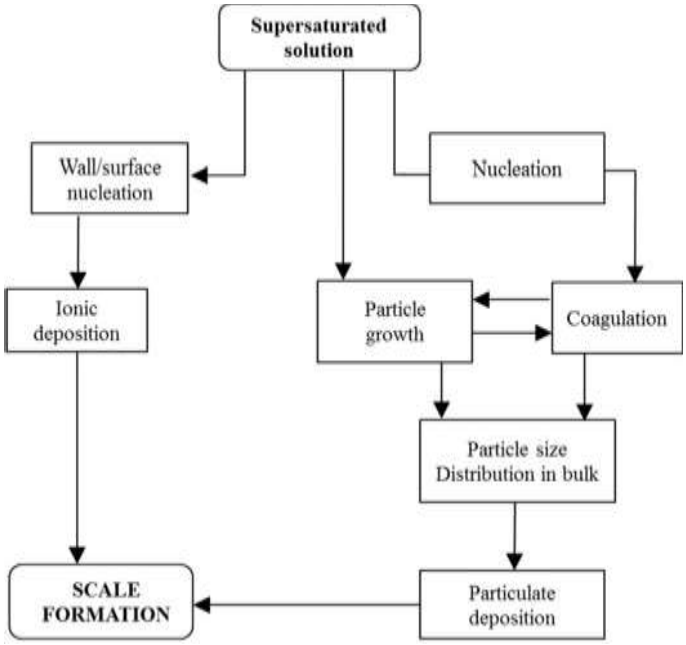

Figure 1.4: Physical processes occurring in pipe flow of supersaturated solutions (Karabelas, 2002)

1.2.5 Biological Fouling

Biological fouling occurs when biological materials (micro and macro-organisms such algae, bacteria, molds, and so on.) grow on the heat transfer surface and, as a result, reduce the heat transfer performance through the surface and process liquid (Mullin, 2001).

1.3 Bayer Process Scaling

This research particularly focused on hydrodynamic effects on Bayer process scaling in the precipitation area. Here, the fundamentals of the Bayer cycle and scaling due to crystallisation of gibbsite are discussed. The Bayer process cycle is used for refining bauxite ore to alumina oxide (Al_2O_3), which is then smelted to produce pure aluminium as shown in Figure 1.5. The process was developed and patented by Karl Josef Bayer in 1888 (Hind et al., 1999), and has become the cornerstone of the aluminium industry worldwide. Production of bauxite reached 20.2 million tonnes, alumina 19.9 million tonnes and aluminium 1.6 million tonnes worldwide by the fiscal year 2014-2015, with Australia the world's largest producer of bauxite and refiner of alumina with just about 22% of the world production (Australian Government, 2017). In the Bayer process, crushed bauxite is subjected to high-temperature (up to 270ºC) and pressure digestion in a concentrated caustic solution in a stirred tank.

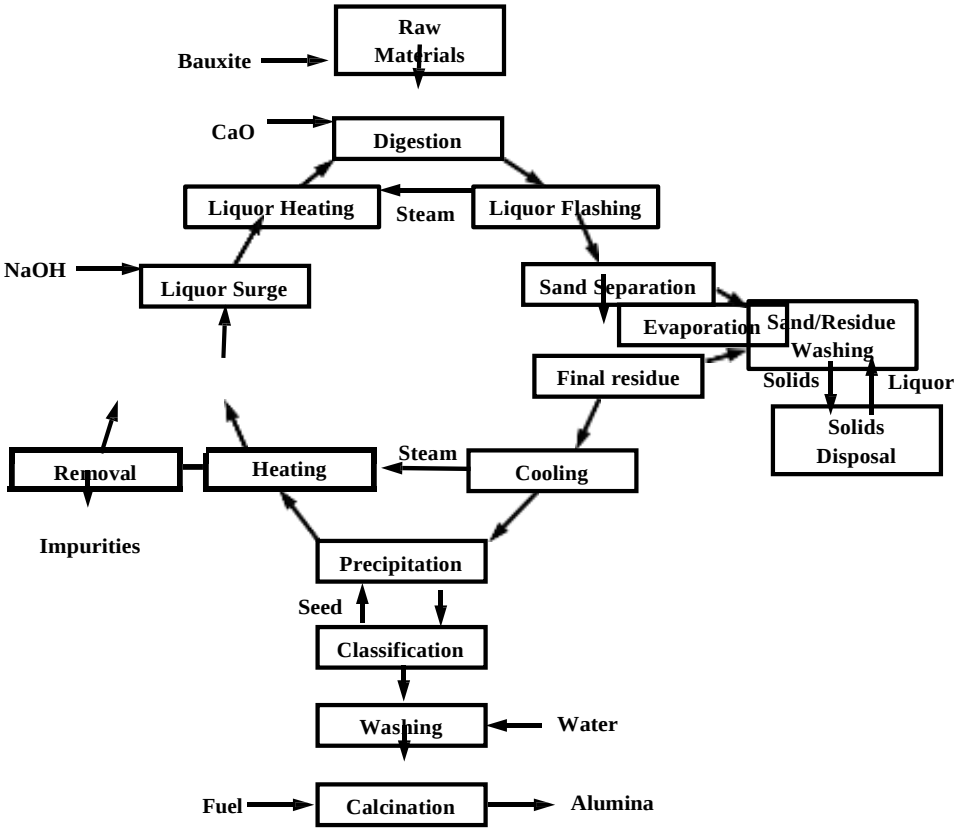

Figure 1.5: Block diagram of Bayer process cycle (Hind et al., 1999)

The resulting liquor, termed pregnant or green liquor, which is supersaturated in sodium aluminate, is then clarified and filtered to remove mud and other insoluble residues. After solids separation, aluminium trihydroxide (gibbsite; $Al(OH)_3$) is precipitated (Hind et al., 1999). This is achieved by cooling the solution and seeding with gibbsite. Then the gibbsite is removed and washed prior to calcination, where the gibbsite is converted to alumina. The extraction process depends almost entirely upon chemical processes occurring at the solid/aqueous interface as shown below (Hind et al., 1999):

Extraction: $Al(OH)_{3(s)} + NaOH_{(aq)} \rightarrow Na^+Al(OH)^-_{4(aq)}$

and $AlO(OH)_{(s)} + NaOH_{(aq)} + H_2O \rightarrow Na^+Al(OH)^-_{4(aq)}$

Precipitation: $Na^+Al(OH)^-_{4(aq)} \rightarrow Al(OH)_{3(s)} + NaOH_{(aq)}$

Calcination: $2Al(OH)_{3(s)} \rightarrow Al_2O_{3(s)} + 3H_2O_{(g)}$

In the Bayer process, caustic liquors are used to dissolve gibbsite from the bauxite ore at high temperature, and then to reprecipitate as a hydrate at low temperature. A consequence of the Bayer process is that, the liquors are purposely kept supersaturated with respect to gibbsite and thus scaling occurs.

Scale formation in alumina refineries is a common phenomenon and it occurs where supersaturated solutions are in contact with solid surfaces. Scale formation mechanism in the Bayer process equipment is complex and is not fully understood yet. Numerous researches indicate that scale growth is strongly affected by fluid velocity while also influenced by a number of other factors such as quality of the bauxite ore, rheological properties of fluid, turbulence and inertia of suspended particles and adhesive property of particles (Das et al., 2016; Hind et al., 1999).

In alumina refineries, the most rapid scale formation occurs in the precipitation area, where alumina is chemically extracted from bauxite. Deposition of scale in the Bayer plants occurs both in liquor and slurry streams. Scale growth rate is different at different parts of the Bayer circuit (four stages such as digestion, clarification, precipitation and calcination as shown in Figure 1.5) without a change in liquor composition, for example, before and after a heat exchanger. Supersaturation is the main driving force of the crystallisation processes and an increase of the supersaturation ratio would result in an increase of scale deposition on the metal surface. The basic scaling mechanisms are of two of types 'growth scale' and 'settled scale' (Hind et al., 1999; Das et al., 2016).

Growth scale is due to the crystallisation of gibbsite from the oversaturated caustic solution. Nucleation can be a slow process in scale growth and is governed by many factors; however, once the nucleii are formed, growth is very predictable by kinetic factors such as temperature and supersaturation. The degree of supersaturation and form of the surface are very critical factors for nucleation. For example, pipe and tank walls are often cooler than the liquor, hence the local supersaturation at the surface will be higher, and nucleation will be more favourable at that point. Another important factor is temperature, for growth of these nucleii at the higher temperature is more rapid even though the supersaturation is less.

In the settled scale, the slurry particles may be settled and cemented by the supersaturated liquor. Settling scale occurs more favourably in low velocity regions of plant equipment or during shut down. The scale can be formed rapidly as only a minor amount of the supersaturated phase needs to be precipitated. Also agitation plays an important role in settling

scale. Examples of each scale type can be found in the same slurry such as in a precipitator and a digest vessel. A growth scale and settled scale can readily be produced in the same environment by placing a flat metal sheet at a 45º angle to the flow direction in a slurry environment. A growth scale forms on the side where flow impinges and settled scale forms on the reverse side.

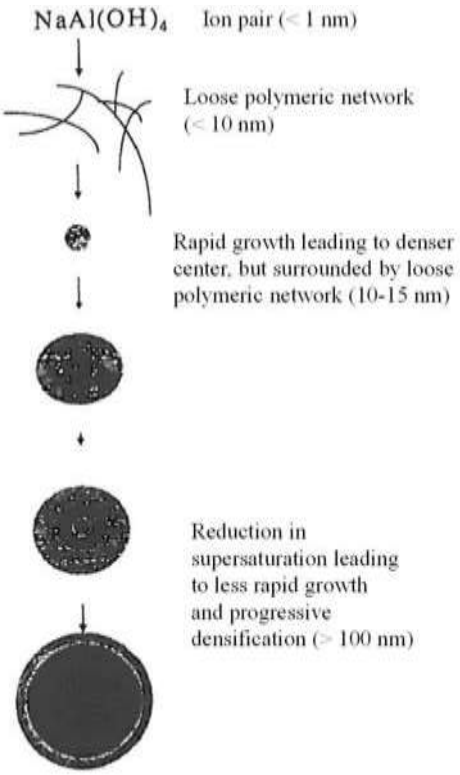

Figure 1.6: Gerson's speculated model of the gibbsite nucleation mechanism and particle growth from supersaturation caustic-aluminate liquors (Watson et al., 1998)

The rate-determining stage in the Bayer process cycle is the crystallisation of gibbsite from the supersaturated caustic-aluminate solution. As reported by Watson et al. (1998), the formation of gibbsite crystals is the most rapid in the temperature range of 60 ºC to 80ºC due to the balance between supersaturation and reaction kinetics. In an ideal supersaturated caustic-aluminate solution, the dissolution of gibbsite phase aluminate-trihydrate occurs according to the simplified chemical reaction (Veesler and Boistelle, 1993):

$$Al(OH)_{3(s)} + OH^{-} \Leftrightarrow Na^{+} Al(OH)_{4(aq)}^{-}$$

The observation of Kali (1997) and Watson et al. (1998) is that the exact mechanism by which the $Al(OH)_4^-$ ions in the supersaturated caustic-aluminate solution nucleate and grow into the crystalline gibbsite is not fully understood.

Watson et al., (1998) concluded that during the development of the aluminium containing particles in caustic-aluminate solutions, there is a considerable time in which the particles are undistinguishable to detection (Watson et al., 1998). Gerson speculated that the nucleation mechanism may be as depicted in Figure 1.6, but has also concluded that more than one crystallisation mechanism is possible (Watson et al., 1998). As reported by King (2013), the kinetics of gibbsite crystal growth is linear. The growth rate, G, of gibbsite crystals is characterised by the equation:

$$G = k\left(C_i - C_s\right)^n \tag{1.1}$$

where C_i is the concentration of process solution at solid-liquid interface [kg/m^3], C_s is the concentration of process solution [kg/m^3], n is the order of reaction and k, a coefficient is a function of the kinetic coefficient k_0 , as follows:

$$k = k_0 \exp\left(\frac{-\Delta G}{RT}\right) \tag{1.2}$$

where ΔG is the overall excess energy [J/m^2], R is the gas constant [J/mol.K] and T is the absolute temperature [K].

1.4 Factors Affecting Scaling

Scaling being a dynamic physiochemical process is influenced by a number of variables categorised as: (i) operating parameters, (ii) process equipment parameters, and (iii) process fluid or solution parameters. Table 1.1 shows a summary of important parameters that affect scaling.

Table 1.1: A summary of parameters affecting scaling

Categories	Variables	Causes
Operating parameters (Hoang et al., 2007; Hoang et al., 2011; Nawrath et al., 2006)	(i) Flow velocity and agitation speed (or shear stress) (ii) Surface temperature (iii) Bulk temperature	(i) Increasing velocity promotes the deposition in the case of mass transfer controlled scaling and vice versa in the case of reaction controlled scaling. (ii) Increasing local surface temperature causes more deposition of inverse soluble salts, and lower temperature promotes the deposition of normal soluble salts. (iii) Similar effect as surface temperature.
Equipment parameters (Azimi et al., 2014; Kaziet al., 2010)	(i) Surface material (ii) Conductivity (iii) Surface energy (iv) Surface structure (roughness)	(i) Different material has different catalytic action and may promote or reduce scaling. (ii) Higher conductive material promotes the scale deposition. (iii) Higher surface energy increases the scale deposition. (iv) Initial scale deposition strongly depends on surface roughness
Process solution parameters (Hoang et al., 2007; Hoang et al., 2011; Nawrath et al., 2006)	(i) Solute concentration (Supersaturation) (ii) Density and viscosity (iii) Impurities and suspended solids	(i) Scale deposition depends on supersaturation. (ii) Density and viscosity have a strong effect on shear rate, and viscosity is playing an important role for the sublayer thickness where initial deposition takes place. (iii) The intrusion of minute impurities promotes the scale deposition acts as a nucleus and sometimes suspended particles (like sand) reduce the scaling.

1.5 Research Problems and Gaps

Based on the available literature, it can be stated that hydrodynamic effects play a dominant role and significantly contribute to both scale growth and its suppression. A limited number of studies have been conducted on the crystallisation scale problem in agitation tanks to examine the hydrodynamic effects on normal soluble salts. Most of the research undertaken for several mineral industries such as alumina, nickel and magnesium was to investigate the chemistry and metallurgical crystallographic approach. Futhermore, the potential hydrodynamic effects on scale mitigation are yet to be fully explored. Therefore, it is essential to investigate the hydrodynamic effects on the crystallisation scaling. It is important to understand the effects of agitation velocity and its contribution so that mitigation and suppression methods can be undertaken. It is seen from the literature that scale can be suppressed by creating more wall shear stress on the scale deposition boundary layer (Hoang et al., 2011; Wu et al., 2012). However, achieving this wall shear stress is not economically viable due to the increased power consumption requirement. One of the most important measures to promote scale suppression on the wall is to de-stabilise the deposition boundary either through increasing the wall velocity or creating pressure fluctuation around the deposition boundary layer by altering the design based on hydrodynamics. However, more research is still needed to clarify the issues mentioned above and to explore the effects of hydrodynamic on the crystallisation scale growth mechanism and its suppression regarding optimum agitation speed, use of baffles and size of impellers.

Based on all the information provided in the above sections, the following research gaps are identified:

- To the best of the author's knowledge from the available literature, no studies have been conducted on crystallisation scale of normal soluble salts in the agitation or precipitation tanks.
- Only a few studies have been conducted on crystallisation scaling of normal soluble salts such as KNO_3.
- Very little research has been done to assess the effects of hydrodynamics on the crystallisation scale growth mechanism and its suppression.
- Little attention has been paid to swirl and non-swirl flow effects on crystallisation scaling in agitationtanks.
- Only a few studies have been conducted on the effects of speed and size of impeller on suppression of crystallisation scale in agitation tanks.

- Limited investigation has been conducted on the effects of material types on freezing crystallisation scaling of normal salt solutions.

Considering the above research problems and gaps, the important research questions that will be addressed in this study are:

(i) What are the effects of hydrodynamics on scaling in mineral industries, namely in the Bayer process of alumina refinery?

(ii) What are the key parameters involved in scale growth and its suppression in terms of hydrodynamics design?

This study will examine the hydrodynamic effects on scale growth and its suppression, and specifically focus on crystallisation scale formation in the agitation or precipitation tank of the Bayerprocess.

1.6 Aim and Objectives

The main aim of this study is to investigate the hydrodynamics effects on the scale growth and its suppression in the agitation tank of the Bayer process. The experimental investigation of crystallisation scale suppression is conducted using a normal soluble salt (KNO_3) solution instead of the real Bayer liquor solutions as it is not safe to handle real Bayer liquor due to its high processing temperature and their caustic property. Moreover, Potassium nitrate (KNO_3) is one of the most temperature sensitive chemicals in its aqueous solubility (17g at 5ºC to 100g at 60ºC per 100g water) which is found suitable for producing crystallized scale by applying a temperature change. The specific objectives of the study are:

- To design and fabricate a suitable laboratory scale tank model, representative of mineral mixing or precipitation tanks to experimentally investigate the hydrodynamics effects on crystallisation scale growth and its suppression.
- To investigate the parameters such as concentration, agitation rate, impeller sizes and baffle effects on the overall scale growth mechanism in the agitation tank.
- To investigate the scale growth effects on the heat transfer coefficient and thermal resistance in the agitation tank.
- To investigate the scaling effects on various materials (Copper, Aluminium, Stainless steel, Mild steel and polycarbonate) and the effect of scale suppression additive on scaling.
- To investigate and analyse the crystallisation scale surface morphology for understanding of scalestructure.

Investigating and achieving these objectives will provide new knowledge and understanding of the hydrodynamics effects on the scale growth which will allow to find the suppression techniques based on hydrodynamics.

1.7 Scope and Limitations of the Study

This research focused on the hydrodynamic effects on crystallisation or mineral scale growth and its suppression in a model agitation tank. Research on the scale problem in the agitation or mixing tanks in mineral processing, chemical industries and refineries is essential, since a solution to this problem will greatly benefit those industries. The investigation of mineral scaling largely depends on understanding the effects of impeller agitation rate (impeller speed), requiring a proper impeller model to develop economically viable outcomes that optimise the power consumption. In addition, it is critical to examine the effects of parameters such as agitation rate, impeller sizes and baffles on the scale growth mechanism to help in the design stage for process optimisation. This experimental investigation also helps in the selection of equipment materials that lessen scale growth on agitation or mixing tanks. Also, examining the benefits of swirl flow (without baffles) and non-swirl flow (with four equally spaced baffles placed on the tank wall) gives new design guidelines for precipitation or mixing tank design experts. The agitation tank without baffles are beneficial because it creates uniform fluid erosion around the tank wall due to swirl phenomena and reduces the scale deposition.

The proposed research will provide new knowledge and data to enhance our understanding of the hydrodynamics effects, not only on scale growth and its suppression, but also on the heat transfer rate and thermal resistance which greatly affect the process efficiency. The study provides a novel approach to elucidating the scaling and its suppression mechanism using for the first time normal soluble salt to generate the crystallisation scale deposition in the agitation tank which effectively replicates many industrial processes. The outcomes of this thesis offer a better understanding of scaling characteristics and provide guidelines for effective design of an agitation tank and selection of suitable impeller blade attracting less or no scale deposition under hydrodynamics conditions.

There are some limitations in this study which are described below:

The experiment to discern the hydrodynamic effects on the crystallisation scale growth phenomenon and its mitigation was conducted using laboratory made process solutions of potassium nitrate (KNO_3). The real industrial process solutions such as the Bayer liquor or black kraft pulp solution are not safe to handle due to high processing temperature, high

pressure and their caustic properties. Also, crystallisation scaling in the agitation tanks was investigated by using only a normal soluble salt rather than an inverse soluble salt which produces freezing crystallisation only.

The results obtained from using KNO_3 solutions will provide the fundamental information which will be related to the crystallisation scale process that occurs in the precipitation tank of Bayer process or agitation tank in other chemical industries.

1.8 Thesis Outline

This thesis contains nine chapters. The outline of these chapters is briefly summarised below:

In Chapter 1, an overview of scaling, mechanisms of crystallisation scaling, types of scaling, processes of scaling, scaling curves, scaling models, factors affecting scaling, and the motivation for this study are presented. The research problems and gaps, aim and objectives, and scopes and limitation of the study are also stated.

In Chapter 2, the literature review relevant to the present study is reported. The literature review covers the history of scaling research, an overview of crystallisation scaling, hydrodynamics aspects of scaling, problems of scaling, an overview of scale mitigation and suppression techniques, economic and environmental impacts of scaling.

In Chapter 3, the mathematical background of crystallisation scaling including modeling of hydrodynamics phenomenon, modeling of scale or crystalline deposit growth phenomenon, modeling heat transfer phenomenon, estimating the average process solution and coolant temperature and estimating the overall heat transfer coefficient and scaling thermal resistance arediscussed.

In Chapter 4, the experimental set-up and necessary apparatus, materials and scale forming solution, data acquisition, experimental procedure, and experiment plan and data collection are explained.

In Chapter 5, hydrodynamic effects on scale growth and suppression including experiment data reproducibility, the effects of supersaturation, effects of agitation rate and effects of baffles on scaling rate are analysed and presented. In addition, a comparison between growth scale on the wall and settled scale on the tank bottom are also explained.

In Chapter 6, hydrodynamics effects on heat transfer including tank wall surface temperature and bulk solution temperature, overall heat transfer coefficient and thermal resistance are analysedand discussed.

In Chapter 7, crystal structure and morphology of crystal surface due to various process parameters such as agitation speed, impeller size, presence of baffles and solution concentration are visualised and discussed.

In Chapter 8, scaling effects on different materials (high to low thermal conductivity material), advantages of scale mitigation additive, effects on heat transfer coefficient and thermal resistance, and crystal surface morphology are analysed and discussed.

In Chapter 9, the findings and concluding remarks of the research are summarised. Recommendations for further study andfuture lines of research are also outlined in this chapter.

CHAPTER 2
LITERATURE REVIEW

This chapter presents a review of the literature highlighting key aspects and importance of scaling, especially the crystallisation scaling mechanism, mitigation, and problems due to scaling currently faced by various industries around the world. The hydrodynamics effects on crystallised scale growth and heat transfer are the main focus here. The literature search for mitigation methods of crystallisation scaling from the hydrodynamics point of view is discussed in details. Furthermore, the environmental and economic impacts due to scaling or fouling in high energy consuming industries are also reviewed.

2.1 Background History of Scaling Research

The term fouling or scaling is defined as the formation of unwanted deposit materials on the heat transfer surfaces that impede heat transfer rate and increase thermal resistance. Scaling is an ancient problem that has been with us since fire was discovered (Somerscales, 1990). Nowadays, it is not only a problem from the viewpoint of economics, but also an environmental issue due to currently imposed restrictions on CO_2 emissions. Scaling or fouling is now an important topic because of its significant effects on the efficiency of energy or heat transfer devices and thus increased energy consumption. Scaling is involved in many parts of heat exchange equipment in different industries around the world. Before 1920, scaling was receiving much attention from engineers, designers and operators into steam boilers and steam condensers. After 1920, it attracted more attention in regard to controlling scaling, particularly in boilers in electricity generation units, because it was not economically viable to shut down these plants for extended periods (Somerscales, 1990). The Wilson plot method was applied to evaluate the thermal resistance for design purposes. In 1922, continuous chlorination was applied to suppress the fouling in condenser cooling water (Boruff and Stoll, 1932). In 1987, a joint committee of Heat Transfer Research Incorporated (HTRI) and the Tubular Exchange Manufacturers Association (TEMA), agreed on a list of fouling factors (TEMA, 1999). In 1959, Kern and Seaton published the first scientific study regarding fouling modelling (Kern and Seaton, 1959; 1959a).

Their proposed model included two successive processes, namely the growth of deposition and the removal of deposition. In 1962, Hasson proposed a noteworthy model that included the mass transfer process with or without chemical reaction (Hasson, 1962). Table 2.1 presents a review of the progress of fouling or scaling research from the 19th century to the present day. The review shows that, prior to 1920, the phenomenon of fouling or scaling in boilers was well recognised and a relationship with the heat transfer surface was established. After 1920, the research focused on determining the thermal resistance and methods to reduce scaling. From 1935 to 1940, TEMA was first to publish the fouling factors of various petroleum feedstocks. In the 1950s, Kern and Seaton (1959a) first modelled the scaling process which included growth and removal processes which was a landmark in scaling research. From 1980 to the present day, more specific research on particular industrial process streams and the modeling of such processes progressed with better understanding of scale mechanisms and various suppression methods.

Table 2.1: Summary of scale research history

Time frame	References	Remarks
Before 1920	1. Leidenfrost (1966) 2. Bathe and Bathe (1943) 3. Partridge (1930) 4. Graham(1860) 5. Breckenridge (1899) 6. Durston(1893) 7. Durston (1893) and Hirsch (1891)	1. First reference about deposits of water drops 2. First to identify the phenomenon of fouling 3. Reported the effect of fouling on boiler efficiency 4. Reported the fouling of fresh and saltwater 5. Reported the effect of fouling on boiler efficiency 6. First to conduct a series of tests of boiler fouling at University of Illinois in 1898 7. Reported the relationship between heat transfer surface temperature and fouling

	8. Hall (Patent in 1834)	8. Patent for prevention of boiler water fouling
1920-1935	1. Hall (1925)	1. First to recognise the solubility product concept to prevent fouling
	2. Wilson (1915)	2. Method for determining fouling thermal resistance
	3. McAdams, Sherwood and Turner (1926)	3. First to demonstrate fouling thermal resistance
	4. Boruff and Stoll (1932)	4. Applied chlorination process to suppress growth of microbial and microbial deposits in condenser water
	5. Frost and Rippe (1931)	5. Use of chlorine in cooling water to improve the long term performance of the condenser
	6. Sieder (1935)	6. Paper presented at ASME about cleanliness factor that expressed fouling performance
1935-1945	1. Gronbeck (1935) (cited in Sieder 1935)	1. Presented fouling for various petroleum feedstocks
	2. Nelson (1935)	2. First calculation of fouling factor for petroleum feedstocks, wax deposits, coke deposits in pipes and precipitation fouling on the shell-tube heat exchangers
	3. TEMA (Standards of Tubular Exchanger Manufacturers Association, TEMA, 1936)	3. Published the first edition of the Standard Tubular Exchanger Manufacturers Association (tabulation of fouling factors used for design)

	4. D. Q. Kern (1966)	4. Proposed the alternative TEMA foulingfactor
1945-1979	1. D. Q. Kern and R. E. Seaton (1959)	1. First landmark fouling model includes the term of growth and removal part
	2. Hasson (Hasson et al., 1968; Hasson and Zahavi, 1970)	2. The first model of precipitation fouling includes the terms mass transport and chemical reaction
	3. Taborek(1972)	3. HTRI (Heat Transfer Research Incorporated) publishedfouling factor results based on the Kern and Seaton equation, reminder that fouling is the major unresolved issue
	4. Conference in Guildford (Proceedings of the International Chemical Engineering Conference on Fouling: Science or Art, University of Surrey, Guildford, England, 1979)	4. First conference on heat transfer fouling
1980 onwards	1. Epstein (1983)	1. Summarised the findings to-date in famous 5×5 matrix
	2. T. R. Bott (1997)	2. Published the mechanism of crystallisation fouling with mechanism aspects
	3. Bohnet and coworkers (1987)	3. Derived mathematical equation of CaSO4 deposition formation includes the mass transport and chemical reaction
	4. Somerscales (1990)	4. Published the historical review of fouling
	5. Whole plant modelling (Müller-Steinhagen et al., 1994; Behbahani et al., 2006; Jamialahmadi and Müller-Steinhagen, 2007;	5. Kraft black liquor in the pulp and paper industry Baye liquor in bauxite refineries, Phosphoric acid plants, Sulfuric

	Yeap et al., 2004; Ishiyama et al., 2009)	acid recovery plant, Crude oil preheat train
	6. Neural Networks (Malayeri and Müller-Steinhagen, 2003; Sheikh et al., 1999)	6. Artificial neural networks is pragmatic alternative to conventionalregressionmethod for better accuracy
	7. CFD Modelling (Brahim et al., 2003)	7. To better understanding of flow and temperature distribution to identify the possible critical areas
	8. Molecular modelling (Puhakka et al., 2007)	8. To better explanation for interaction mechanisms between heat transfer surfaces anddeposits

2.2 Fundamentalof Scaling

This section briefly describes the fundamentals of scaling process which include initiation, transport, attachment, removal and aging of scale deposit. Essentially, the scale growth behaviour comprises induction, transition and scaling, as well as scaling growth rate characteristics such as linear, decreasing rate and asymptotic regarding of scaling curves. Also presented in this section, the mathematical equation used for scale modeling available in the literature.

2.2.1 Scaling or Fouling Process

Scaling is a complex physiochemical process and it follows certain steps in the formation of scaling on the heat exchange surface, namely initiation, transport, attachment, removal and aging. Epstein (1983) first summarised the scaling mechanism and phases in his famous 5×5 matrix, as presented in Figure 2.1 and discussed here.

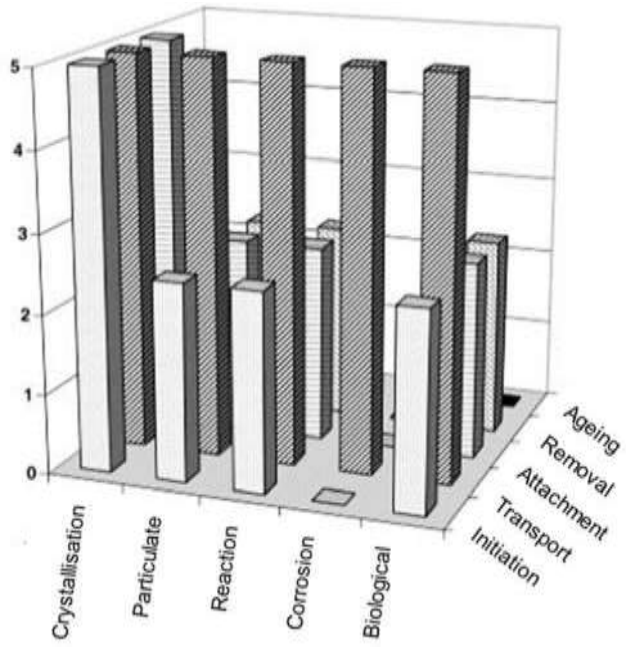

Figure 2.1: Epstein's 5×5 matrix: perceived level of understanding (increasing from 0 to 5) versus fouling mechanisms and types of fouling (Epstein, 1983)

2.2.1.1 Initiation

In all industrial or laboratory scaling processes, it is essential to allow a certain delay time varying from a few seconds to a few months before appreciable scaling starts. The delay period decreases with temperature decrease in normal soluble salts and increases with temperature increase in the inverse soluble salts due to supersaturation. Greater surface roughness is also significant to reduce the delay period as it acts as additional nucleation sites and also decreases the thickness of the viscous sub-layer and enhances the eddy transport to the solid heat exchange surface (Epstein, 1983).

2.2.1.2 Transport

Transport is best understood in the scaling or fouling stages (Epstein, 1983). In this stage, scaling components or species from the bulk solution are transported to the heat exchange surface across a viscous sublayer. The following equation can express the local scale deposition flux due to concentration gradient (Melo et al., 1987).

$$\frac{d\dot{m}_d}{dt} = \beta(C_b - C_i) \qquad (2.1)$$

where C_b is the bulk concentration of process solution [kg/m^3], $\dot{m}_d$ is the scale mass deposited per unit area [kg/m^2] and C_i is the concentration of process solution at the solid-liquid interface [kg/m^3].

2.2.1.3 Attachment

For crystallisation scaling, crystal deposits are assumed to adhere to the surface where nucleation has already occurred. The attachment is governed by a surface integration method which, in the case of stoichiometric equality in solutions of crystallising cations and anions, is expressed by (Melo et al., 1987) as:

$$\frac{d\dot{m}_d}{dt} = K_R^*(C_i - C_s)^n \tag{2.2}$$

Where, K_R^* is the crystal growth rate constant, C_s is the saturation concentration of process solution [kg/m^3] and n is the order of reaction.

2.2.1.4 Removal

In this stage, the removal of crystal deposits from the heat exchange surface occurs by various mechanisms such as erosion, spalling, breaking and dissolution. The shear stress imposed by fluid flow or agitation is mainly responsible for removal of scale deposits. The scale removal model originally proposed by Kern and Seaton (1959a) and further developed by Taborek et al. (1972) is expressed as:

$$\frac{dm_r}{dt} = k_{rem}\tau_s\delta \tag{2.3}$$

where, k_{rem} is the proportionality constant for scale removal, τ_s is the shear stress [N/m^2], σ_s is the shear strength [N/m^2] and δ is the scale deposit thickness [m].

2.2.1.5 Aging

Crystal deposits commence aging as soon as having been attached to the heat exchange surface. During aging, crystals may change their chemical structure, for example, by dehydration or polymerisation.

2.2.2 Scaling Curves

Numerous researchers have studied different aspects of crystallisation scaling or fouling. It is observed that there is no scale deposition for some time after a new or clean heat exchange

surface has been brought into operation. This period is called the 'initiation period' or 'time delay' (Bansal et al., 2008; Bohnet, 1987). The scaling or fouling curve is illustrated in Figure 2.2. The initial scale deposits on the heat exchange surface can cause a favourable effect on the heat transfer rate to increase corresponding negative thermal fouling resistance. The negative fouling occurs due to changing flow characteristics near the heat transfer wall as the result of augmented turbulence when the scale deposit penetrates into the viscous sublayer (Bansal et al., 2008; Bohnet, 1987). This beneficial heat transfer effect may continue until the additional thermal resistance is overcome by the favourable effect of turbulence. The period from the beginning of the scaling process until the fouling resistance again becomes zero is termed the 'roughness delay time' (Bansal et al., 2008; Bohnet, 1987).

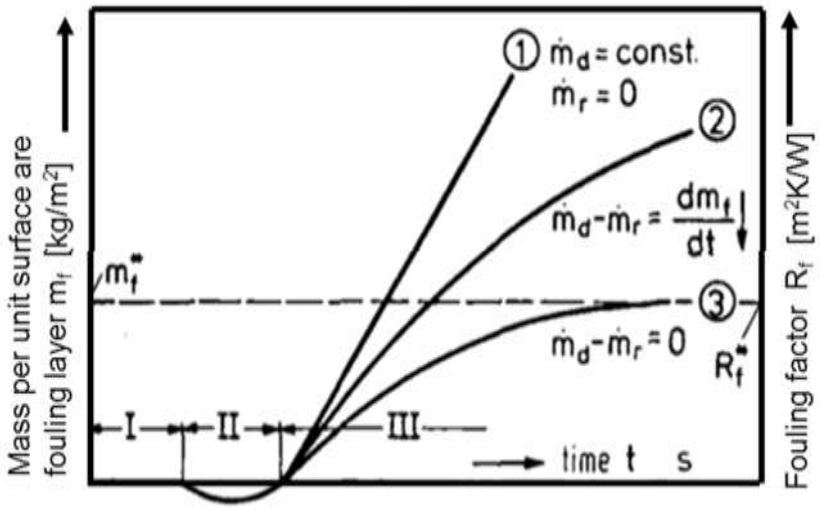

Figure 2.2: Scaling or fouling curves: I. induction, II. transition, III. scaling; 1 growth rate is constant, 2 growth rate decreases with time, 3 growth rate decreases with time and falls to zero (Bohnet, 1987)

The linear scaling or fouling curve occurs when scale deposit mass (also thermal resistance) increases with time and the removal term is virtually zero. Linear behaviour is mainly observed for very strong scale deposits where the deposition is faster than removal or the removal rate is negligible (Bansal et al., 2008; Bohnet, 1987). Falling scale behaviour is obtained when scale deposition decreases with time and the result of the net effect of the build up of deposits is that the removal rate increases with time for lower mechanical strength deposits (Bansal et al., 2008; Bohnet, 1987). An asymptotic scale curve commonly occurs in various scaling

experiments reported in the literature (Bansal et al., 2008; Bohnet, 1987; Crittenden et al., 2015; Fernandez-Torres et al., 2001; Hasan et al., 2012a; Jamialahmadi and Müller-Steinhagen, 2007; Karabelas, 2002; Müller-Steinhagen, 2010; Mwaba et al., 2006a; Mwaba et al., 2006b; Najibi et al., 1997). The asymptotic behaviour is observed for weak deposits where the removal rate increases with time and eventually becomes equal to the deposition rate (Bansal et al., 2008; Bohnet, 1987).

2.2.3 Scaling Models

Crystallisation scaling is considered as a common scaling that occurs in various industrial processes. The mathematical model of crystallisation scaling has long been studied and is well developed. The first pioneer model by Kern and Seaton (1959a) is considered as a base model of crystallisation scaling for further development. Table 2.2 shows a summary of historical works on modeling of deposition due to crystallisation .

Table 2.2: A summary of crystallisation scaling models

Authors	Models or related works	Remarks
(Kern and Seaton, 1959a)	$\frac{dm}{dt} = \frac{dm_d}{dt} \frac{dm_r}{dt}$ The details of this model are described in Chapter 4, which includes deposition and removal terms.	Considered as first pioneer work for both crystallisation and chemical reaction scaling.
(Taborek et al., 1972)	$\frac{dx_f}{dt} = C_1 P_d \omega^n \exp\left(\frac{-E}{RT_s}\right) - C_2 \tau x^m$ where C_1, C_2 are constant, x_f is the deposit thickness, E is the activation energy, P_d is a scaling probability, ω water quality factor, T_s is the surface temperature, is	Critiqued to have too many unknown parameters and complex crystallisation and particulate scaling mechanisms.

	the shear stress, and ψ is a scale strength factor.	
(Hasson et al., 1968)	$\dot{m}_{scale} = \frac{\left(\left[Ca(HCO_3)_2\right] - K_s'\right)}{(1/k_m) + (1/k_r)}$ where $\dot{m}_{scale}$ is scaling mass flux, K' is the molar solubility product, k_m is the mass transfer coefficient at the deposit-fluid interface, k_r is the reaction rate associated with the formation of the crystalline solid on the fouled surface.	Used for investigation of scaling in pipes, they established the classic diffusion model which explains the dynamic of scaling mass flux.
(Hasson, 1981)	$\frac{dm_f}{dt} = K' A_g P_{st} \omega \exp\left(\frac{-E}{RT_s}\right)$ where m_f is a deposit mass, K' is constant, A_g is a crystal nucleation and growth area, ω water quality factor, P_{st} is sticking probability.	Removal term is not considered; also contains several unknown parameters.
(Müller-Steinhagen and Branch, 1988)	$\dot{m}_{scale} = \frac{\beta\left[Ca^{2+}\right]\left[\left(1+\frac{4ac}{b^2}\right)^{0.5}-1\right]b}{2a}$ where β is mass transfer coefficient, *a,b,c* are model parameters.	Developed from Hasson's diffusion model, but using the diffusion of ionic species from the bulk to the surface instead of ion concentrations at the fluid-solid interface.

2.3 Overview of Crystallisation Scaling

Crystallisation scale deposition commonly occurs in many mineral refining processes, such as alumina, nickel and magnesium refining. Very limited information exists in the literature about

scaling due to the crystallisation of normal solubility salts and the effect of hydrodynamics on its mechanism and mitigation or suppression in agitation tanks. Due to insufficient literature, there is a lack of experimental evidence and physical understanding regarding normal solubility salts compared with inverse solubility salts. The mechanism of crystallisation scaling (or some mathematical modelling) and its suppression have been studied by many researchers. A number of papers and patents have been published in the field of crystallisation scaling on heat exchanger surfaces under the condition of convective heat transfer or sub-cooled boiling. The available information can be found in the literature as books (Bott,1985; Garret-Price, 1985; Melo et al., 1987), review papers (Epstein, 1983; Somerscales, 1990; Zhao and Chen, 2013) and research papers (Amjad, 1988; Andritsos and Karabelas, 2003; Behbahani et al., 2006; Azimi et al., 2014; Bansal et al., 2005; Bansal et al., 2008; Bott, 1997; Brahim et al., 2003; Briançon et al., 1997; Crittenden et al., 2015; Deev et al., 2009; Demopoulos, 2009; Fahiminia et al., 2007; Fernandez-Torres et al., 2001; Hasson and Zahavi, 1970; Helalizadeh et al., 2000; Karabelas, 2002; Kazi et al., 2015a; Kazi et al., 2015b; Kazi et al., 2012; Kern and Seaton, 1959a; Mwaba et al., 2006a; Mwaba et al., 2006b; Najibi et al., 1997; Nawrath et al., 2006; Pääkkönen et al., 2015; Rosmaninho et al., 2008; Rosmaninho et al., 2007).

This study is focused on hydrodynamic effects on scale deposition in the precipitation tank of the Bayer process. The scale formation causes severe difficulties in alumina refinery plants such as reduction of heat transfer efficiency due to the increase of thermal resistance, production limitations from reduced flows and contamination of the gibbsite product by surface adsorption. The scale formation mechanism in the Bayer process equipment is still not well understood. Silica in bauxite can occur in many forms, including kaolinite ($Al_2O_3.SiO_2.2H_2O$), halloysite ($Al_2O_3.SiO_2.4H_2O$), quartz (SiO_2), kyanite ($Al_2O_3.SiO_2$), montmorillonite group, feldspathic silicates and alumina silica gels (Meikle, 1973). The dissolved silica precipitates as sodium aluminosilicate scale throughout alumina plants. As mentioned before, potassioum nitrate solutions will be used for this study. However, scarcely any experimental work on the crystallisation scaling of potassium nitrate (normal soluble salt) can be found in the literature. In the following paragraphs, some of the recent investigations on crystallisation scaling (normal and inverse solubility salts) are reviewed.

2.3.1 Mechanism of Crystallisation Scaling or Fouling

Crystallisation is at the heart of many natural or industrial processes such as the Bayer process to extract alumina from bauxite through the formation of gibbsite crystals, production of many

pharmaceuticals, many chemical industries and the formation of bones and teeth. The sequence of events that leads to crystallisation scaling can be seen in Figure 2.3.

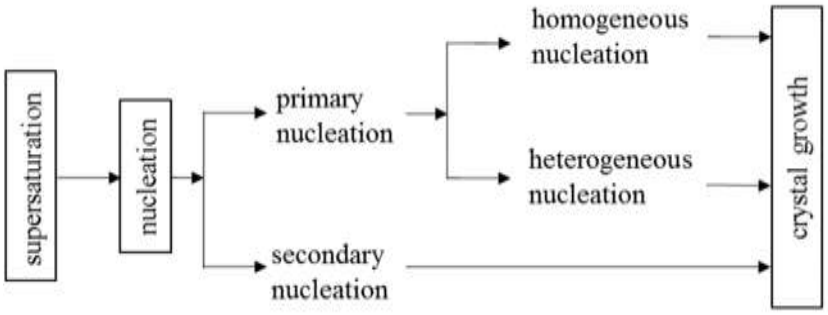

Figure 2.3: Crystal forming steps (Mullin, 2001)

Supersaturation is the main driving force for the formation of crystalline deposits on a solid surface attributable to a temperature differential between the heat exchange surface and the process solution of soluble salts. The driving force for crystallisation scaling from an aqueous solution as a function of supersaturation is given in the equation (Mullin, 2001):

$$\Delta\beta = k_B T \ln(S+1) \tag{2.4}$$

where $\Delta\beta$ is the degree of driving force, generalised by the difference of the chemical potentials between the solid and liquid process solution, S is the supersaturation ratio which is often articulated by the ratio of the bulk concentration to the saturation concentration, T is the absolute temperature [K] and k_B is the Boltzmann constant [J/K.mol].

Supersaturation itself is not sufficient to start crystallisation without nucleation sites. The formation of crystals usually requires the presence of solid bodies in the solution such as embryos, impurities, nuclei or artificial crystal seeds that leads to the formation of crystal nuclei (Zhao and Chen, 2013). The crystal formation process can be described as either primary or secondary nucleation. Primary nucleation is the result of homogeneous nucleation without any aid of foreign bodies or nucleation sites. In homogeneous nucleation, the overall Gibbs free energy change, ΔG_{homo} between a small particle of solute and solute in the solution is expressed by the following equation (Mullin, 2001):

$$\Delta G_{homo} = \Delta G_S + \Delta G_V = 4\pi r^2 \gamma + \frac{4}{3v}\pi r^3 \Delta G \tag{2.5}$$

where ΔG_s is the sum of surface excess free energy [J/m^2], ΔG_v is the free energy change of the transformation per unit volume [J/m^3], r is the small solid solute particle (assumed to be a sphere of radius r for simplicity) [m] and is the interfacial tension between the developing crystalline surface and the supersaturated solution [N/m^2].

For heterogeneous nucleation, nucleation can start growing at relatively low supersaturation wth the presence of foreign particles or impurities (generally called nucleation sites), the overall Gibbs free energy change ΔG_{hetero} is expressed as follows (Mullin, 2001):

$$\Delta G_{hetero} = \varphi \Delta G_{homo} \quad (2.6)$$

where φ is the value of factor between 0 and 1.

2.3.2 Crystallisation Scaling or Fouling of Normal Soluble Salts

The characteristic of normal soluble salts, for example, potassium nitrate (KNO_3) (Ashley, 1976; Nývlt and Veverka, 1997) and sodium sulphate (Na_2SO_4) (Hasan et al., 2012a), is for solubility in water to increase with increase of temperature as shown in Figure 2.4(a). The crystallisation scaling of normal soluble salt is sometimes called freezing scaling or fouling (or precipitation). Freezing scaling or fouling describes the phenomenon where a scale deposit layer is formed on the heat transfer surface (or sub-cooled surface) whose temperature is lower than the bulk solution temperature via crystallisation of dissolved species (Fernandez-Torres et al., 2001).

Fernandez-Torres presented the theoretical study of freezing solidification fouling for liquids in laminar flow through a duct which was controlled by heat and mass transfer rather than by activation control (Fernandez-Torres et al., 2001). They gave a theoretical model of fouling which was capable of predicting different regimes of fouling behaviour (for example, no fouling, linear fouling, falling fouling and asymptotic fouling) without knowledge of crystallisation kinetics and negligible shear removal effect. Fitzgerald et al. (2004) investigated an experimental model of coring of palm oil fats in distribution lines by using a model solution of tri-palmitin (PPP) in a non-crystallising paraffin solvent. It was observed that freezing fouling (or deposition due to normal soluble salt) strongly related to the degree of supercooling of the liquid and a higher velocity reduced the deposition thickness due to the stronger shear rate, but the tradeoff was the extra energy requirement.

Hasan et al. (2012a) performed experiments on the crystallisation fouling of sodium sulfate (Na_2SO_4) under cross flow conditions during convective heat transfer. They have shown that the crystallisation process was activation control and that solution temperature (or via hot solution Reynolds number, Re_h) and surface temperature (or via cold water Reynolds number inside the tube, Re_c) have significant effects on the fouling rate. They showed that an increase in the fouling layer thickness does not necessarily lead to an increase in the thermal resistance due to enhancing the overall heat transfer coefficient with increasing cold water Reynolds number (Breckenridge, 1899). The asymptotic value of thermal resistance decreased by 27% with increase of Re_c from 7500 to 2500 and 20% for an increase of Re_h from 250 to 485 due to increasing surface wall temperature.

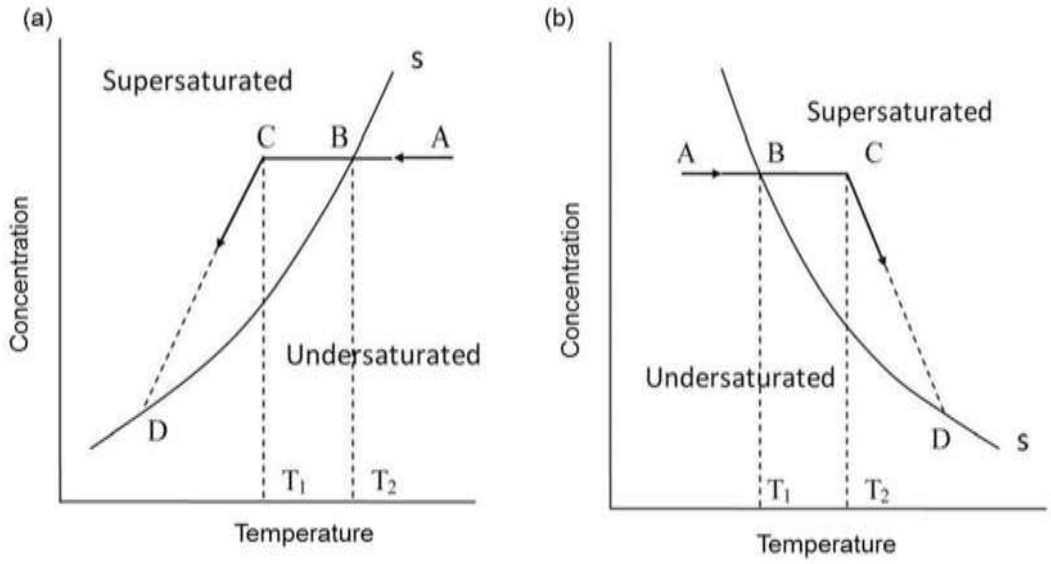

Figure 2.4: (a) Solubility curve of normal soluble salts (Seidell, 1942), and (b) Solubility curve of inverse soluble salt (Silcock, 1979)

Nývlt and Veverka (1997) experimentally investigated scale formation of different normal solubility salts including KNO_3, $ZnSO_4$, $FeSO_4.7H_2O$, $MgSO_4.7H_2O$ and $Na_2B_4O_7.10H_2O$ on cooling surfaces in crystallisers by introducing a critical temperature difference and critical time in the cooling finger apparatus. They observed two distinct mechanisms of scale formation: it produced a compact smooth scale layer by crystal growth due to nucleation on the cooling surface and created a porous layer due to sticking of suspended particles impacting

on them. They also observed the hydrodynamic effect of particle suspension on scale formation which exhibited two different phenomena. Firstly, as stronger impacts of particles onto the scale may enhance the growth and secondly, decline the scale deposition as rapidly streaming solution can wash away the crystalline deposit which was not sticking firmly.

Ashley (1976) experimentally investigated prevention of potassium nitrate and brine freezing scale deposition on heat exchange surfaces by impeller agitation combined with ultrasound (or direct sonification). It was reported that lower agitation (for example, 100 rpm) created heavy deposition and violent (or strong) agitation (for example, 900 rpm) showed almost no scaling on the cooling coil. Ashley (1976) also proved that scale deposition could be alleviated by applying ultrasound vibration with a combination of gentle agitation (for example, 100 rpm).

2.3.3 Crystallisation Scaling or Fouling of Inverse Soluble Salts

The characteristic of inverse soluble salts, for example, calcium carbonate ($CaCO_3$) (Karabelas, 2002; Kazi et al., 2015b ; Liu et al., 2011; Pääkkönen et al., 2015; Tai and Chen, 1998; Wang et al., 2011;), calcium sulfate ($CaSO_4$) (Hasson and Zahavi, 1970; Kazi et al., 2013; Kazi et al., 2010; Najibi et al., 1997) and coprecipitation of $CaCO_3$ and $CaSO_4$ (Chong and Sheikholeslami, 2001; Helalizadeh et al., 2000; Höfling et al., 2003) is for solubility in water to decrease with an increase of temperature as shown in Figure 2.4(b). The crystallisation scaling or fouling of inverse soluble salt is defined as scale formed on the heated surface.

Crittenden et al. (2015) investigated the calcium sulphate crystallisation fouling with enhanced heat transfer surfaces using a simple stirrer batch cell. They have shown that shear stress is a more effective process parameter to reduce the fouling by the modification of smooth surfaces by incorporating raised helical threads on the surface or changing the turbulence structure. Hoang et al. (2011) studied the effects of process parameters (for example, supersaturation ratio, runtime, flow rate, velocity, pipe diameter, Reynolds number and surface material) on gypsum scale formation in pipes. They have shown that the scale mass increased with flow velocity (or flow rate) and pipe diameter due to an increase of solution volume and amount scale forming substances. Hoang et al. also investigated the effects of the solution on the formation of calcium sulphate scales on pipes (Hoang et al., 2007). The results showed that high solution temperatures reduced the induction time and significantly enhanced the scale rate and various hydrated and anhydrous deposits formed if the temperature was above 40°C.

Kazi et al. performed many experiments on calcium sulphate scaling during convective heat transfer in different pipe materials (Kazi et al., 2012; Kazi et al., 2010). It was observed that

scaling rate was enhanced with increasing of thermal conductivity and surface roughness. Kazi et al. (2013) also investigated the fibre characteristics (fibre concentration, fibre length and fibre flexibility) on heat transfer fouling. The induction time of heat transfer fouling was effectively extended and the heat transfer rate was augmented during the induction period when fibre concentration was above about 0.025% in the fouling solution.

Bansal et al. proposed the deposition rate law which was a modification of classical deposition rate theory by inclusion of nucleation sites (Bansal et al., 2008; Bansal et al., 2005). They investigated the calcium sulphate crystallisation fouling in a plate heat exchanger and results showed that crystallisation rate was enhanced significantly by the addition of nucleation sites during the fouling process. Bansal et al. (2001) studied comparisons between double-pipe and plate heat exchanger during calcium sulfate crystallisation fouling with same flow condition. They showed that the fouling of plate heat exchanger 20-25 times less than double-pipe heat exchanger in the presence of particles and 15 times less when the particles were filtered out with similar flow velocity and results were very close with similar shear stress condition.

Mwaba et al. (2006a) produced the semi-empirical correlation for calcium sulfate crystallisation fouling on the heat transfer surfaces with inclusion of the effects of nucleation phase. They reported three distinct time regions, namely nucleation, growth and asymptotic, and showed that overall fouling curves exhibit a S-curve. It is significant to include the nucleation phase in the development of correlation, because nucleation enhances the convective heat transfer due to increase of the surface area and increase of turbulence close to the wall. Mwaba et al. also experimentally investigated the effect of parameters (for example, surface temperature, flow velocity and degree of supersaturation) on the calcium sulphate crystallisation scaling on heated copper plate (Mwaba et al., 2006b). They have shown that the induction period is reduced by lowering the flow velocity and is augmented with increasing degree of supersaturation.

Najibi et al. (1997) undertook a series of experiments on calcium sulphate scale formation during sub-cooled flow boiling in a vertical annulus. They found that the scale deposition rate is controlled by different mechanisms (mass transfer control, surface reaction control and interaction bubble formation on the heated surface), depending on flow velocity and surface temperature. For the range of velocity from 60 to 140 cm/s, a linear fouling curve with asymptotic behaviour was observed, which is caused by pure crystallisation without the presence of suspended particles. Jamialahmadi et al. also investigated the effect of calcium

sulphate scale deposition on pool boiling heat transfer from a steel circular heater (Jamialahmadi and Muller-Steinhagen, 2004; Jamialahmadi et al., 1989). They have shown that the heat transfer coefficient at the liquid-solid interface changes throughout the deposition process due to the evolution of the bubble formation mechanism. They also observed that deposition rate increases and heat transfer coefficient decreases as concentration and heat flux increases.

Helalizadeh et al. (2000) performed many experiments to investigate the crystallisation scale deposition from a mixture of calcium sulphate and calcium carbonate on the heat transfer surfaces during convective heat transfer and sub-cooled boiling. They noticed that deposition rate was controlled either by mass transfer and chemical reaction depending on flow velocity and surface temperature. They also reported from scanning electron microscopy and X-ray analysis that the adhesion strength of deposits from the mixture was approximately between $CaSO_4$ and $CaCO_3$. Helalizadeh et al. proposed the mechanistic model that includes transport and reaction mechanisms for deposition from a mixture of calcium sulphate and calcium carbonate on the heat transfer surface based on the experimental force convective data (Helalizadeh et al., 2005). The boiling effect is also considered by the inclusion of an enhancement factor, E.

2.4 Hydrodynamics Aspects of Scaling

Most of the parameters that play a critical role in scale formation and its suppression are related to hydrodynamics or fluid dynamics which will be discussed here (Nawrath et al., 2006; Wu et al., 2012). However, only limited information is available in the literature about the effects of hydrodynamics on the scaling mechanism and its mitigation in agitation tanks. This section reviews the scale growth mechanism and factors involved in reducing scale on the process equipment through hydrodynamics or fluid dynamics design.

Many researchers (Yu et al., 2002; Nawrath et al., 2006; Xing et al., 2005) suggest that scale growth in processing equipment is affected by a number of factors including supersaturation in solution, phase transformation, run time, form of material surfaces and flow characteristics (velocity, flow rate and Reynolds number). In the chemical industry, slurry mixing tank agitators are often designed on the basis of achieving off-bottom suspension to resist the settle time for crystallisation (Ibrahim and Nienow, 1996; Nienow, 1997; Wu et al., 2001). In this case, axial flow impellers pumping downward with vertical baffles are more energy efficient than radial turbines (Ibrahim and Nienow, 1996; Nienow, 1997; Wu et al., 2001) and the energy

efficiency for off-bottom solids suspension is sensitive to impeller off-bottom clearance and impeller diameter (Chapman et al., 1983; Wu et al., 2007; Wu et al., 2012; Wu et al., 2006c; Wu et al., 2011; Wu et al., 2002; Wu et al., 2010).

Several investigations have attempted to reveal the effects of hydrodynamics or flow velocity on the crystallisation scale formation during convective heat transfer on the tube rather than the agitation tank. The literature reported that a higher velocity sometimes reduced the scale deposition (Webb and Li, 2000; Hasson and Zahavi, 1970; Hasan et al., 2012a) and sometimes showed the opposite trend (Helalizadeh et al., 2000; Hoang et al., 2011) depending on whether the crystallisation process was activation control or mass transfer control or a combination of both (Bansal et al., 2008; Helalizadeh et al., 2000). In the case of mass transfer control scaling, crystalline scale deposition increased with velocity due to more transfer of salt to the surface occurring due to the higher velocity and, on the other hand, crystalline scale deposition decreased with higher velocity in the case of activation control due to more fluid shear stress.

Hasan et al. (2012a) performed experiments on the effects of temperature and hydrodynamics on the normal soluble salt of sodium sulfate crystallisation fouling under cross flow conditions. They have shown the effects of cold water Reynolds (Re_c) number passing through the inside of the tube and hot solution Reynolds number (Re_h) outside the tube on the scale deposition and fouling layer thickness. It was revealed that an increase of Re_c leads to a decrease in the thermal fouling resistance due to the increase of internal heat transfer coefficient and a corresponding increase of fouling layer thickness. In contrast, an increase of Re_h leads to a decrease in fouling resistance and consequently the eroding of the crystalline fouling layer due to shear forces. Hoang et al. (2011) experimentally investigated the effects of process parameters on Gypsum (calcium sulfate) scale formation in pipes as supersaturation ratio, run time, operational hydrodynamic conditions (flow rate, fluid velocity, pipe diameter, and Reynolds number) and surface material. They found that the scale deposition increased on the coupon inside the pipe at a higher velocity.

The Kern and Seaton model (1959a) is accepted as the first model to describe the fouling or scaling process. Bott (1997) stated that the increasing of velocity has opposing effects on the crystallisation scaling process. Thus, an increase of velocity promotes the scale deposition if mass transfer effect dominates (as is likely to occur with pure salts) or decrease the scale deposition if the interfacial shear rate has a greater effect (particularly for mixed crystal system where the deposit structure is likely to be weaker). Crittenden et al. investigated the

crystallisation fouling with enhanced heat transfer surfaces (Crittenden et al., 2015). They found that fouling rates reduced by increasing the surface shear rate by surface enhancement (either fine wires were attached to it or helical threads form on the surface). It was noticed that positive helix surface leads to reduced scale formation due to higher stress rate than other surfaces such as a negative helix or smooth surface. Young et al. studied effects of shear rate and surface temperature on fouling deposition of crude oils using a simple batch stirred cell system (Young et al., 2011). They also found that an increase in surface shear stress leads to decrease of crude oil fouling deposit.

Cowan and Weintritt (1976) conducted an experiment with a high velocity which can curtail or accelerate scale deposition due to the formation of a boundary layer next to the pipe wall. Yu et al. (2005) investigated in dynamic fouling-loop in which they experimented with the effects of thermodynamic conditions such as surface superheat, fluid velocity and bulk subcooling on sugar mill evaporators. The fouling mechanism was particulate deposition of silica and calcium oxalate colloidal species strengthened by consolidation; fouling rate increased with decreasing interfacial energy barrier between the surface and foulant. Xing et al. (2005) experimentally obtained that at higher ion concentration, the fouling rate increases linearly with surface temperature and the effect of flow velocity on deposition rate is very strong. It is clear that the scaling is a physico-chemical process which can be affected by fluid dynamics through its effect on heat and mass transfer. Therefore, fluid velocity is seen to play a critical role in scale formation and suppression mechanism.

2.5 Hydrodynamics Aspects of the Bayer Process Scaling

Very limited work has been done on scale formation mechanisms in slurry pipes and slurry tanks used in minerals processing industries such as aluminium refineries. In the extensive literature, most of the topics are related to fouling in evaporators (Yu et al., 2002), membranes used in the reverse osmosis processes in desalination plants (Neofotistou and Demadis, 2004) and heat exchangers (Coletti and Macchietto, 2011). Loan et al. (2008) in the CSIRO (Commonwealth Scientificand Industrial Research Organisation), experimentally investigated scale formation in slurry tanks by X-ray photoelectron spectroscopy and observed that, at the initial stage, scale is formed as a result of precipitation reactions other than solids settling.

A novel scale-velocity model was developed by Wu et al. (2012) for explaining the scale growth and suppression in an alumina refinery. In this model, a relationship between the fluid flow velocity and scale formation is schematically presented in Figure 2.5. There are four

regimes identified to understand the scale growth mechanism, namely regimes (A) mass transfer control, (B) chemical reaction control, (C) suppression by erosion and (D) erosion damage. In regime A, the initial scale is null at zero velocity as followed by a molecular diffusion-rate controlled process. Then the scale growth rate starts very rapidly as fluid velocity increases due to an increased effect of mass transfer. This explanation is strongly supported by the study (Hoang et al., 2011) in which an increase in gypsum scale growth rate with increasing fluid velocity was observed in the range from 0 to 0.07 m/s.

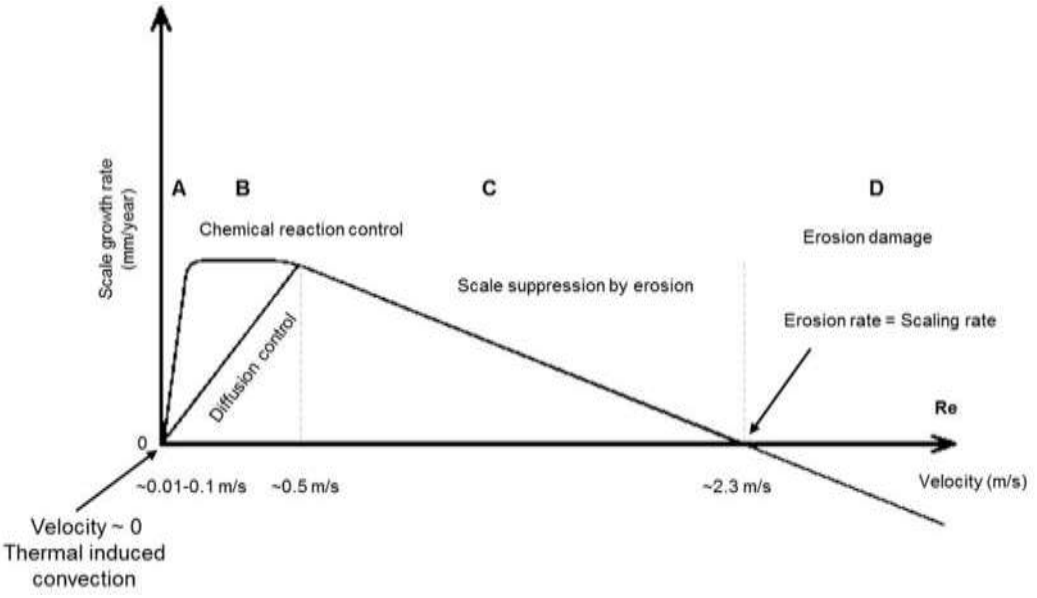

Figure 2.5: Relationship between the precipitation or chemical reaction driven scale growth rate and fluid velocity (Wu et al., 2012)

In regime B, for fluid velocity larger than 0.1 m/s, the chemical reaction rate may start to control the overall rate of scaling as increasing fluid velocity does not affect the overall rate of scale growth. On the other hand, when chemical reaction is relatively fast, the rate of scale growth continuously increases with increasing fluid velocity.

In regime C, the rate of scale growth gradually decreases with increase in fluid velocity. In this regime, an increase in fluid velocity results in more erosion, which slows down the scale growth. Nawrath et al. (2006) conducted detailed plant tests on scale growth of a supersaturated aluminate solution in a precipitation circuit at the Queensland Alumina (QAL) refinery in Australia. Measurements of scale growth were conducted in a series of different diameter pipes

connected through the fittings and it was concluded that scale growth decreases with increasing slurry velocity in the range from 0.5 to 1.7 m/s as presented in Figure 2.6.

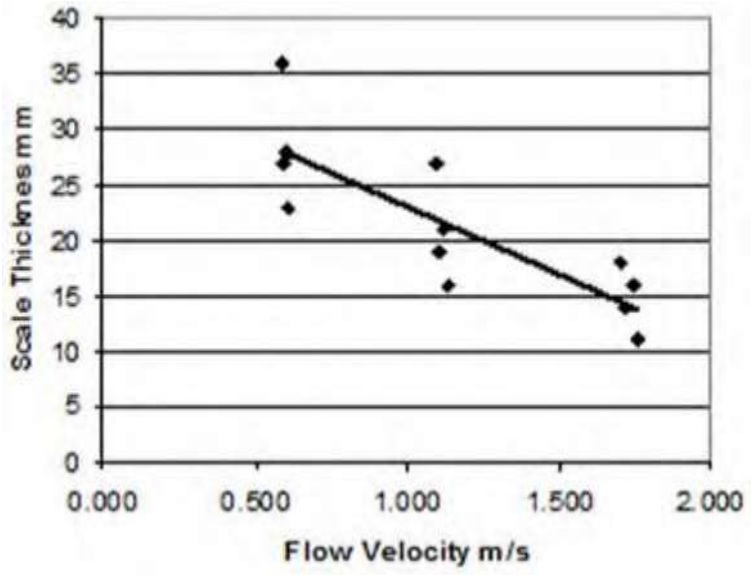

Figure 2.6: Maximum scale thickness versus fluid velocity based on tests using pipes in the precipitation area at QAL (Nawrath et al., 2006)

In regime D, the material surface suffers net loss due to the effect of erosion exceeding scale growth. Wu et al. (2011) reported on erosion of the impeller tip operating in a slurry vessel due to the increase of tip velocity of the blade as shown in Figure 2.7. The erosion increased with the increase of blade radius, due to increased tip velocity.

Wu et al. (2012) concluded that regimes C and D are more important for scale suppression in terms of fluid dynamics design, and hydrodynamic lift and drag forces play a minor role in the nucleation of slurry particles to inhibit the scale growth. They invented a new precipitation tank design with swirl flow technology (SFT). It is the long term experience that the velocity near the wall surface is a critical factor for suppression of scale growth. The non-dimensional velocity efficiency parameter (η) along the tank height can be described (Wu et al., 2006b) by:

$$\eta = \frac{\square V}{(P/\rho A)^{1/3}} \tag{2.7}$$

where P is the agitator power input, ρ is slurry density, A is the tank wetted surface area excluding the bottom and V is the velocity outside of the boundary layer.

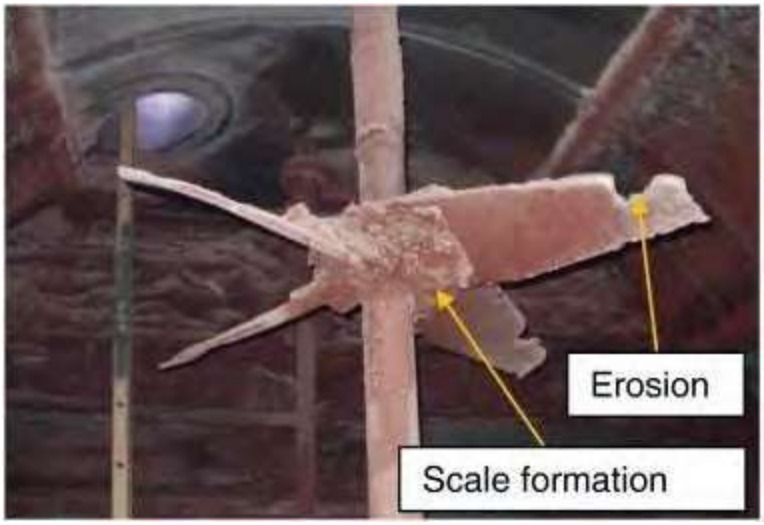

Figure 2.7: Coexistence of scale formation and erosion on an axial flow impeller, after operating in a Ni-laterite HPAL autoclave for an extended period of time (Wu et al., 2012)

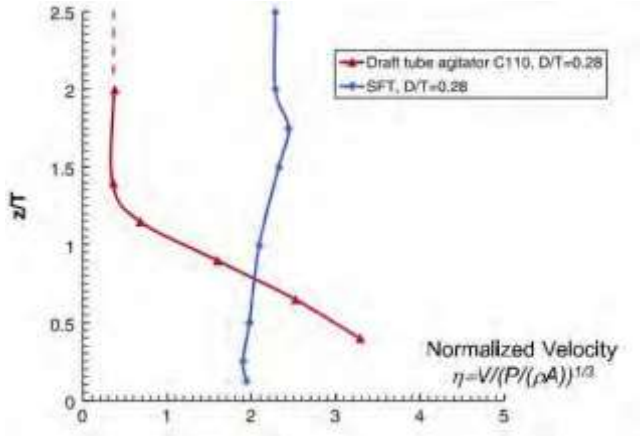

Figure 2.8: Laboratory precipitators: non-dimensional velocity efficiency parameter profile along tank height, measured near the wall (outside the flow boundary layer) (Wu et al., 2012)

From their experiment, Wu et al. (2012) concluded that SFT creates a more uniform higher absolute velocity adjacent to the tank surface when compared with the conventional draft tube agitator design configurations as shown in Figure 2.8. This higher velocity near the adjacent wall was seen more favourable to suppress the scale deposition. For a detailed investigation, CFD modelling was conducted on the full-scale cone-bottom and flat-bottom precipitation tanks with the conventional draft-tube agitator and the swirl flow agitator (SFT). It was observed that the swirl flow agitator is more energy efficient with the cone-bottom tank than

the flat-bottom tank. Nawrath et al. (2006) and Deev et al. (2009) conducted extensive laboratory experiments to discern the effect of fluid dynamics of flow through the model of a concentric reducer used for connecting pipes of two different diameters. They measured the stream-wise and cross-stream velocity components of water flow through the concentric reducer by particle image velocimetry (PIV) technology. They found that the cross-stream component of the fluctuating velocity varies significantly and, at a distance from the wall of 0.05R, the component becomes five times larger than that at the walls of the straight pipes connected to the reducer.

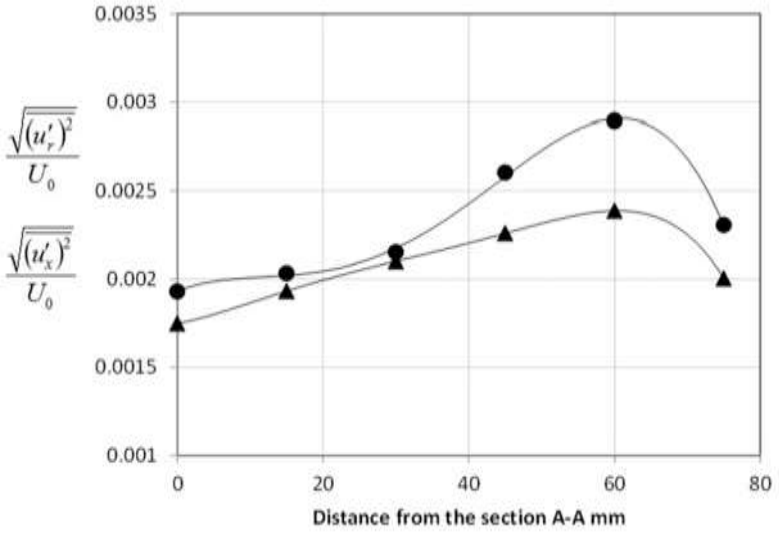

Figure 2.9: Variations of normalised fluctuating components and along the X-axis at the distance of 0.08 R from the internal surface of the reducer: Re=27,130 and V=0.268 m/s (101.8 mm φ pipe) (Das et al., 2016)

Das et al. numerically investigated the effect of velocity components (cross-stream and stream-wise velocity) of water flow through the concentric reducer commonly used in the pipe network of the Bayer process (Das et al., 2015; Das et al., 2016). They concluded that the cross-stream u'_r fluctuating velocity component is a dominant parameter controlling the variation of the particle deposition rate as the flow passes through the reducer as shown in Figure 2.9. The flow velocity of fluid and geometry of the pipe fittings affect the particles deposition rate. The cross-stream, u'_r fluctuating velocity component in the reducer is greater than stream-wise u'_x

fluctuating velocity component in the reducer; it is believed that this is one of the reasons for more particle deposition as well as more scale growth in the concentric reducer. In contrast, stream-wise u_x' fluctuating velocity component is responsible for the erosion of deposited particles on a solid wall (Das et al., 2015; Das et al., 2016).

2.6 Problems of Scaling

The main characteristic of scale deposit material is that it has low thermal conductivity which creates a major resistance to heat transfer (Das et al., 2016; Kazi et al., 2012; Nawrath et al., 2006; James, 1990; TEMA, 1999). The scale deposit on the heat transfer surface reduces the process efficiency and causes other difficulties such as pressure drop, probe malfunction, partial or complete blockage of the piping system and promotes damage of process equipment (Das et al., 2016; Kazi et al., 2012; Nawrath et al., 2006). Figure 2.10 shows the scale problem in a shell-tube heat exchanger and pipes in the Bayer process cycle equipment in the alumina industry.

Figure 2.10: Negative effect of excessive inlet baffle spacing on deposit formation (left, (Müller-Steinhagen, 2011)) and scale growth observed in components of the pipe (right, (Nawrath et al., 2006))

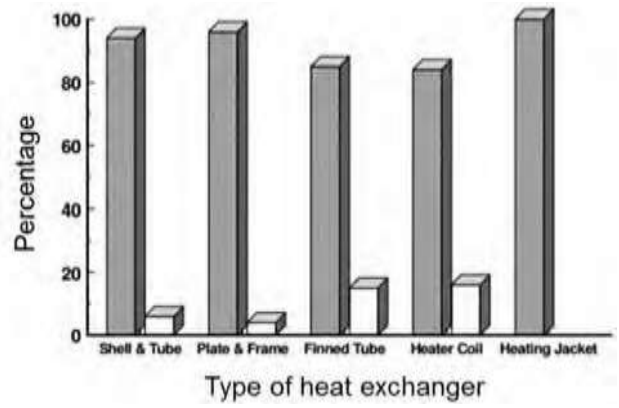

Figure 2.11: Fouling on various heat exchanger types (Steinhagen et al., 1993)

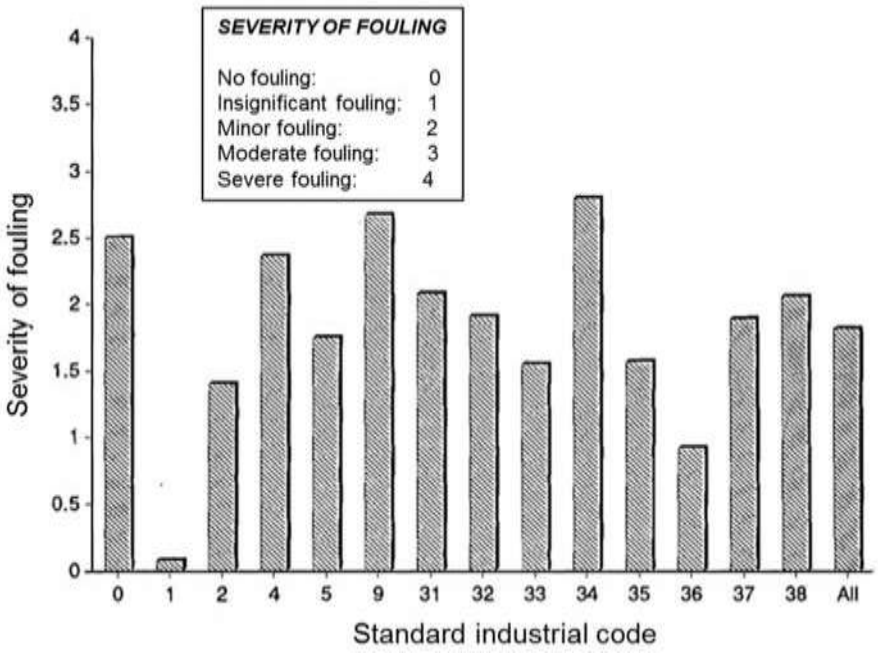

Figure 2.12: Degree of fouling for different industries, for SIC code see Table 2.2 (Steinhagen et al., 1993)

Figure 2.11 shows the percentage of fouling and non-fouling on various types of heat exchangers commonly used in industry. The severity of fouling or scaling in different sectors is shown in Figure 2.12 against standard industrial code, as severity between 0 (no fouling) and 4 (severe fouling). Table 2.3 shows the standard industrial codes. The fouling problem with code 0 (no code available) is not representative because of the small number of industries in this group.

Table 2.3: Standard Industrial Code (SIC) (Steinhagen et al., 1993)

Code 0	No codingavailable
Code 1	Agriculture, forestry andfishing
Code 2	Mining and quarrying
Code 4	Electricity, gasand water
Code 5	Buildingandconstruction
Code 9	Community, social and personal service
Code 30	Manufacture, notspecified
Code 31	Manufacture of food, beverage and tobacco
Code 32	Textile, wearing apparel and wood products
Code 33	Manufacture of wood and wood products
Code 34	Manufacture of paper products, printing
Code 35	Manufacture of chemicals, petroleum
Code 36	Manufacture of nonmetallic mineral products
Code 37	Basic metal industries
Code 38	Manufacture of fabricated metal products, machinery and equipment
Code 39	Othermanufacturingindustries

The main operational obstacle created by scaling or fouling is thermal resistence of the heat transfer surface because of the low conductivity of scale deposit. Figure 2.13 shows the effect of total scaling resistance in reducing the clean overall heat transfer coefficient of heat transfer (James, 1990). Table 2.4 presented some TEMA values of overall thermal resistance (James, 1990; TEMA, 1999). It is seen that higher fouling resistance occurs in crude oil refinery and process liquid streams than liquid water streams.

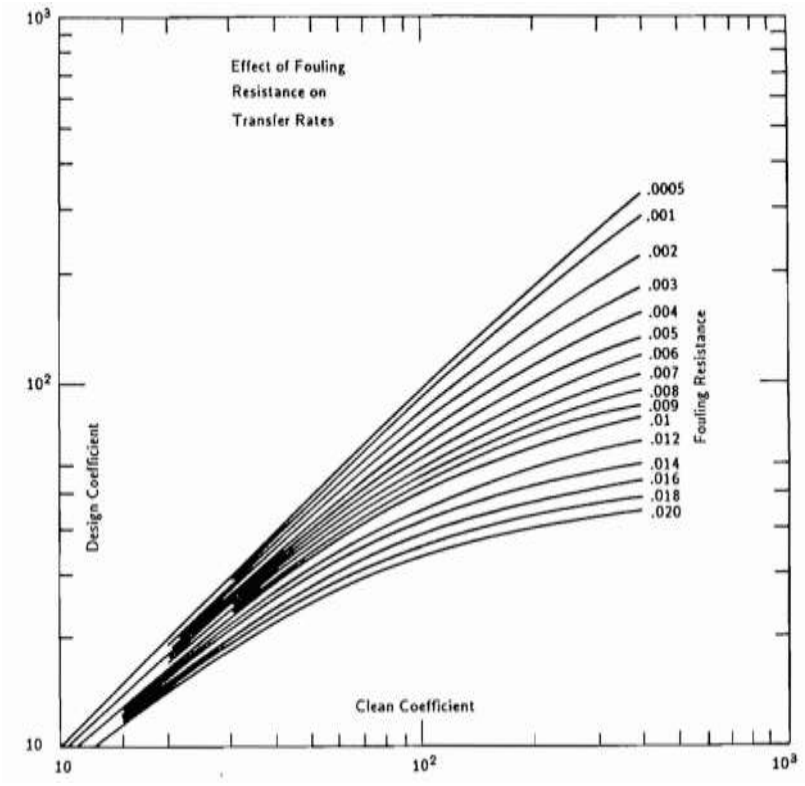

Figure 2.13: Effect fouling resistance on heat transfer rates (James, 1990)

Table 2.4: TEMA fouling resistance values for water and other fluids (James, 1990; TEMA, 1999)

Fluid	Fouling Resistance (10^{-4} m^2.K/W)	Fluid	Fouling Resistance (10^{-4} m^2.K/W)
1. Liquid Water Streams		**5. Chemical Process**	
Artificial spray pond water	1.75-3.5	**Strams**	
Boiler blowdown water	3.5-5.3	Acid gas	3.5-5.3
Brackish water	3.5-5.3	Natural gas	1.75-3.5
Closed-cycle condensate	0.9-1.75	Solvent vapor	1.75
Closed-loop treated water	1.75	Stable overhead products	1.75
Distilled water	0.9-1.75	**6. Crude Oil Refinery**	
Engine jacket water	1.75	**Streams**	
River water	3.5-5.3	Temperature at 120°C	3.5-7
Seawater	1.75-3.5	Temperature at 120°-180°C	5.25-7
Treated boiler feedwater	0.9	Temperature at 180°-230°C	7-9
		Temperature > 230°C	9-10.5

Treated cooling tower water			
2. Industrial Liquid Streams	1.75-3.5	**7. Petroleum Streams**	
		Lean oil	3.5
Ammonia (oil bearing)		LPG	1.75-3
Engine lube oil	5.25	Natural gasolene	1.75-3.5
Ethanol	1.75	Rich oil	1.75-3.5
Ethylene glycol	3.5	**8. Process Liquid Streams**	
Hydraulic fluid	3.5	Bottom products	1.75-3.5
Industrial organic fluids	1.75	Caustic solutions	3.5
Methanol	1.75-3.5	DEA solutions	3.5
Refrigerants	3.5	DEG solutions	3.5
Transformer oil	1.75	MEA solutions	3.5
No. 2 fuel oil	1.75	TEG solutions	3.5
No. 6 fuel oil	3.5	**9. Crude and Vacuum liquids**	
3. Cracking and Coking unit Streams	0.9	Atmospheric tower bottoms	12.3
		Gasolene	3.5
Bottom slurry oils		Heavy fuel oil	5.3-12.3
Heavy coker gas oil	5.3	Heavy gas oil	5.3-9
Heavy cycle oil	7-9	Kerosene	3.5-5.3
Light coker gas oil	5.3-7	Light distillates and gas oil	
Light cycle oil	5.3-7	Naphtha	3.5-5.3
Light liquid products	3.5-5.3	Vacuum tower bottoms	
Overhead vapors	3.5	**10. Industrial Gas or Vapor streams**	
4. Light-END Processing Streams	3.5		
		Ammonia	1.75
Absoption oils		Carbon dioxide	3.5
Alkylation trace acid streams	3.5-5.3	Coal flue gas	17.5
Overhead gas	3.5	Compressed air	1.75
Overhead liquid products	1.75	Exhaust steam (oil bearing)	2.6-3.5
Overhead vapors	1.75	Natural gas (flue gas)	9
Reboiler streams	1.75	Refrigerant (oil bearing)	3.5
	3-5.3	Steam (non-oil bearing)	9

2.7 Overview of Scale Mitigation and Suppression Techniques

It is important to discern the scale formation mechanism before attempting to optimise efforts to suppress the scale growth. Reduction of scale has remained a challenge and detailed research is needed to address this critical and important issue adequately. Various techniques or methods used to mitigate or suppress fouling or scaling in either on-line or off-line conditions include changing operating conditions (feed dilution, thermal shock and shear stress increase),

mechanical interventions (projectiles, inserts, wire brushes), and chemical or physical interventions (surface coating, ultrasound and electric/magnetic).

Müller-Steinhagen (1998) investigated the integral mitigation approach of scaling in the evaporator of a Kraft pulping process and shell-tube heat exchanger of a Bayer bauxite refinery process using real process solutions from several industries. In the Kraft pulping process, the deposits mainly included Burkeite and calcium carbonate, and PTFE coating on heat transfer surfaces significantly prolonged the scale occurrence time and fluidised particles were also shown to reduce deposition.

In the Bayer process cycle, the scale deposits were mostly DSP (Desilication product) with very low thermal conductivity of about 0.3 W/Mk (Müller-Steinhagen et al.,1994b). The experiment with subcooled nucleate boiling significantly reduced scale deposition by the mechanism of creating intense agitation in the sublayer by bubbles formation on the heat transfer surface. Müller-Steinhagen et al. (1994) have investigated some techniques to mitigate or suppress the heat exchanger scaling in Bauxite refineries such as chemical additives to reduce the effective supersaturation of the process solution, surface coating or electropolishing of heat transfer surfaces to reduce the Gibbs energy (or stickiness), turbulence promoters (for example, wire inserts) to reduce temperature-controlled scale deposition and creating a fluidised bed to reduce scaling (Müller-Steinhagen et al., 1994). Table 2.5 shows some chemical inhibitors used to reduce scale deposition significantly for particular foulants.

Table 2.5: Categorization of chemical inhibitor agents for different fouling mechanisms (Müller-Steinhagen, 2010)

Fouling mechanism	Foulant	Inhibitor agent
Crystallisation, precipitation	Ca^{2+}, Mg^{2+} $CaCO_3$ $CaSO_4$	Ion exchange pH control Scale inhibitors (for example, ethylenediaminetetraacetic acid [EDTA])
	Soft and hard scalants	Adsorption agents (for example, polyphosphates)

	Soft and hard scalants	Crystalline weakening agents (polycarboxylic acid)
Particulate	Particulate matter	Surfactants or dispersants
Chemical reaction	Oxygen (polymerization) Metals (reaction catalyst) Insoluble hydrocarbon particle	Antioxidants Metal deactivators Dispersants
Biofouling	Micro- and Macroorganisms	Oxidants (biocide, chlorine)
Corrosion fouling	Passivating oxide layer	Passivating oxidants and pH control

Kazi et al. conducted detailed experiments on calcium sulfate scale mitigation in a heat exchanger with natural fibres (bleached kraft softwood fibre, softwood pulp fibre and hardwood eucalypt pulp fibre) (Kazi et al., 2013; Kazi et al., 2012; Kazi et al., 2010). They reported that fibres significantly increase heat transfer rates by extending the induction period when fibre concentration is above about 0.025% in the scaling solution. They also observed that gum arabic additive also reduced the rate of $CaCO_3$ scale formation on the heated surface (Kazi et al., 2015a).

Crittenden et al. (2015) investigated the effects of surface shear stress on scaling from saturated $CaSO_4$ solution using a simple batch stirrer. It was observed that scale reduction occurred due to enhanced turbulence creating an increase of shear stress (shear stress increase by wire filled on stirrer). Förster et al. (1999) studied the pulsation techniques (single stroke high velocity superimposed on the stationary flow) as a mitigation of scaling on the heat transfer surface. The pulsating flow considerably decreased scale deposition on the pipe surface due to an abrupt increase of the shear stress. Hasan et al. performed many experiments on the potential of turbulence generator to suppress Na_2SO_4 crystallisation scaling under cross flow conditions (Hasan et al., 2012b). The asymptotic value thermal resistance was reduced by up to 85% due to lowering the surface temperature by the using turbulence generators, resulting in decreased fouling. Tijing et al. (2009) demonstrated the potential of the oscillating electric field to mitigate mineral scaling in a counterflow heat exchanger. The thermal resistance reduction up to 60% by the application of maximum frequency 13.56 MHz.

Azimi et al. (2014) investigated the effect of surface energy on reducing $CaSO_4$ scale formation. They showed that a 90% reduction in weight gain due to scale formation was achieved by

reducing surface energy from 52 mJ/m^2 (uncoated glass) to 10 mJ/m^2 (fluorosilane-coated glass). Zettler et al. investigated the influence of heat transfer surface properties and characteristics on fouling mitigation in plate heat exchangers (Zettler et al., 2005). They found that modified surface techniques (reduced surface energy by Ion bean implantation, Ion sputtering, Carbo-Nitriding and oxidising, Ni-P-PTFE coating and electroploshing) effectively reduced scale formation but no certain relationship between energy and scale formation was determined. Hasson et al. (1998) also investigated the potential of various anti-scalants (Calgon, Aqua-Mag, Dequest 2060, Flocon 100 and Cyanamer P-70) to suppress $CaCO_3$ deposition. Both chemical and mechanical process have a scale mitigation potential and also have some disadvantage. Table 2.6 shows the limitations of various chemical and mechanical mitigation systems.

Table 2.6: Limitations of various chemical and mechanical mitigation systems (Müller-Steinhagen et al., 2011)

Mitigation systems	
Chemical	Mechanical
Environmental hazards	Lack of effective control and timing
Health hazards	Ineffective distribution
Increased costs	Increased pressure drop
Over-dosage	Limited to certain chemicals
Possible corrosion impacts	Abrasive impacts
	Require modification of heat exchanger

2.8 Economic Impacts of Scaling

Scaling or fouling is still a big unresolved issue in respect of economic aspects or financial losses. Due to limited research, only a few accurate estimations are available regarding the financial losses caused by scaling or fouling in various industries. However, it is an enormous cost for the mineral industry and for other chemical and process industries where the impacts are manifested through increased capital expenditure and reduced capacity. It has been estimated that direct costs involved in removing scale may be as much as one-quarter of the operational expenses of an alumina refinery (Nawrath et al., 2006). One of the major devices in which scaling or fouling occurs, used in almost every processing industry, is a heat

exchanger. The economic penalties that occur from scaling in heat exchangers are due to excess heat transfer surface area, maintenance, fluid treatment, additional hardware, additional fuel consumption and loss of production (Müller-Steinhagen, 2011). The annual net expenses due to scaling resistance account for nearly 0.25% of Gross Domestic Product (GDP) in industrialised countries as shown by different studies from the 1980s and early 1990s (Garrett - Price, 1985; Pritchard, 1988; Steinhagen et al., 1993). Table 2.7 shows the cost segmentations due to fouling in the USA and UK. The total scaling or fouling costs for each SIC code in New Zealand are presented in Table 2.8; the total costs for all industries in New Zealand is about $46 million. The proportions of various scaling related expenses are shown in Figure 2.14, the major cost factor being maintenance costs of about 72% and the smallest cost factor being lost production of about 2.8% (Steinhagen et al., 1993).

Table 2.7: Costs due to scaling or fouling in USA and UK (Garrett - Price, 1985; Steinhagen et al., 1993; Woods et al., 1976; Pritchard, 1988)

Cost items	Expenditure
Capital expenditure	Up to £100 million in 1987, England US$960-280 million in 1982, USA
(i) Excess heat transfer surface area Between 10-500% Between 11-67%, TEMA	(i) 25% additional capital cost corresponding 30-40% excessarea £5 million in 1968 and £20 million in 1977, UK US$320 million in 1982, USA
(ii)Transport and installation costs (cost due to oversized equipment)	(ii) US$640-960 million per year, USA
(iii) Capital costs for antifouling equipment	(iii) Not estimated
Fuel costs	(i) £100-200 million in 1978, UK (ii) US$700-35,500 million, USA
Maintenance costs	(i) 15% of the maintenance costs of process plant and 50% of that due to fouling (ii) US$2,000 million in 1982, USA
Costs due to production loss	(i) £100 million in 1978, UK (ii) US$200 million in 1984, USA

Table 2.8 Total scaling costs in New Zealand in 1988, in $US/10^3

SIC code	Companies using heat exchangers	Average cost	Total cost
1	120	-	-
2	11	-	-
4	11	10	110
5	35	142	4,970
31	642	7.5	4,815
32	157	10.5	1,648
33	192	1.75	336
34	234	8.7	2,036
35	419	13.3	5,573
36	117	5.8	679
37	44	177	7,788
38	355	10.5	3,727
All industries	2,554	18	45,921

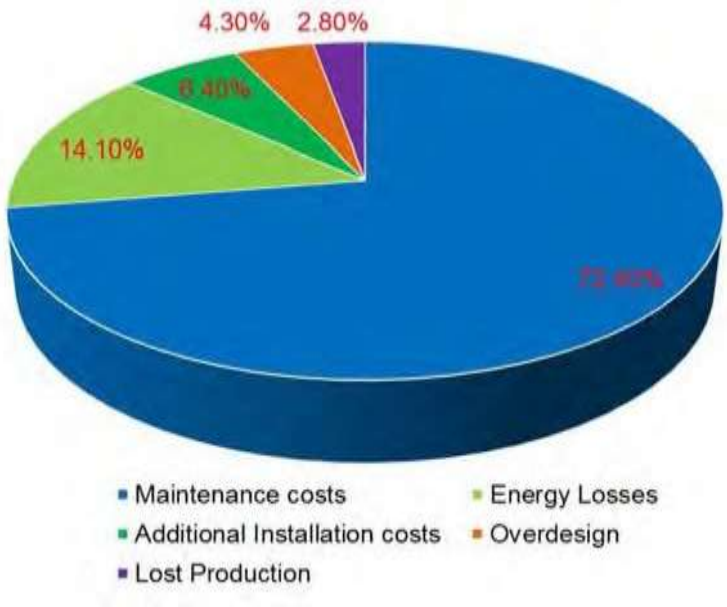

Figure 2.14: Scaling-related costs in New Zealand in 1988 (Steinhagen et al., 1993)

Müller-Steinhagen reported that the total annual costs of scaling for highly industrialised countries such as the United States and the United Kingdom are about 0.25% of their GNP and, for less industrialised countries like Australia and New Zealand, the total scaling costs are around 0.15% of GNP (Müller-Steinhagen, 1993). Müller-Steinhagen (1993) has summarised the total scaling costs of various industrialised countries based on 1984 figures as shown in Table 2.9. For scaling in the hydrocarbon industry, the expenditure for the USA is US$1.36 billion, and worldwide (without Eastern bloc countries) is US$ 4.41 billion (presented in Table 2.10).

Table 2.9: Estimated fouling or scaling costs incurred in some countries (Müller-Steinhagen, 1993)

Country	Fouling costs US$ Millions	GNP (1984) US$ Millions	Fouling costs % of GNP
US (1982)	3860-7000	3,634,000	0.12-0.22
	8000-10,000		0.28-0.35
Japan	3062	1,225,000	0.25
West Germany	1533	613,000	0.25
UK (1978)	700-930	285,000	0.20-0.33
Australia	260	173,000	0.15
New Zealand	35	23,000	0.15
Total industrial World	26,850	13,429,000	0.20

Table 2.10: Estimated fouling or scaling costs incurred in some countries- 2002 (Bansal et al., 2005)

Country	Fouling costs US$ Millions	GNP (2002) US$ Millions	Fouling costs % of GNP
USA	25,518	10,207,039	0.25
Japan	10,810	4,323,919	0.25
Germany	4,691	1,876,340	0.25
UK	3,777	1,510,771	0.25
France	3,405	1,362,077	0.25
China	1,851	1,234,157	0.15
India	742	494,817	0.15
Australia	576	384,075	0.15
New Zealand	78	52,248	0.15

Table 2.11: Fouling or scaling related expenditure in refineries (Bohnet, 1987)

	USA					Non-communist world				
	Mill. t/a	US$ Millions				Mill. t/a	US$ Millions			
	Capacity	Energy	Through-put	Maintenance and cleaning	Total	Capacity	Energy	Through-put	Maintenance and cleaning	Total
Crude distillation	992.4	183.6	671.4	6.3	861.3	3418.3	632.4	2312.6	21.7	2966.7
Hydrotreating	413.5	89.2	85.0	4.2	178.4	1185.4	255.6	243.7	11.9	511.2
Visbreaking	12.2	37.3	9.2	2.6	49.1	82.7	254.3	63.0	10.8	335.3
Reforming	209.5	162.6	106.4	2.3	271.3	463.1	359.5	235.2	5.0	599.7
Total		427.7	872.0	15.4	1360.1		1501.8	2854.5	56.6	4412.9

2.9 Environment Impacts of Scaling

Due to the increased world population and global industrialisation, there will inevitably be increasing problems such as food shortages, scarcity of safe drinking water and global warming. In particular, the concern is climate change, with the growth of population and industrialisation continuing to increase green gas emissions, particularly CO_2, NO_X and SO_X emissions are increasing. Scaling on processing equipment in many industries is a major operational problem that compromises energy recovery and environmental welfare. Scaling in processing equipment such as heat exchangers, precipitation tanks and condensers creates several problems including loss of heat transfer, flow blockage or pressure loss, under-deposit corrosion and flow maldistribution. All of these problems due to scaling will have severe adverse impacts on cost, safety, health and the environment through decreased production efficiency, increased maintenance requirements, increased energy consumption, increased heat transfer surface regarding cost, mitigation and cleaning regarding safety and health issues and increased emissions regarding an environmental problem. It is indicated that CO_2 emissions due to human activity were 2.6 billion tons in 2002, and this will increase up to 4.2 billion tons per year in 2030 (Parfit, 2005). However, about 750 crude oil refineries worldwide currently produce 87 million barrels of refined oil per day (Müller-Steinhagen et al., 2009). Literature shows that 10% of total CO_2 emissions (approximately 88 million tons) per annum are due to scaling in crude oil refineries.

2.10 Summary

The literature review was undertaken based on the significance of crystallisation scaling and its mitigation techniques in the various industrial processes with an emphasis on the effects of hydrodynamics on crystallisation scale formation and its suppression. The effects of hydrodynamics in heat exchangers, especially in the agitation or precipitation tanks, have been presented. This review contributes to a greater understanding of how hydrodynamics play an important role in mitigation or suppression of crystallisation scaling on the heat transfer or exchange surfaces. It also provides an awareness about economic and environmental impacts due toscaling.

CHAPTER 3
THEORETICAL CONSIDERATION FOR THE CRYSTALLISATION SCALING

This chapter presents the theoretical and mathematical background to analyse the crystallisation scale in the agitation tank. The mathematical formulation is important for elucidating and explaining the mechanism of scaling process. It is rather difficult to model crystallisation scaling by a single phenomenon or equation. In particular, crystallisation scaling of normal or inverse soluble salt which comprises of different transport mechanism, is analysed here. The crystalline scale deposit in the agitation tank of normal soluble salt, for example, KNO_3 can occur by three different phenomena simultaneously, such as (i) fluid dynamics or hydrodynamics phenomenon, (ii) scale growth phenomenon and(iii) heattransfer phenomenon. These phenomena have been discussed in the following sections.

3.1 Hydrodynamics Phenomenon and Parameters

The fluid dynamic or hydrodynamic effects play a critical role in the growth and its suppression mechanism of crystallisation scaling in the agitation tank or other heat exchange equipment in the mineral or chemical process industry. The hydrodynamic effects on the crystallisation scaling in the agitation tank are also related to the flow condition (lower, moderate or strong agitation), tank condition with non-swirl flow or swirl flow without baffles, impeller type (axial, radial or mixed flow blade) sizes and location of the impeller either concentric or eccentric.

In agitation tank scale experiments, the crucial parameter is the impeller rotational speed or rotational Reynolds number which reveals the effects of shear stress of the bulk solution (Dream et al., 1999; Kumar et al., 2011; Sánchez Pérez et al., 2006). For the mixing test using agitation by impeller blade, the rotational Reynolds number is usually defined as:

$$\mathrm{Re} = \frac{D^2 N \rho}{\mu} \qquad (3.1)$$

where,

= Crystalline solution density [kg/m^3]

N = Impeller rotational speed [rev/s]

D = Agitator or impeller diameter [m]

= Dynamic viscosity or crystalline solution [Pa.s]

The averaged shear rate over the agitation tank wall is proportional to the rotational speed of the impeller (Wu et al., 2006a) which is as follows:

$$\gamma = K_s N \tag{3.2}$$

where,

= Shear rate [s^{-1}]

N = Impeller rotational speed [rev/s]

K_s = Non-dimensional constant,

K_s = 7 N_Q for axial impeller

= 14 N_Q for radial impeller

Alternatively, the shear rate is calculated using the impeller tip speed over the distance between the tip and agitation tank wall (Kumar, 2009) as follows:

$$\gamma = ND / (T - D) \tag{3.3}$$

where,

T = Agitation tank diameter [m]

The non-dimensional impeller flow number (Wu et al., 2010) is defined as follows:

$$N_Q = \frac{Q}{ND^3} \tag{3.4}$$

where,

Q =Impeller flow rate [m^3/s]

Pumping flow rate (the flow rate through the impeller zone), $Q = \left(\frac{N_Q}{P_o^{1/3}} \right) \left(\frac{P}{\rho} D^4 \right)^{1/3}$

The energy dissipation rate is measured through the non-dimensional power number (Wu et al., 2010) which is as below:

$$P_o = \frac{P}{\rho N^3 D^5} \tag{3.5}$$

The impeller exit velocity is measured by non-dimensional efficiency coefficient (Wu et al., 2010) as below.

$$\eta = \frac{V}{\left(P/\left(\rho T^2\right)\right)^{1/3}} = \frac{V}{\left(P/\left(\rho A\right)\right)^{1/3}} \tag{3.6}$$

For axial flow impeller, the averaged velocity at impeller exit is, $V = \frac{4}{\pi}\left(\frac{N_Q}{P_o^{1/3}}\right) D^{-2/3} \left(\frac{P}{\rho}\right)^{1/3}$

where,

P = Agitator power [W]

V = Velocity [m/s]

A = Tank wetted surface area excluding the bottom [m^2]

3.2 Scale or Crystalline Deposit Growth Phenomenon

Crystallisation scaling of normal or inverse soluble salt occurs when dissolved solute in the process solution precipitate out or crystallise on the heat exchange or transfer surface due to supersaturation. The supersaturation is a main driving force for crystallisation scaling and is achieved by either lower or higher surface temperature in the case of normal or inverse soluble salt, respectively. In the resultant scale growth phenomenon, two concurrent mechanisms (Müller-Steinhagen, 2011) are involved in the agitation tank. The first mechanism is growing up of crystal deposit on the heat transfer surface due to the local supersaturation. The second mechanism is removing accumulated crystal deposit due to the fluid shear stress imposed by the impeller agitation. The mechanism of crystallisation scaling is shown in Figure 3.1. Depending on the conditions, crystallisation scaling can be diffusion controlled, surface reaction controlled, or a combination of both. If the migration of ions from bulk solution to the solid-liquid interface is controlled by mass transfer or diffusion mechanism, then it can be modeled (Bansal et al., 2005; Bansal et al., 2008; Bohnet, 2005; Fahiminia et al., 2007; Mwaba et al., 2006a; Mwaba et al., 2006b) as follows:

$$\frac{d\dot{m}_d}{dt} = \beta(C_b - C_i) \tag{3.7}$$

where,

$\dot{m}_d$ = Scale mass deposited per unit area [kg/m^2]

β = Mass transfer coefficient [m/s]

C_b = Bulk concentration of process solution [kg/m^3]

C_i = Concentration of process solution at solid-liquid interface [kg/m^3]

In the case of KNO_3 scaling, K^+ and NO^{3-} ions are transported from the bulk process solution to the solid-liquid interface or heat transfer surface due to the concentration difference. In crystallisation scaling process, K^+ and NO^{3-} ions are mingled at the interface of solid-liquid to build a crystal lattice to form KNO_3 crystals. In the surface reaction controlled condition, the resultant accumulation of solid deposit is modeled (Bansal et al., 2005; Bansal et al., 2008; Fahiminia et al., 2007; Mwaba et al., 2006a; Mwaba et al., 2006b,) by the following equation:

$$\frac{d\dot{m}_d}{dt} = K_R^* (C_i - C_s)^n \tag{3.8}$$

where,

K_R^* = Crystal growth rate constant [m^4/kg.s]

C_s = Saturation concentration of process solution [kg/m^3]

n = Order of reaction

The order of reaction n usually determined empirically. However, several researchers (Hoang et al., 2011; Mwaba et al., 2006a; Mwaba et al., 2006b) have reported that surface reaction controlled crystallisation, n can range from 1 to 4 or more, depending on the experimental condition. The crystal growth rate constant, K_R^* depends on the solid-liquid interface temperature and Arrhenius expression (Bott, 1997; Fahiminia et al., 2007; Mwaba et al., 2006b); this dependency is described in the following equation:

$$K_R^* = K_{ro} \exp\left(-\frac{\Delta E}{R T_{gi}}\right) \tag{3.9}$$

where,

K_{ro} = Pre-exponential constant [m ^{4}/kg.s]

ΔE = Activation energy [J/mol]

R_g = Gas constant [J/mol.K]

T_i = Temperature at the solid-liquid interface [°C]

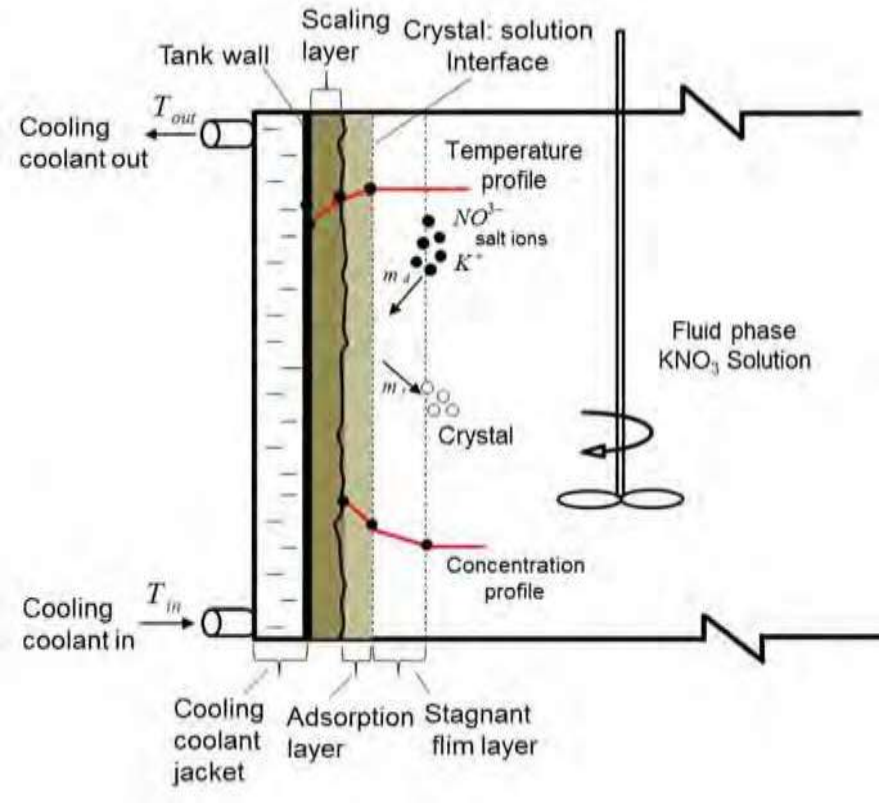

Figure 3.1: Mechanism of KNO_3 crystallisation scaling mechanism in the agitation tank

In the agitation tank scale experiment conditions, the concentration at solid-liquid interface C_i is not known or it is a very cumbersome process to determine this parameter. It is usually congenial to exclude it from the analysis. In this condition, it is assumed that steady-state conditions exist at the solid-liquid interface (Mwaba et al., 2006b). In steady-state condition at the interface of solid-liquid, then Eqs. (3.7) and (3.8) are identical, then on rearranging quadratic Eq. (3.10) (Bansal et al., 2008; Fahiminia et al., 2007; Mwaba et al., 2006b) is obtained, if the order of reaction $n = 2$.

$$\left(\frac{dm_d}{dt}\right)^2 - \left[2\beta(C_b - C_s) + \frac{\beta^2}{K^*_R}\right]\left(\frac{dm_d}{dt}\right) + \left[\beta(C_b - C_s)\right]^2 = 0 \quad (3.10)$$

If $\frac{dm_d}{dt} < \beta(C_b - C_s)$, the solution of quadratic Eq. (3.10) is shown as Eq. (3.11). The rate of crystals deposit mass or scale accumulation (Bansal et al., 2008; Fahiminia et al., 2007; Mwaba et al., 2006b) on the solid surface per unit area is given by Eq. (3.11).

$$\frac{dm_d}{dt} = \beta\left[\frac{1}{2}\left(\frac{\beta}{K^*_R}\right) + (C_b - C_s) - \sqrt{\frac{1}{4}\left(\frac{\beta}{K^*_R}\right)^2 + \left(\frac{\beta}{K^*_R}\right)(C_b - C_s)}\right] \quad (3.11)$$

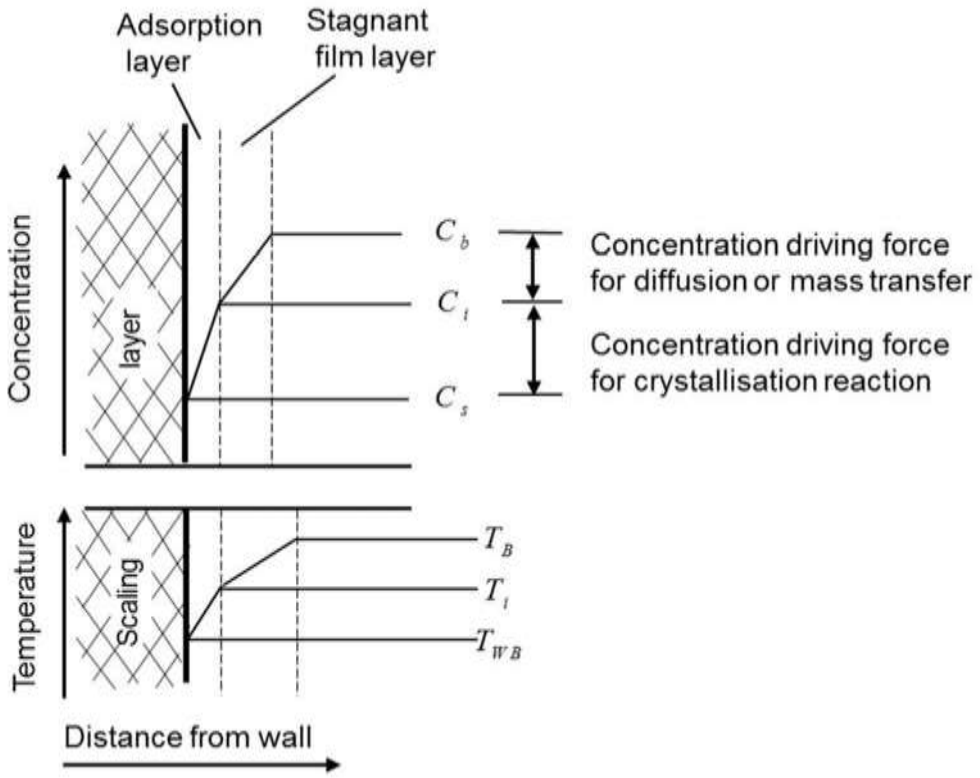

Figure 3.2: Concentration and temperature profile at agitation tank wall

Kern and Seaton (1959a) observed that modeling of scaling processes is a balance between opposing transport process to and from the heat transfer surface, namely, deposition and removal as shown in Figure 3.1. It was observed that along with the scale deposition mechanism on the agitation tank wall, another mechanism occurred: the removal of scale deposits from the heat exchange surface of the tank wall (Müller-Steinhagen, 2011). The scale

removal rate from the tank wall is directly proportional to the wall shear stress of the bulk flow (Mwaba et al., 2006b).

The rate of scale deposit removal can be expressed (Mwaba et al., 2006b) as

$$\frac{d\,\dot{m}_r}{dt} = k_{rem}\frac{\tau_s}{\sigma_s}\delta \tag{3.12}$$

where,

k_{rem} = Proportionality constant for scale removal [m^3/ kg.s]

τ_s = Shear stress [N/m^2]

o_s = Shears strength [N/m^2]

δ= Scale deposit thickness [m]

The resultant formula for scale modeling (Bansal et al., 2008; Bott, 1997; Müller-Steinhagen, 2011; Mwaba et al., 2006b) is as follows:

Net scale deposition rate = Rate of scale deposition – Rate of scale removal

$$\frac{dm}{dt} = \frac{d\,\dot{m}_d}{dt} - \frac{d\,\dot{m}_r}{dt} \tag{3.13}$$

The scaling thermal resistance, R_{scale}, is calculated as (Mwaba et al., 2006b)

$$R_{scale} = \frac{\delta}{k_{scale}} \tag{3.14}$$

where, the thickness, δ, is given by (Mwaba et al., 2006b)

$$\delta = \frac{m}{\rho_{scale}} \tag{3.15}$$

where,

k_{scale} = Thermal conductivity of scale deposit [W/m.K]

ρ_{scale} = Density of scale deposit [kg/m^3]

Assume constant values of k_{scale} and ρ_{scale}, and substituting Eqs. (3.14) and (3.15) in Eq. (3.13) gives the rate of scaling thermal resistance (Fahiminia et al., 2007; Mwaba et al., 2006b) as follows:

$$\frac{dR_{scale}}{dt} = \frac{1}{\rho_{scale}\, k_{scale}} \left[\frac{d\, m_d}{dt} - \frac{d\, m_r}{dt} \right] \tag{3.16}$$

3.3 Heat Transfer Phenomena

A heat transfer fluid (or coolant) was circulated through the external jacket to cool down the working fluid in the tank. In this process, water-ethylene glycol mixture (50% + 50%) was used as the heat transfer fluid and the energy was transported where there is no phase change. Figure 3.3 shows a schematic representation of energy and material flow between cooling jacket and the agitated tank. The amount of thermal energy given off by the KNO_3 crystallised solution and the amount of thermal energy gained by the water-ethylene coolant is taken as equal because the system is perfectly insulated.

The agitation tank is shown in Figure 3.3, where the heated KNO_3 solution is contained in the tank. The coolant circulated through the external cooling jacket absorbed the heat from the process solution agitated in the tank.

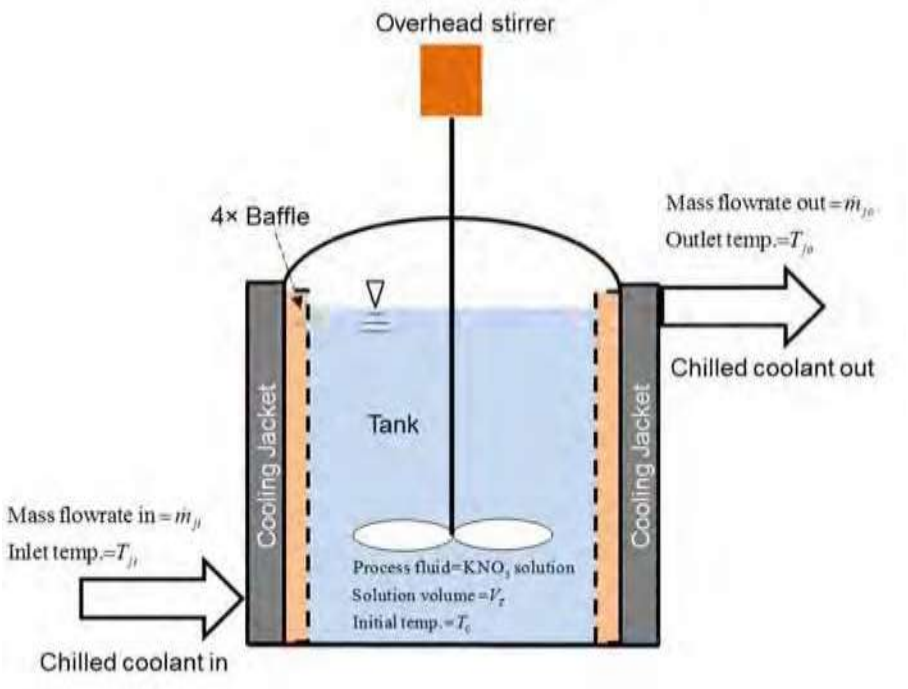

Figure 3.3: Schematic representation of energy and material flow in the lab scale agitation tank

3.3.1 Estimation of the Average Process Solution and Coolant Temperature

This section describes the material and energy balance equations to evaluate the tank and jacket temperatures. The following assumptions were considered for simplification in the calculation.

1. Constant volume of process solution in the agitation tank and constant volume flow rate through the external cooling jacket.
2. Constant density and heat capacity for both the process solution and coolant.
3. The conduction mechanism governs the rate of heat transfer from the process solution (KNO_3 solution) in the tank to the coolant in the external jacket (water-ethylene glycol mixture) through the tank wall material (SS316).

Material balance in the agitation tank:

Accumulation = Input-Output

$$\Rightarrow \frac{d(\rho V_T)}{dt} = 0$$

$$\Rightarrow V_T = C \tag{3.17}$$

where,

V_T = Volume of process solution [m^3]

ρ = Density of process solution [kg/m^3]

t = Time [s]

Assuming constant density and constant volume of scale process solution and there is no entering or leaving of process solution from the system, energy balance in the agitation tank:

Accumulation = Energy in by flow + Energy out by flow + Energy out by heat transfer + other energy

$$\Rightarrow q_{accu} = q_{in} + q_{out} + Q_{heat} + q_{loss} + q_{shaft} + q_{KE} + q_{PE}$$

$$\Rightarrow \frac{dV_T \rho C_P (T_B - T_{ref})}{dt} = 0 + 0 + Q_{heat} + q_{loss} + 0 + 0 + 0$$

$$\Rightarrow \frac{dV_T \rho C_P (T_B - T_{ref})}{dt} = Q_{heat} + q_{loss} \quad (3.18)$$

where,

C_P = Heat capacity of process solution [J/kg.K]

T_B = Bulk temperature of process solution [°C]

T_{ref} = Reference temperature [°C]

Here, the kinetic and potential energy changes and the shaft work done by the mixing impellers is neglected.

On the basis of assumptions of constant density, volume and heat capacity, the Eq. (3.18) can be written by Eq. (3.19).

$$\Rightarrow \frac{d(T_B - T_{ref})}{dt} = \frac{Q_{heat} + q_{loss}}{V_T \rho C_P} \quad (3.19)$$

Assuming the system to be perfectly insulated ($q_{loss} = 0$) and T_{ref} is a constant, then the Eq. (3.20) can be obtained as:

$$\Rightarrow \frac{d(T_B - T_{ref})}{dt} = \frac{Q_{heat}}{V_T \rho C_P} = \frac{UA(T_J - T)}{V_T \rho C_P} \quad (3.20)$$

where,

T_J = Average coolant temperature [°C]

Q_{heat} = Amount of heat content in the process solution [W]

A = Heat transfer area of the agitation tank [m^2]

U = Overall heat transfer coefficient [$W/m^2.K$]

Material balance through the jacket:

Accumulation = Input-Output

$$\Rightarrow \frac{d(\rho_j V_j)}{dt} = \dot{m}_{ji} - \dot{m}_{jo}$$

Assuming constant density and constant volume, $\frac{dV_j}{dt}=0$

Then, $\dot{m}_{ji}=\dot{m}_{jo}=\dot{m}_j$ (3.21)

where,

V_j = Volume of coolant flow through the jacket [m^3]

ρ_j = Density of coolant [kg/m^3]

$\dot{m}_{ji}$ = Mass flow rate at jacket inlet [kg/s]

$\dot{m}_{jo}$ = Mass flow rate at jacket outlet [kg/s]

Assuming constant density and constant volume of coolant fluid so, the flow rate of coolant through the external jacket is constant.

Energy balance through the jacket:

Accumulation = Energy in by flow + Energy out by flow + Energy out by heat transfer + other energy

$$\Rightarrow q_{accu}=q_{in}+q_{out}+Q_{heat}+q_{loss}+q_{KE}+q_{PE} \quad (3.22)$$

The kinetic and potential energy changes between the inlet and outlet streams of the jacket assumed to be neglected. Then the Eq. (3.22) reduces as follows:

$$\Rightarrow \frac{dV_j\rho_j C_{Pc}(T_{jo}-T_{ref})}{dt} = q_{in}+q_{out}+Q_{heat}+q_{loss}+0+0+0$$

$$\Rightarrow \frac{dV_j\rho_j C_{Pc}(T_{jo}-T_{ref})}{dt} = q_{in}+q_{out}+Q_{heat}+q_{loss}$$

Assuming the system to be perfectly insulated ($q_{loss}=0$) and T_{ref} is a constant, so

$$\frac{dV_j\rho_j C_{Pc}(T_{jo})}{dt} = q_{in}+q_{out}+Q_{heat} = \dot{m}_j\rho_j C_{Pc}\left[\left(T_{ji}-T_{ref}\right)-\left(T_{jo}-T_{ref}\right)\right]+Q_{heat}$$

$$\Rightarrow \frac{dT_{jo}}{dt} = \frac{\dot{m}_j}{V_j}\left[\left(T_{ji} - T_{ref}\right) - \left(T_{jo} - T_{ref}\right)\right] + \frac{Q_{heat}}{V_j \rho_j C_{Pc}}$$

$$\Rightarrow \frac{dT_{jo}}{dt} = \frac{\dot{m}_j}{V_j}\left(T_{ji} - T_{jo}\right) + \frac{Q_{heat}}{V_j \rho_j C_{Pc}}$$

$$\Rightarrow \frac{dT_{jo}}{dt} = \frac{\dot{m}_j}{V_j}\left(T_{ji} - T_{jo}\right) + \frac{UA(T_j - T)}{V_j \rho_j C_{Pc}} \qquad (3.23)$$

where,

T_{ji} = Average inlet coolant temperature [°C]

T_{jo}= Average outlet coolant temperature [°C]

$\dot{m}_j$ = Average coolant flow rate [kg/s]

C_{Pj} = Specific heat capacity of coolant [J/kg.K]

3.3.2 Estimating the Overall Heat Transfer Coefficient and Scaling Thermal Resistance

Figure 3.4 shows the schematic of the temperature profile between the coolant fluid (in the jacket) and the heated KNO_3 process solution (in the agitated tank).

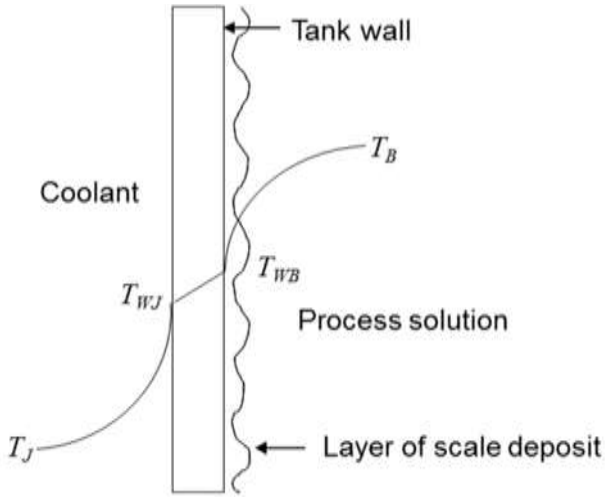

Figure 3.4: Schematic of the temperature profile between the cooling coolant (in the jacket) and heated KNO_3 solution (in the agitated tank)

The crystallisation scaling on the agitation tank wall has a significant influence on heat transfer rate and thermal resistance. The consequences of scale deposit on the tank wall are reduced overall heat transfer rate and enhanced thermal resistance between the process solution and the coolant.

This part described the mathematical equations to calculate the overall heat transfer coefficient (OHTC) and scale thermal resistance. The following assumptions are considered to simplify the calculation.

1. One-dimensional flow of heat across the radial direction. The energy balance equation is composed of a series of resistances which relate the bulk solution temperatures of the agitated liquid in the tank and the coolant through the jacket outside of tank wall.

2. The physical properties of process solution and the coolant (that is, temperature, heat capacity, viscosity, and so on.) are uniform throughout the whole process solution volume in the agitation tank and external jacket, respectively.

3. The transport mechanism for heat transfer from the tank wall to the coolant fluid is convectiveheattransfer.

4. The heat transfer through the agitated tank wall is based on conduction.

5. The rate of heat transfer through each mechanism from the heated scale forming solutions to the coolant is equal.

The amount of heat transfer from the process solution to the coolant occurs through three energy transport mechanisms from the process solution to the coolant through the heat exchange surface of the agitation tank wall (Çengel, 2004).

Convection in the process solution side: $q_{solution} = h_i A_i \left(T_B - T_{WB}\right)$ (3.24)

Conduction through the wall: $q_{wall} = \frac{2\pi k L}{\ln\left(r_o / r_i\right)}\left(T_{WB} - T_{WJ}\right)$ (3.25)

Convection in the coolant side: $q_{coolant} = h_o A_o \left(T_{WJ} - T_J\right)$ (3.26)

The resistance equation across the process solution (KNO_3 solution) in the tank is:

$$R_{Solution} = \frac{1}{h_i A_i} \quad (3.27)$$

The resistance equation for the coolant fluid (a mixture of water and ethylene glycol) in the jacket is:

$$R_{Coolant} = \frac{1}{h_0 A_0} \tag{3.28}$$

The resistance equation for conduction through the tank wall (SS 316) is:

$$R_{Wall} = \frac{\ln(r_o / r_i)}{2\pi kL} \tag{3.29}$$

where,

h_i = Heat transfer coefficient of process solution side [W/m^2.K]

h_o = Heat transfer coefficient of coolant side [W/m^2.K]

A_i = Heat transfer surface area of process solution side [m^2]

A_o = Heat transfer surface area of coolant side [m^2]

r_i= Inner radius of tank [m]

r_o = Outer radius of tank [m]

T_B = Average bulk solution temperature [°C]

T_{WB} = Average tank wall temperature process solution side [°C]

T_J = Average coolant temperature [°C]

T_{WJ} = Average tank wall temperature coolant side [°C]

k= Thermal conductivity of tank wall material [W/m.K]

L = Solution height inside the tank [m]

Hence, to addition of Eq. (3.24), Eq. (3.25) and Eq. (3.26), and put the resistance value from Eq. (3.27) to Eq. (3.29), then the resultant form is given as:

$$(T_B - T_J) = (q_{Coolant} / R_{Coolant}) + (q_{Wall} / R_{Wall}) + (q_{Solution} / R_{Solution}) \; R_{Wall} = \frac{\ln(r_o / r_i)}{2\pi kL} \tag{3.30}$$

At steady state, the heat transfer through each mechanism is equal and can be represented by $Q_{Overall}$, the overall heat transfer rate:

$$q_{Coolant}=q_{Wall}=q_{Solution}=Q_{Overall} \tag{3.31}$$

$$Q_{Overall}=\left(T_B-T_J\right)\ /\left(\left(1/R_{Coolant}\right)+\left(1/R_{Wall}\right)+\left(1/R_{Solution}\right)\right) \tag{3.32}$$

$$Q_{Overall}=\left(T_B-T_J\right)\ /R_{Overall} \tag{3.33}$$

The overall thermal resistance is given by Eq. (34).

$$R_{Overall}=\sum 1\ /\left(h_k A_k\right)+\left(\left(\ln\left(r_0/r_i\right)\right)/2\pi kL\right) \tag{3.34}$$

$$R_{Overall}=1\ /\left(U_{Overall}*A\right)=\left(1/\ A_i h_i\right)+\left(\left(\ln\left(r_0/r_i\right)\right)/2\pi\,k\,L\right)+\left(1/\ A_o h_o\right) \tag{3.35}$$

The overall heat transfer coefficient ($U_{Overall}$) based on the inside agitation tank wall heat transfer area can be calculated as (Çengel, 2003):

$$U_{Overall}\ =\frac{1}{\left(1/h_i\right)+\left(\left(A_i\ln\left(r_0/r_i\right)\right)/2\pi kL\right)+\left(\left(A_i/A_o\right)\left(1/h_o\right)\right)} \tag{3.36}$$

The additional resistance term as scale resistance occurs due to formation of scale deposition from the process solution on the agitation tank wall. Eq. (3.37) and Eq. (3.38) express the final form of overall heat transfer coefficient and overall scaling thermal resistance comprising effects of crystallisation scaling.

$$U_{Overall-Scale}\ =\frac{1}{\left(1/h_i\right)+\left(\left(A_i\ln\left(r_0/r_i\right)\right)/2\pi\,k\,L\right)+\left(\left(A_i\ln\left(r_i/r_{scale}\right)\right)/2\pi\,k\,L\right)+\left(A_i/A_o\right)\left(1/h_o\right)} \tag{3.37}$$

$$R_{Overall-Scale}=\sum 1\ /\left(h_k A_k\right)+\left(\left(\ln\left(r_0/r_i\right)\right)/2\pi kL\right)+\left(\left(\ln\left(r_i/r_{scale}\right)\right)/2\pi kL\right) \tag{3.38}$$

The crystalline scale deposit layer creates resistance on heat transfer and consequently decreases overall heat transfer coefficient which is expressed by the Eq. (3.39) and Eq. (3.40) respectively.

$$R_{Scale}=R_{Overall-Scale}-R_{Overall} \tag{3.39}$$

$$U_{Scale}=U_{Overall}-U_{Overall-Scale} \tag{3.40}$$

The values of h_i and h_o are based on the empirical equation. The inside convective heat transfer coefficient for an agitated tank with 3-bladed axial flow impeller (A310) is estimated from the following correlation (Dream et al., 1999):

$$N_{Nu} = 0.68 \left(N_{\mathrm{Re}}\right)^{0.67} \left(N_{\mathrm{Pr}}\right)^{0.33} \left(N_{\mu}\right)^{0.14}$$

$$\Rightarrow h_i = 0.68 \left(\frac{k_s}{D_T}\right) \left(\frac{D_A^2 N \rho}{\mu}\right)^{0.67} \left(\frac{C_p \mu}{k}\right)^{0.33} \left(\mu_s / \mu_{ws}\right)^{0.14} \qquad (3.41)$$

here,

Nusselt number: $N_{Nu} = \frac{h_i D_T}{k}$

Agitator Reynolds number: $N_{\mathrm{Re}} = \frac{D_A^2 N \rho}{\mu}$

Prandlt number: $N_{\mathrm{Pr}} = \frac{C_p \mu}{k}$

Viscosity number: $N_{\mu} = \mu_s / \mu_{ws}$

where,

h_i = Convective heat transfer coefficient inside vessel [W/m^2.K]

D_T = Agitation tank diameter [m]

k_s = Thermal conductivity of process solution [W/m.K]

D_A = Agitator diameter [m]

N = Agitator speed [rev/s]

ρ = Density of process solution [kg/m^3]

C_p = Heat capacity of process solution [J/kg.K]

μ_s = Viscosity of process solution at bulk solution temperature [Pa.s]

μ_{ws} = Viscosity of process solution at wall temperature [Pa.s]

The following correlation for the coolant (50% water and 50% Ethylene Glycol) in the external jacket can be used to estimate the heat transfer coefficient (Dream et al., 1999):

$$N_{Nu} = 1.02\left(N_{\mathrm{Re}}\right)^{0.45}\left(N_{\mathrm{Pr}}\right)^{0.33}\left(D_e/L\right)^{0.4}\left(D_{jo}/D_{ji}\right)^{0.8}\left(\mu_c/\mu_{wc}\right)^{0.14}\left(N_{Gr}\right)^{0.05}$$

$$\Rightarrow h_o = 1.02\left(k_c/D_e\right)\left(\frac{D_e V \rho_e}{\mu_c}\right)^{0.45}\left(\frac{C_{pc}\mu_c}{k_c}\right)^{0.33}\left(D_e/L_c\right)^{0.4}\left(D_{jo}/D_{ji}\right)^{0.8}\left(\mu_c/\mu_{wc}\right)^{0.14}\left(\frac{D_e^3 \rho_c^2 g\beta\,\Delta t}{\mu_c^2}\right)^{0.05}$$

(3.42)

here,

Nusselt number: $N_{Nu} = \dfrac{h_o D_e}{k_c}$

Agitator Reynolds Number: $N_{\mathrm{Re}} = \dfrac{D_e V \rho_c}{\mu_c}$

Prandlt number: $N_{\mathrm{Pr}} = \dfrac{C_{pc}\mu_c}{k_c}$

Viscosity number: $N_{\mu} = \mu_c/\mu_{wc}$

Equivalent diameter: $D_e = D_{jo} - D_{ji}$

Equivalent area: $A_x = \pi\left(D_{jo}^2 - D_{ji}^2\right)/4$

Equivalent velocity: $V = Q/A_x$

where,

h_o = Convective heat transfer coefficient inside jacket [W/m^2.K]

D_e = Equivalent jacket diameter [m]

D_c = Mean diameter of coolant jacket [m]

D_{jo} = Outside jacket diameter [m]

D_{ji} = Inside jacket diameter [m]

k_c = Thermal conductivity of coolant [W/m.K]

A_x = Equivalent area of external coolant jacket [m]

Q = Coolant flow rate through jacket [m^3/sec]

V = Equivalent velocity of coolant through the jacket [m/s]

ρ_c = Density of coolant [kg/m^3]

C_{pc} = Heat capacity of coolant [J/kg.K]

μ_c = Viscosity of cooling coolant at bulk coolant temperature [Pa.s]

μ_{wc} = Viscosity of cooling coolant at wall temperature [Pa.s]

L_c = Coolant height in jacket [m]

β_c = Coefficient of volumetric expansion [-]

Δt_G = Temperature difference between the wall and bulk solution [°C]

3.4 Summary

The theoretical and mathematical consideration to determine the different parameters by using the experimental values and standard values from empirical equations have been reviewed and discussed. The famous Kern and Seaton scale deposition model Eq. (3.13) was used to determine the net scale deposition rate. This equation includes two terms: (i) the first term is the scale deposition term which was calculated using the Eq. (3.8) based on the surface reaction principle rather than the pure mass transfer transport phenomena determined by experimental observation (detailed presentation is given at section 5.2 in Chapter 5); (ii) the second term was calculated using the Kern and Seaton scale deposit removal mechanism caused by the shear stress and fluid erosion. It is imperative to use correct empirical equation for Nusselt number (N_{Nu}) which is more coherent with experimental condition to determine overall heat transfer coefficient (OHTC) and thermal resistance (TR). The empirical Eqs. (3.41) and (3.42) were used to determine the Nusselt number for bulk scale forming inside the agitation tank, and coolant in the external jacket, respectively, to allow calculation of OHTC and TR.

CHAPTER 4
EXPERIMENTAL DESIGN AND METHODOLOGY

This chapter presents the experimental design, methodology and plans for undertaking various tests and experiments to achieve the objectives of the research. One of the essential and significant tasks of this study was to design and fabricate a lab scale agitation tank which represents replicas of precipitation and agitation tank of many mineral and chemical industries. Various scale experiments were conducted in this tank using laboratory made KNO_3 aqueous solutions which will be discussed here. This agitation tank crystalline scale experiment is seen as identical with the precipitation process in the Bayer process and mixing process of other chemical industries. The following sections describe the scale experiment set up, materials and method and data acquisition in details.

4.1 Experimental

The rig design for the agitation tank scale experiment is necessary to maintain the standard scale-up ratio of tank diameter to impeller diameter, impeller height to impeller diameter, baffle width to tank diameter and solution height to tank diameter to reflect real operation conditions in the industry as shown in Table 4.1. In the crystallisation scale experiment, it is crucial to set up solution temperature, coolant flow temperature, solute concentration and commencement of crystal growth timing. In the agitation tank scale experiment, at the beginning of each test some time (time between the beginning of experiment and starting of impeller rotation) needs to be allowed for initiation of crystal growth on the heat transfer surface. Particularly, for the high agitation experiment (impeller speed from 300 rpm to above) a time of minimum 60 sec was allowed for each experiment. A thermocouple was fitted inside the tank to record temperature for the flow condition of the tank. For the measurement of agitation tank wall temperature, four thermocouples were carefully fitted at four points behind the baffles. It was important to measure the scale growth rate after a specific time interval. Sample coupon was used to collect scale weight at a specific time interval and the scale collection by the coupon sample was also verified by measuring the gross accumulated scale weight on the tank wall and settled scale on the bottom after each experiment. The experimental details are presented below.

4.1.1 Experimental Setup and Apparatus

The schematic diagram and the photograph of the experimental set up with necessary apparatus required for this study are shown in Figure 4.1 and Figure 4.3, respectively. The experimental setup consists of agitation tank and external cooling jacket around the tank. The agitation tank is comprised of two flow loops. The first flow loop is the agitation tank itself where the process solution is agitated at constant impeller speed in the tank.

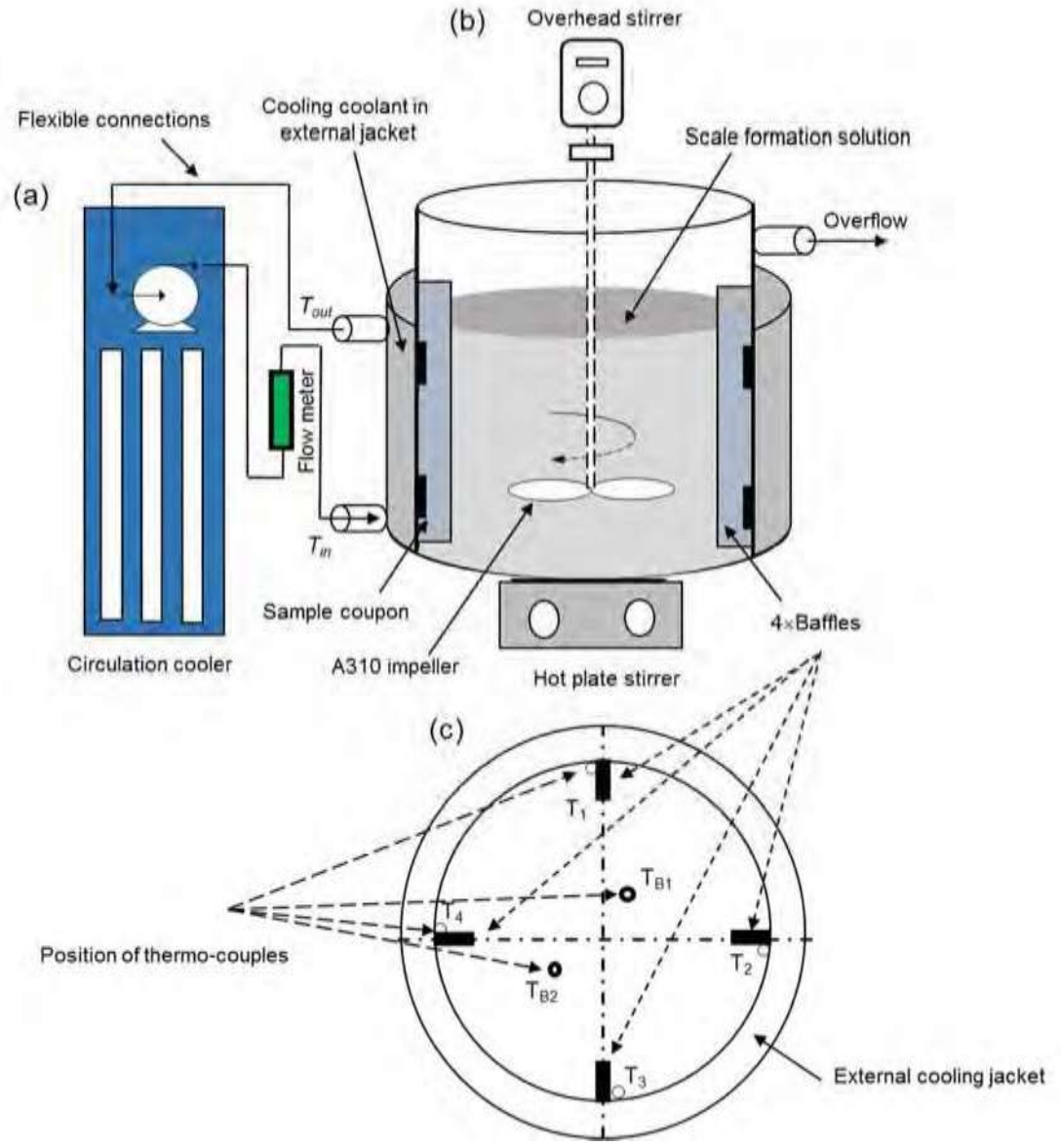

Figure 4.1: Schematic diagram of the experimental setup (a) Low-temperature coolant circulator, (b) Lab-scale agitation tank with low-temperature circulator, (c) Position of baffles and thermocouples for measuring the wall and bulk solution temperature

The second flow loop is the flow of a coolant at constant flow rate through the external jacket from lab-scale circulator by high capacity flexible pipe as shown in Figures 4.1 and 4.3. The coolant is circulated by a circulator which is regulated by a flow meter and the solution in the tank is stirred by overhead stirrer. The experimental set up is comprised of a thermostatically controlled magnetic heater, and thermocouples also. The apparatus that were used in the experiment are briefly described in this section.

4.1.1.1 Scale Building Agitation Tank

The design and fabrication of agitation tank as shown in Figure 4.2 is a major part of this project. The agitation tank was fabricated from SS316 stainless steel at Raskin workshop at Rockhampton, Queensland. The agitation tank and external cooling jacket were fabricated from two concentric cylinders of different diameters and welded on a bottom plate and the top part of the external jacket with a concentric plate of the same thickness of material SS316 stainless steel. The dimensions of the tank are: inner diameter 210 mm, height 330 mm and thickness of wall 3 mm. The external jacket inner diameter 216 mm, outer diameter 250 mm and height 300 mm. The scale experiment tank consists of cooling coolant flow loop with an external jacket, and an overhead stirred tank containing the scaling solution. The agitation tank also has the option of fixing the baffle as required. The dimension of four identical baffles were cut from the SS316 plate with the length same as the tank height, width of 15 mm and thickness of 5 mm. The agitation tank also comprises of inlet, outlet and overflow port with the dimension of 9.52 mm each. The inlet and outlet of external jacket were attached to a circulator via a flow meter and high capacity flexible pipe to maintain a constant coolant flow rate in the external jacket. The detailed dimensions of the tank and associated parts are given in Table 4.1.

Table 4.1: Tank dimensions and values

Dimensions	Values
Inner diameter of tank (D)	210 mm
Height of tank (T)	330 mm
Thickness of tank wall	3 mm
Capacity of tank (1)	11.43 litre
Height of solution (H)	210 mm
Impeller diameter (d)	86, 114 and 180mm

Height of impeller from bottom of tank	Corresponding height of impeller diameter 86, 114 and 180 mm, respectively
Dimension of baffle	330 mm ×15 mm ×5 m
Dimension of external jacket	Inner diameter 213 mm, outer diameter 266 mm and height 300 mm
Capacity of external tank	4.64 litre
Dimension of sample coupon	5 mm ×5 mm ×1.5 mm
Dimension of magnetic stirrer	215 mm ×360 mm ×112 mm
Dimension of inlet, outlet and overflow pipes	9.52 mm
Capacity of flowmeter	0-20 LPM
Capacity of lab circulator	7 litre
Capacity of overhead stirrer	10-2000 rpm

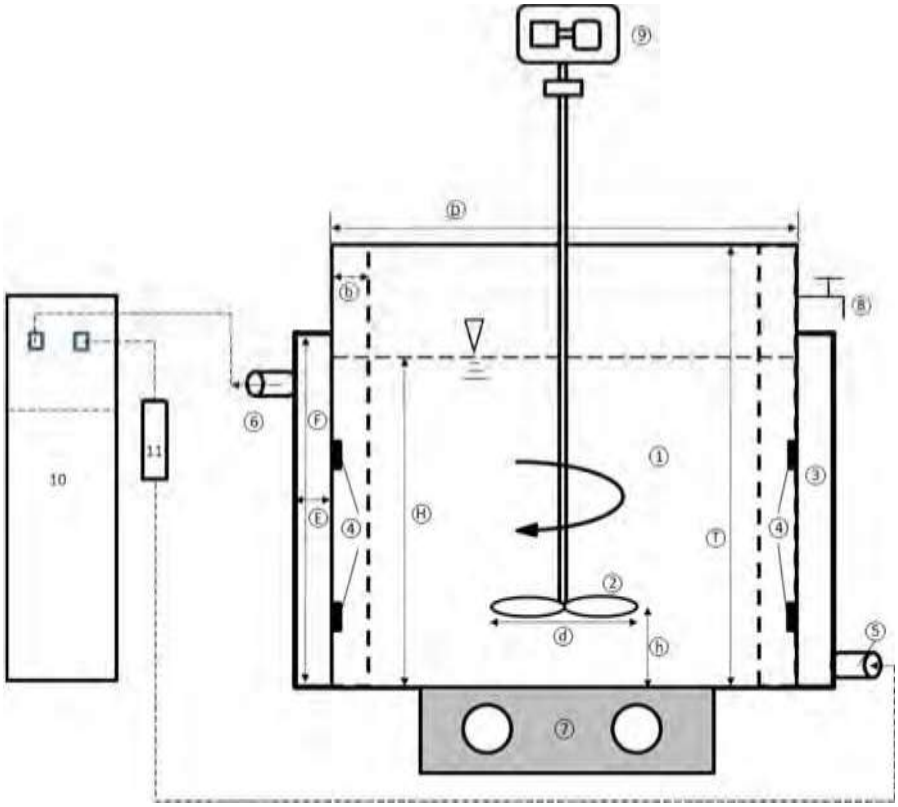

Figure 4.2: Apparatus of agitation tank scale experiment: 1-agitation tank, 2-impeller, 3-external cooling jacket, 4-sample coupons, 5-inlet coolant flow, 6-outlet coolant flow, 7-magnetic stirrer, 8-overflow port, 9-overhead motor drive, 10-low-temperature lab circulator and 11-flowmeter

Table 4.2: Tank dimensions and characteristics

Parameters	Range of values
Tank material	SS 316
Surface roughness, R_a	0.6
D	0.21 m
$\frac{H}{D}, \frac{d}{h}$	1
$\frac{d}{D}$	1/2.4, 1/3.8, 1/3
$\frac{b}{D}$	$\frac{1}{14}$

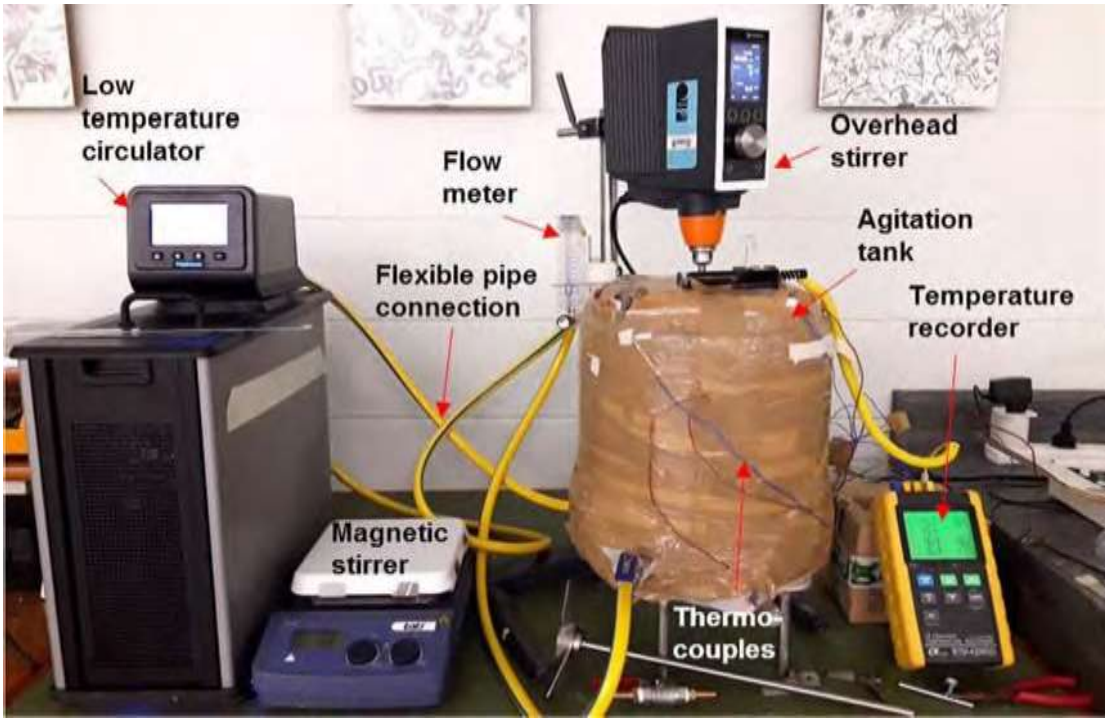

Figure 4.3: Agitation tank setup with necessary connection of the flow loop

The geometric dimensions and proportions of agitation tank are given in Table 4.2. The single parameter of temperature (solution and coolant) is very important in the stage of scale formation. The temperature profile of the process solution in the agitation tank to cooling coolant in the jacket through the tank wall is shown in Figure 4.4. The scale experiment was

performed by using different sizes of axial flow impeller. The flow patterns of axial flow impeller is shown in Figure 4.5.

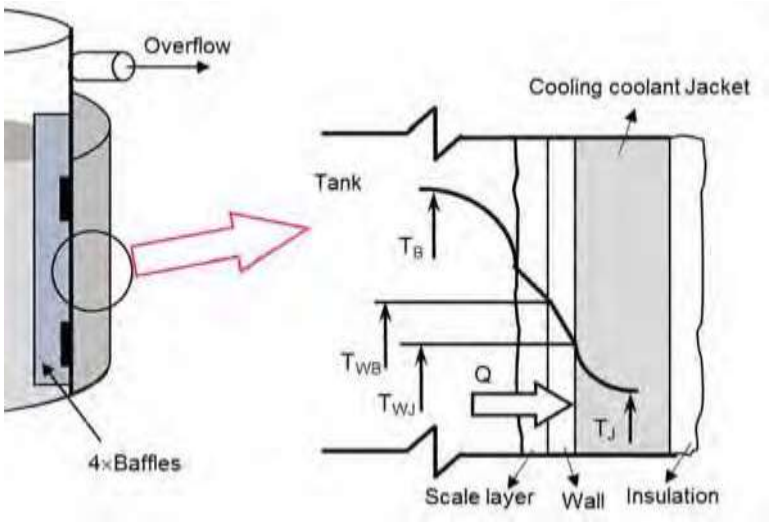

Figure 4.4: Temperature profile through the bulk process solution to coolant

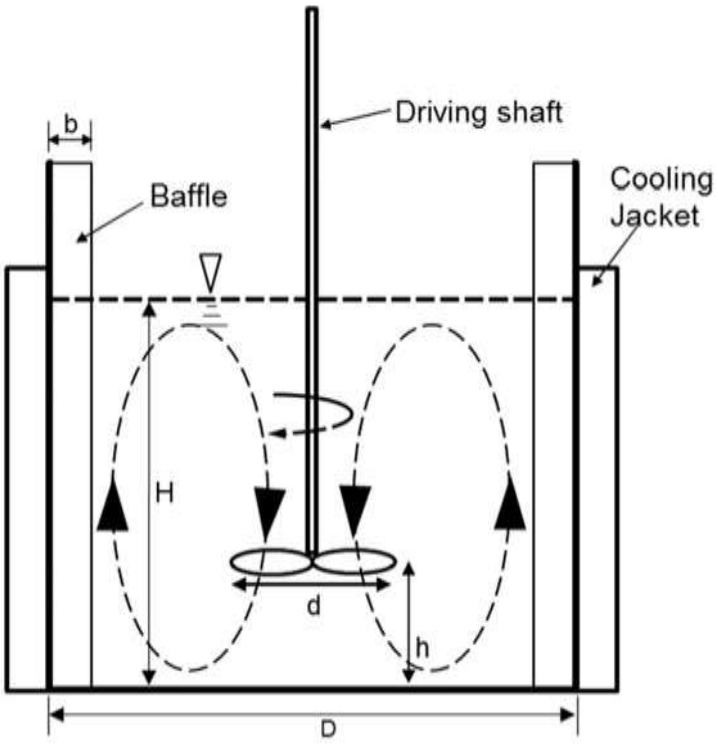

Figure 4.5: Flow pattern in the agitation tank

4.1.1.2 Low-Temperature Coolant Circulator

The advanced programmable temperature controller circulator model AP07R-20 (Poly Science Inc., USA) with a reservoir capacity of 7 litres was used to circulate coolant in an outer jacket around the agitation tank as shown in Figure 4.2. The low-temperature coolant (50% water + 50% ethylene glycol) circulation is through the centrifugal pump in the circulator which can operate at 35 L/min with a temperature range of -20 to 200°C. The coolant temperature was maintained at - 4°C and agitation tank wall temperature approximately at -3.7±0.2°C. The flow of coolant was varied as required for maintaining stable experiment conditions.

Figure 4.6: Agitation tank

Figure 4.7: Position of baffle and agitator in the tank

4.1.1.3 Overhead Stirrer

The variable speed overhead stirrer (110-240 V and 100 W, speed range 10 to 2000 rpm, model: value/precision 100, Heidolph, Germany) was used to rotate the A310 impeller which is shown in Figure 4.3. The torque and speed for a specific test were saved in the computer via USB cable and those data were used to calculate rotational Reynolds number and power consumption by the impeller.

4.1.1.4 Agitation Impeller

For experiment, the A310 model impeller (Lightnin, USA) of three different sizes of axial flow impellers (diameter: 86, 114 and 160 mm) were used to examine the effects of shear rate on the crystalline scale deposit which is shown in Figure 4.8.

Figure 4.8: A310 model axial flow impeller (Lightnin, USA)

4.1.1.5 Hot Plate Magnetic Stirrer

The hot plate magnetic stirrer (200-240V, 50/60 Hz, 1050W, and accuracy ± 0.2°C) with the capability of 20 litres and as shown in Figure 4.3 was used to heat up the scaling solution. The constant temperature of bulk scaling forming solution was maintained automatically at a set temperature by the hot plate magnetic stirrer.

4.1.1.6 Rotameter

The FR2000 (Brooks Instruments, USA) rotameter as in Figure 4.3 was used to measure the flow rate of the coolant. It also regulated the coolant flow rate as required to adjust the appropriate heat flux to the agitation tank wall.

4.1.1.7 Thermocouple and Temperature Recorder

The k-type thermocouple was used to measure the temperature at various points of scale experiment set up. The BTM-4208SD model 12 channels temperature recorder as shown in Figure 4.3 was used to record the temperature. The average temperature at different point of scaling wall, bulk solution temperature, and inlet and outlet temperature of coolant were measured to evaluate the overall heat transfer coefficient and thermal resistance due to surface crystallisation of normal soluble salt.

4.1.1.8 Scale Collection Coupon Sample

The stainless steel coupon was used to collect the scale weight. Total eight little coupon samples each with a dimension: 15 mm × 15 mm × 1.5 mm were used to collect the scale weight at different time intervals. The coupons were installed inside the tank wall aligned with the surface curve for minimum flow disturbance by using chemical solution proof glue. After the experiment, the solutions were drained and the coupons were carefully taken out. Then the total weight of the sample coupon was measured to calculate the scale weight by subtraction of coupon weight from the total weight.

4.2 Materials and Scale Forming KNO_3 Solutions

4.2.1 Materials

In this agitation tank scale experiment, the potassium nitrate (KNO_3) (AR grade, Auschem Ltd.) was used as a scale forming reagent. For the experiment, laboratory made KNO_3 solutions were used to investigate the hydrodynamic effects on crystallisation scaling because the real Bayer liquor or other chemical solutions were not safe to handle due to the high processing temperature and their caustic properties. In addition, the KNO_3 is an ionic compound, and it is safe to handle. Also, KNO_3 is one of the most temperature sensitive chemicals due to its aqueous solubility (17g at 5°C to 100g at 60°C per 100g water) which is understood to being suitable for producing crystalline scale simply by applying temperature change.

4.2.2 Preparation of Potassium Nitrate (KNO_3) Solution

The KNO_3 solution was prepared by dissolving KNO_3 in distilled water with the required proportions for maintaining desired concentration of 4.5, 4.75 and 5.25 mol/dm^3.

$$KNO_{3(S)} + H_2O_{(l)} = K^+_{(aq)} + NO^-_{3(aq)} + H_2O_{(l)}$$
$$KNO_{3(S)} = K^+_{(aq)} + NO^-_{3(aq)} \quad (4.1)$$

KNO_3 is a neutral normal solubility salt that cannot be hydrolyzed in water, and it dissociates in water only, as shown in Eq. (4.1). Therefore, there is no bond formation between water and KNO_3. The molecules are interspersed within the molecules of water. At first, distilled water was heated up to 48°C in a glass beaker, then KNO_3 was gradually added and stirred to produce the solution. The solubility of KNO_3 is entirely dependent on the temperature. The solubility curve of KNO_3 as a function of temperature is shown in Figure 4.9.

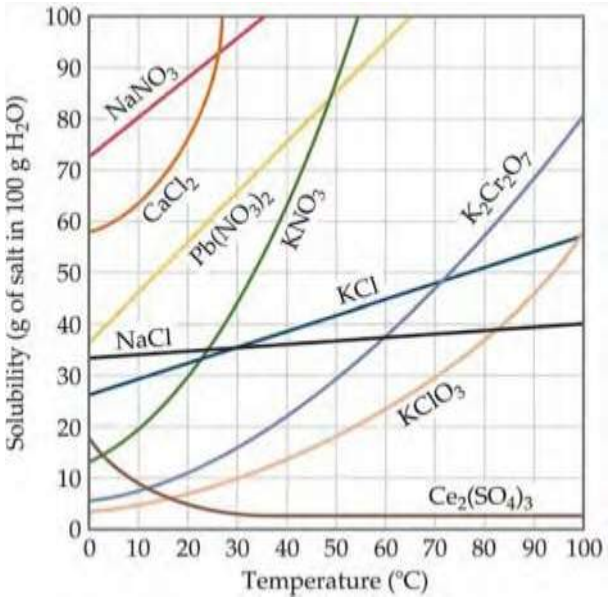

Figure 4.9: Solubility of potassium nitrate (KNO_3) as a function of temperature

The solutions of various concentrations of KNO_3 were prepared for the scale experiment as per the following proportions which are shown in Table 4.3.

Table 4.3: Solutions concentration

Water [litre]	KNO_3 [gm]	Concentration [mol/dm^3]
7	3185	4.50
7	3362	4.75
7	3716	5.25

4.3 Test Data Measurement

For each experiment, the measured parameters were: the bulk solution temperatures, wall temperatures, coolant flow temperatures, solution conductivity, coolant flow rate, and impeller speed and torque. Four k-type thermocouples were installed inside the tank wall at an equal space to measure the scale forming wall temperature at four different points, namely T_1, T_2, T_3, and T_4 as shown in Figure 4.1 (c). In addition, two thermocouples were inserted in the scale solution to measure the bulk solution temperatures of T_{B1} and T_{B2}, respectively. Moreover, the other two thermocouples were also used to measure the inlet and outlet bulk temperatures of cooling coolant inserted at the inlet (T_{in}) and outlet (T_{out}) of the external cooling jacket. All eight thermocouples were connected to a 12 channel BTM-4208SD data logger to record the temperature at every 10 seconds. The HI98192 model conductance cell recorded the conductivity itself and FR2000 series flow meter measured the coolant flow rate with accuracy of ± 3%. The Hei-Torque precision 100 model recorded the torque and rpm data in PC through the mini-USB interface.

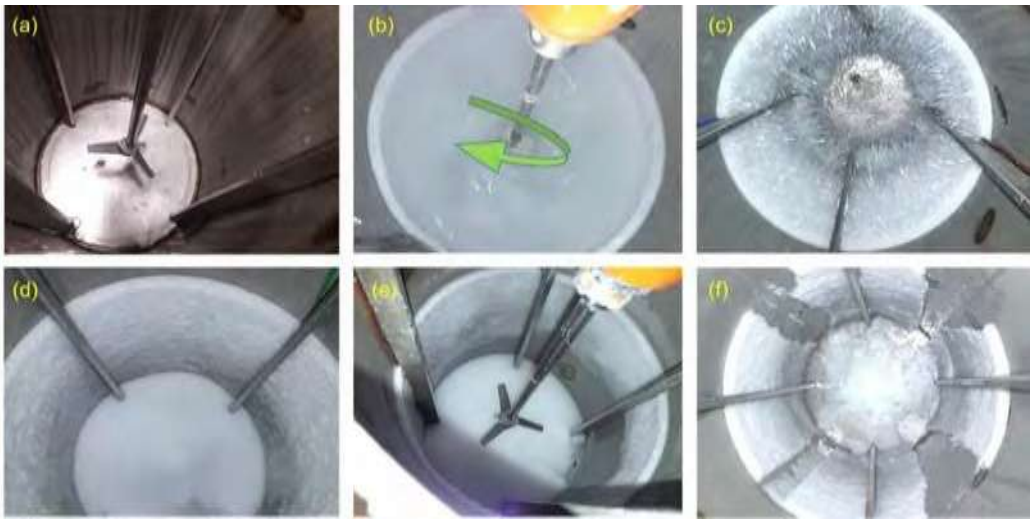

Figure 4.10: Agitation tank condition at various modes (a) At empty condition, (b) At operation mode, (c) Scale growth at low agitation (100 rpm) condition, (d) Scale growth at moderate agitation (300 rpm) condition, (e) Scale growth at strong agitation (500 rpm) condition, (f) At de-scaling condition

After every experiment, the scale growth rate on both the wall and the bottom of the tank was measured by direct measurement of scale weight and measurement of averaged scale weight

using sample coupon. The data for the scale growth rate and averaged scale thickness on the tank wall are presented in details in Appendix B and one set of data shown in Table 4.4.

The scale pattern, formed scale and presence of foreign products were inspected visually. The photographs of different conditions of the agitation experiment tank are shown in Figures 4.10 (a-f). Figure 4.10 (a) shows the empty condition before commencement of experiment, Figure 4.10 (b) shows the experiment run, then the scale growth at different agitation conditions are shown in Figures 4.10 (c), (d), (e) and finally the descaling operation as shown in Figure 4.10 (f).

4.4 Experimental Procedure and Plan

This section presents the experimental plan for scale deposition test run in the agitation tank as shown in Tables 4.4 and 4.5. The series of experiment (total number of experiment of 114) were conducted to examine the effects of different sizes of impellers (86, 114 and 160 mm), at various rate of agitations (100, 200, 300, 400, 500, 600 and 700 rpm) and with different KNO_3 concentrations (4.50, 4.75 and 5.25 mol/dm^3).

Table 4.4: Experimental data collection plan for impeller diameter of 86 or 114 mm with different concentration (4.50, 4.75 and 5.25 mol/dm^3) with baffles and without baffles condition

Agitator rpm	Scaling rate (wall and bottom)	Scale weight (wall and bottom)	Scale thickness	Wall temp. four points	Solution temp. (bulk)	Coolant temp. (inlet, outlet, bulk)	Agitator torque and power	Electrical conductivity (EC)
100	√	√	√	√	√	√	√	√
200	√	√	√	√	√	√	√	√
300	√	√	√	√	√	√	√	√
400	√	√	√	√	√	√	√	√
500	√	√	√	√	√	√	√	√
600	√	√	√	√	√	√	√	√
700	√	√	√	√	√	√	√	√

For each experiment, the following data were measured: scale weight, scale thickness, the temperature at different thermocouple positions, agitation speed and torque to achieve the target of the experiment. The time duration for each experiment was 80 minutes and scale weight measured at every 5 minutes interval. For each diameter of the impeller, 7 experiments were conducted at seven different speeds of 100 to 700 rpm at 100 rpm intervals (except for 160 mm impeller which was conducted at five different speeds of 100 to 500 rpm at 100 rpm interval).

Table 4.5: Experimental data collection plan for impeller diameter of 160 mm with different concentration (4.50, 4.75 and 5.25 mol/dm^3) with baffles and without baffles condition

Agitator rpm	Scaling rate (wall and bottom)	Scale weight (wall and bottom)	Scale thickness	Wall temp. at four points	Solution temp. (bulk)	Coolant temp. (inlet, outlet, bulk)	Agitator torque and power	Electrical conductivity (EC)
100	√	√	√	√	√	√	√	√
200	√	√	√	√	√	√	√	√
300	√	√	√	√	√	√	√	√
400	√	√	√	√	√	√	√	√
500	√	√	√	√	√	√	√	√
600	-	-	-	-	-	-	-	-
700	-	-	-	-	-	-	-	-

4.5 Experiment and Data Collection

Before starting the scaling experiment, the prepared scale forming solution with predetermined concentration was heated to the required temperature. The coolant temperature of - 4°C and tank wall temperature of - 3.7 ± 0.2°C were checked before commencement of experiment with fully insulated agitation tank. After running the test for 80 minutes, the solution was completely drained. The scaling rate was measured on the wall of the agitation tank and data are shown in Appendix B, in Tables B.2, B.4, B.6, B.8 and B.10. The settled scale was measured on the bottom of the tank and these data are shown in Tables B.1, B.3, B.5, B.7, B.9 and B.11 with baffles and without baffles conditions in Appendix B. For each experiment, the average scale thickness was also measured and presented in Appendix B, Tables B.12, B.13 and B.14. The OHTC and TR were calculated based on the average bulk solution temperature, average coolant temperature and average tank wall temperature have been discussed in detail in Chapter 6.

Table 4.6: Wall scale growth rate at various agitation rate with baffles (KNO_3 concentration of 4.5 mol/dm^3)

Experiment. No	rpm	Impeller diameter 86 mm (a)		Impeller diameter 114 mm (b)		Impeller diameter 160 mm (c)	
		Total scale weight [g]	Scale rate [g/cm^2/hr	Total scale weight (g)	Scale rate [g/cm^2/hr	Total scale weight [g]	Scale rate [g/cm^2/hr]
Expt. 1(a, b, c)	100	1510	1.090	1340	0.968	1100	0.794
Expt. 2(a, b, c)	200	1190	0.859	900	0.650	500	0.361
Expt. 3(a, b, c)	300	850	0.614	465	0.336	245	0.177
Expt. 4(a, b, c)	400	625	0.451	340	0.246	140	0.101
Expt. 5(a, b, c)	500	530	0.383	245	0.177	85	0.061
Expt. 6(a, b)	600	430	0.311	195	0.141	-	-
Expt. 7(a, b)	700	380	0.274	170	0.123	-	-

4.6 Summary

The novel laboratory model agitation tank replicating the precipitation and mixing tank of mineral and chemical industries was carefully designed and fabricated. The design criteria were selected based on the available literature in which the experimental results reflect the real world conditions. Every connection point was sealed and the tank was properly insulated before the experiment. The temperature readings were monitored and observed carefully. The scale forming solution concentrations and other relevant parameters of data were also monitored. The whole scale weight of the scale depositions on the sample coupon were also collected and dried for weight measurement. Finally, the collected data were analysed and synthesised to show the hydrodynamic effects on scale deposition and heat transfer which are presented and discussed in detail in Chapters 5 and 6.

CHAPTER 5
HYDRODYNAMIC EFFECTS ON SCALE GROWTH AND SUPPRESSION

This chapter presents the experimental data and results in detail. The results are primarily on the hydrodynamic or fluid dynamic effects on scale growth and its suppression in the case of crystallisation scaling. A series of experiments were conducted to investigate the effects of varying operating parameters (impeller agitation speed, impeller size, the degree of supersaturation, and baffles) on the crystallisation scaling rate in the agitation tank. The scaling experiments were performed at agitation speeds varying from 100 to 700 rpm and at three different solution concentrations (4.5, 4.75 and 5.25 mol/dm^3) in both the baffled and unbaffled tank conditions.

5.1 Experimental Procedure and Data Collection

Experimental procedure and data collection on the hydrodynamic effects were discussed in detail in Chapter 4, section 4.4 and section 4.5. However, for relevance and clarity, a brief statement on experimental procedure is provided. The properly insulated stainless steel (SS 316) agitation tank with total capacity of 11 litres was filled with a heated KNO_3 solution, heated to a predetermined temperature 48 ± 1.8°C, which turned highly supersaturated at agitation wall temperature. The coolant circulator was connected with the external cooling jacket to cool down the agitation tank wall with the temperature at - 3.7 ± 0.2°C. The coolant flow rate was adjusted to obtain the required heat flux for the bulk liquid solution by convection mechanism through the tank wall. The solution was agitated by the impeller blade positioned at the centre of the tank and the agitation speed was set from 100 to 700 rpm. The average coolant temperature was calculated by taking the average of the inlet and outlet temperatures of the coolant through the external cooling jacket.

The measurements of the scale growth rate which included the scale growth on the tank wall and the tank bottom were performed using two different methods. The first method was used to measure the scale deposits on sample coupons positioned at different locations on the tank wall after a specified time interval, and the second method was used to weigh the total mass of

the scale deposit on the bottom manually removed and cleaned with caution. After completion of each experimental run, the solution from the agitation tank was completely drained out through the bottom; then the scale was dried slowly for 24 hours by an air-dryer.

5.2 Experimental Data Reproducibility

The crystallisation scale deposition rate of KNO_3 solution on the surface wall of the agitation tank as a function of time for three separate scale experiments were run under the same conditions of KNO_3 concentration of 4.5 mol/dm^3, bulk temperature of 48°C, temperature difference of (ΔT) 51.75°C for an agitation speed of 300 rpm and the baffled condition, as presented in Figure 5.1. It is observed that the data reproducibility from these different runs of the experiment are within good agreement, showing an average root mean square (RMS) error of 7.5%.

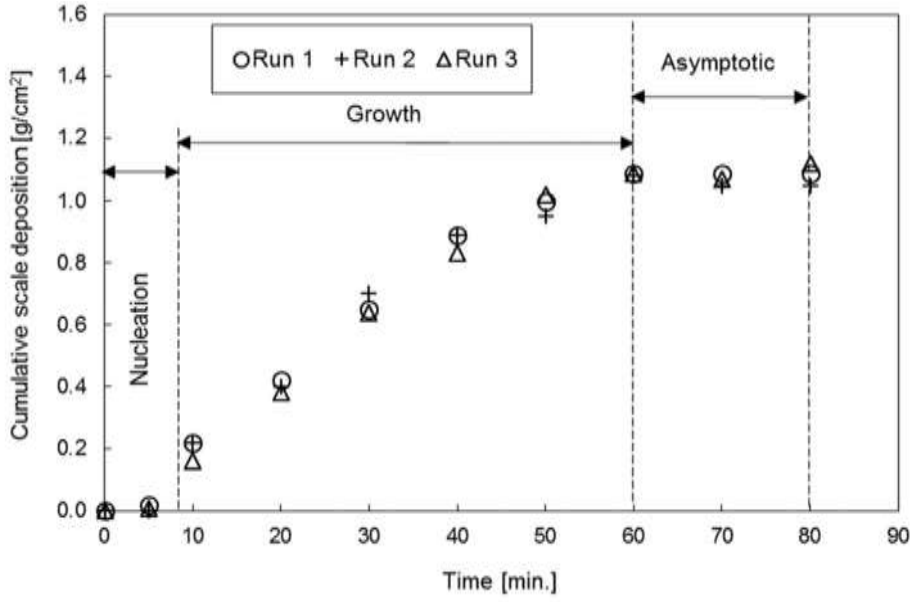

Figure 5.1: Scale deposition rate on stainless steel (SS 316) agitation tank wall as a function of time for three separate runs of the experiment under the conditions of bulk temperature 48°C, ΔT=51.75°C, agitation speed of 300 rpm and KNO_3 concentration of 4.5 mol/dm^3 with the baffled condition

Figure 5.2 presents scale growth rate as a function of agitation speed ranging from 100 to 700 rpm for three separate experiments run under similar conditions and the results show good reproducibility with a RMS error of 10.5%. The variation in different runs is believed to have

occurred due to the slight variation in wall temperature (within ±0.70°C) and the possible inclusion of foreign material in the KNO_3 solution from various lots of the AR grade KNO_3 stock from the supplier. Similar results have also been reported in the literature by several authors (Gill and Nancollas, 1980; Kazi et al., 2015b; Kazi et al., 2012).

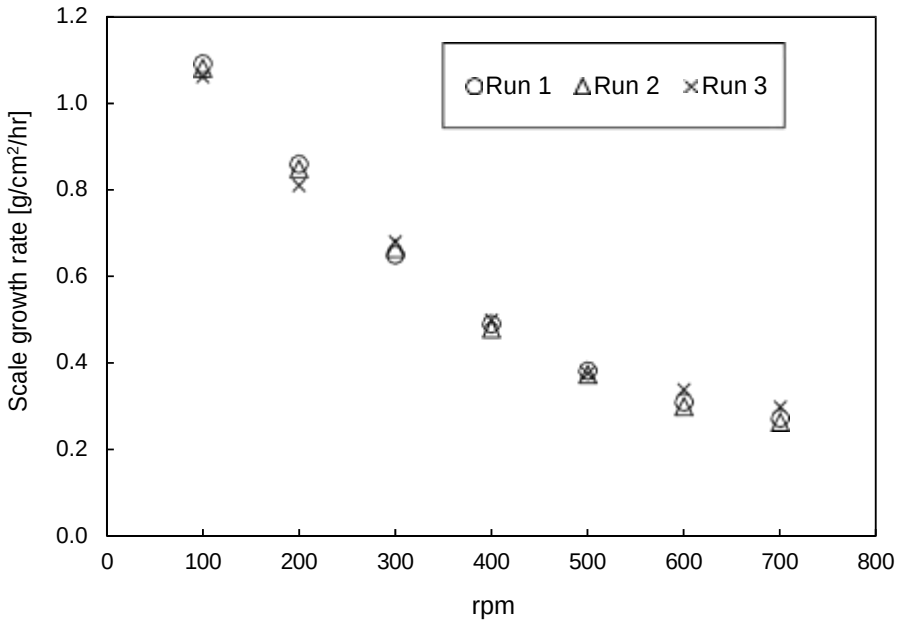

Figure 5.2: Scale deposition growth rate on stainless steel (SS 316) agitation tank wall as a function of agitation rate for three separate runs of the experiment under the conditions of bulk temperature 48°C, ΔT=51.75°C and KNO_3 concentration of 4.5 mol/dm^3 with the baffled condition

5.3 Effect of Supersaturation

The scale growth rate of KNO_3 solution follows Eq. (5.1) below (Hoang et al., 2011):

$$\Omega_d = \frac{C_b - C_s}{\frac{1}{k_m} + \frac{1}{k_r (C_i - C_s)^{n-1}}} \tag{5.1}$$

where, Ω_d is the mass of crystal solid deposit in unit time or scaling rate [g/hr], C_b is the concentration of the crystal-forming substance in the bulk solution [mol/dm^3], C_s is the equilibrium saturation concentration [mol/dm^3] C_i is the concentration of solute in the solution

at the interface with the tank wall, k_m is the mass transfer coefficient [g dm^3/mol/hr], k_r is the reaction rate constant and n is the order of the crystal growth process, and the values of n are more than one (Hoang et al., 2011; Mwaba et al., 2006b).

The order of the crystal growth process n is calculated from the slope of the curves as shown in Figures 5.3 (a, b, c) with the baffled condition and in Figures 5.4 (a, b, c) without the baffles. When the crystallisation process is controlled by the surface attachment reaction, and if n >1, then $C_b \approx C_s$ and Eq. (5.1) reduces to:

$$\Omega_d = k_r (C_i - C_s)^n \tag{5.2}$$

For example, using the equation of the line plots of $\log \Omega_d$ versus $(C_i - C_s)$ as shown in Figure 5.3(a), the value of n can be found to be varying from 1.09 to 2.3, for different impeller speeds of 86 mm diameter are shown in Table 5.1.

Table 5.1: Scale growth equation and R^2 value for different impeller speeds of 86 mm diameter

rpm	log equation	R^2 value
100	$\log \Omega_d = 1.0897\,(C_i - C_s) + 1.566$	$R^2 = 0.9968,\ n = 1.0897$
200	$\log \Omega_d = 1.4622\,(C_i - C_s) + 2.3403$	$R^2 = 0.9994,\ n = 1.4622$
300	$\log \Omega_d = 1.7645(C_i - C_s) + 2.0549$	$R^2 = 0.9515,\ n = 1.7645$
400	$\log \Omega_d = 2.0714(C_i - C_s) + 1.7977$	$R^2 = 0.9949,\ n = 2.0714$
500	$\log \Omega_d = 2.3168(C_i - C_s) + 1.566$	$R^2 = 0.9964,\ n = 2.3168$
600	$\log \Omega_d = 2.2743\,(C_i - C_s) + 1.5042$	$R^2 = 0.9749,\ n = 2.2743$
700	$\log \Omega_d = 1.6944(C_i - C_s) + 1.747$	$R^2 = 0.9132,\ n = 1.6944$

These results indicate that the crystallisation scale deposition of KNO_3 on the wall of the agitation tank is a surface reaction controlled process as n is equal to or greater than 1.

(a)

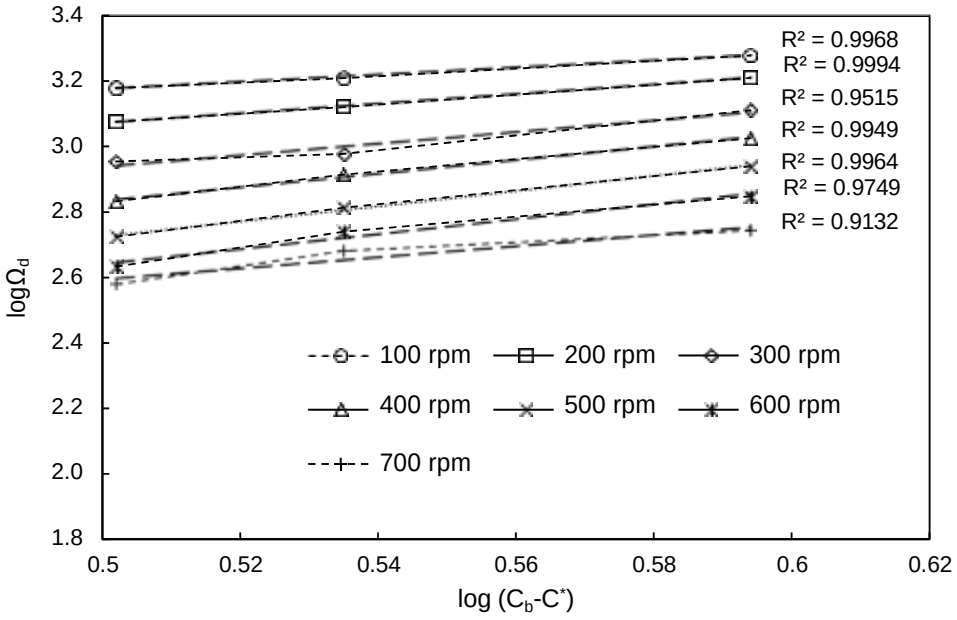
3.4
3.2
3.0
2.8
2.6
2.4
2.2
2.0
1.8
0.5
0.52
0.54
0.56
0.58
0.6
0.62
logΩd
log (Cb-C*)
R² = 0.9968
R² = 0.9994
R² = 0.9515
R² = 0.9949
R² = 0.9964
R² = 0.9749
R² = 0.9132
100 rpm
200 rpm
300 rpm
400 rpm
500 rpm
600 rpm
700 rpm

(b)

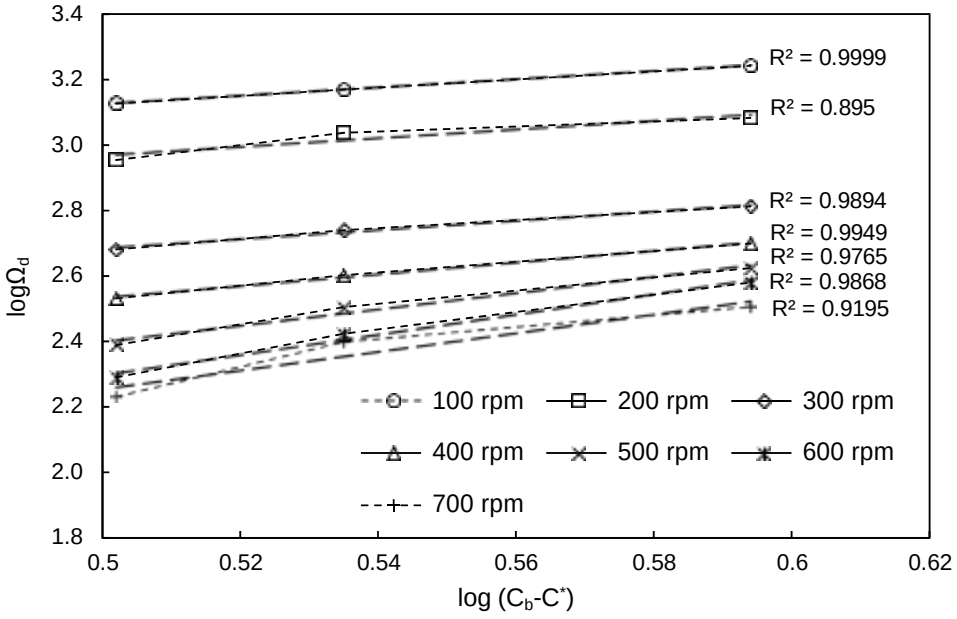
3.4
3.2
3.0
2.8
2.6
2.4
2.2
2.0
1.8
0.5
0.52
0.54
0.56
0.58
0.6
0.62
logΩd
log (Cb-C*)
R² = 0.9999
R² = 0.895
R² = 0.9894
R² = 0.9949
R² = 0.9765
R² = 0.9868
R² = 0.9195
100 rpm
200 rpm
300 rpm
400 rpm
500 rpm
600 rpm
700 rpm

(c)

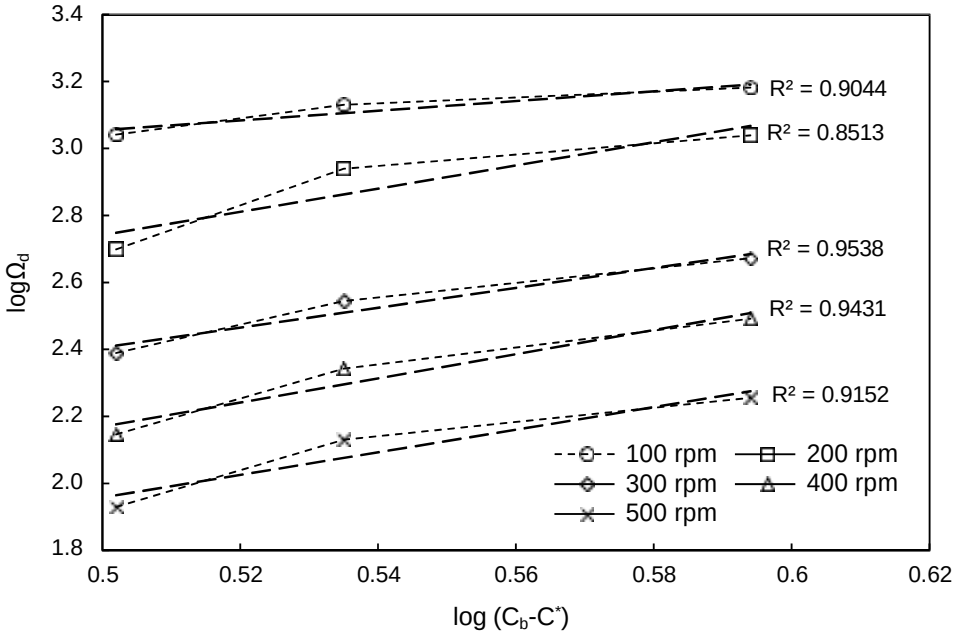

Figure 5.3: The relationship between scale mass and supersaturation of KNO_3 at bulk temperature 48°C, ΔT=51.75°C, C_b = 4.50 mol/dm ^{3} with baffles and run time 80 min: (a) impeller diameter of 86 mm, (b) impeller diameter of 114 mm, and (c) impeller diameter of 160 mm

Figures 5.5 (a, b, c) show the effect of scaling rate as a function of supersaturation ratio. In crystallisation scaling, supersaturation is the main driving force of the scaling process. It is seen from Figures 5.5 (a, b, c) that the scaling rate increases with the increasing of supersaturation ratio at the wall temperature, which is below the saturation temperature because of normal soluble salt.

(a)

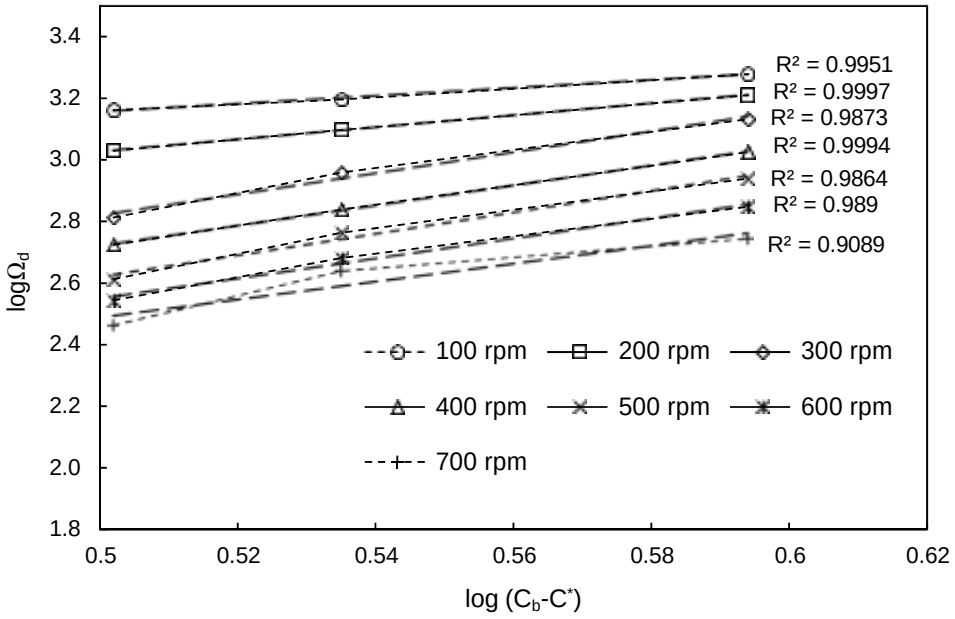
3.4
3.2
3.0
2.8
2.6
2.4
2.2
2.0
1.8
logΩd
0.5
0.52
0.54
0.56
0.58
0.6
0.62
log (Cb-C*)
R² = 0.9951
R² = 0.9997
R² = 0.9873
R² = 0.9994
R² = 0.9864
R² = 0.989
R² = 0.9089
100 rpm
200 rpm
300 rpm
400 rpm
500 rpm
600 rpm
700 rpm

(b)

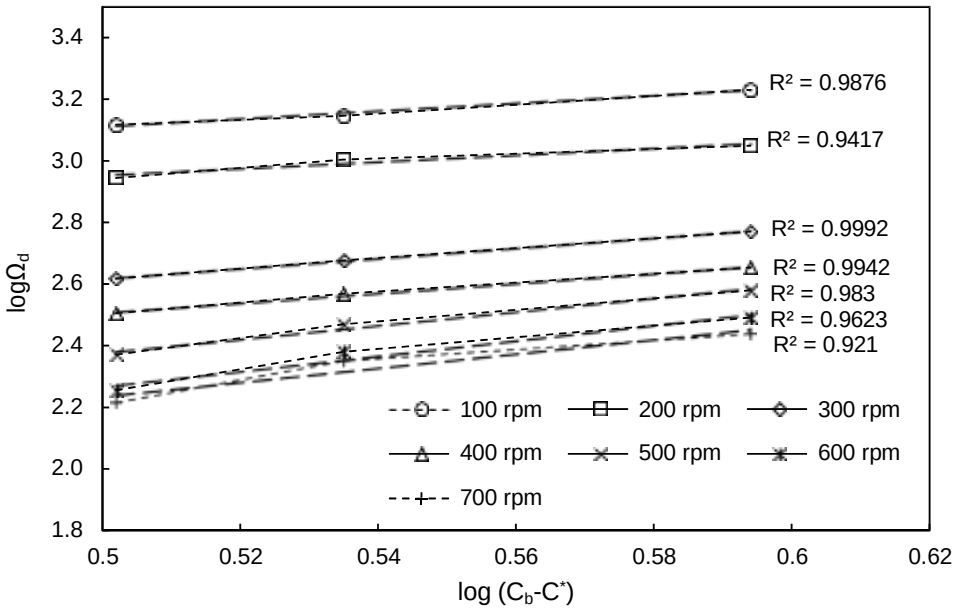
3.4
3.2
3.0
2.8
2.6
2.4
2.2
2.0
1.8
logΩd
0.5
0.52
0.54
0.56
0.58
0.6
0.62
log (Cb-C*)
R² = 0.9876
R² = 0.9417
R² = 0.9992
R² = 0.9942
R² = 0.983
R² = 0.9623
R² = 0.921
100 rpm
200 rpm
300 rpm
400 rpm
500 rpm
600 rpm
700 rpm

(c)

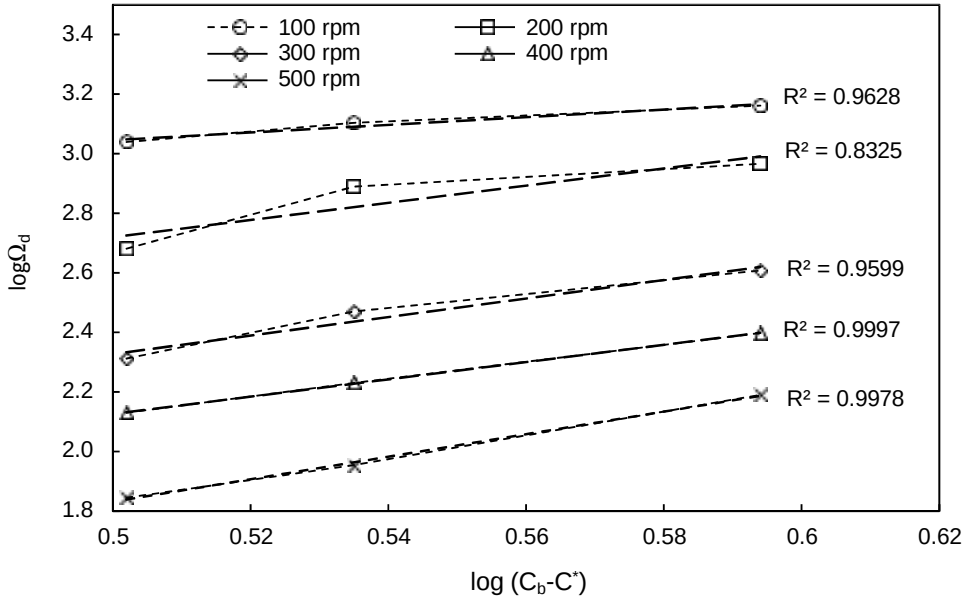

Figure 5.4: The relationship between scale mass and supersaturation of KNO_3 at bulk temperature 48°C, ΔT=51.75°C, C_p = 4.50 mol/dm^3 without baffles and run time 80 min: (a) impeller diameter of 86 mm, (b) impeller diameter of 114 mm, and (c) impeller diameter of 160 mm

(a)

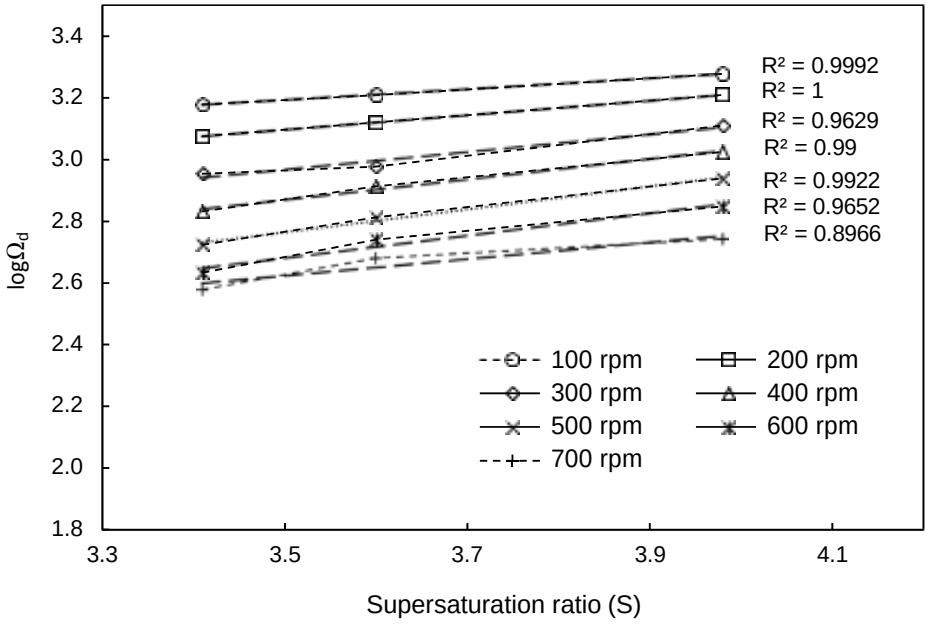

(b)

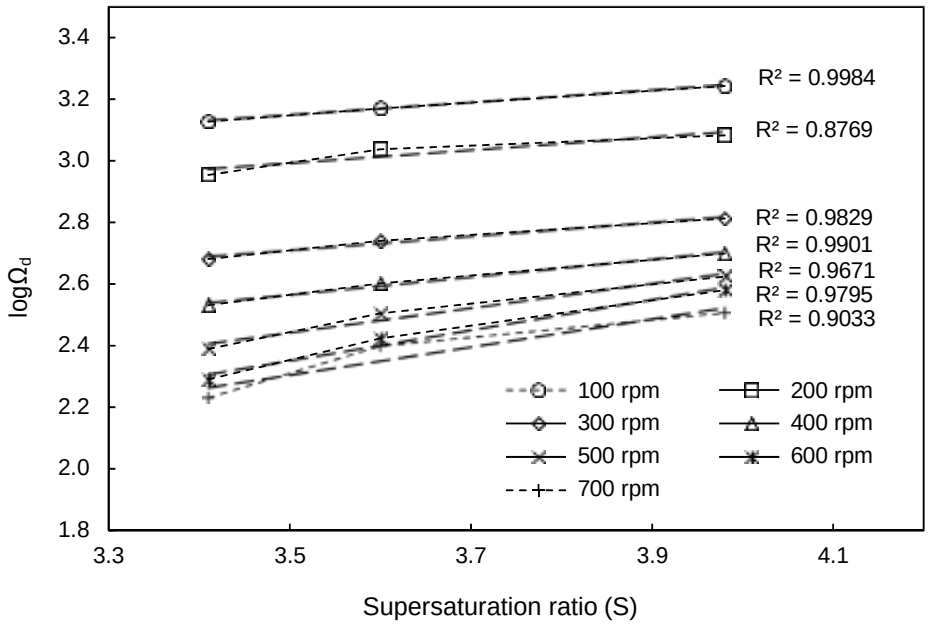

(c)

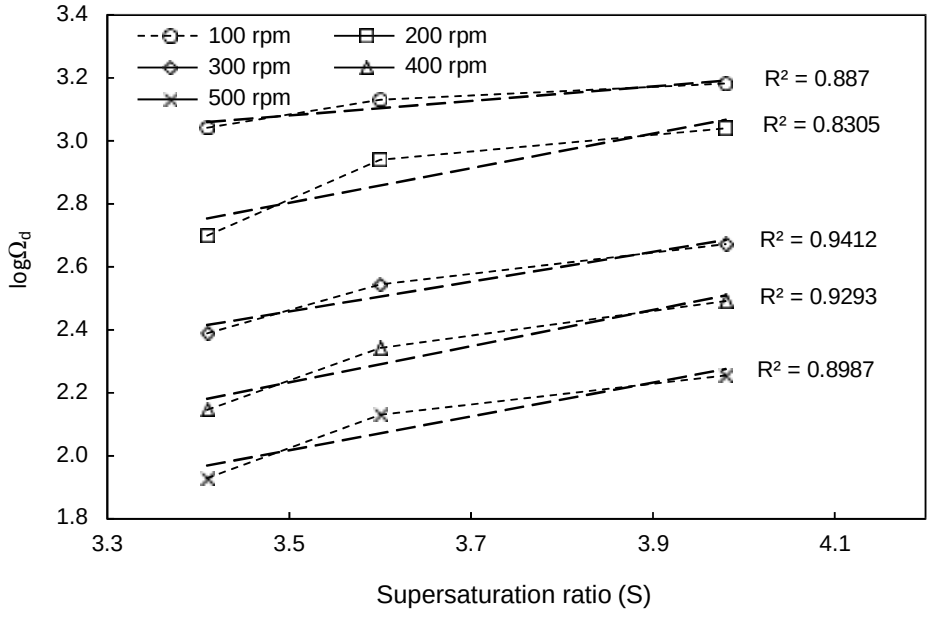

Figure 5.5: The relationship between scale mass and supersaturation ratio of KNO_3 at bulk temperature 48°C, ΔT=51.75°C, $C_b = 4.50$ mol/dm ^{3} with baffles and run time 80 min: (a) impeller diameter of 86 mm, (b) impeller diameter of 114 mm, and (c) impeller diameter of 160 mm

5.4 Effect of Agitation Rate

The scale experiment indicates that quantitatively the scale growth rate is enhanced at lower impeller agitation speeds and is reduced at higher agitation speeds. The hydrodynamic effects on scale growth and its suppression in the agitation tank with three different impeller sizes at a rotational speed ranging from 100 to 700 rpm and for solutions with various supersaturation levels were considered. The impeller agitation rate is also expressed by impeller rotational Reynolds number shown in Table 5.1 using equation (3.1). The Reynolds number increased with the increase of impeller speed. It also increases with impeller size and slightly decreased with the increase of KNO_3 concentration for the corresponding agitation speed and impeller size. Table 5.2 shows the shear rate using equation (3.2) and blade tip velocity corresponding to specific impeller speeds and both these parameters were increased with the impeller speed. In the subsequent discussion, the effects of hydrodynamics on the scale growth and its suppression mechanism is discussed with regard to impeller speed expressed as rpm instead of the other parameters (Reynolds number, shear rate and blade tip velocity).

Table 5.2: Reynolds number variations by KNO_3 concentration for different impeller sizes and speeds

rpm	*Re* for KNO_3 con. of 4.50 mol/dm^3			*Re* for KNO_3 con. of 4.75 mol/dm^3			*Re* for KNO_3 con. of 5.25 mol/dm^3		
	dia. 86 mm	dia. 114 mm	dia. 160 mm	dia. 86 mm	dia. 114 mm	dia. 160 mm	dia. 86 mm	dia. 114 mm	dia. 160 mm
100	8023.90	14099.33	27773.37	7878.14	13843.20	27268.84	7842.10	13779.88	27144.12
200	15999.75	28114.22	55380.43	15709.10	27603.50	54374.40	15637.25	27477.25	54125.71
300	24023.65	42213.55	83153.80	23587.24	41446.70	81643.24	23479.36	41257.14	81269.84
400	32047.55	56312.87	110927.17	31465.38	55289.90	108912.09	31321.47	55037.02	108413.96
500	40023.41	70327.77	138534.24	39296.35	69050.21	136017.64	39116.62	68734.4	135395.55
600	48047.31	84427.10	166307.61	47174.49	82893.41	163286.49	46958.73	82514.28	162539.68
700	56071.21	98526.42	194080.98	55052.63	96736.60	190555.33	54800.83	96294.17	189683.80

Table 5.3: Shear rate and blade tip speed for different impeller sizes and speeds

rpm	Shear rate [1/sec]			Blade tip velocity [m/s]		
	dia. 86 mm	dia. 114 mm	dia. 160 mm	dia. 86 mm	dia. 114 mm	dia. 160 mm
100	1.1582	1.9831	5.3440	0.4510	0.5978	0.8390
200	2.3095	3.9544	10.6560	0.8992	1.1920	1.6730
300	3.4677	5.9375	16.0000	1.3502	1.7898	2.5120
400	4.6260	7.9206	21.3440	1.8012	2.3876	3.3510
500	5.7773	9.8919	26.6560	2.2494	2.9818	4.1850
600	6.9355	11.8750	32.0000	2.7004	3.5796	5.0240
700	8.0937	13.8581	37.3440	3.1514	4.1774	5.8630

This part of the analysis reveals the implication of agitation rate on the cumulative scale growth rate at three different sizes of the impeller (diameters of 86, 114 and 160 mm). Table 5.3 and Table 5.4 show the percentage increase of wall scale growth rate at concentrations of 4.75 mol/dm^3 and 5.25 mol/dm^3 compared with a concentration of 4.50 mol/dm^3, respectively.

Table 5.4: Percentage (%) increase of wall scale growth rate at KNO_3 concentration of 4.75 mol/dm^3 compared with concentration of 4.50 mol/dm^3

rpm	Impeller dia. 86 mm		Impeller dia. 114 mm		Impeller dia. 160 mm	
	With baffles	Without baffles	With baffles	Without baffles	With baffles	Without baffles
100	6.79	7.64	9.34	6.50	18.52	16.93
200	9.85	14.40	17.43	12.87	42.53	38.06
300	10.53	24.18	15.45	16.16	30.00	30.51
400	23.78	23.19	15.00	16.22	36.36	32.35
500	18.46	29.31	23.44	27.12	37.04	27.78
600	21.82	27.08	26.42	31.25	-	-
700	20.83	33.33	32.00	33.33	-	-

The wall scale growth rate constantly increases with the increase of KNO_3 concentration. The percentage of scale growth rate at light agitation has little variation among the impeller sizes because light agitation is most favourable to the growth of scale deposit on the agitation tank wall irrespective of impeller sizes. The percentage of scale growth rate was higher at strong agitation than light agitation. These results reveal that the effects of strong agitation played a more beneficial role in the mitigation of scale growth than the light agitation.

The percentage increase of wall scale shown in Table 5.3 and Table 5.4 also reveals the effects of concentration and percentage of scale growth rate increase with the increase in KNO_3 concentration.

Table 5.51: Percentage (%) increase of wall scale growth rate at KNO_3 concentration of 5.25 mol/dm^3 compared with concentration of 4.50 mol/dm^3

rpm	Impeller dia. 86 mm		Impeller dia. 114 mm		Impeller dia. 160 mm	
	With baffles	Without baffles	With baffles	Without baffles	With baffles	Without baffles
100	20.44	17.43	23.34	23.00	27.63	27.24
200	26.54	24.11	25.62	21.43	50.25	48.11
300	34.11	35.21	28.46	29.66	47.87	49.38
400	41.04	39.77	32.00	31.11	54.84	54.00
500	39.08	44.59	41.81	43.42	52.78	58.06
600	39.01	44.44	48.68	46.77	-	-
700	31.41	42.12	46.88	45.45	-	-

Table 5.5 and Table 5.6 show the percentage increase of the bottom settled scale growth rate at concentrations of 4.75 mol/dm^3 and 5.25 mol/dm^3 compared with a concentration of 4.50 mol/dm^3, respectively. Strong agitation increased the bottom settled scale growth rate and reduced the wall scale growth rate. The consequence of the increase of concentration was to increase the settled scale.

Table 5.6: Percentage (%) increase of bottom settled scale growth rate at KNO_3 concentration of 4.75 mol/dm^3 compared with concentration of 4.50 mol/dm^3

rpm	Impeller dia. 86 mm		Impeller dia. 114 mm		Impeller dia. 160 mm	
	With baffles	Without baffles	With baffles	Without baffles	With baffles	Without baffles
100	40.74	44.44	19.20	26.23	14.81	9.41
200	19.05	20.49	11.11	20.00	8.27	11.17
300	8.61	14.71	8.84	11.79	8.28	10.63
400	7.81	14.43	6.80	10.66	4.36	4.56
500	8.08	16.44	7.79	7.09	4.19	5.28
600	10.26	13.33	7.69	6.02	-	-
700	7.42	10.77	6.35	9.38	-	-

Table 5.7: Percentage (%) increase of bottom settled scale growth rate at KNO_3 concentration of 5.25 mol/dm^3 compared with concentration of 4.50 mol/dm^3

rpm	Impeller dia. 86 mm		Impeller dia. 114 mm		Impeller dia. 160 mm	
	With baffles	Without baffles	With baffles	Without baffles	With baffles	Without baffles
100	80.72	80.88	59.68	62.69	56.88	53.89
200	44.08	45.51	53.33	53.13	32.98	30.28
300	32.02	36.96	36.88	35.42	28.81	27.10
400	36.82	37.23	35.64	35.37	29.10	28.36
500	36.81	37.67	32.44	31.77	30.28	31.46
600	34.78	34.23	30.89	27.95	-	-
700	31.70	33.31	28.56	28.75	-	-

Figures 5.6 (a, b, c), 5.7 (a, b, c) and 5.8 (a, b, c) show the variation in the cumulative scale deposition rate as a function of time at different agitation speeds with KNO_3 concentrations of 4.50, 4.75 and 5.25 mol/dm^3, respectively. The scaling rate on the cooling surface is a function of two consecutive mechanisms of crystallisation: (i) initial heterogeneous nucleation, and (ii)

growth of tiny crystals (Bott, 1996; Bott, 1997; Briançon et al., 1997; Kazi et al., 2015a; Rankin and Adamson, 1973). The growth of crystals on the cooling surface is the result of two major processes: (i) the transport of solute from scaling solutions to the boundary layer of the cooling surface by a diffusion process, and (ii) integration of tiny crystals into a larger crystal lattice (Bott, 1996; Bott, 1997; Rankin and Adamson, 1973). The extent of prevailing supersaturation will determine the rate of crystallisation and when supersaturation is attained at the cooling surface region. The diffusion or mass transport is a prerequisite transport mechanism for creating the scaling layer by incorporation of the new crystalline material into the previous scaling layer. However, the prime cause of crystallisation scaling is a local supersaturation of solute in the process solution. When the solubility product of K^+ and NO_3^- ions exceeds the saturation limit, KNO_3 crystallises and forms scale.

(a)

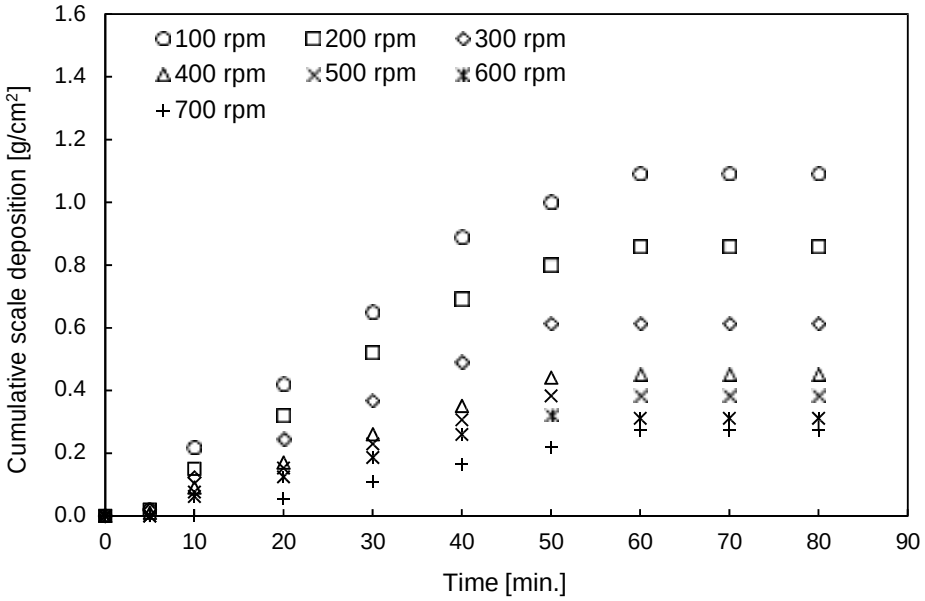

The total cumulative scale growth curve is explained in terms of three regimes, namely nucleation, growth and asymptotic (Mwaba et al., 2006a; Mwaba et al., 2006b). In the nucleation regime, scale growth rate is quite negligible because it requires the initiation of scale crystallisation on the wall surface of the tank due to supersaturation of KNO_3 solution. In the growth regime, heterogeneous scale deposition increases rapidly with time as the crystallisation scale rate is much higher than the scale removal rate by the action of fluid erosion. The

asymptotic behaviour regime of the scaling curve occurs for the period between 60 mins and 80 mins where the rate of scale removal is equal to the rate of scale deposition.

(b)

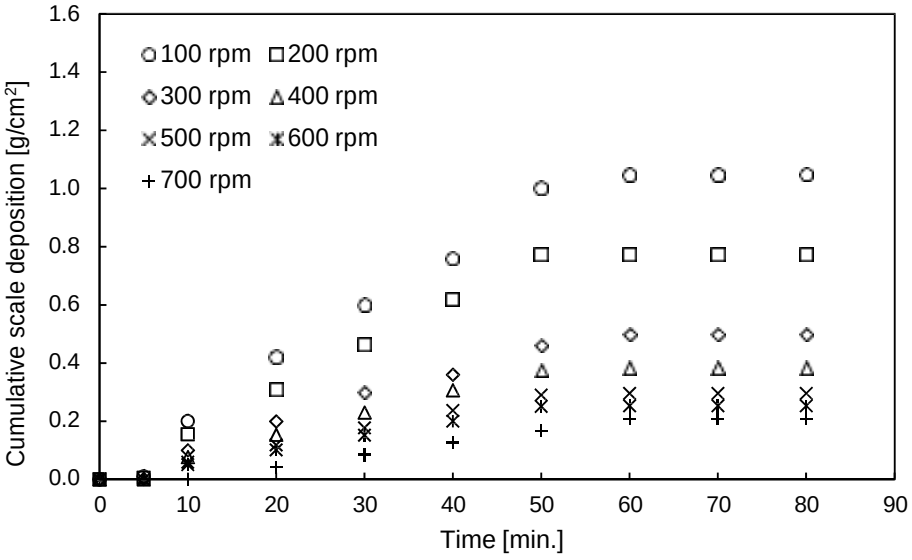

(c)

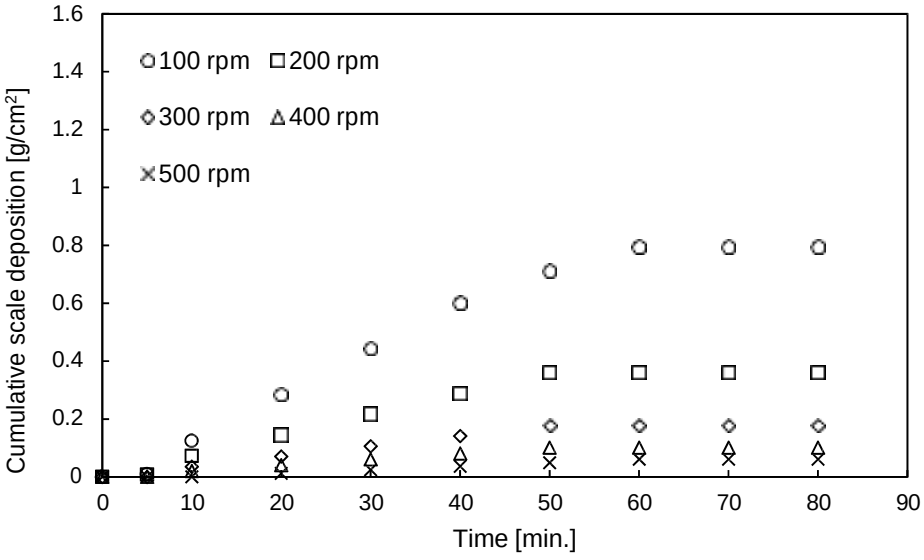

Figure 5.6: Deposition of KNO_3 as a function time, baffles and agitator speed. Experiments were performed at bulk temperature 48°C, ΔT=51.75°C, and KNO_3 $C_b = 4.50\,\text{mol/dm}^3$: (a) impeller diameter of 86 mm, (b) impeller diameter of 114 mm, and (c) impeller diameter of 160 mm

(a)

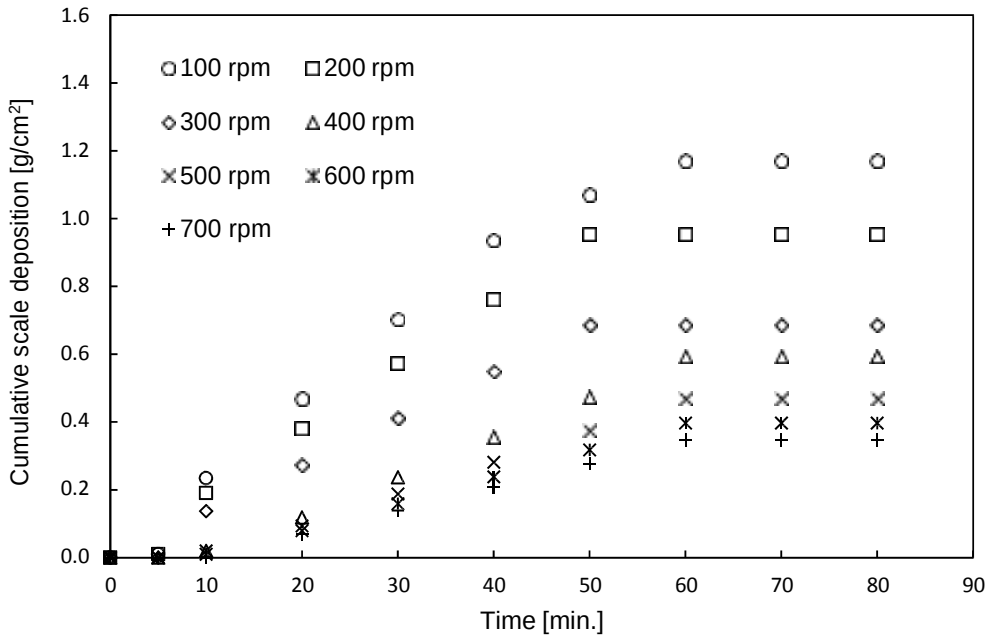
100 rpm
200 rpm
300 rpm
400 rpm
500 rpm
600 rpm
700 rpm
Cumulative scale deposition [g/cm²]
Time [min.]
0.0
0.2
0.4
0.6
0.8
1.0
1.2
1.4
1.6
0
10
20
30
40
50
60
70
80
90

(b)

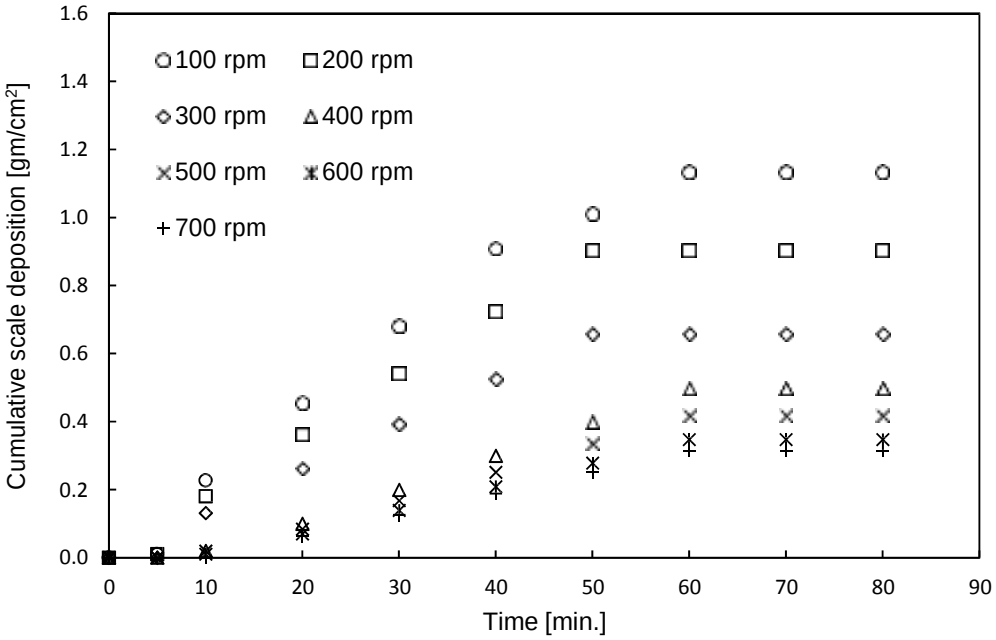
100 rpm
200 rpm
300 rpm
400 rpm
500 rpm
600 rpm
700 rpm
Cumulative scale deposition [gm/cm²]
Time [min.]
0.0
0.2
0.4
0.6
0.8
1.0
1.2
1.4
1.6
0
10
20
30
40
50
60
70
80
90

(c)

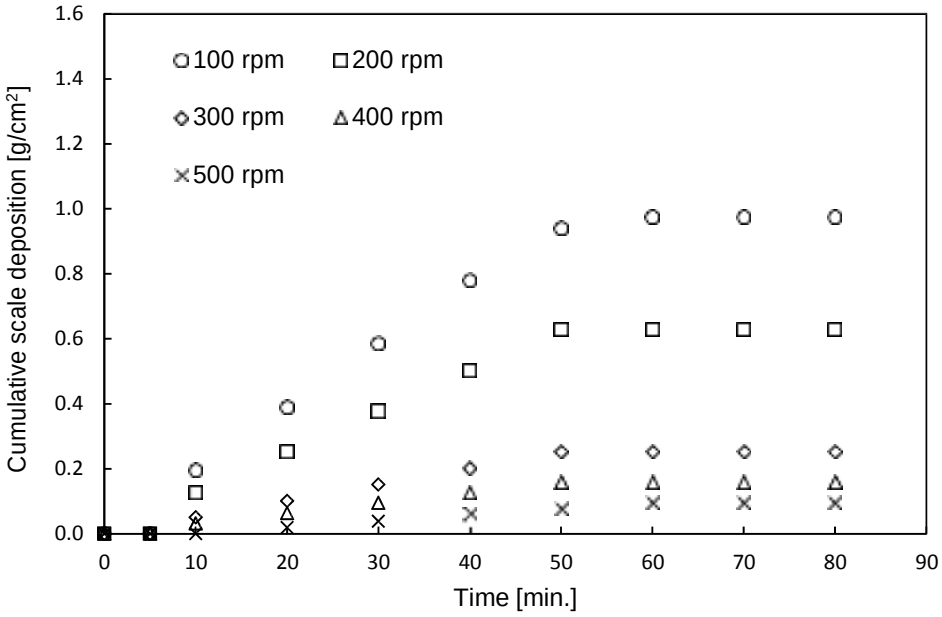

Figure 5.7: Deposition of KNO_3 as a function time, baffles and agitator speed. Experiments were performed at bulk temperature 48°C, ΔT=51.75°C, and KNO_3 C_b=4.75mol/dm^3: (a) impeller diameter of 86 mm, (b) impeller diameter of 114 mm, and (c) impeller diameter of 160 mm

(a)

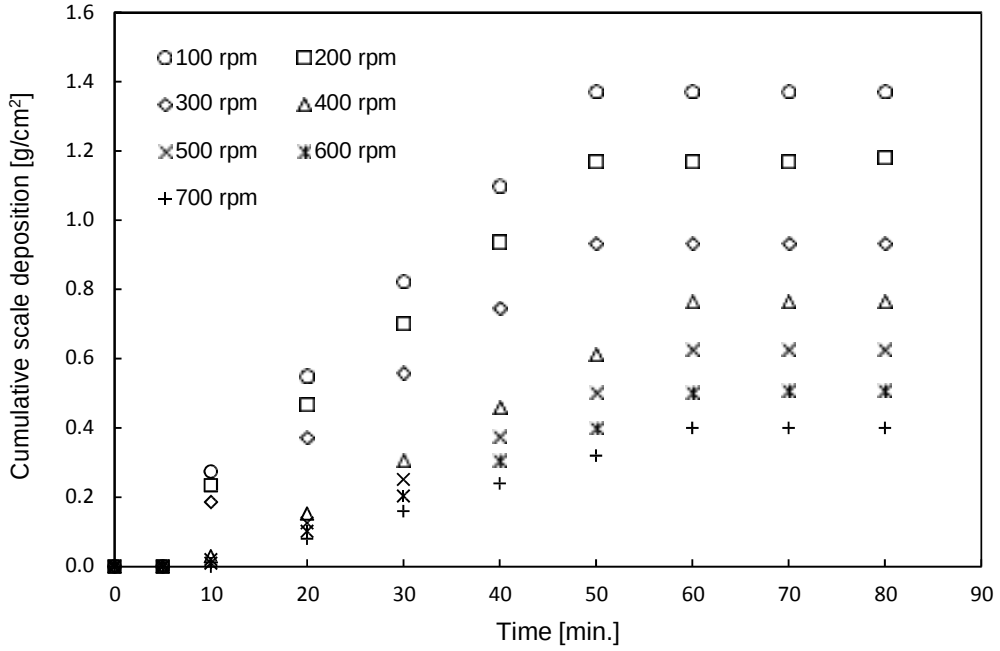

(b)

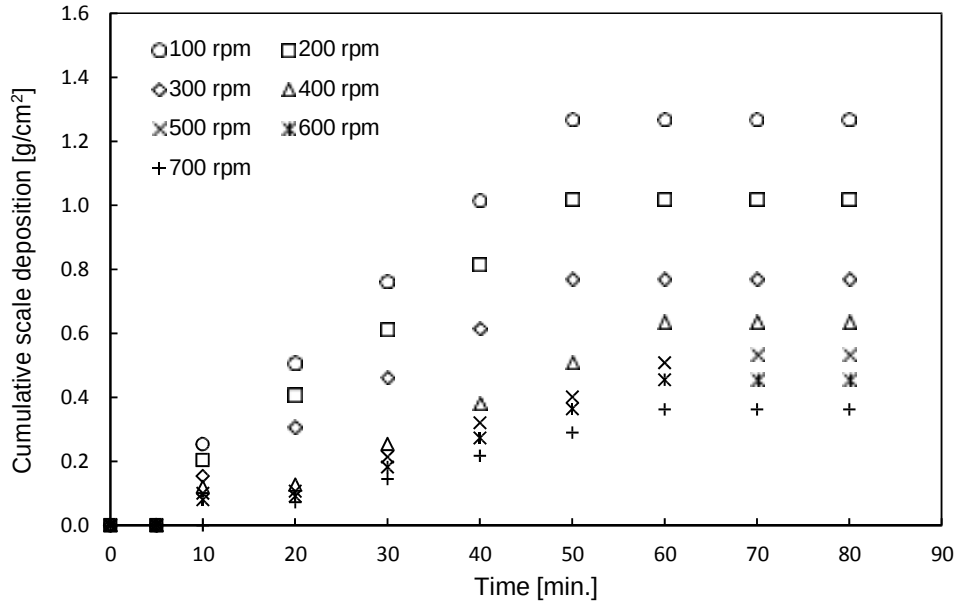

(c)

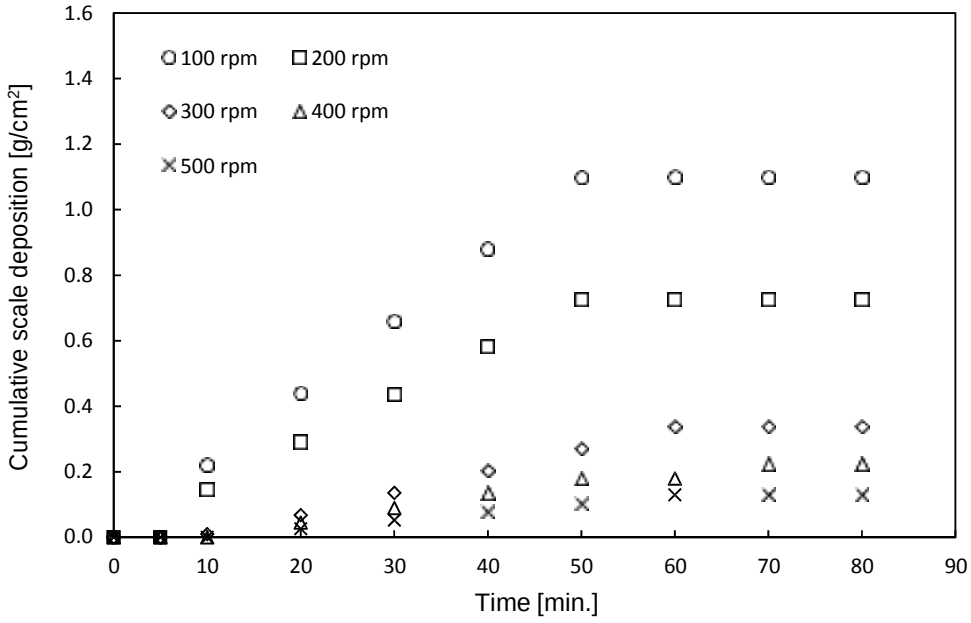

Figure 5.8: Deposition of KNO_3 as a function time, baffles and agitator speed. Experiments were performed at bulk temperature 48°C, ΔT=51.75°C, and KNO_3 C_b=5.25 mol/dm^3: (a) impeller diameter of 86 mm, (b) impeller diameter of 114 mm, and (c) impeller diameter of 160 mm

From Figures 5.6 (a, b, c), 5.7 (a, b, c) and 5.8 (a, b, c), it is evident that the scaling rate decreases with the increase in agitation speed from 100 to 700 rpm for all the impeller sizes. These results clearly show that the higher the agitation speed imposed, the more is the shear rate imposed on the scale deposition layer by axial flow impeller (Nawrath et al., 2006; Wu et al., 2012) and hence the higher agitation speed leads to lower scale growth rate.

5.5 Effects of Baffles on Scaling Rate

This section of the analysis reveals the effects of the presence or absence of four equally spaced baffles on the cumulative scale growth rate as shown in Figure 5.9 (a, b, c). For all the impeller sizes, the scale deposition rate is higher in a baffled tank in comparison to an unbaffled tank. This phenomenon can be explained by two reasons. Firstly, the baffles themselves act as nucleation sites as they provide more surface area. Secondly, the presence of baffles diminishes the effect of fluid erosion around the baffles because of lower flow velocity. On the other hand, the fluid erosion was distributed uniformly on the wall in the unbaffled tank and it was easier to wash off crystal deposits by the action of fluid erosion than in the baffled tank.

(a)

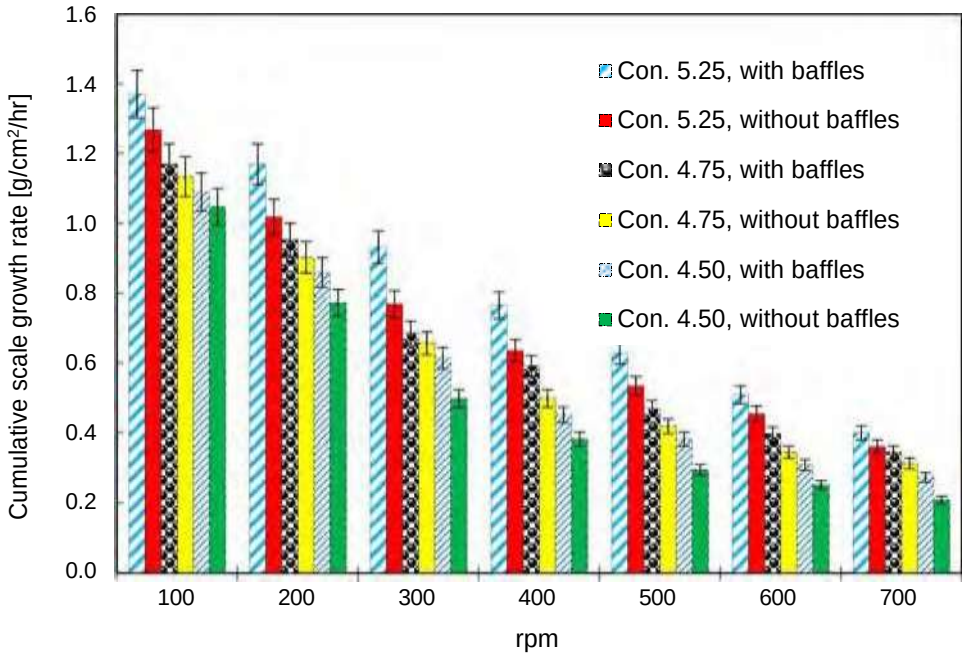

(b)

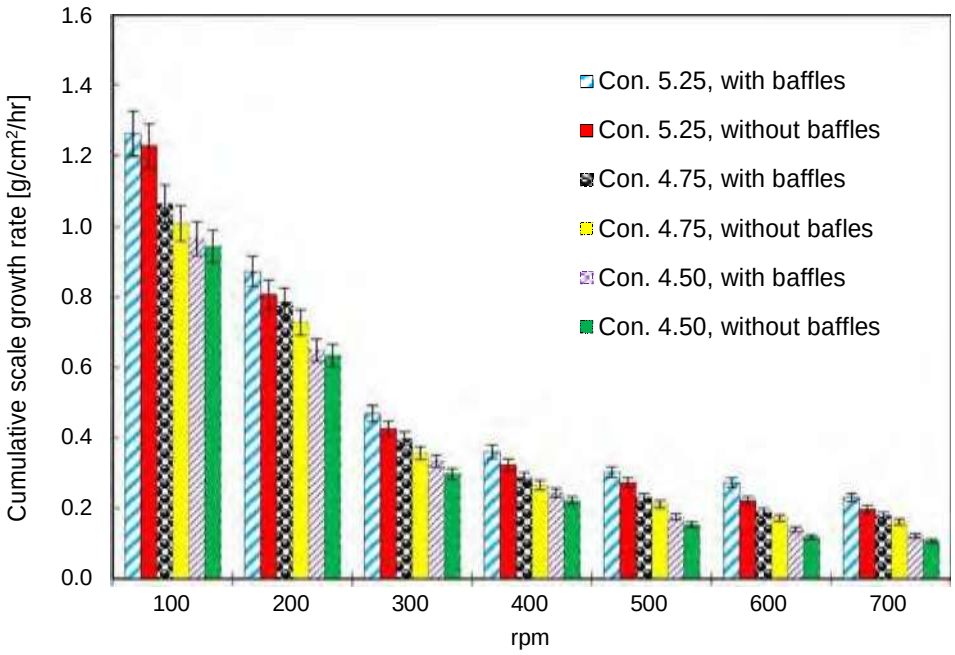

(c)

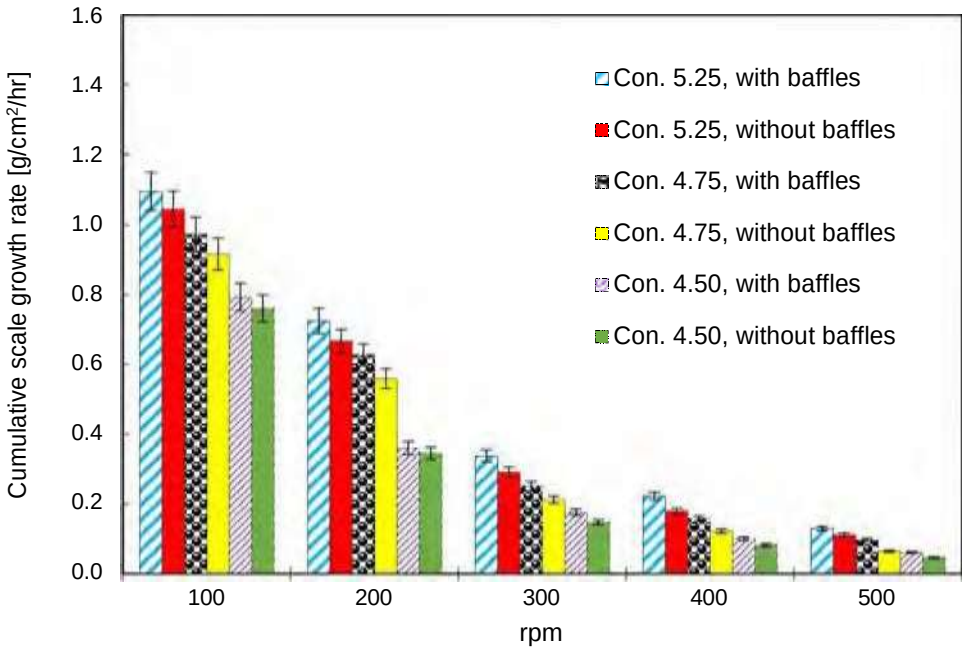

Figure 5.9: Effect of baffles on scale growth rate at bulk temperature 48°C, ΔT=51.75°C: (a) impeller diameter of 86 mm, (b) impeller diameter of 114 mm, and (c) impeller diameter of 160 mm

Figure 5.10 (a, b, c) shows the comparison of settled bottom scale growth rate as a function of agitation rate with and without the presence of baffles. Compared with the wall scale growth rates, the results exhibit opposite trends for settled scale growth rate showing increases with the increase of both agitation rate and the impeller sizes. Overall, these results reveal the favourable hydrodynamic effects of increasing the shear rate on crystalline scale deposit through increasing the agitation rate on the mitigation of wall scale growth with the consequence of increasing settled scale on the bottom of the agitation tank.

From Figure 5.10 (a, b, c), an increase of settled scale deposit with increasing of agitation rate and a lessening of wall scale growth can be discerned. For all the impeller sizes, the settled scale deposit is higher in an unbaffled tank in comparison to a baffled tank. This can be explained by the fact that the unbaffled tank creates a swirl flow that has the benefit of developing a uniformly higher shear rate on the wall in comparison with the baffled tank. It can be stated that settled scale increases with higher agitation speed (corresponding shear rate).

(a)

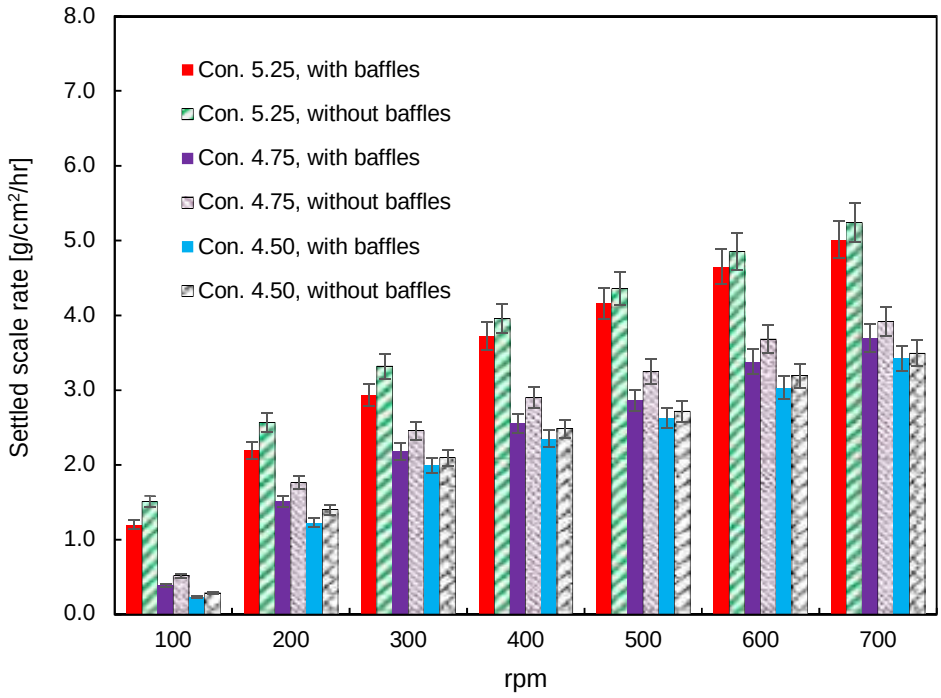

(b)

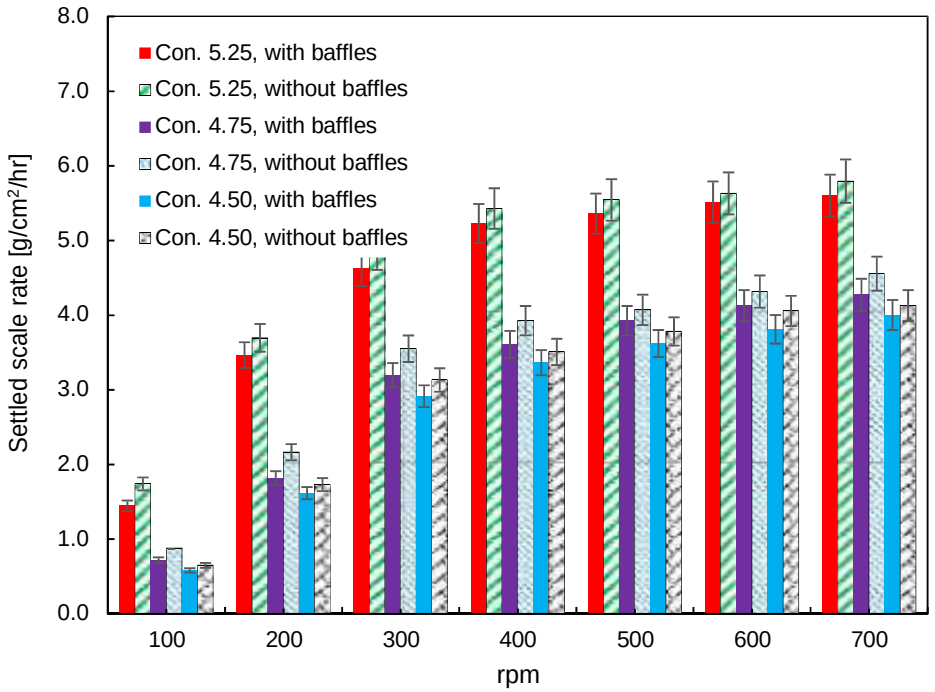

(c)

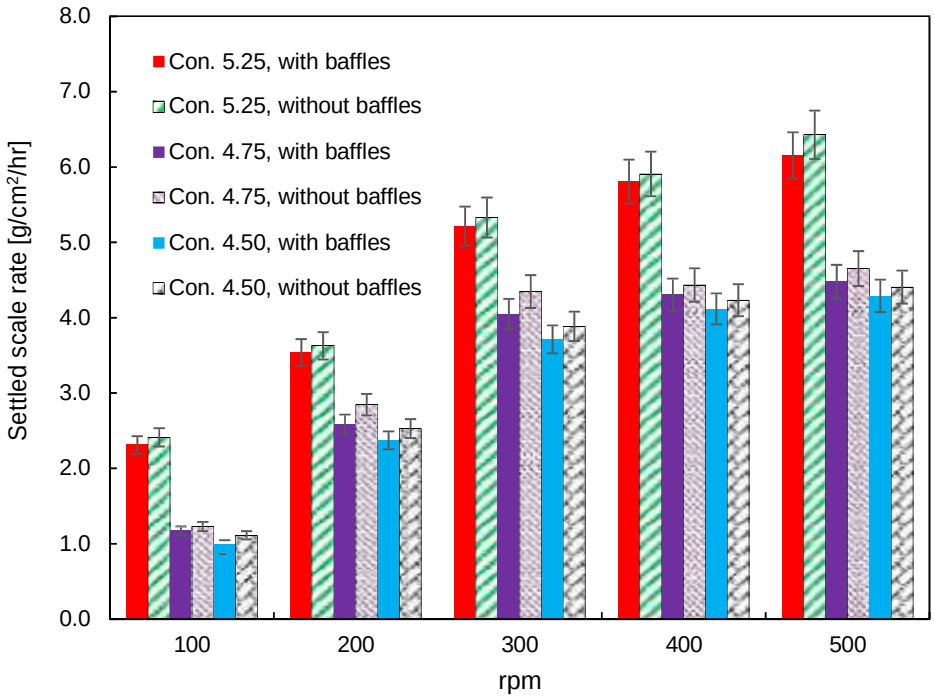

Figure 5.10: Bottom settled scale growth rate at bulk temperature 48°C, ΔT=51.75°C: (a) impeller diameter of 86 mm, (b) impeller diameter of 114 mm, and (c) impeller diameter of 160 mm

5.6 Comparison between Scale Growth on Wall and Settled Scale on Bottom

Figures 5.11 and 5.12 present simultaneous comparisons between scale growth on the wall and the settled scale on the bottom for the baffled and unbaffled tanks, respectively. In general, the growth of scale on the wall creates operational problems due to decreased heat transfer rate and the settled scale on the bottom creates a maintenance problem due to the difficulties with drain out. Figure 5.11(a) shows the results for the smaller impeller of diameter 86 mm. At lower agitation speed (for example, 100 rpm), the settled scale on the bottom is negligible compared to the scale growth on the wall at low concentration solutions. This result implies that negligible fluid erosion is applied on the wall scale layer by the low agitation speed (Wu et al., 2012). The accumulation of settled scale on the bottom is rapidly enhanced with the increase in fluid erosion imposed by the high agitation speed. It is discerned from Figures 5.11(b) and 5.11(c) that the settled scale on the bottom increases with the increasing impeller size (for example, 114 and 160mm). The comparison between scale growth on the wall and settled scale on the bottom with the condition of unbaffled tank indicates a similar trend as for a baffled tank as shown in Figure 5.12. This confirms that, in the unbaffled tank condition, settled scale deposit on the bottom is higher than scale growth on the wall due to the higher shear rate imposed on the wall because of the swirl flow created in the unbaffled tank.

(a)

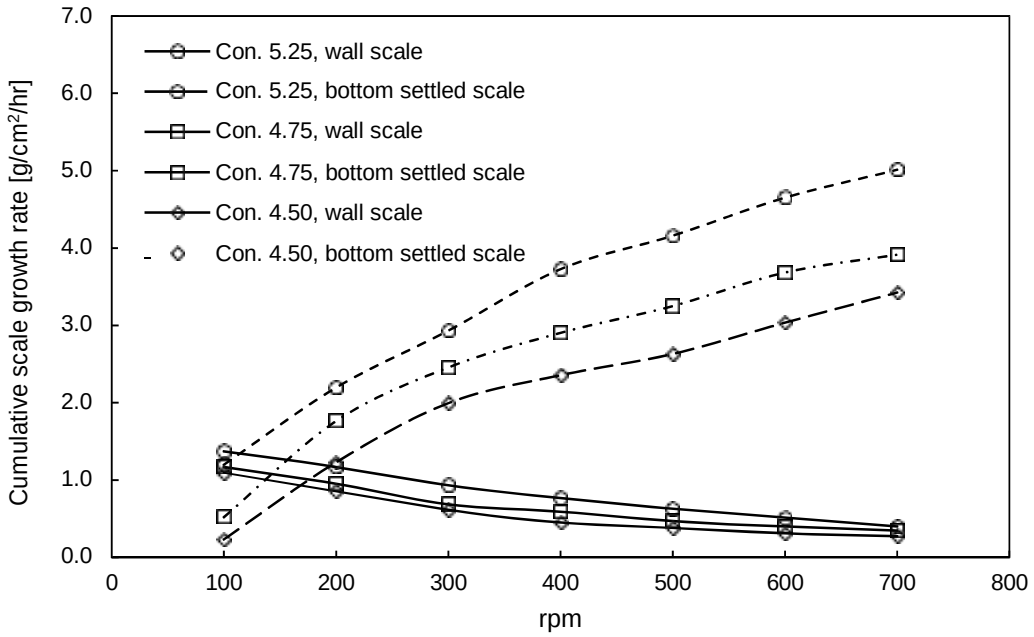

(b)

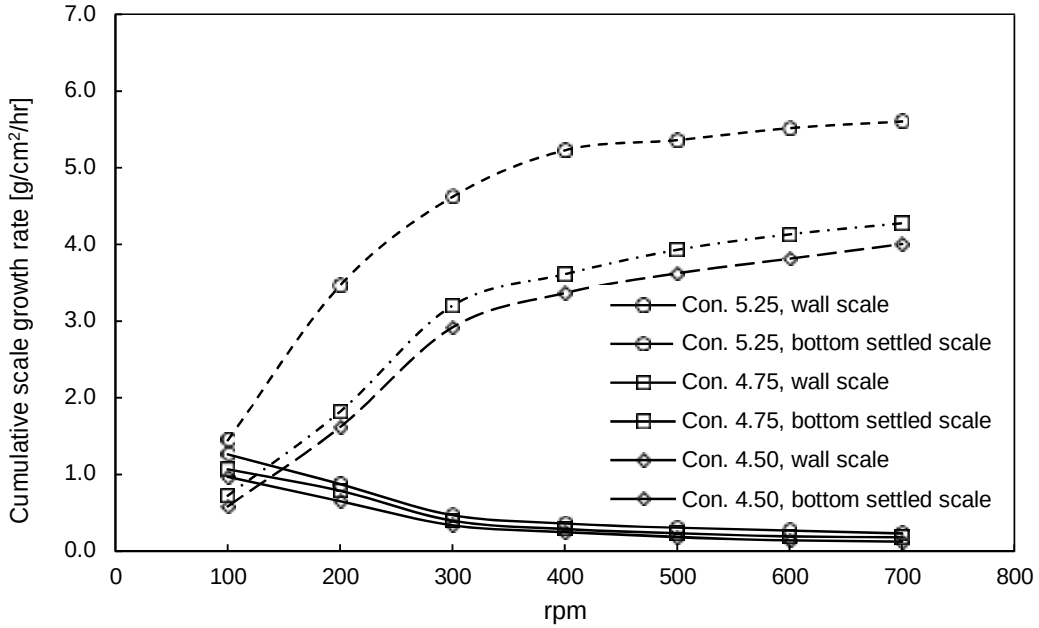

(c)

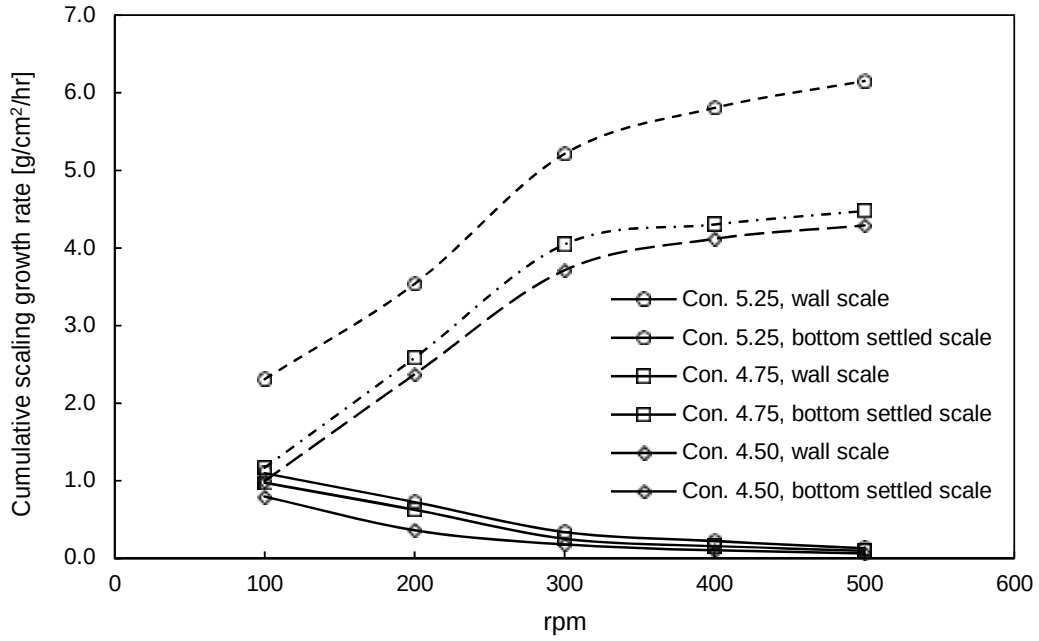

Figure 5.11: Comparison of bottom settled scale with wall scale growth at bulk temperature 48°C, ΔT=51.75°C: (a) impeller diameter of 86 mm, (b) impeller diameter of 114 mm, and (c) impeller diameter of 160 mm with baffles

(a)

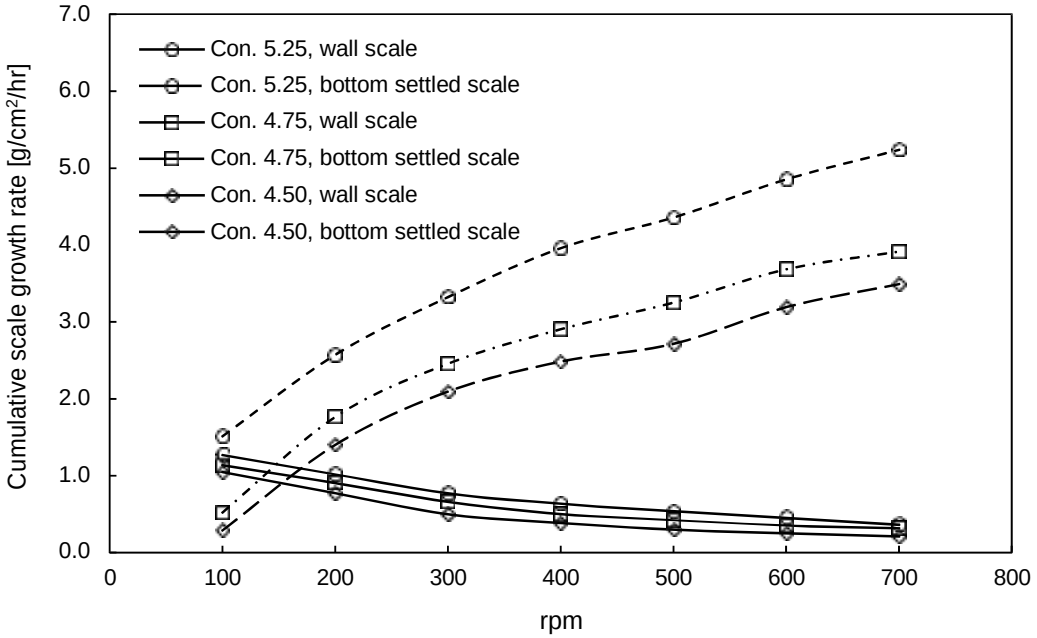
Cumulative scale growth rate [g/cm²/hr]
7.0
6.0
5.0
4.0
3.0
2.0
1.0
0.0
0
100
200
300
400
500
600
700
800
rpm
Con. 5.25, wall scale
Con. 5.25, bottom settled scale
Con. 4.75, wall scale
Con. 4.75, bottom settled scale
Con. 4.50, wall scale
Con. 4.50, bottom settled scale

(b)

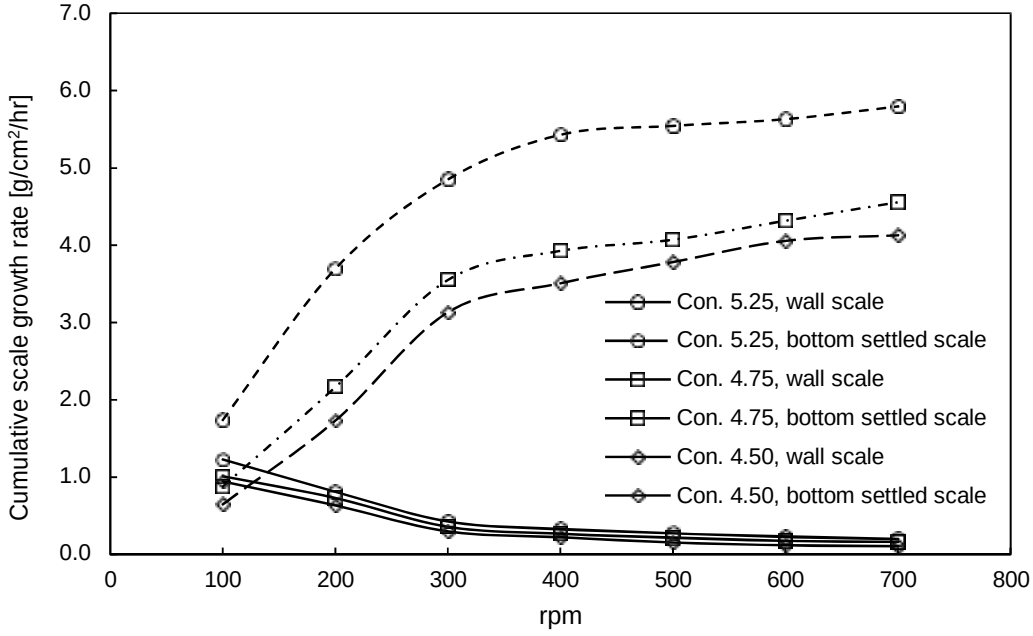
Cumulative scale growth rate [g/cm²/hr]
7.0
6.0
5.0
4.0
3.0
2.0
1.0
0.0
0
100
200
300
400
500
600
700
800
rpm
Con. 5.25, wall scale
Con. 5.25, bottom settled scale
Con. 4.75, wall scale
Con. 4.75, bottom settled scale
Con. 4.50, wall scale
Con. 4.50, bottom settled scale

(c)

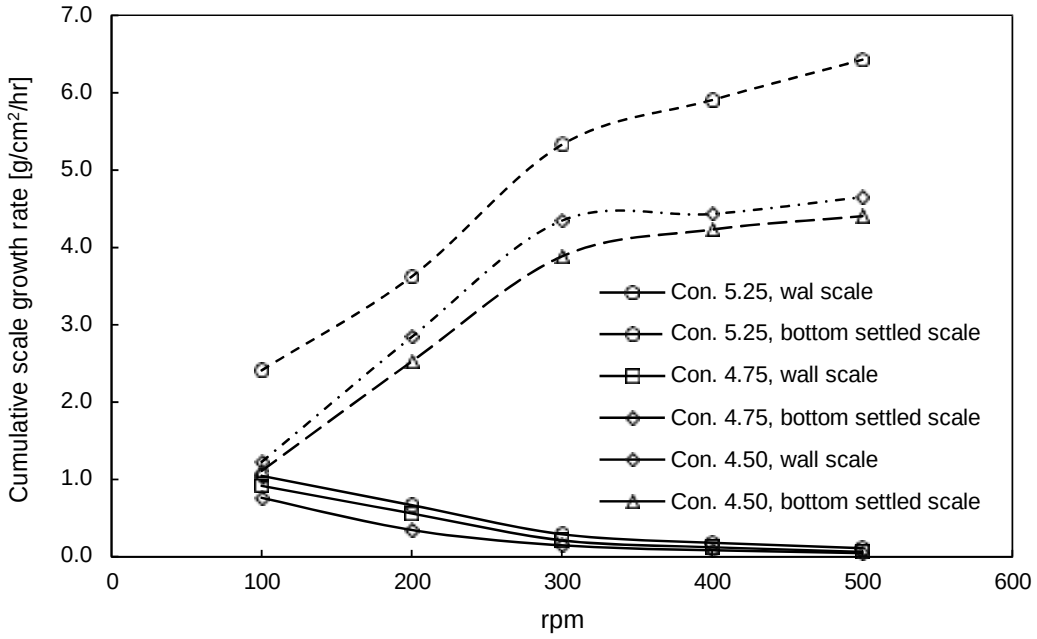

Figure 5.12: Comparison of bottom settled scale with wall scale growth at bulk temperature 48°C, ΔT=51.75°C: (a) impeller diameter of 86 mm, (b) impeller diameter of 114 mm, and (c) impeller diameter of 160 mm without baffles

5.7 Summary

This chapter reveals the effects of hydrodynamics on the scale growth (wall and bottom) and their suppression or mitigation. It was found that supersaturation was the main driving force for crystallisation scale deposition. It is seen that a higher agitation rate suppressed the scale deposit on the agitation tank wall and a lower agitation rate enhanced the scale deposit. Growth of scale deposit on the wall was also suppressed by the application of the higher shear rate created with an increase of impeller size. The unbaffled tank had the benefit in the mitigation of scale deposit on the wall because of the more uniform shear rate with the condition of swirl flow against the tank wall in comparison with the baffled tank. All of the above three conditions were found not beneficial to the settled scale deposit which increased under these conditions. It is significant to design the agitation tank to mitigate or suppress the scale deposit through consideration of these hydrodynamics effects.

CHAPTER 6
HYDRODYNAMIC EFFECTS ON HEAT TRANSFER

This chapter presents the hydrodynamic effects on the heat transfer characteristics in the agitation tank due to scale formation of normal soluble salt on the wall. The scale formation on the heat transfer surfaces reduces the efficiency of process equipment because the scale deposit material has low thermal conductivity which creates a major resistance to heat transfer. This experimental investigation has focused on the effect of surface crystallisation of potassium nitrate on the heat exchange surfaces on the wall of the agitation tank. The crystallisation scale rate on the wall of the agitation tank was found to be controlled by the wall temperature and supersaturation ratio, indicating that surface integration (or surface reaction or activation control) governs the scale growth process. The impeller agitation rate affects the scaling rate on the agitation wall, and it shows a decreasing scaling rate with an increasing agitation rate. It was observed that there was a significant variation of overall heat transfer coefficients (OHTCs) and scaling thermal resistance (TR) coefficients with different agitation rates (100 to 700 rpm), with varying impeller diameter (86, 114 and 160 mm), for the tank with and without baffles, and for various solution concentrations (4.50, 4.75 and 5.25 mol/dm^3). The following sections discuss the hydrodynamic effects on the heat transfer rate and thermal resistance.

6.1 Experimental Procedure and Data Collection

The experimental procedure was explained in the previous Chapter 5 in section 5.1. The experiment procedure is the same since the heat transfer data were collected from the same experiment under different experimental conditions. The overall heat transfer coefficients (OHTC) and the thermal resistance (TR) were calculated from the relevant experimental data on the basis of the average temperatures of agitation tank wall and the bulk solution. The heat transfer values were calculated and a single representative case has been presented here and the other results and data are presented in Appendix C. The values of heat transfer coefficient of solution side, h_i and heat transfer coefficient of coolant side, h_o were calculated using the empirical Eqs. (3.41) and (3.42) respectively, which were presented in Chapter 4. Table 6.1 shows the values of h_i and h_o for concentration of 4.50 mol/dm^3, at different impeller

diameters and baffled tank conditions. The value of h_i increases with increase of agitation speed (corresponding Reynolds number) and for bigger impeller sizes while the value of h_o remain constant.

Table 6.1: Values of h_i [W/m^2.K] and h_o[W/m^2.K] at KNO_3 concentration of 4.75 mol/dm^3 and baffled tank and clean condition

	rpm	86 mm	114 mm	160 mm
h_i	100	1639.815	2392.32084	3767.799
	200	2603.829	3798.71773	5982.811
	300	3418.887	4987.80298	7855.568
	400	4147.049	6050.11593	9528.663
	500	4812.901	7021.52649	11058.59
	600	5439.698	7935.95849	12498.78
	700	6032.708	8801.09809	13861.34
h_o	157.2857			

Table 6.2 presents the values of thermal resistance $R_{Overall}$ and overall heat transfercoefficient $U_{Overall}$ at clean condition based on the Eqs. (4.35) and (4.36) respectively, discussed in Chapter 4.

Table 6.2: Values of $R_{Overall}$ [m^2.K/W] and $U_{Overall}$ [W/m^2.K] at clean condition

	rpm	86 mm	114 mm	160 mm
$R_{Overall}$	100	0.050495883	0.049110635	0.048008644
	200	0.048865432	0.047993044	0.047299042
	300	0.048204247	0.047539835	0.047011283
	400	0.047833365	0.047285614	0.046849868
	500	0.04759245	0.047120479	0.046745017
	600	0.047419558	0.04700197	0.046669771
	700	0.047289059	0.04691252	0.046612976
	rpm	86 mm	114 mm	160 mm

$U_{Overall}$	100	143.0130851	147.047008	150.4223284
	200	147.7848862	150.4712294	152.6790399
	300	149.8119514	151.9057086	153.6136006
	400	150.9735374	152.7223969	154.1428547
	500	151.737772	153.2576169	154.4886023
	600	152.2910113	153.6440357	154.7376857
	700	152.7112731	153.936996	154.9262254

The values of overall heat transfer coefficient at scaled condition $U_{Overall-Scale}$ and overall thermal resistance at scaledcondition $R_{Overall-Scale}$ vary asymptotically with time; these values are shown in Table 6.3 and calculations based on the Eqs. (4.37) and (4.38) respectively, as discussed in details in Chapter 4. The value of $R_{Overall-Scale}$ increases with time asymptotically due to the growth of scale and the value of $U_{Overall-Scale}$ decreases due to the thermalresistance of scale deposit layer.

Table 6.3: Values of $U_{Overall-Scale}$[W/m^2.K] and $R_{Overall-Scale}$[m^2.K/W] at KNO_3 concentration of 4.75 mol/dm^3, rpm 100 and baffled tank condition

Time [Sec]	Scale thickness [mm]	R_{scale} [m^2.K/W]	$R_{Overall-Scale}$ [m^2.K/W]	$U_{Overall-Scale}$ [W/m^2.K]
0	0	0	0.050495883	143.0131089
1	0	0	0.050495883	143.0131089
2	0	0	0.050495883	143.0131089
3	0.04	0.000459454	0.050955337	141.7235891
4	0.08	0.000919083	0.051414966	140.4566378
5	0.867	0.009998097	0.06049398	119.3767223
6	1.734	0.020079786	0.070575669	102.3238325
7	2.601	0.030246477	0.08074236	89.43970525
8	3.468	0.040499615	0.090995498	79.36186937
9	4.335	0.050840682	0.101336565	71.26324757
10	5.202	0.061271201	0.111767084	64.61269663
12	6.069	0.071792732	0.122288615	59.05351582
15	6.936	0.082406877	0.13290276	54.33726594

20	7.803	0.093115282	0.143611165	50.2855931
25	8.67	0.103919635	0.154415518	46.7671428
30	9.537	0.114821672	0.165317555	43.68303524
35	10.404	0.125823174	0.176319057	40.9574136
40	11.271	0.136925974	0.187421857	38.53111179
45	12.138	0.148131955	0.198627838	36.3573032
50	12.6	0.154146113	0.204641996	35.28880998
55	12.9	0.158067535	0.208563418	34.6253076
60	13	0.159377515	0.209873398	34.40918467
70	13	0.159377515	0.209873398	34.40918467
80	13	0.159377515	0.209873398	34.40918467

6.2 Tank Wall Surface Temperature and Bulk Solution Temperature

Figure 6.1 shows the variation of bulk solution temperature as a function of experiment run time for the KNO_3 concentration of 4.75 mol/dm^3, impeller diameter of 114 mm and different agitation speeds of 100, 300, 500 and 700 rpm.

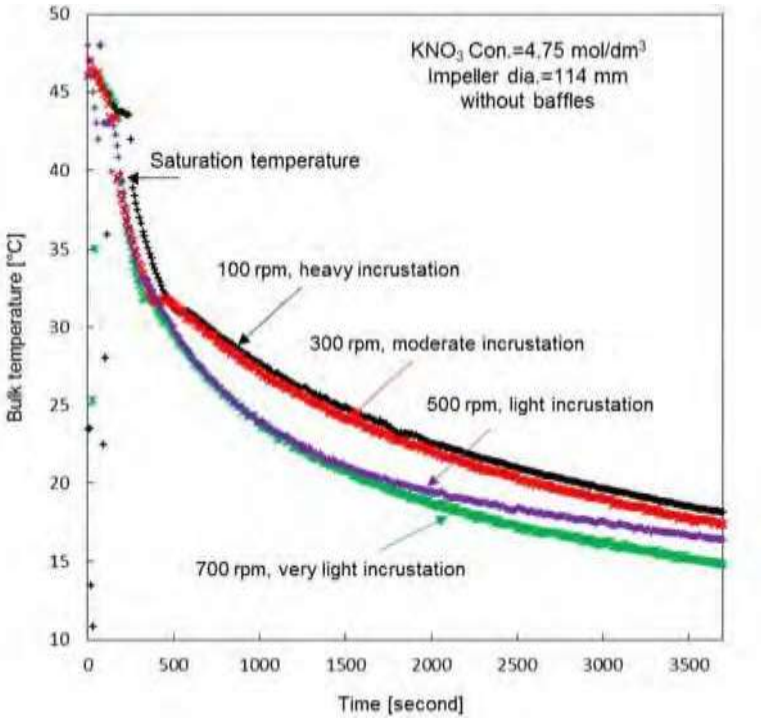

Figure 6.1: Variation of bulk solution temperature as a function of run time at different agitationrates

It is seen from the results that the bulk solution temperature decreases appreciably with time at increasing agitation speeds. The intense agitation increases the heat transfer flux between external jacket coolant and bulk solution and diminishes the temperature difference between the tank wall and bulk solution. Figure 6.2 compares the effects of agitation rate on local wall temperature and KNO_3 scale deposition. Higher deposition rates occur at lower wall temperatures in the case of normal solubility salt. At the lowest agitation rate (100 rpm), heavy crystalline scale deposits grew on the low-temperature agitation wall. It is evident that heavy encrustation rapidly occurs as soon as the saturation temperature has been passed. The moderate agitation speed (300 rpm) appeared to be fairly efficient at agitation of the bulk solution, allowing only the large crystalline scale deposits to settle on the bottom.

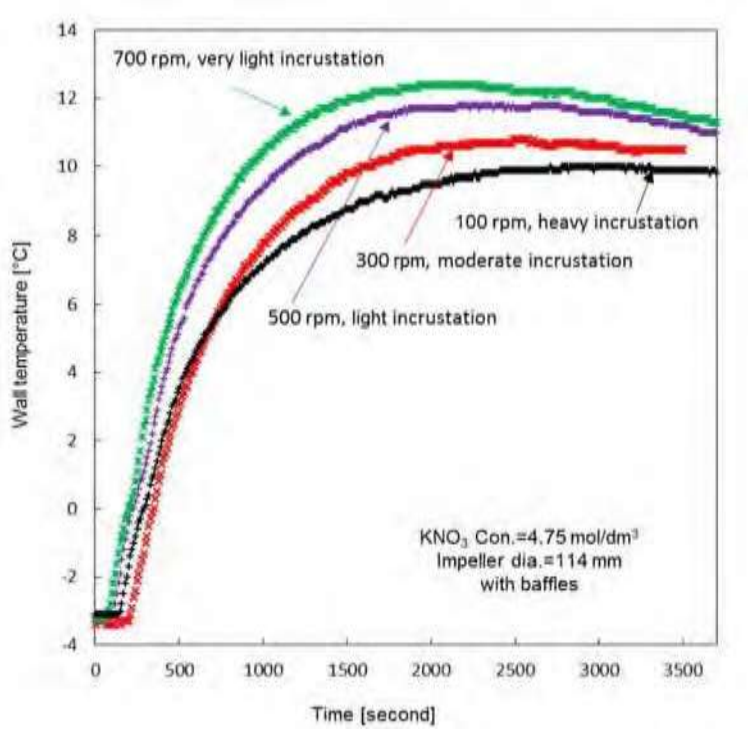

Figure 6.2: Variation of tank wall temperature as a function of run time at different agitation rates

It can be seen that this degree of agitation prevented immediate encrustation, but light encrustation of crystal deposit eventually clings to the tank wall due to lower agitation. It can be concluded that this degree of agitation prevented immediate encrustation, but eventually moderate or light (300 and 500 rpm respectively) encrustation occurred. The higher agitation rates (500 rpm and 700 rpm) can be described as strong bulk agitation of the scale solution as it increased the wall temperature more rapidly than other lower and moderate agitation cases (100 rpm and 300 rpm). At these conditions, all crystals were kept suspended in the solution, while very light encrustation (sometimes no encrustation) took place on the wall, and most of the suspended crystals settled down on the bottom of the tank during the of scale experiment.

6.3 Hydrodynamic Effects on Overall Heat Transfer Coefficient (OHTC)

The plots of variation of average OHTC, $U_{overall}$ with time for agitation speeds from 100 to 700 rpm, at bulk temperature 48°C, ΔT=51.75°C, $C_b = 4.50$ mol/dm ^{3} both with baffles and without baffles are presented in Figures 6.3 and 6.4 respectively. Table 6.4 sets out the percentage reduction of OHTC due to the the level of scale deposition that occurs on the tank wall after 80 minutes under different agitation intensities with the conditions of KNO_3 concentration of

4.5 mol/dm^3 and the impeller diameters of 86 mm, 114 mm and 160 mm compared with the OHTC for a clean tank wall. In all cases, the OHTC of the process solution of heat flux through the coolant in the external jacket and into the bulk solution in the agitation tank decreases asymptotically with time by 75% to 38% for the impeller diameter of 86 mm, 73% to 23% for impeller diameter of 14 mm and 72% to 2.6% for the impeller diameter of 160 mm depending on the agitation intensity affecting scale deposition on the wall with the baffled tank condition. In the case of the unbaffled condition, OHTC decreases by 70% to 29% for the impeller diameter of 86 mm, 64% to 19% for the impeller diameter of 114 mm and 55% to 0.6% for the impeller diameter of 160 mm. The implication is that light bulk agitation (100, 200 and 300 rpm) allows heavier crystallisation encrustation on the tank wall compared with strong agitation (600 and 700 rpm). It can be seen that, for all cases, OHTC reduction with the baffled condition is greater than with the unbaffled condition. It is revealed that lesser scale deposit occurs in the unbaffled condition compared with the baffled condition due to the creation of swirl flow condition.

Table 6.4: Reduction of OHTC (U_{ovrd}) for KNO_3 concentration of 4.5 mol/dm^3 for various impeller sizes and speeds at time 80 min

rpm	Impeller dia. 86 mm		Impeller dia. 114 mm		Impeller dia. 160 mm	
	With baffles	Without baffles	With baffles	Without baffles	With baffles	Without baffles
100	75.9%	70.5%	73.1%	64.5%	72%	55.3%
200	60.4%	59.1%	55.3%	54%	50.1%	32.8%
300	56.1%	54.9%	49.1%	48.3%	13.1%	11.1%
400	54.1%	51%	46.7%	43.4%	9.1%	5.2%
500	51.4%	48%	43.7%	41.2%	2.6%	0.6%
600	44%	34.5%	38.5%	28.1%	-	-
700	38%	29.9%	23.5%	19.6%	-	-

(a)

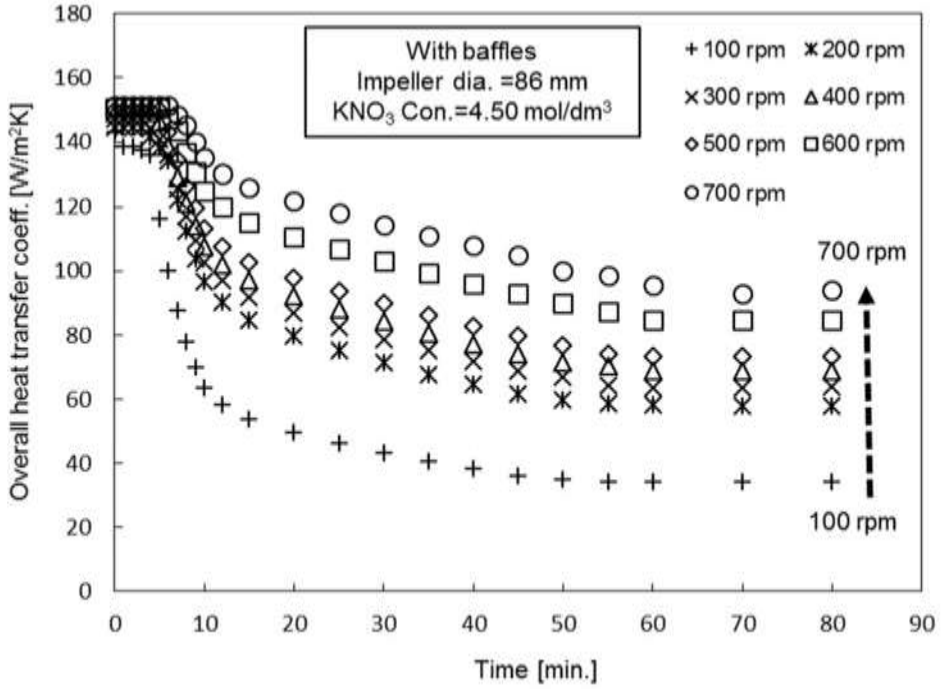
With baffles
Impeller dia. =86 mm
KNO3 Con.=4.50 mol/dm3
100 rpm
200 rpm
300 rpm
400 rpm
500 rpm
600 rpm
700 rpm
700 rpm
100 rpm
Overall heat transfer coeff. [W/m2K]
Time [min.]

(b)

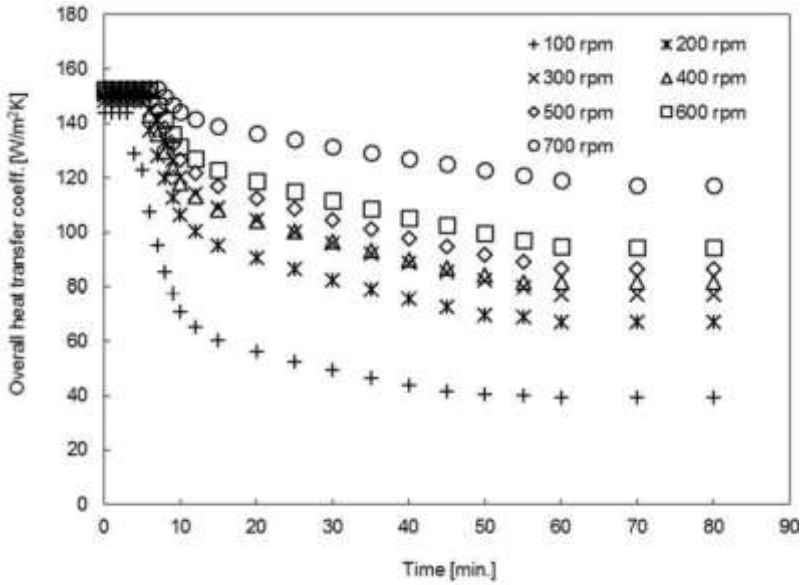
100 rpm
200 rpm
300 rpm
400 rpm
500 rpm
600 rpm
700 rpm
Overall heat transfer coeff. [W/m2K]
Time [min.]

(c)

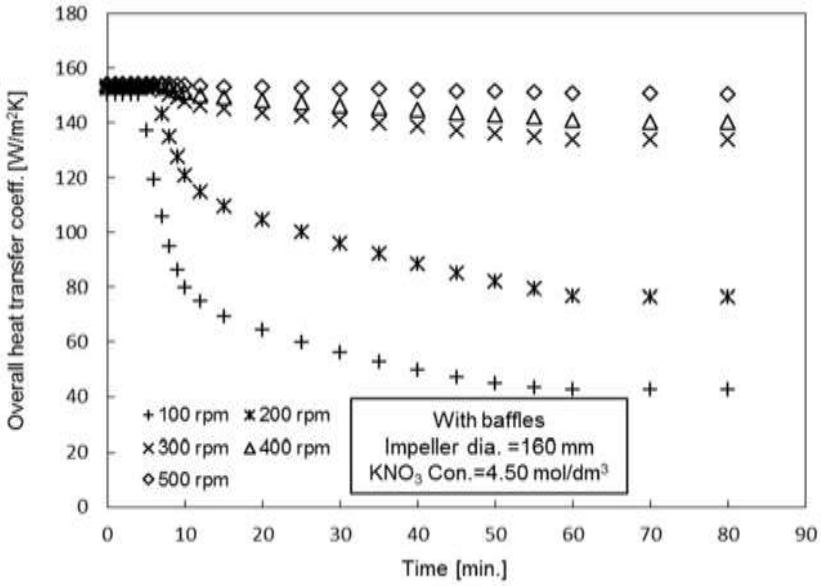

Figure 6.3: Variation of overall heat transfer coefficient (OHTC) with time at different agitation rates for KNO_3 concentration of 4.50 mol/dm^3 and with baffles: (a) impeller diameter of 86 mm, (b) impeller diameter of 114 mm, and (c) impeller diameter of 160 mm

(a)

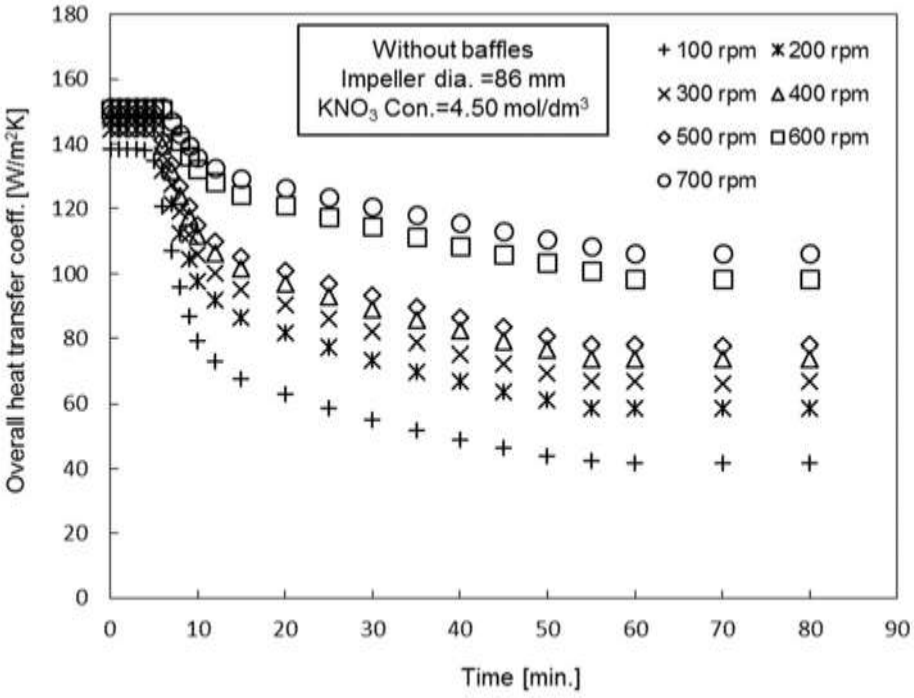
Without baffles
Impeller dia. =86 mm
KNO3 Con.=4.50 mol/dm3
+ 100 rpm
* 200 rpm
× 300 rpm
△ 400 rpm
◇ 500 rpm
□ 600 rpm
○ 700 rpm
Overall heat transfer coeff. [W/m2K]
Time [min.]

(b)

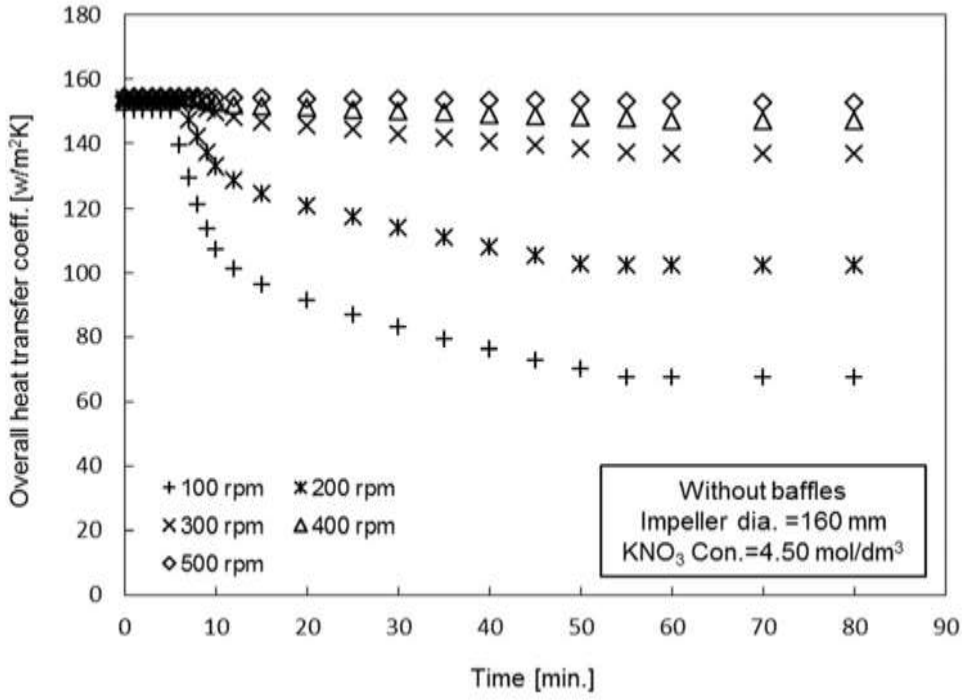
+ 100 rpm
* 200 rpm
× 300 rpm
△ 400 rpm
◇ 500 rpm
Without baffles
Impeller dia. =160 mm
KNO3 Con.=4.50 mol/dm3
Overall heat transfer coeff. [w/m2K]
Time [min.]

(c)

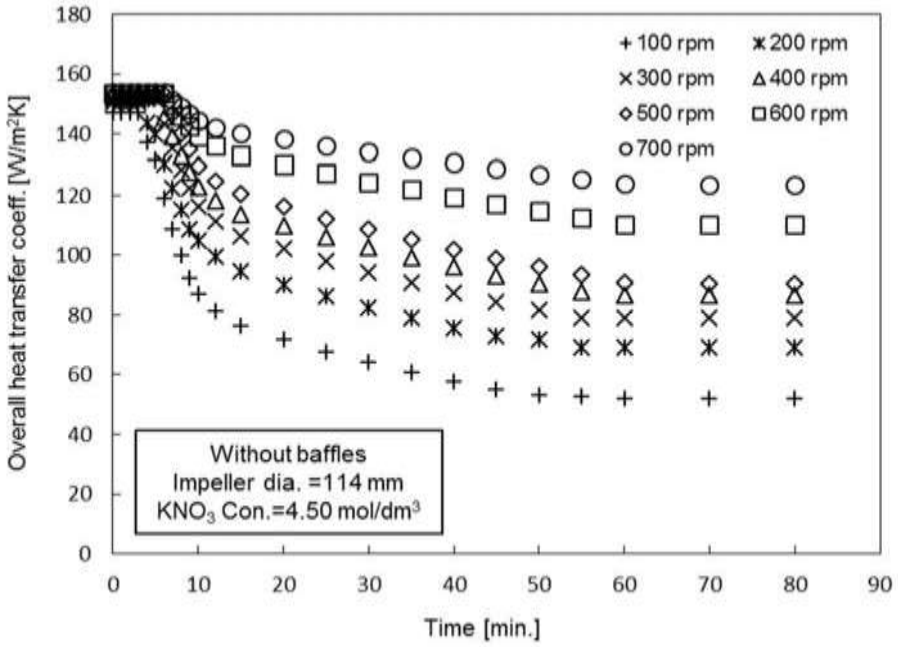

Figure 6.4: Variation of overall heat transfer coefficient (OHTC) with time at different agitation rates for KNO_3 concentration of 4.50 mol/dm^3 and without baffles: (a) impeller diameter of 86 mm, (b) impeller diameter of 114 mm, and (c) impeller diameter of 160 mm

The plots of variation of average OHTC, $U_{overall}$ with time for agitation speeds from 100 to 700 rpm, at bulk temperature 48°C, ΔT=51.75°C, C_b=4.75 mol/m^{3}both with baffles and without baffles are presented in Figures 6.5 and 6.6 respectively. Table 6.8 sets out the percentage reduction of OHTC due to the level of scale deposition that occurs on the tank wall after 80 minutes under different agitation intensities with the conditions of KNO_3 concentration of 4.75 mol/dm^3 and the impeller diameters of 86 mm, 114 mm and 160 mm compared with the OHTC for a clean tank condition. The OHTC decreases asymptotically with time by 79% to 40% for the impeller diameter of 86 mm, 74% to 30% for the impeller diameter of 114 mm and 72% to 3.8% for the impeller diameter of 160 mm depending on agitation intensity due to crystallisation scale deposition on the wall with the baffled tank condition. In the case of the unbaffled condition, OHTC decreases by 74% to 36% for the impeller diameter of 86 mm, 66% to 26% for the impeller diameter of 114 mm and 63% to 2.6% for the impeller diameter of 160 mm.

Table 6.5: Reduction of OHTC ($U_{overall}$) at KNO_3 concentration of 4.75 mol/dm^3 for various impeller sizes and speeds at time 80 min

rpm	Impeller dia. 86 mm		Impeller dia. 114 mm		Impeller dia. 160 mm	
	With baffles	Without baffles	With baffles	Without baffles	With baffles	Without baffles
100	79.1%	74.8%	74.1%	66.7%	72.6%	63.3%
200	64.6%	64.6%	58%	56%	52.6%	46.7%
300	61.7%	57.7%	54.3%	51.6%	15.6%	13.1%
400	58.6%	54.6%	50.6%	46.7%	10.3%	9.1%
500	55.6%	50.9%	46.4%	43.7%	3.8%	2.6%
600	46.7%	42.8%	42.4%	35.3%	-	-
700	40.7%	36.8%	30.7%	26.8%	-	-

(a)

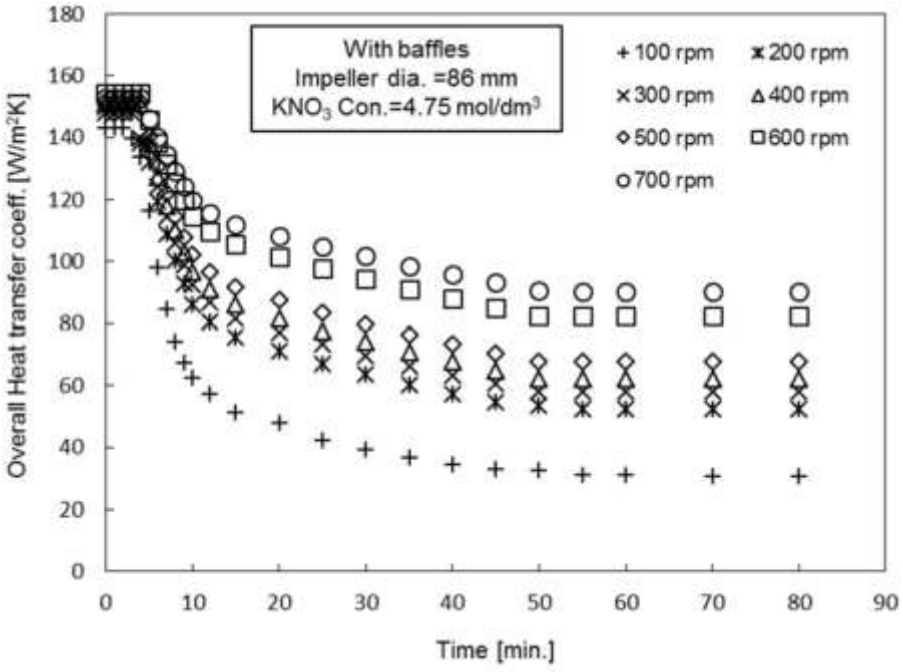

(b)

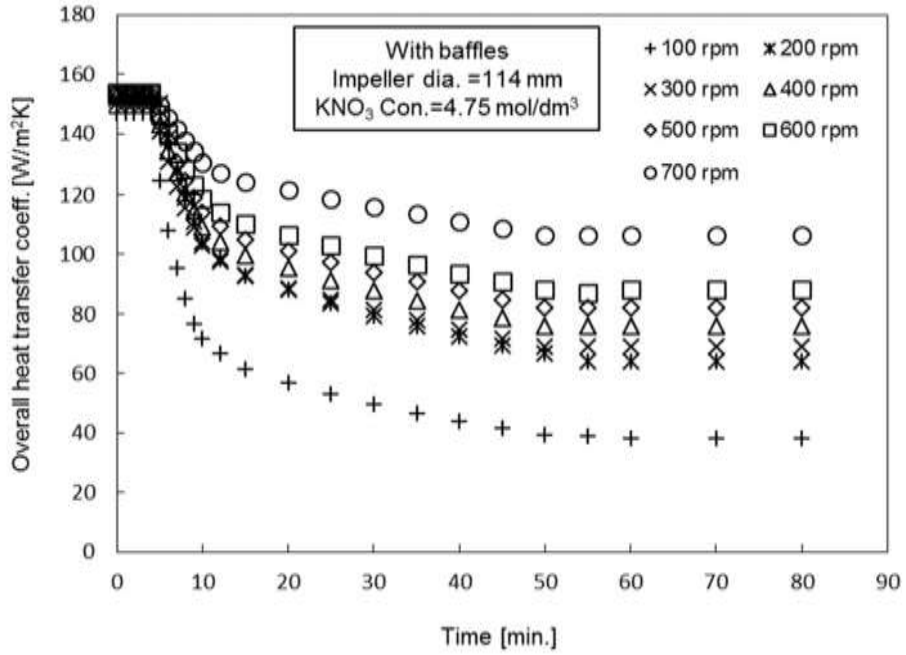

(c)

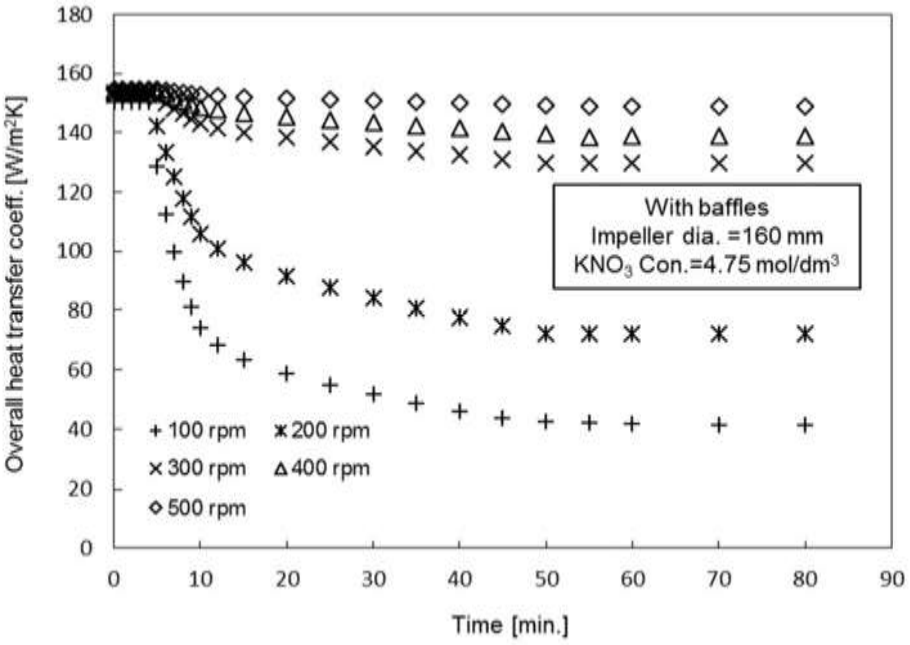

Figure 6.5: Variation of overall heat transfer coefficient (OHTC) with time at different agitation rates for KNO_3 concentration of 4.75 mol/dm^3 and with baffles: (a) impeller diameter of 86 mm, (b) impeller diameter of 114 mm, and (c) impeller diameter of 160 mm

(a)

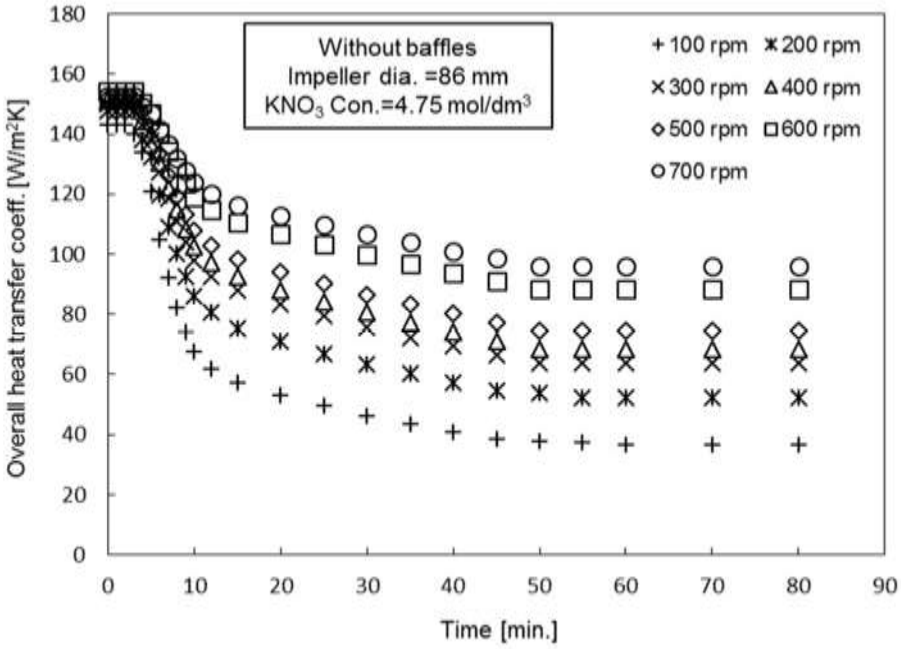
Without baffles
Impeller dia. =86 mm
KNO3 Con.=4.75 mol/dm3
100 rpm
200 rpm
300 rpm
400 rpm
500 rpm
600 rpm
700 rpm
Overall heat transfer coeff. [W/m2K]
Time [min.]

(b)

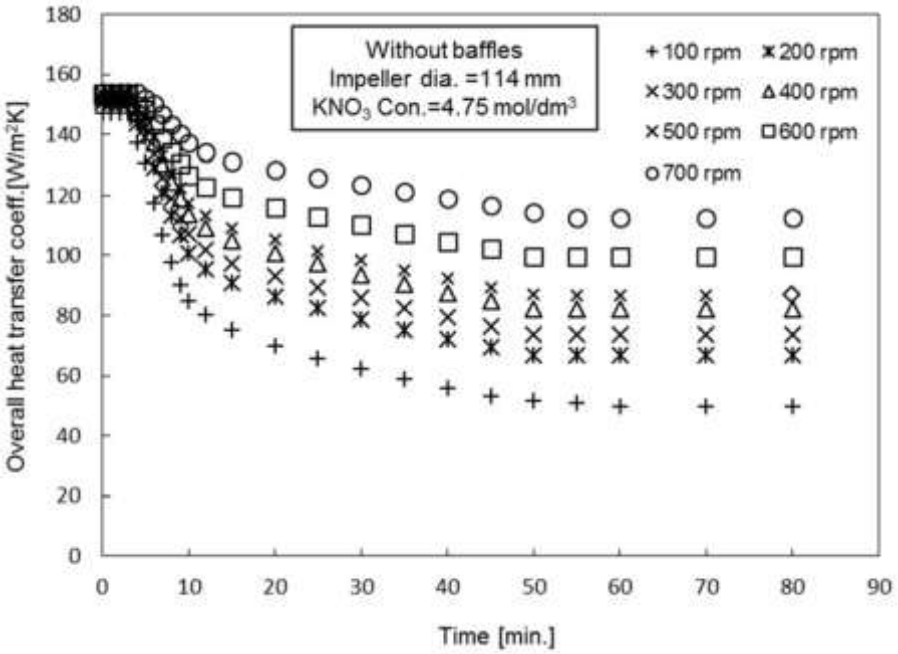
Without baffles
Impeller dia. =114 mm
KNO3 Con.=4.75 mol/dm3
100 rpm
200 rpm
300 rpm
400 rpm
500 rpm
600 rpm
700 rpm
Overall heat transfer coeff.[W/m2K]
Time [min.]

(c)

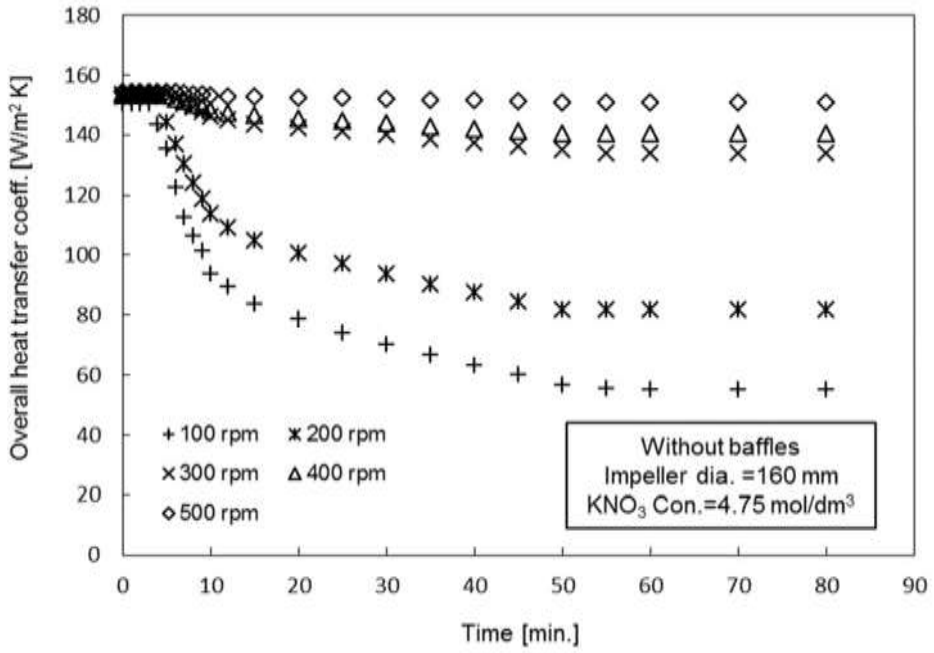

Figure 6.6: Variation of overall heat transfer coefficient (OHTC) with time at different agitation rates for KNO_3 concentration of 4.75 mol/dm^3 and without baffles: (a) impeller diameter of 86 mm, (b) impeller diameter of 114 mm, and (c) impeller diameter of 160 mm

Table 6.9 sets out the percentage reductions of OHTC magnitude due to the level of scale deposition that occurs on the tank wall after 80 minutes for different agitation intensities with the conditions of KNO_3 concentration of 4.5 mol/dm^3 and impeller diameters of 86 mm, 114 mm, and 160 mm with the baffled and unbaffled tanks compared with the OHTC for a clean tank. The plots of variation of average OHTC, $U_{overall}$ with time for agitation speeds from 100 to 700 rpm, at bulk temperature 48°C, ΔT=51.75°C, $C_b = 4.25\,mol/dm^3$ both with baffles and without baffles are presented in Figures 6.7 and 6.8 respectively. In all cases, the OHTC of the process solution of heat flux through the coolant in the external jacket and into the bulk solution in the agitation tank decreases asymptotically with time by 80% to 46% for the impeller diameter of 86 mm, 75% to 35% for the impeller diameter of 114 mm and 74% to 12% for the impeller diameter of 160 mm depending on agitation intensity with the baffled tank condition. In the case of the unbaffled condition, OHTC decreases by 77% to 42% for the impeller diameter of 86 mm, 73% to 31% for the impeller diameter of 114 mm and 72% to 4% for the impeller diameter of 160 mm.

Table 6.6: Reduction of OHTC ($U_{overall}$) at KNO_3 concentration of 5.25 mol/dm^3 for various impeller sizes and speeds at time 80 min

rpm	Impeller dia. 86 mm		Impeller dia. 114 mm		Impeller dia. 160 mm	
	With baffles	Without baffles	With baffles	Without baffles	With baffles	Without baffles
100	80.4%	77.6%	75.5%	73.4%	74.6%	72%
200	70.1%	65.9%	62%	60%	55.2%	52.6%
300	66.4%	64.4%	57.6%	55.6%	19.6%	14%
400	63.5%	61.5%	55.2%	50%	16.8%	11%
500	60.3%	56.3%	51.6%	48.3%	12.9%	4.5%
600	57.8%	50.6%	46.4%	38.5%	-	-
700	46.7%	42.7%	35.9%	31.3%	-	-

(a)

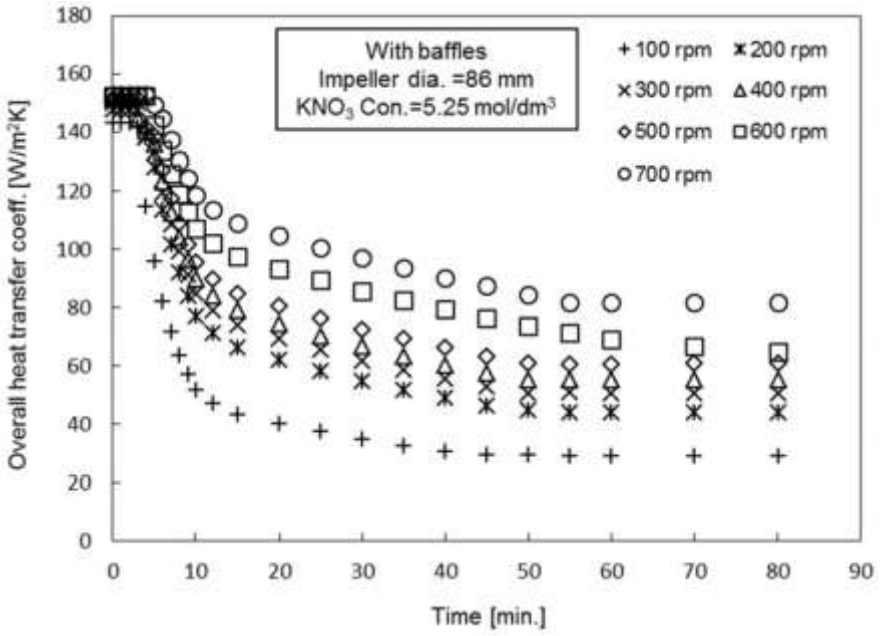

(b)

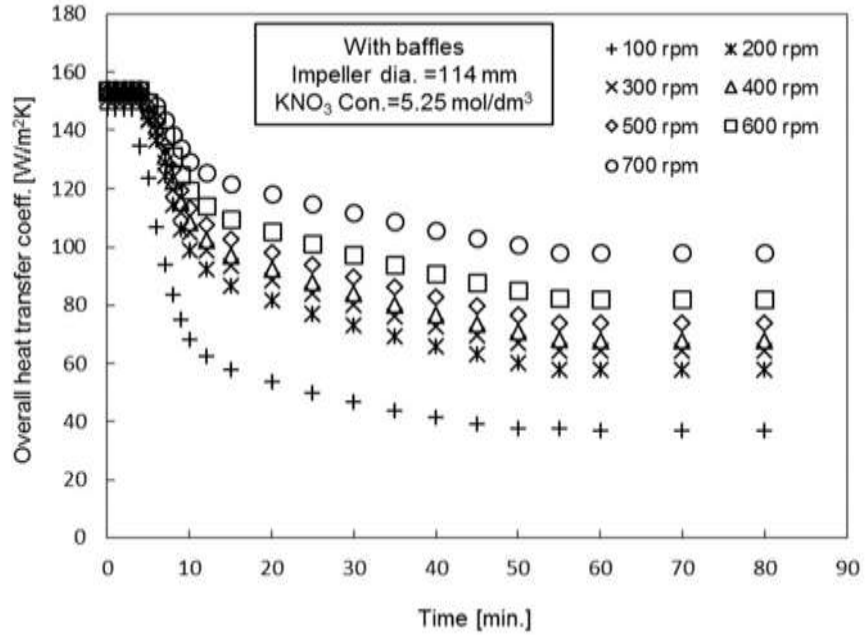

(c)

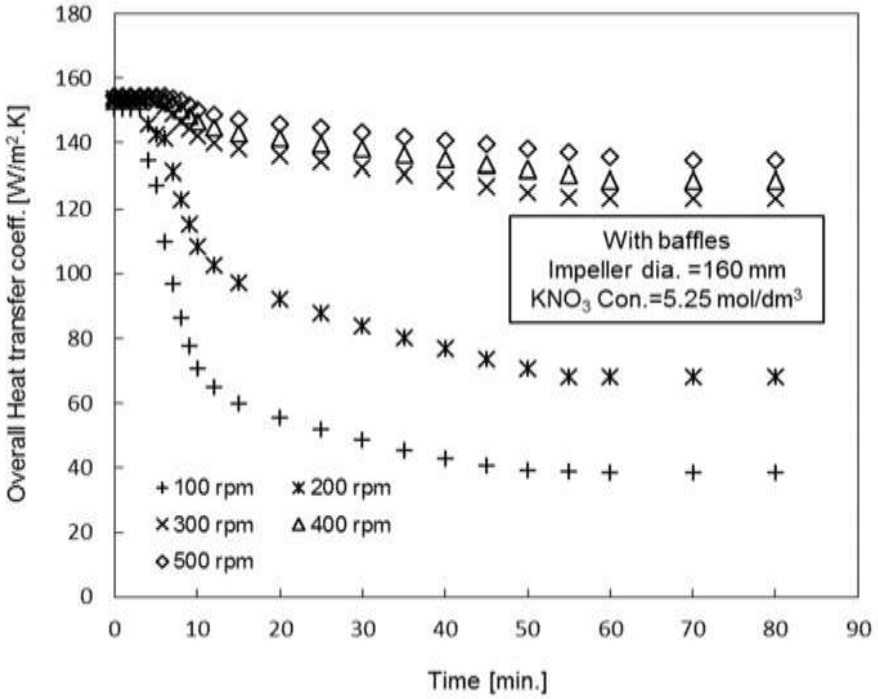

Figure 6.7: Variation of overall heat transfer coefficient (OHTC) with time at different agitation rates at KNO_3 concentration of 5.25 mol/dm^3 and with baffles: (a) impeller diameter of 86 mm, (b) impeller diameter of 114 mm, and (c) impeller diameter of 160 mm

(a)

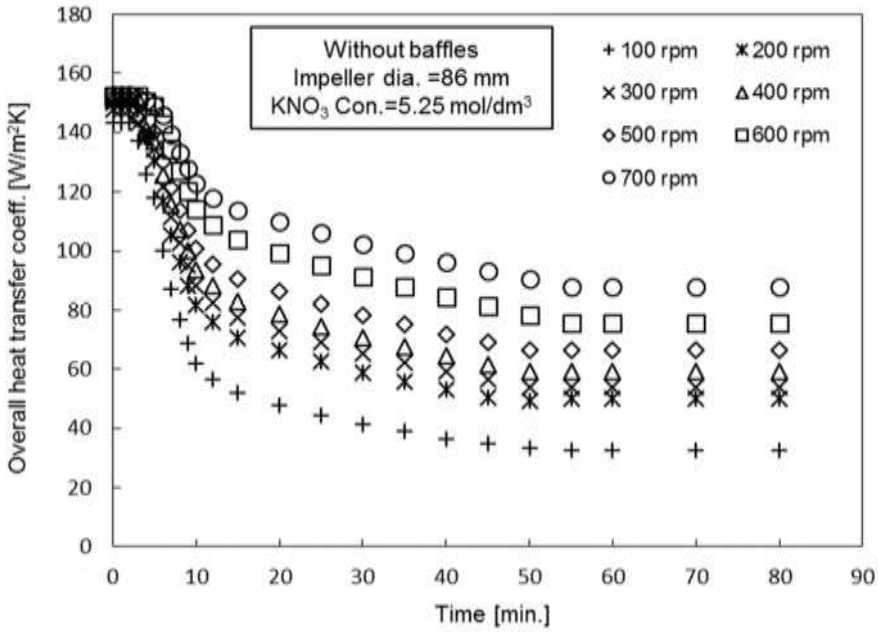
Without baffles
Impeller dia. =86 mm
KNO3 Con.=5.25 mol/dm3
100 rpm
200 rpm
300 rpm
400 rpm
500 rpm
600 rpm
700 rpm
Overall heat transfer coeff. [W/m2K]
Time [min.]

(b)

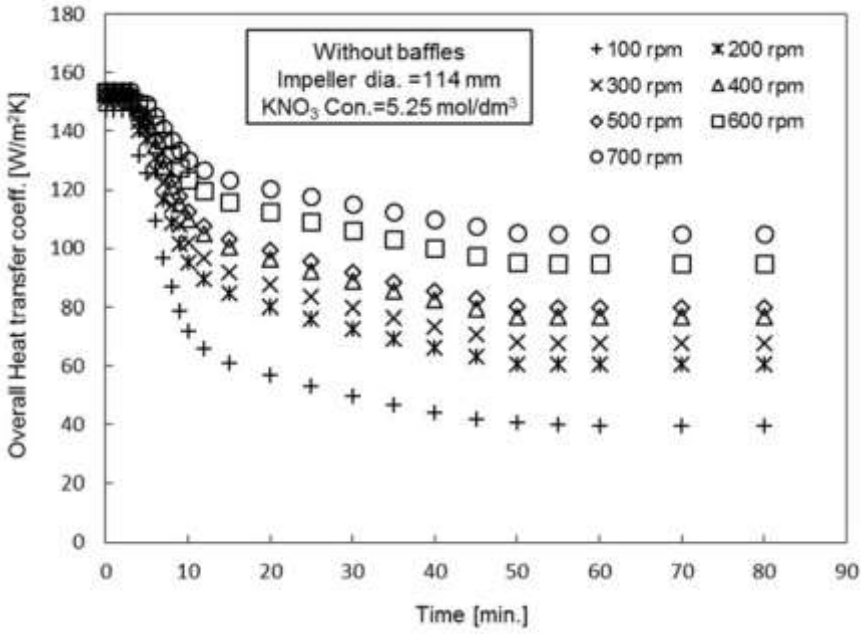
Without baffles
Impeller dia. =114 mm
KNO3 Con.=5.25 mol/dm3
100 rpm
200 rpm
300 rpm
400 rpm
500 rpm
600 rpm
700 rpm
Overall Heat transfer coeff. [W/m2K]
Time [min.]

(c)

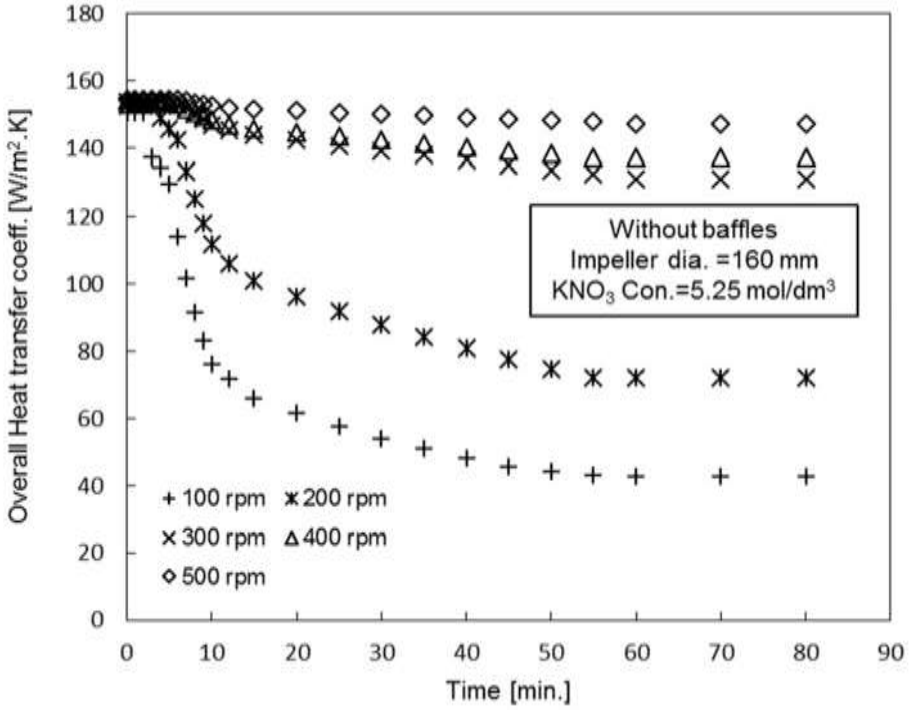

Figure 6.8: Variation of overall heat transfer coefficient (OHTC) with time at different agitation rates at KNO_3 concentration of 5.25 mol/dm^3 and without baffles: (a) impeller diameter of 86 mm, (b) impeller diameter of 114 mm, and (c) impeller diameter of 160 mm

The effect of KNO_3 concentration or degree of supersaturation on the OHTC as a function of agitation rate is revealed through Figures 6.3 to 6.8. In crystallisation scaling, supersaturation is the main driving force of the scaling process. It can be attributed to an increase in the degree of supersaturation (either increase of solute concentration or decrease of heat exchange surface temperate or a combination of both) which results in an increase of scale deposit as a consequence of the reduction of OHTC. From the above results, it is discerned that the magnitude of OHTC decreases more rapidly under light agitation than for strong (or violent) agitation in all cases of impeller size.

6.4 Hydrodynamic Effects on Thermal Resistance (TR)

This part of the analysis reveals the implication of agitation rate (or impeller speed) on the scaling thermal resistance (TR) at different concentrations and sizes of the impeller as shown in Figures 6.9 (a, b, c) to 6.14 (a, b, c). Figures 6.9 (a, b, c), 6.11(a, b, c) and 6.13 (a, b, c) show the variation in scaling thermal resistance (TR) with time as a function of agitation rate with

the baffled condition for concentrations of 4.50, 4.75 and 5.25 mol/dm^3, respectively. The variation of thermal resistance (TR) with time as a function of agitation rate with the unbaffled condition for concentrations of 4.50, 4.75 and 5.25 mol/dm^3 are shown in Figures 6.10 (a, b, c), 6.12 (a, b, c) and 6.14 (a, b, c), respectively. It is seen that the TR increases asymptotically to a limit at which the value of the rate of removal of scale deposits from the tank wall equals the rate of scale deposition.

The augmentation of TR is also a function of agitation speed, that is, the higher the agitation, the lower the TR. Former studies show that the solution velocity or impeller speed (proportional to impeller rotational Reynolds number) can variously enhance the crystallisation scaling (Helalizadeh et al., 2000; Hatch, 1973), decrease the scale deposit (Marshall et al., 2003; Hasson and Zahavi, 1970), or have no effect (Helalizadeh et al., 2000) in some cases, depending on whether scaling is mass transfer or surface reaction (or activation) control. For the present study, Figures 6.9 (a, b, c) to 6.14 (a, b, c) reveal that, as the impeller speed (or impeller rotational Reynolds number) is increased, the scaling resistance (TR) decreases. The TR decreases appreciably as the agitation rate increases, having three possible effects, two of which lead to a reduction in scaling, and the other leads to an increase in scaling. As the impeller agitation speed (or impeller rotational Reynolds number) increases, the heat transfer coefficient between the bulk solution and tank wall surface increases by thinning of the thermal boundary layer in the wall vicinity due to increased eddy diffusion; this leads to a diminished temperature differential which in turn decreases the crystalline deposit because the salt is of normal solubility. Also, with the increase of impeller speed, the fluid erosion effect increases due to the more severe shear force on the crystalline scale layer, which reduces the growth of the layer on the tank wall and augments the bottom settled scale deposit.

The third effect, which enhances the scaling, that is, increasing impeller speed introduces more salt to the wall of the agitation tank by increasing mass transport via turbulent eddies due to thinning of the viscous sublayer, which then leads to enhancing the concentration of solute near the heat transfer surface. From all the results shown in Figures 6.9 (a, b, c) to 6.14 (a, b, c), it is seen that the scaling resistance reduces with the increase of impeller speed. This can be explained either by the crystallisation scaling being a surface reaction or activation control or because the temperature differential between the transfer surface and bulk solution reduces substantially. Hence, heat transfer surface temperature and activation energy play major roles in crystallisation scaling in the agitation tank and the diffusion or mass transfer does not control the scaling process (Hasan et al., 2012a).

(a)

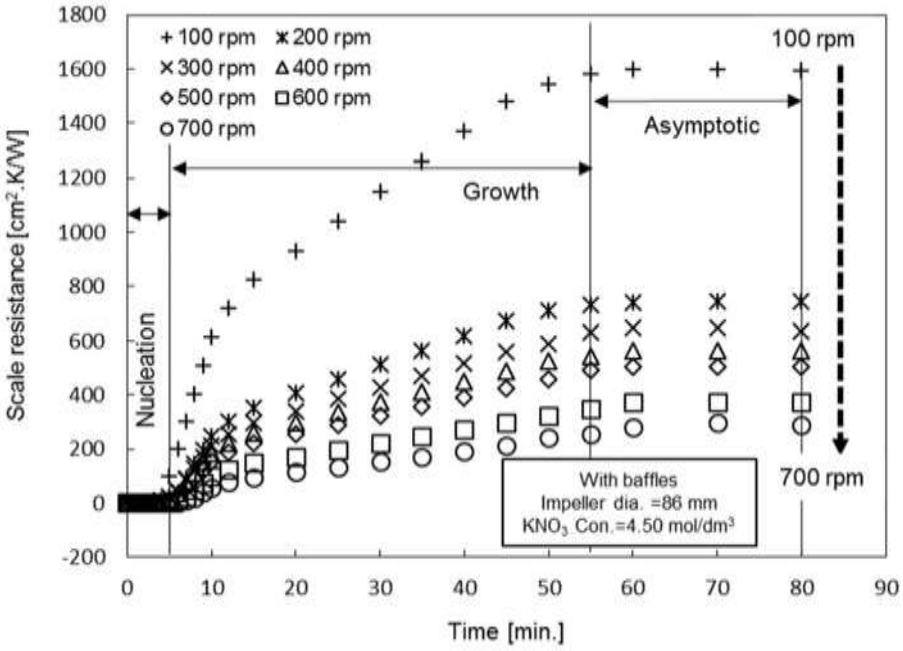
+100 rpm
*200 rpm
×300 rpm
△400 rpm
◇500 rpm
□600 rpm
○700 rpm
100 rpm
Asymptotic
Growth
Nucleation
700 rpm
With baffles
Impeller dia. =86 mm
KNO3 Con.=4.50 mol/dm3
Scale resistance [cm2.K/W]
Time [min.]

(b)

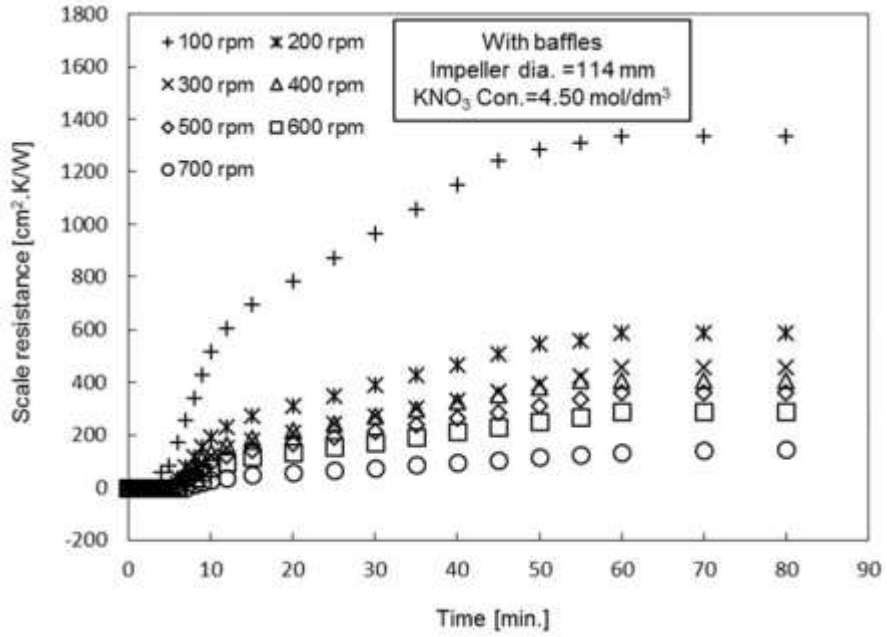
+100 rpm
*200 rpm
×300 rpm
△400 rpm
◇500 rpm
□600 rpm
○700 rpm
With baffles
Impeller dia. =114 mm
KNO3 Con.=4.50 mol/dm3
Scale resistance [cm2.K/W]
Time [min.]

(c)

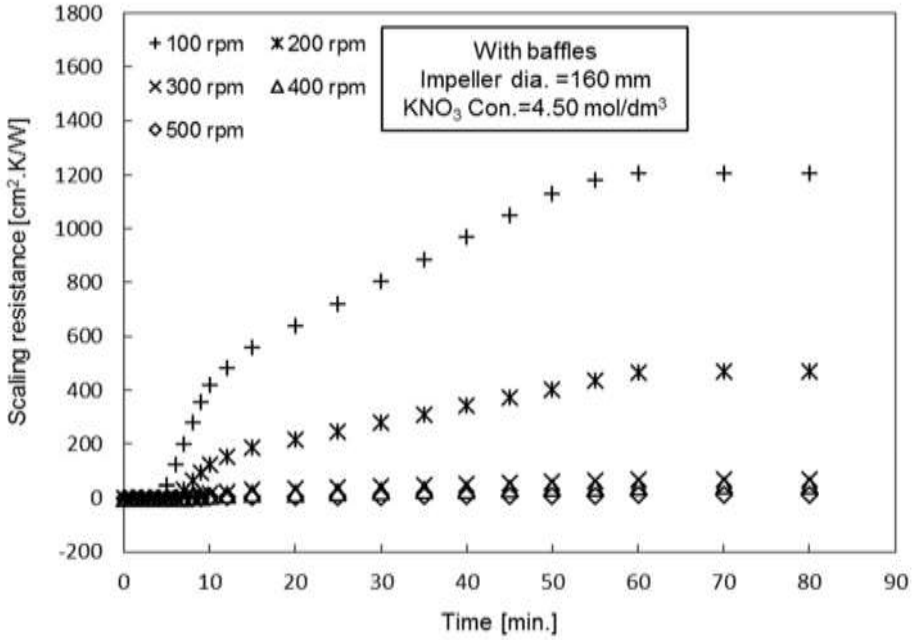

Figure 6.9: Scaling thermal resistance (TR) as a function of time at different agitation rates at KNO_3 concentration of 4.50 mol/dm^3 and with baffles: (a) impeller diameter of 86 mm, (b) impeller diameter of 114 mm, and (c) impeller diameter of 160 mm

Tables 6.4, 6.5 and 6.6 show the effects of KNO_3 concentration on the thermal resistance (TR) due to crystallisation scale deposition in baffled and unbaffled tank conditions. Increasing the concentration leads to increases in TR by introducing more scale deposit due to higher supersaturation at tank wall temperature. The effects of impeller diameters of 86 mm, 114 mm and 160 mm are shown in Tables 6.4, 6.5 and 6.6, respectively. It is evident that an increase of impeller size results in a decrease in scale growth rate. Firstly, the increase in fluid erosion introduced by larger impeller size leads to an increase in heat transfer coefficient, which leads to a decrease in the crystal growth on the wall and reduces the thermal resistance (TR) due to scaledeposit.

Secondly, as the agitation rate increases with impeller size, the temperature difference between the bulk solution and the crystal growth surface on the tank wall is reduced. The lower temperature differential causes a decline of the local supersaturation at the tank wall, which decreases the crystal deposition on the wall because of normal solubility salt, so the suspended crystals tend to settle on the bottom of the tank. For all cases, an asymptotic plot is observed

where the removal rate of crystal from the wall increases with time and the rate of crystal deposition eventually equals the removal rate, and the scale curve then levels off . Also, the values of TR shown in Tables 6.4, 6.5 to 6.6 reveal the effects of the four equally spaced baffles on the TR and the relation with crystalline scale deposit. The variation of thermal resistance (TR) with time as a function of agitation rate with the unbaffled condition for concentrations of 4.50, 4.75 and 5.25 mol/dm^3 are shown in Figures 6.10 (a, b, c), 6.12 (a, b, c) and 6.14 (a, b, c), respectively.

For all the impellers, the TR is higher in a baffled tank in comparison to an unbaffled tank; two reasons can explain this. Firstly, the baffles themselves act as nucleation sites as they provide more surface area; secondly, the presence of baffles diminishes the effect of fluid erosion because of the lower flow velocity. On the other hand, an unbaffled tank creates swirl flow in the tank and the fluid erosion is distributed uniformly on the wall, and it is easier to wash off crystal deposits by the action of fluid erosion. This result implies that an increase in crystalline deposition leads to augmentation of TR and crystalline scale layer thickness and reductions in OHTC under baffled conditions.

Table 6.7: Values of TR, $R_{scale} \times 10^3$ [cm^{2}K/W] at various KNO_3 concentrations with impeller diameter of 86 mm at time 80 min

rpm	Concentration 4.50 mol/dm^3		Concentration 4.75 mol/dm^3		Concentration 5.25 mol/dm^3	
	With baffles	Without baffles	With baffles	Without baffles	With baffles	Without baffles
100	159.37	120.68	185.88	146.34	199.35	172.55
200	123.47	73.26	89.36	83.19	114.35	95.56
300	112.67	58.83	76.44	64.87	94.31	85.65
400	104.92	49.22	68.51	57.62	83.19	74.61
500	98.58	44.44	58.83	49.22	70.95	61.24
600	85.24	25.53	40.87	34.95	64.07	48.02
700	76.80	20.26	32.59	27.88	40.87	34.95

Table 6.8: Values of TR, $R_{scale} \times 10^3$[cm^2 K/W] at various KNO_3 concentrations with impeller diameter of 114 mm at time 80 min

rpm	Concentration 4.50 mol/dm^3		Concentration 4.75 mol/dm^3		Concentration 5.25 mol/dm^3	
	With baffles	Without baffles	With baffles	Without baffles	With baffles	Without baffles
100	133.44	89.36	139.87	95.56	147.63	133.44
200	58.83	56.54	64.87	60.04	77.05	70.95
300	45.64	43.97	57.03	50.42	64.87	58.83
400	40.88	36.13	48.03	40.88	58.83	46.83
500	36.13	32.59	40.88	36.18	50.42	43.25
600	29.15	18.51	34.95	25.53	40.88	29.06
700	14.44	11.53	20.85	17.35	26.70	21.78

Table 6.9: Values of TR, $R_{scale} \times 10^3$[cm^2 K/W] at various KNO_3 concentrations with impeller diameter of 160 mm at time 80 min

rpm	Concentration 4.50 mol/dm^3		Concentration 4.75 mol/dm^3		Concentration 5.25 mol/dm^3	
	With baffles	Without baffles	With baffles	Without baffles	With baffles	Without baffles
100	120.68	58.83	127.04	83.19	139.87	120.68
200	46.83	23.19	52.81	40.88	58.83	52.82
300	6.91	5.75	86.44	6.19	11.53	8.06
400	4.60	2.29	5.18	4.60	9.22	5.75
500	1.21	0.57	1.72	1.15	6.91	2.29
600	-	-	-	-	-	-
700	-	-	-	-	-	-

(a)

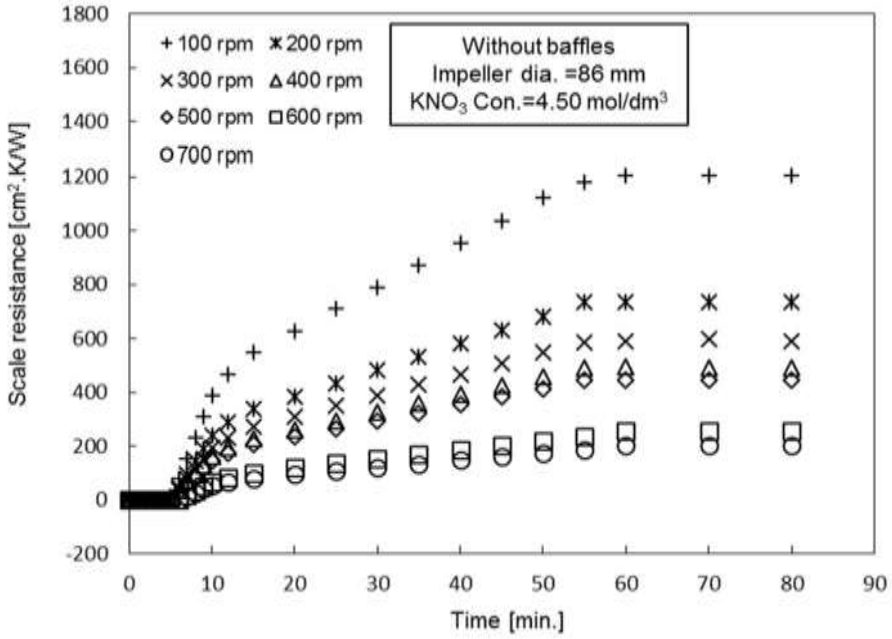
+100 rpm
*200 rpm
×300 rpm
△400 rpm
◇500 rpm
□600 rpm
○700 rpm
Without baffles
Impeller dia. =86 mm
KNO3 Con.=4.50 mol/dm3
Scale resistance [cm2.K/W]
Time [min.]

(b)

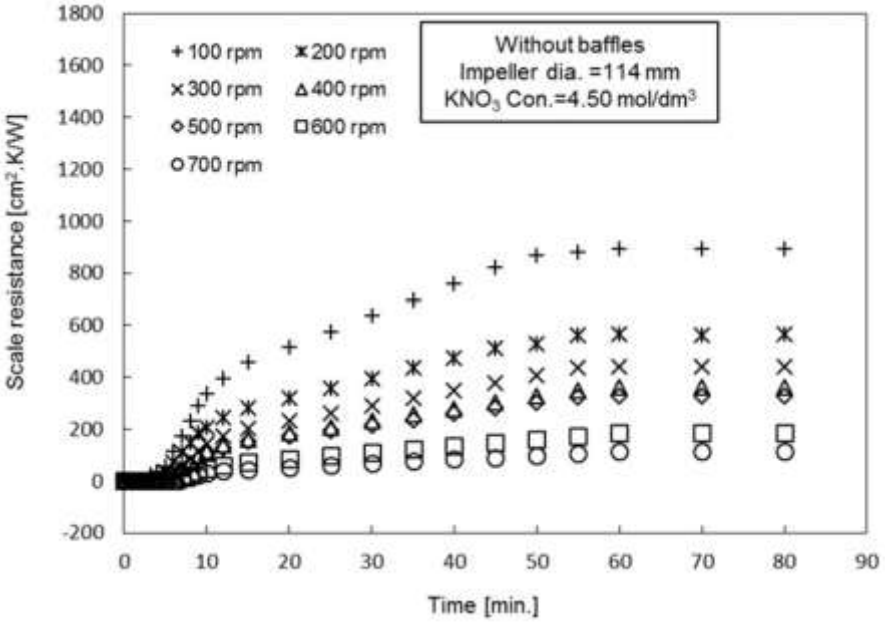
+100 rpm
*200 rpm
×300 rpm
△400 rpm
◇500 rpm
□600 rpm
○700 rpm
Without baffles
Impeller dia. =114 mm
KNO3 Con.=4.50 mol/dm3
Scale resistance [cm2.K/W]
Time [min.]

(c)

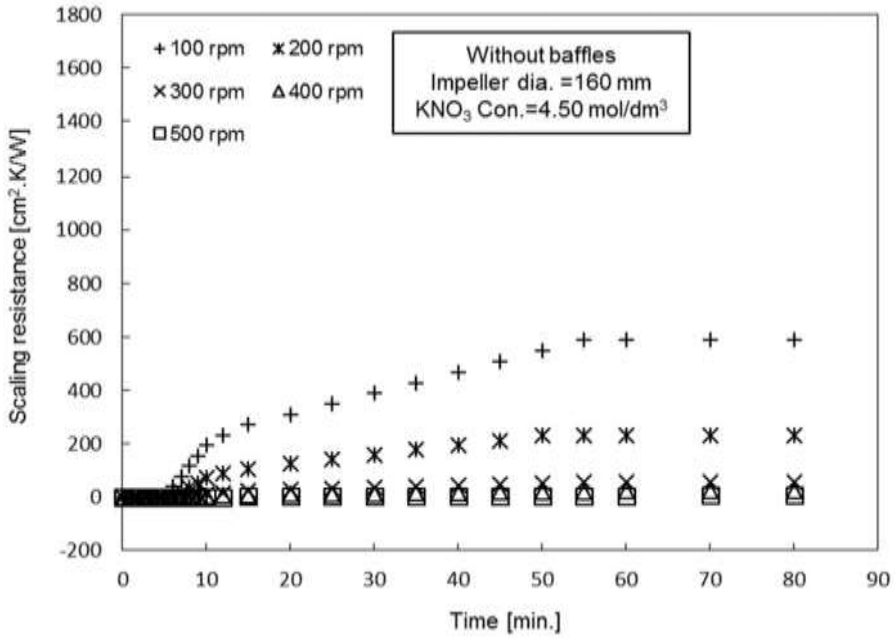

Figure 6.10: Scaling thermal resistance (TR) as a function of time at different agitation rates at KNO_3 concentration of 4.50 mol/dm^3 and without baffles: (a) impeller diameter of 86 mm, (b) impeller diameter of 114 mm, and (c) impeller diameter of 160 mm

(a)

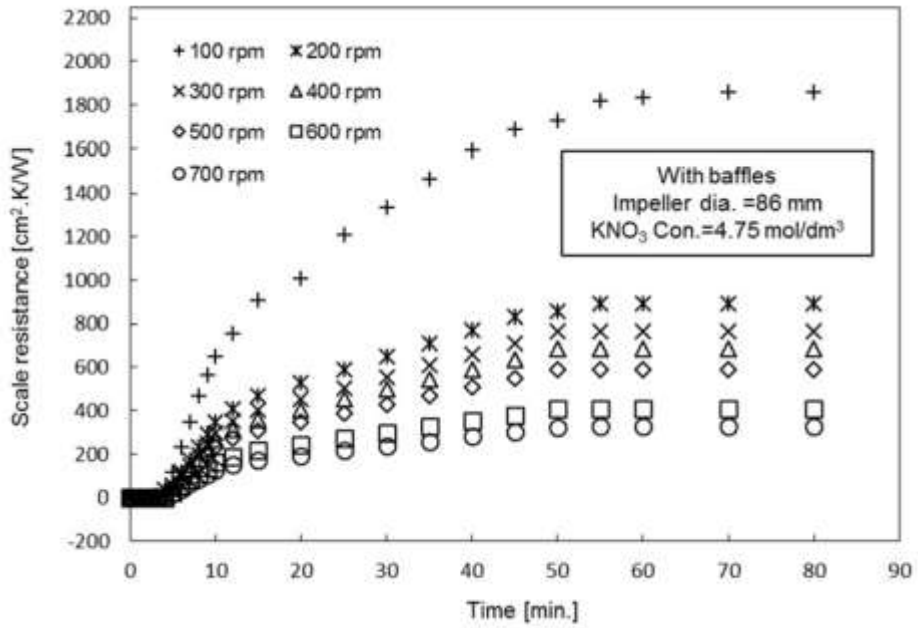

(b)

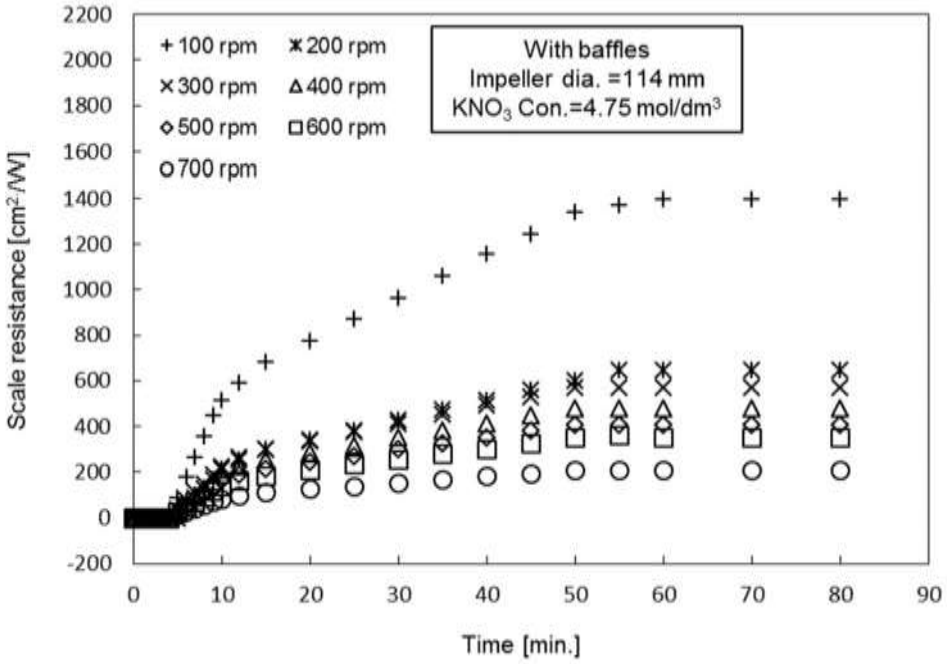

(c)

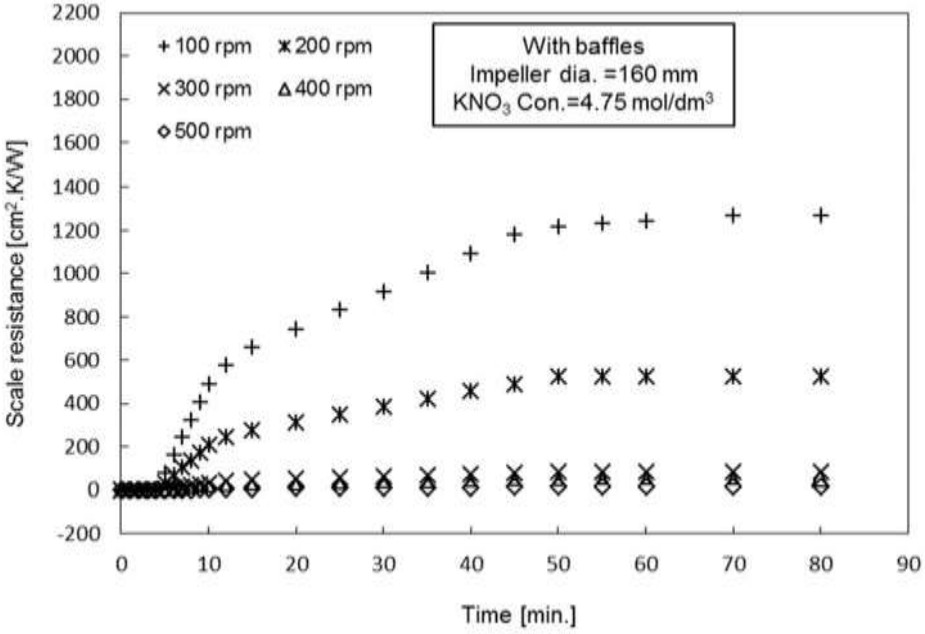

Figure 6.11: Scaling thermal resistance (TR) as a function of time at different agitation rates at KNO_3 concentration of 4.75 mol/dm^3 and with baffles: (a) impeller diameter of 86 mm, (b) impeller diameter of 114 mm, and (c) impeller diameter of 160 mm

(a)

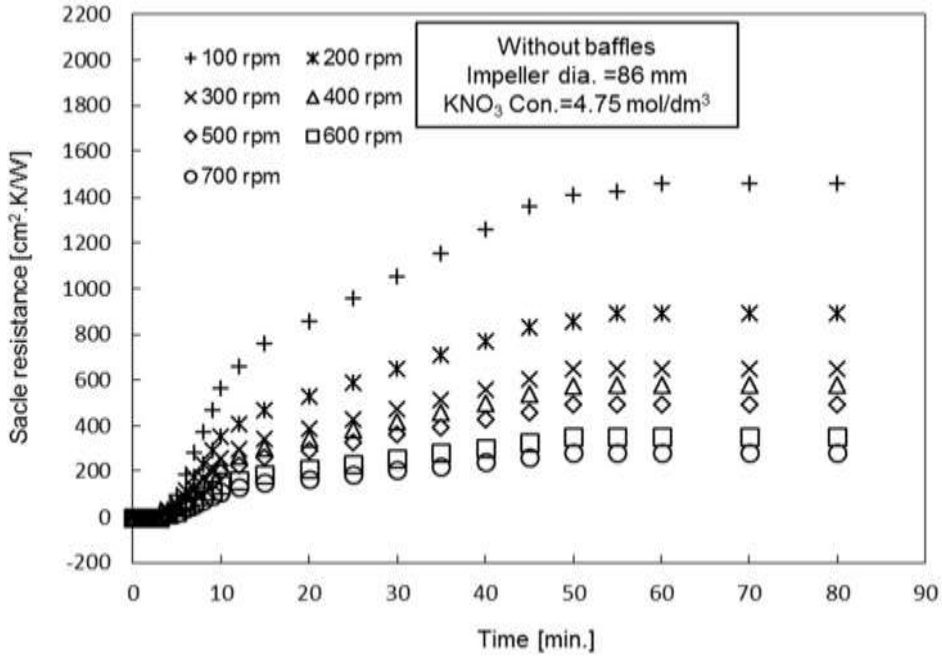
Without baffles
Impeller dia. =86 mm
KNO3 Con.=4.75 mol/dm3
+ 100 rpm
* 200 rpm
× 300 rpm
△ 400 rpm
◇ 500 rpm
□ 600 rpm
○ 700 rpm
Sacle resistance [cm2.K/W]
Time [min.]

(b)

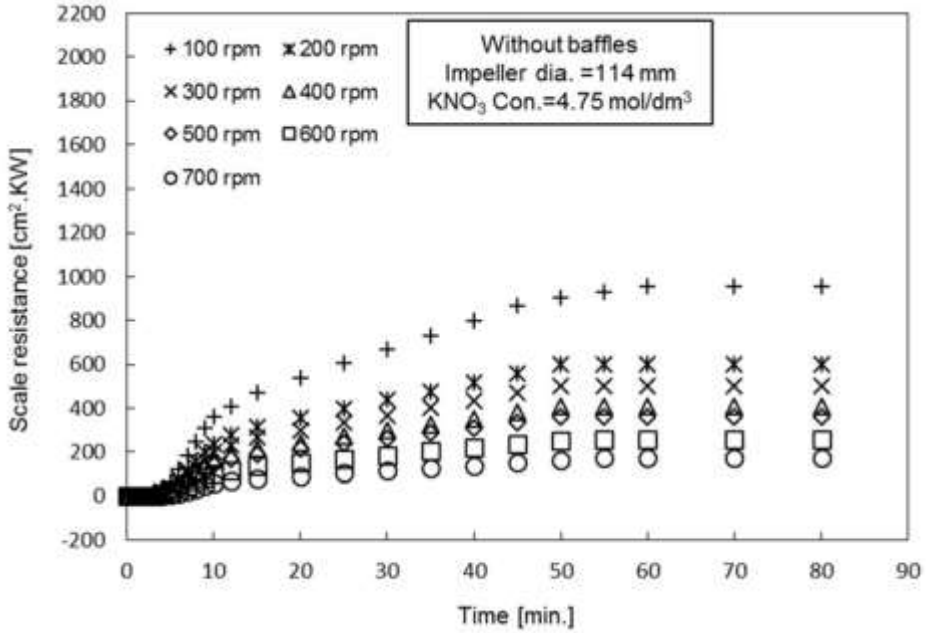
Without baffles
Impeller dia. =114 mm
KNO3 Con.=4.75 mol/dm3
+ 100 rpm
* 200 rpm
× 300 rpm
△ 400 rpm
◇ 500 rpm
□ 600 rpm
○ 700 rpm
Scale resistance [cm2.KW]
Time [min.]

(c)

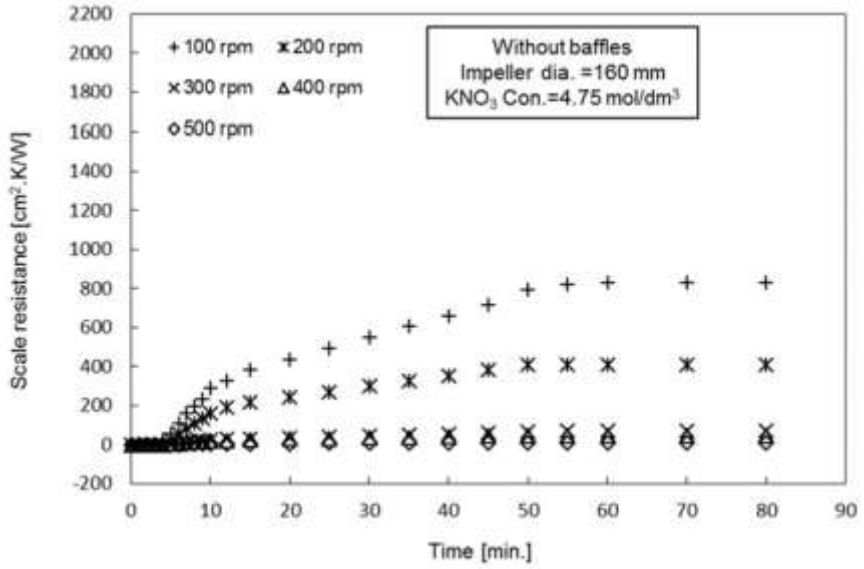

Figure 6.12: Scaling thermal resistance (TR) as a function of time at different agitation rates at KNO_3 concentration of 4.75 mol/dm^3 and without baffles: (a) impeller diameter of 86 mm, (b) impeller diameter of 114 mm, and (c) impeller diameter of 160 mm

(a)

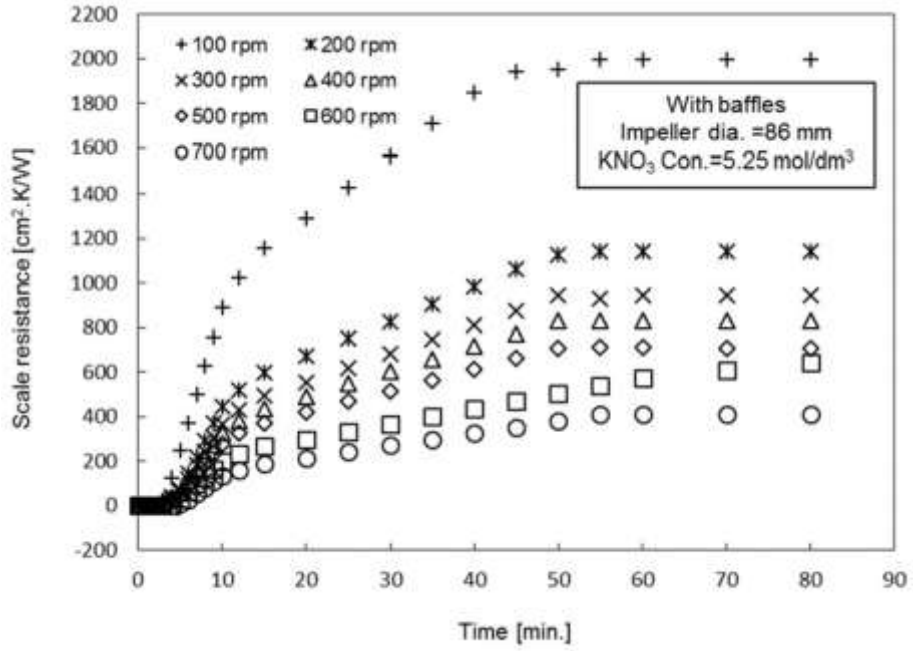

(b)

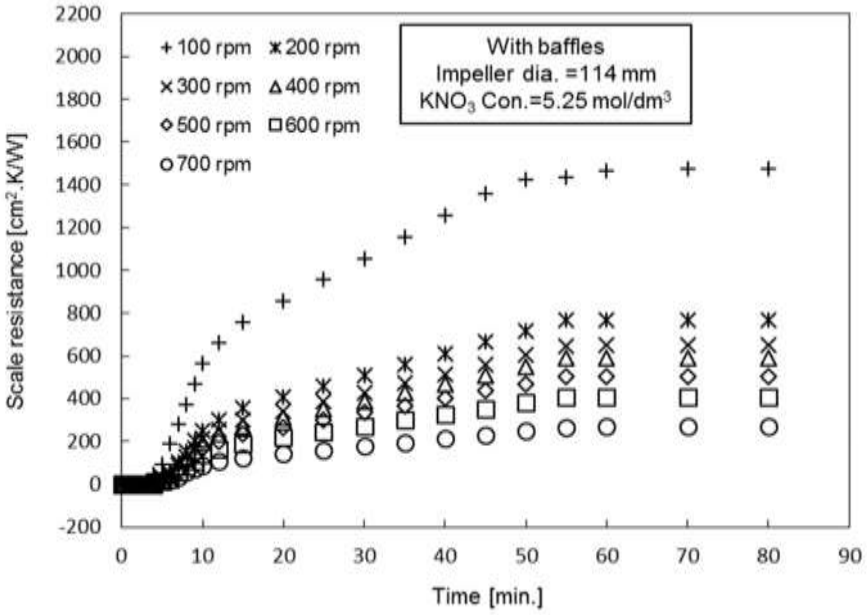

(c)

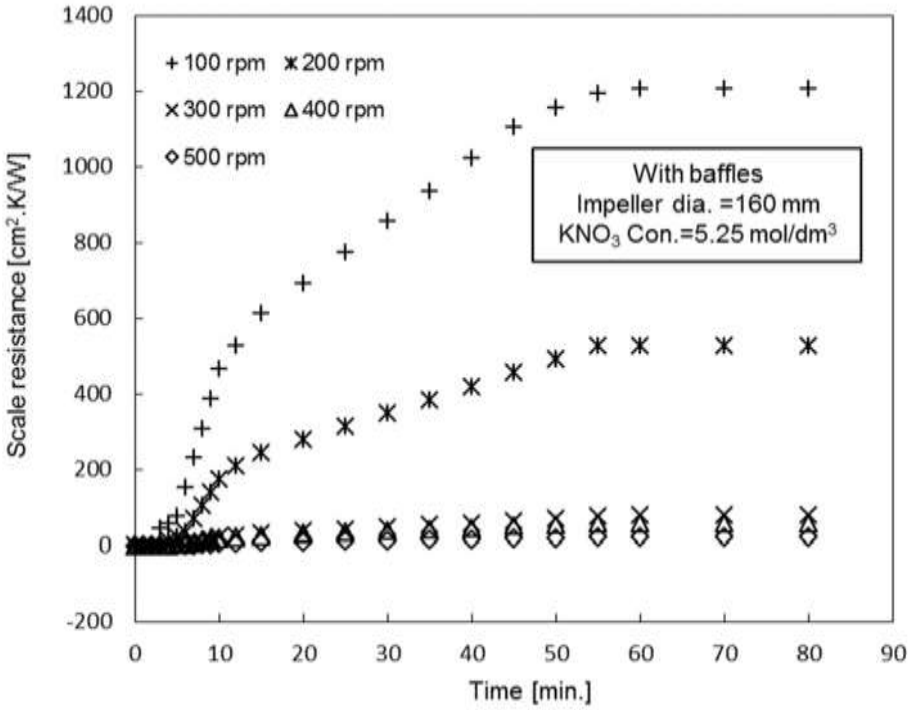

Figure 6.13: Scaling thermal resistance (TR) as a function of time at different agitation rates at KNO_3 concentration of 5.25 mol/dm^3 and with baffles: (a) impeller diameter of 86 mm, (b) impeller diameter of 114 mm, and (c) impeller diameter of 160 mm

(a)

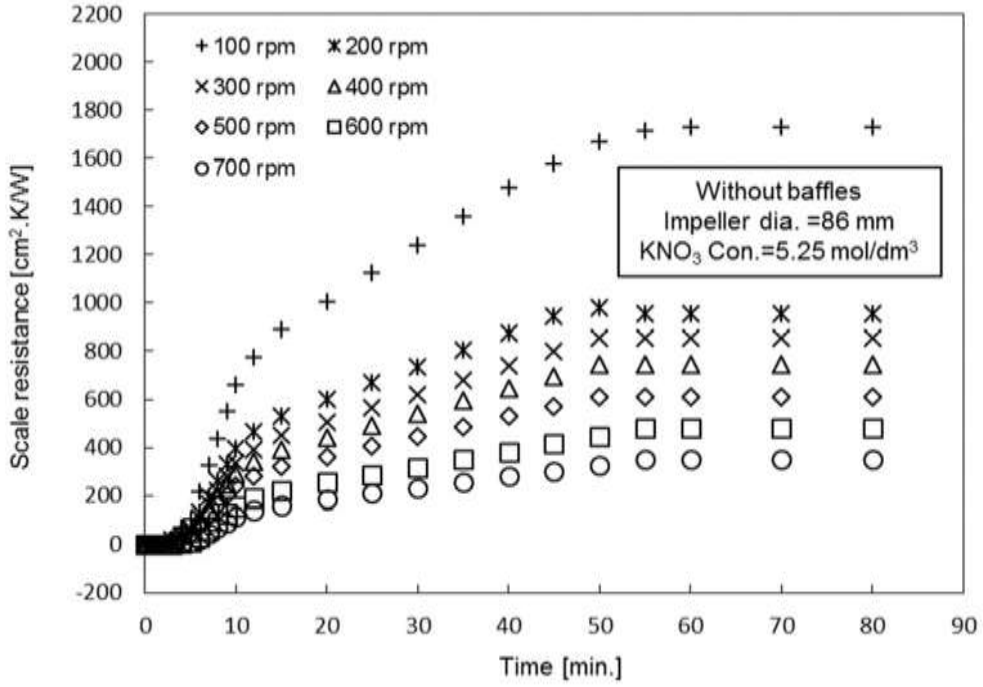
100 rpm
200 rpm
300 rpm
400 rpm
500 rpm
600 rpm
700 rpm
Without baffles
Impeller dia. =86 mm
KNO3 Con.=5.25 mol/dm3
Scale resistance [cm2.K/W]
Time [min.]

(b)

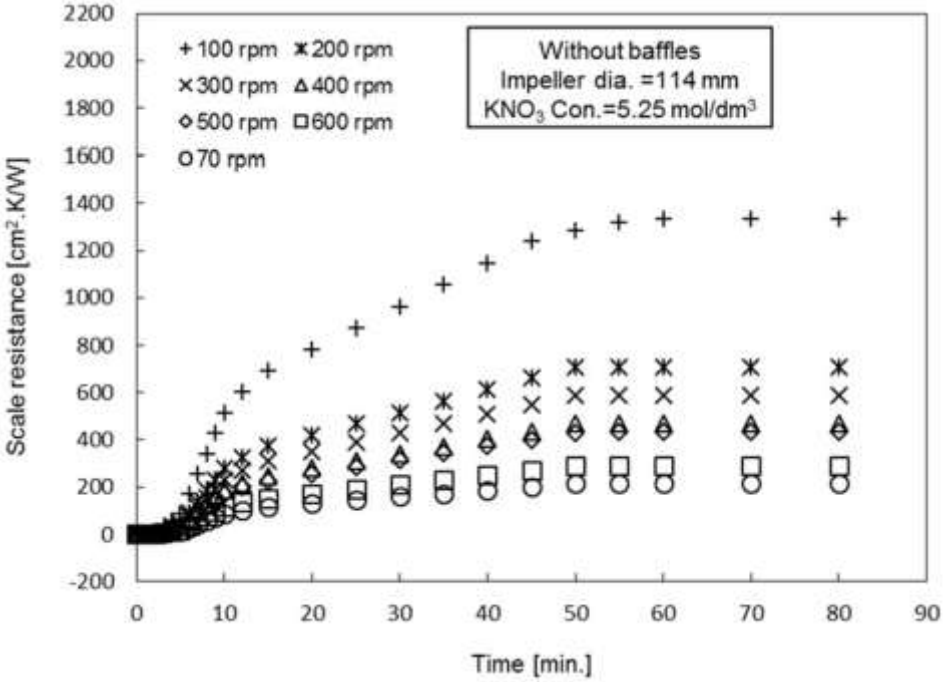
100 rpm
200 rpm
300 rpm
400 rpm
500 rpm
600 rpm
70 rpm
Without baffles
Impeller dia. =114 mm
KNO3 Con.=5.25 mol/dm3
Scale resistance [cm2.K/W]
Time [min.]

(c)

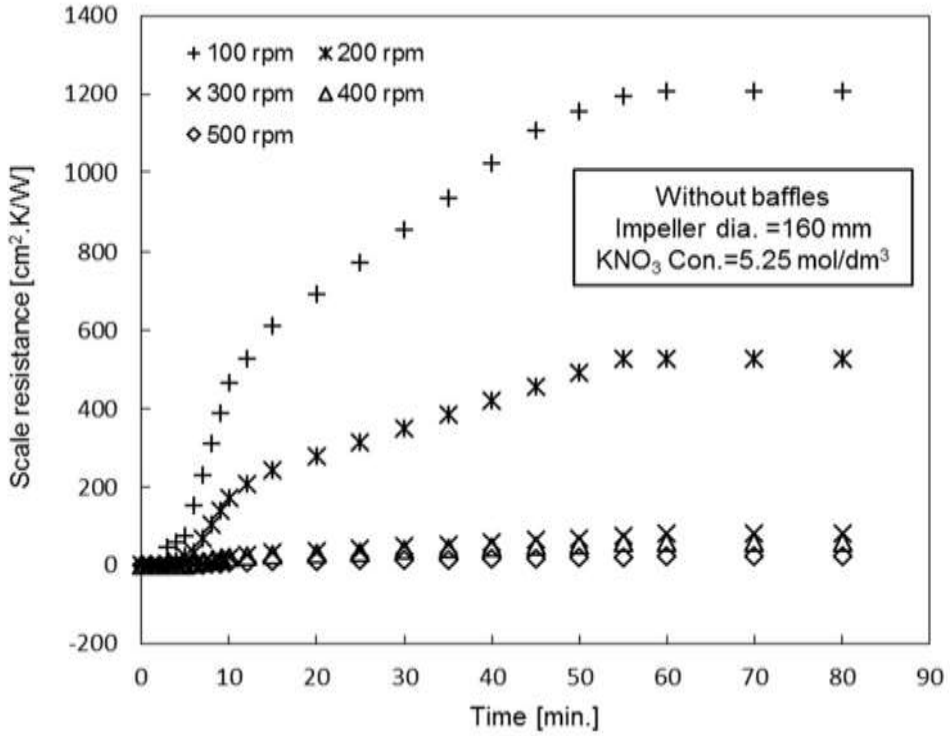

Figure 6.14: Scaling thermal resistance (TR) as a function of time at different agitation rates at KNO_3 concentration of 5.25 mol/dm^3 and without baffles: (a) impeller diameter of 86 mm, (b) impeller diameter of 114 mm, and (c) impeller diameter of 160 mm

Figures 6.15 (a, b), 6.16 (a, b) and 6.17 (a, b) show the asymptotic variation of crystalline scale layer thickness as a function of agitation rate at different KNO_3 scale forming solution concentrations for the impeller diameters of 86 mm, 114mm and 160mm, respectively.

(a)

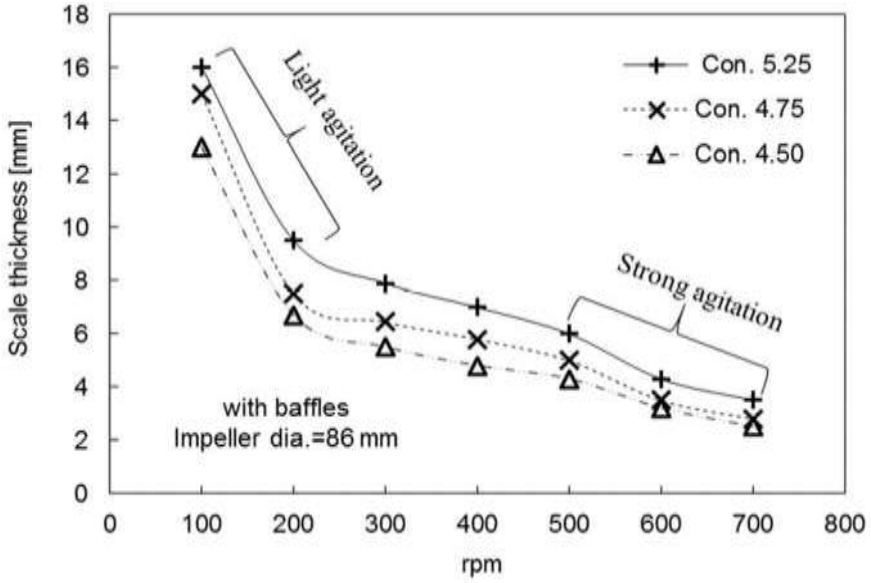

(b)

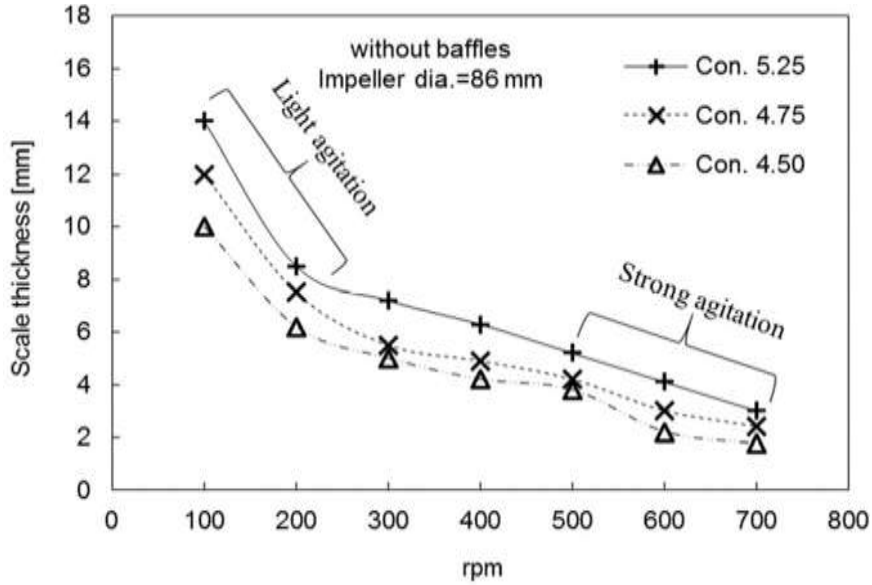

Figure 6.15: Thickness of scaling layer as a function agitation rate for impeller diameter of 86 mm: (a) with baffles, and (b) without baffles

It is seen that crystalline scale thickness decreases with the increasing agitation rate and this asymptotic decrease leads to the decrease of TR and an increase of OHTC. It should be noted

that the asymptotic thickness of the scaling layer increases with concentration in the case of smaller size impellers (86 mm and 114 mm) than the larger one (160 mm).

(a)

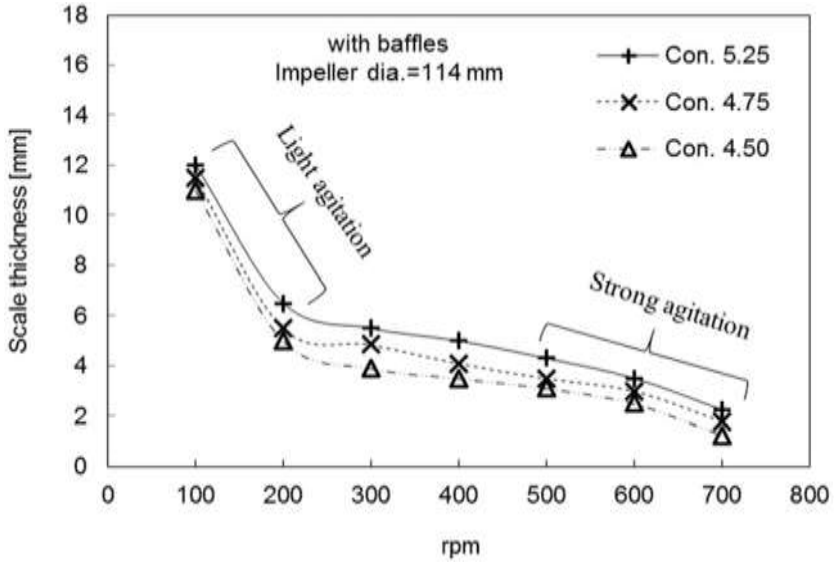

(b)

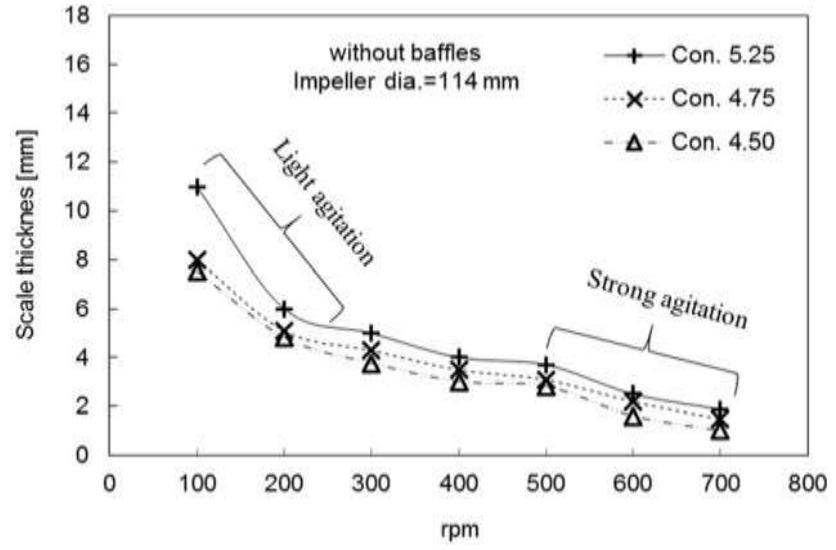

Figure 6.16: Thickness of scaling layer as a function agitation rate for impeller diameter of 114 mm: (a) with baffles, and (b) without baffles.

(a)

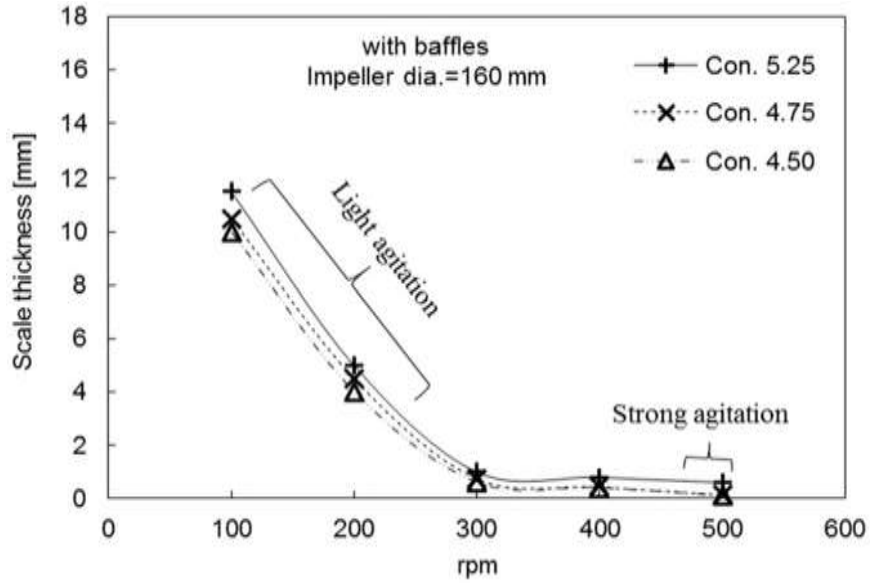

(b)

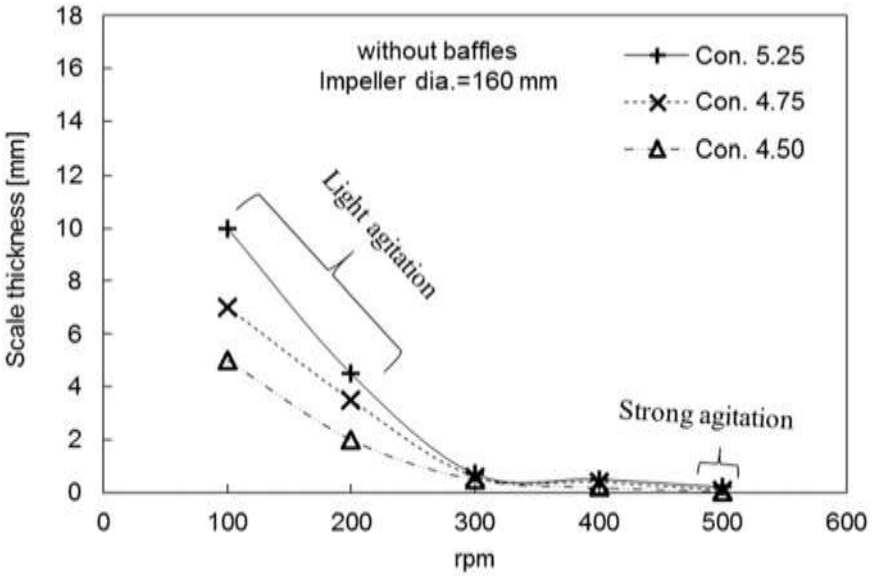

Figure 6.17: Thickness of scaling layer as a function agitation rate for impeller diameter of 160 mm: (a) with baffles, and (b) without baffles

6.5 Uncertainty Analysis

An uncertainty analysis of the measured values is significant to validate the accuracy of the experimental results. The uncertainty analysis was performed in this study to validate the data obtained from the experimental measurements.

When one variable X_i is considered in a particular experiment which includes a known uncertainty of δX_i, the relationship between the measured value and its uncertainty is expressed as follows (Moffat, 1988):

$$X_i = X_i(\text{measured}) \pm \delta X_i \tag{6.1}$$

If R is represented as a function of a set of independent measured variables $(X_1, X_2, X_3, ...X_n)$, the data interpretation program can be represented by (Moffat, 1988):

$$R = R(X_1, X_2, X_3, ...X_n) \tag{6.2}$$

If, when the equation is a pure "product form" as Eq. (6.5), then the relative uncertainty can be represented as equation (6.6).

$$R = X_1^{a}, X_2^{b}, X_3^{c}, ...X_M^{m} \tag{6.3}$$

$$\frac{\delta R}{R} = \sqrt{\left(a\frac{\delta X_1}{X_1}\right)^2 + \left(b\frac{\delta X_2}{X_2}\right)^2 + \left(c\frac{\delta X_3}{X_3}\right)^2 + ... + \left(m\frac{\delta X_m}{X_m}\right)^2} \tag{6.4}$$

The uncertainty analysis is important especially when the measured scaling resistances have small values. This is a single representative case which is found to express typical scaling resistance behaviour in the experiments.

The uncertainties of scaling resistance and overall heat transfer coefficient largely depend on h_i and h_o. The heat transfer coefficient (h_i) of the bulk solution is a function of thermal conductivity (k), bulk solution density (ρ) and viscosity of bulk solution (μ_s).

$$\Rightarrow h_i = 0.68 \left(\frac{k}{D_T}\right)\left(\frac{D_A^2 N \rho}{\mu}\right)^{0.67}\left(\frac{C_{ps}\mu}{k}\right)^{0.33}\left(\frac{\mu_s}{\mu_{ws}}\right)^{0.14} \tag{6.5}$$

The uncertainty of heat transfer coefficient (h_i) of the bulk solution can be calculated as

$$B_{h_i} = \sqrt{\left(\frac{\partial h}{\partial k} B_k\right)^2 + \left(\frac{\partial h}{\partial N} B_N\right)^2 + \left(\frac{\partial h}{\partial \rho} B_\rho\right)^2 + \left(\frac{\partial h}{\partial \mu_s} B_{\mu_s}\right)^2} \tag{6.6}$$

Table 6.10: Conditions of KNO_3 solution in the example case for agitation rate N=100 rpm, concentration of 4.50 mol/dm^3 and with baffles

Parameter	Numerical value	Bias uncertainty
k[W/mK]	0.6346	±0.0054
ρ [kg/m^3]	1170	±20
μ_s [Pa.s]	0.00065	±1.2×10^{-6}

The operational conditions with their bias uncertainties at the 95% confidence level are presented for the example case in Table 6.10. The values listed in Table 6.10 are substituted into Eq. (6.9) and, taking the partial derivatives, the example case is:

$$\frac{B_{h_i}}{h_i} = \sqrt{\left(\frac{0.67}{k} B_k\right)^2 + \left(\frac{0.67}{\rho} B_\rho\right)^2 + \left(\frac{-0.2}{\mu_s} B_{\mu_s}\right)^2} \tag{6.7}$$

$$\frac{B_{h_i}}{h_i} = \sqrt{\left(\frac{0.67}{0.6346}.0.0054\right)^2 + \left(\frac{0.67}{1170}.20\right)^2 + \left(\frac{-0.2}{0.00065}.1.2\times10^{-6}\right)^2} = 1.28\%$$

Table 6.11: Conditions of coolant in the example case for agitation rate N=100 rpm

Parameter	Numerical value	Bias uncertainty
k_c [W/mK]	0.3596	±0.061
ρ_c[kg/m^3]	1079.3	±25
V_c[m/s]	0.00938	±0.00052
μ_c[Pa.s]	0.009618	±6.3×10^{-5}

The uncertainty of h_o at the 95% confidence level is presented for the example case in Table 6.8. The heat transfer coefficient (h_o) of the bulk solution is a function of thermal conductivity

(k_c), coolant density (ρ), coolant flow velocity (V) and viscosity of coolant (μ_c).

$$\Rightarrow h_o = 1.02\left(\frac{k_c}{D_e}\right)\left(\frac{D_e V \rho_c}{\mu_c}\right)^{0.45}\left(\frac{C^{pc}\mu_c}{k_c}\right)^{0.33}\left(\frac{D_e}{L}\right)^{0.4}\left(\frac{D_{jo}}{D_{ji}}\right)^{0.8}\left(\frac{\mu_c}{\mu_{wc}}\right)^{0.14} \times\left(\frac{D_e^3 \rho_c^2 g \beta \Delta t}{G/\mu_c^2}\right)^{0.05} \quad (6.8)$$

$$B_{h_o} = \sqrt{\left(\frac{\partial h}{\partial k_c}B_{k_c}\right)^2 + \left(\frac{\partial h}{\partial V}B_V\right)^2 + \left(\frac{\partial h}{\partial \rho_c}B_{\rho_c}\right)^2 + \left(\frac{\partial h}{\partial \mu_c}B_{\mu_c}\right)^2} \quad (6.9)$$

$$\frac{B_{h_o}}{h_o} = \sqrt{\left(\frac{0.67}{k_c}B_{k_c}\right)^2 + \left(\frac{0.45}{V}B_V\right)^2 + \left(\frac{0.45}{\rho_c}B_{\rho_c}\right)^2 + \left(\frac{0.37}{\mu_c}B_{\mu_c}\right)^2} \quad (6.10)$$

$$\frac{B_{h_o}}{h_o} = \sqrt{\left(\frac{0.67}{0.3596}.0.061\right)^2 + \left(\frac{0.45}{0.00938}.0.00052\right)^2 + \left(\frac{0.45}{1079.3}.25\right)^2 + \left(\frac{0.37}{0.009618}.0.000063\right)^2}$$

$$= 11.6\%$$

Table 6.12: Various measured values for agitation rate N=100, concentration of 4.50 mol/dm^3 and with baffles and impeller diameter of 86 mm

Parameter	Numerical value	Bias uncertainty
h_i [W/m²K]	1639.815	±20.9
h_o[W/m²K]	157.2857	±18.2
r_{scale}[m]	0.095	±12.8
A_i[m²]	0.138474	-
A_0[m²]	0.140452	-
$R_{overall}$[cm²K/W]	0.050495883	-
$U_{Overall}$[W/m²K]	143.0130851	-
$R_{Overall-Scale}$[cm²K/W]	1593.775149	-
$U_{Overall-Scale}$[W/m²K]	34.40918	-

The uncertainty of overall scaling resistance under clean wall conditions depends on heat transfer coefficient (h_i) of bulk solution and heat transfer coefficient (h_0) of coolant.

$$R_{Overall} = 1/(U_{Overall} * A) = (1/A_i h_i) + ((\ln(r_0/r_i))/2\pi k L) + (1/A_o h_o) \tag{6.11}$$

$$B_{R_{overall}} = \sqrt{\left[\left(\frac{\partial R_{overall}}{\partial h_i} B_{h_i}\right)^2 + \left(\frac{\partial R_{overall}}{\partial h_0} B_{h_0}\right)^2\right]} \tag{6.12}$$

$$B_{R_{overall}} = \sqrt{\left[\left(-\frac{1}{h_i A_i} B_{h_i}\right)^2 + \left(-\frac{1}{h_o A_0} B_{h_0}\right)^2\right]} \tag{6.13}$$

$$B_{R_{overall}} = \sqrt{\left[\left(-\frac{1}{1639.815 \times 0.138474}.20.9\right)^2 + \left(-\frac{1}{157.2857 \times 0.140452}.18.2\right)^2\right]} = 0.828\times10^{-2}$$

At the 95% confidence level, the scaling resistance is therefore

$$R_{Overall} = 0.050495883 \ \frac{m^2K}{W} \pm 0.828\times10^{-2} \ \frac{m^2K}{W}$$
$$= 0.050495883 \ \frac{m^2K}{W} \pm 16.4\%$$

The uncertainty of overall heat transfer coefficient under clean wall conditions depends on heat transfer coefficient (h_i) of bulk solution and heat transfer coefficient (h_0) of coolant.

$$U_{Overall} = \frac{1}{(1/h_i) + ((A_i \ln(r_0/r_i))/2\pi kL) + ((A_i/A_o)(1/h_o))} \tag{6.14}$$

$$B_{U_{overall}} = \sqrt{\left[\left(\frac{\partial U_{overall}}{\partial h_i} B_{h_i}\right)^2 + \left(\frac{\partial U_{overall}}{\partial h_0} B_{h_0}\right)^2\right]} \tag{6.15}$$

$$B_{U_{overall}} = \left(\frac{1}{R_{overall}}\right)^2 \sqrt{\left[\left(-\frac{1}{h_i A_i} B_{h_i}\right)^2 + \left(-\frac{1}{h_o A_0} B_{h_0}\right)^2\right]} \tag{6.16}$$

At the 95% confidence level, the heat transfer coefficient is therefore

$$U_{Overall} = 143.0130851 \frac{W}{m^2K} \pm 27.556 \frac{W}{m^2K}$$

$$= 143.0130851 \frac{W}{m^2K} \pm 19.26\%$$

The uncertainty of overall scaling resistance under scaling conditions depends on heat transfer coefficient (h_i) of bulk solution, scale radius (r_{scale}) and heat transfer coefficient (h_0) of coolant.

$$R_{Overall-Scale} = 1/(h_i A_i) + \left(\left(\ln(r_0/r_i)\right)/2\pi k L\right) + \left(\left(\ln(r_i/r_{scale})\right)/2\pi k L\right) + 1/(h_0 A_0) \tag{6.17}$$

$$B_{R_{overall-scale}} = \sqrt{\left[\left(\frac{\partial R}{\partial h_i} B_{h_i}\right)^2 + \left(\frac{\partial R}{\partial r_{scale}} B_{r_{scale}}\right)^2 + \left(\frac{\partial R}{\partial h_0} B_{h_0}\right)^2\right]} \tag{6.18}$$

$$B_{R_{overall-scale}} = \sqrt{\left[\left(-\frac{1}{h_i A_i} B_{h_i}\right)^2 + \left(-\frac{1}{r_{scale}} B_{r_{scale}}\right)^2 + \left(-\frac{1}{h_0 A_0} B_{h_0}\right)^2\right]} \tag{6.19}$$

At the 95% confidence level, the scaling resistance is therefore

$$B_{R_{overall-scale}} = 0.1593775149 \frac{m^2K}{W} \pm 0.033469277 \frac{m^2K}{W}$$

$$= 0.1593775149 \frac{m^2K}{W} \pm 21.7\%$$

The uncertainty of overall heat transfer coefficient under scaling conditions depends on heat transfer coefficient (h_i) of bulk solution, scale radius (r_{scale}) and heat transfer coefficient (h_0) of coolant.

$$U_{Overall-Scale} = \frac{1}{(1/h_i) + \left(\left(A_i \ln(r_0/r_i)\right)/2\pi k L\right) + \left(\left(A_i \ln(r_i/r_{scale})\right)/2\pi k L\right) + (A_i/A_o)(1/h_o)} \tag{6.20}$$

$$B_{U_{overall-scale}} = \sqrt{\left[\left(\frac{\partial U}{\partial h_i} B_{h_i}\right)^2 + \left(\frac{\partial U}{\partial r_{scale}} B_{r_{scale}}\right)^2 + \left(\frac{\partial U}{\partial h_0} B_{h_0}\right)^2\right]} \tag{6.21}$$

$$B_{U_{overall-scale}} = \left(-\frac{1}{R_{overall-scale}}\right)^2 \sqrt{\left[\left(-\frac{1}{h_i A_i} B_{h_i}\right)^2 + \left(-\frac{1}{k_{scale}} B_{r_{scale}}\right)^2 + \left(-\frac{1}{h_0 A_0} B_{h_0}\right)^2\right]} \quad (6.22)$$

At the 95% confidence level, the scaling resistance is therefore

$$B_{U_{overall-scale}} = 34.40918 \frac{W}{m^2 K} \pm 7.568 \frac{W}{m^2 K}$$

$$= 34.40918 \frac{W}{m^2 K} \pm 21.9\%$$

In this study, the temperature is varied from -4°C to 48°C, and the uncertainties of the experimental results would mainly occur due to the temperature fluctuations in the bulk solution as well as the coolant. Therefore, the maximum uncertainty in the scaling resistance and the overall heat transfer coefficient are determined to be with ±22%.

6.6 Summary

This chapter reveals that the agitation tank hydrodynamics has significant effects on the heat transfer and thermal resistance. This is of more concern when considering the costs involved in high energy consuming industries. From the above discussion, it can be concluded that the crystallisation scaling process of KNO_3 in the agitation tank is a surface reaction or activation control process. The scale thickness decreases with the increase in agitation rate as well as impeller size which produces more shear force on the crystalline layer. A higher differential temperature between the bulk solution and the heat transfer surface promotes crystalline scale growth of normal solubility salt. The overall heat transfer coefficient increases with the increase of agitation rate. The thermal resistance decreases with the increase of agitation rate. The unbaffled tank shows benefits because of its increasing of OHTC and decreasing of TR and crystalline scale thickness. From a practical point of view, the overall results indicate that the best way to reduce crystalline scale deposition is to determine the appropriate size of the impeller at the maximum economic agitation rate and to lower the temperature differential between the bulk solution and the heat transfer surface in cases of normal soluble salts or freezing scaling.

CHAPTER 7 SCALE CHARACTERISATION

This chapter analyses the surface structure and morphology of the crystalline scale deposits on the stainless steel agitation tank wall. The scale characteristics are examined by using a camera to view the scale topology and scanning electronic microscope (SEM) for microscopic structure of crystal deposits.

7.1 Scale Deposit Structure

The photographs as presented in Figures 7.1 (a) to (d) show the KNO_3 scale formation on stainless steel SS316 surface at different agitation speeds of 100, 300, 500 and 700 rpm, respectively, for the impeller diameter of 86 mm and KNO_3 concentration of 4.50 mol/dm^3. Initially, it was observed that the porous and uniform scale layer was formed at the lower agitation, and more compact and non-uniform scale layer was formed at the higher agitation. The scale deposition at low agitation speed (for example, 100) is presented in Figure 7.1 (a) for the impeller diameter of 86 mm and baffled condition, 7.3 (a) for the impeller diameter of 86 mm and unbaffled condition, and 7.6 (a) for the impeller diameter of 114 mm and baffled condition, in which the crystal surface shows large needle-like shape. The likely cause of the large, porous needle-like shape is due to the lower fluid erosion and possible growing up of the crystals freely outwards from the wall. During the experiment, it was also observed that the needle like shape grows up very fast because of the protruding shape acting as a strong nucleation site at low agitation.

At moderate agitation, the scale deposition becomes more dense and the surfaces are covered with uniform scale deposition, as shown in Figure 7.1 (b), 7.1 (c), 7.3 (b), 7.3 (b) and 7.7 (a), (b), (d), (e) in crystal structure. Conversely, at high agitation speed (for example, 500 rpm to up) as shown in photographs (Figure 7.1 (c), 7.1 (d), 7.6 (d), and 7.7 (c) (f)), the crystal surface structure is more compact and less porous which can be attributed to the high fluid erosion (Kazi et al., 2012; Kazi et al., 2010). It is noted that cleaning of this compact crystallisation scaling surface from the wall of agitation tank is rather a difficult process.

The scale deposits from the SS316 tank wall were collected on a sample holder with carbon sticky glue surface, and crystal structure morphology was examined by using microscopic techniques of scanning electronic microscope (SEM). A typical microscopic picture from SEM

analysis is given in Figure 7.2 at agitation speed 100 rpm, KNO_3 concentration of 4.50 mol/dm^3 and with baffles.

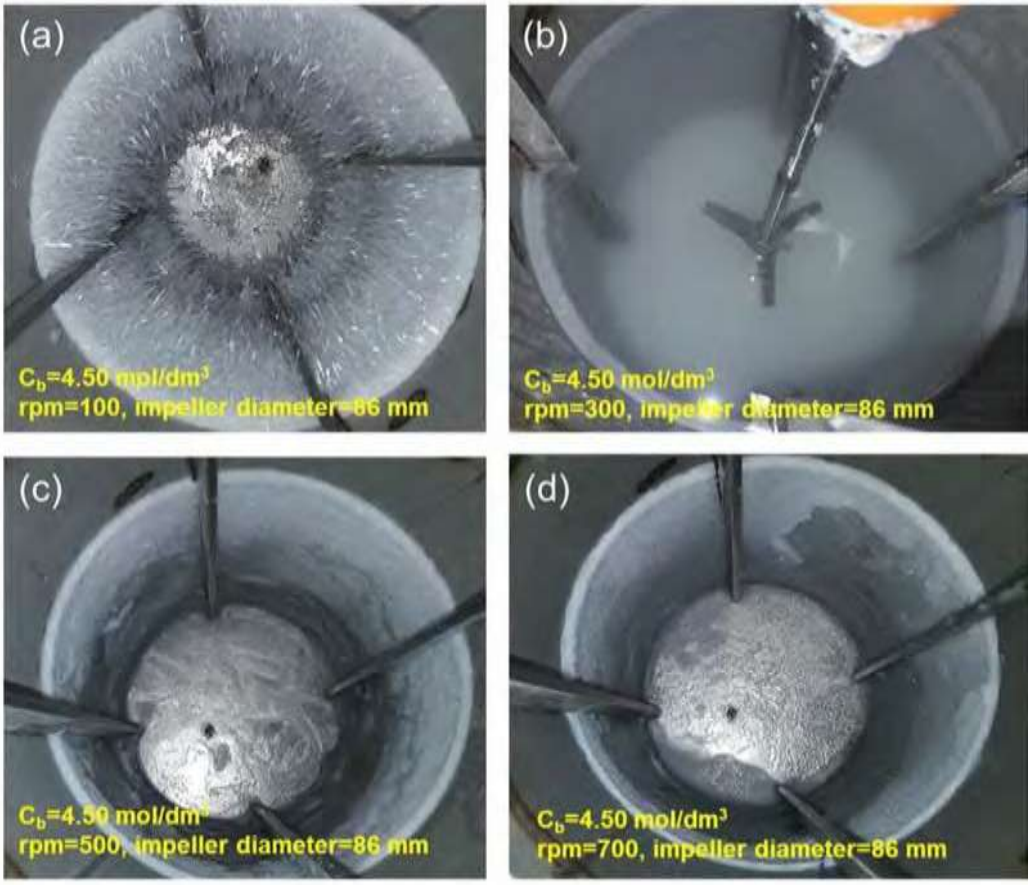

Figure 7.1: Crystal growth on SS 316 agitation tank wall surface exposed to a solution of KNO_3 at bulk temperature 48°C, ΔT=51.75°C, C_b=4.50 mol/dm^3, impeller diameter of 86 mm and baffled tank condition

7.2 Crystal Morphology

Figure 7.2 shows the scale deposit at the bulk liquid-solid scale interface at the end of the experiment. Figure 7.2 (a) shows the KNO_3 scale deposit with various crystals sizes and porosity. It is observed that some of the smaller crystals appear to attach with scale deposit loosely. The likely explanation of tiny and broken crystals are that they originated from either bulk crystallisation or tiny crystals breaking from the scale deposit layer due to the fluid erosion

by shear stress. Figure 7.2 (b) shows the broken crystals spread over the layer of scale deposits, Figure 7.2 (c) represents the tiny crystals accumulated on the large one, and Figure 7.3 (d) shows the large crystal broken by fluid shear.

(a)

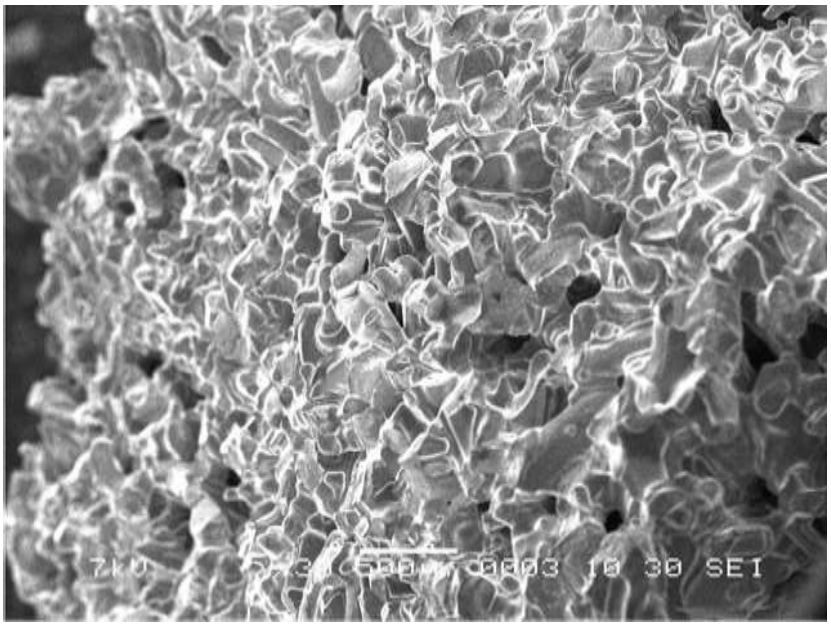

(b)

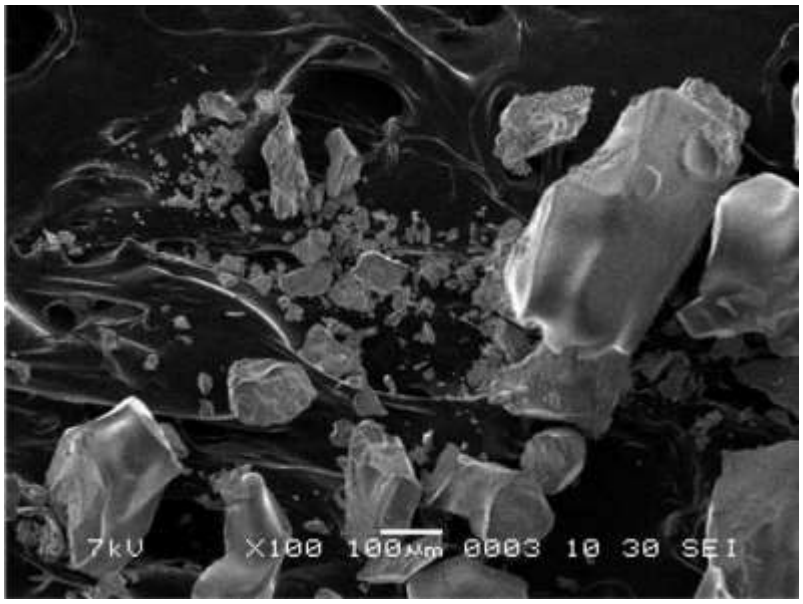

(c)

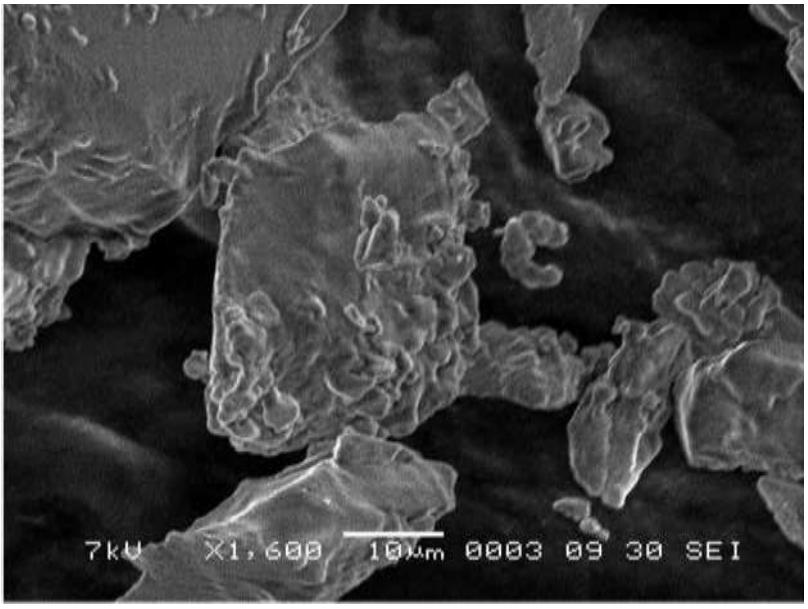

(d)

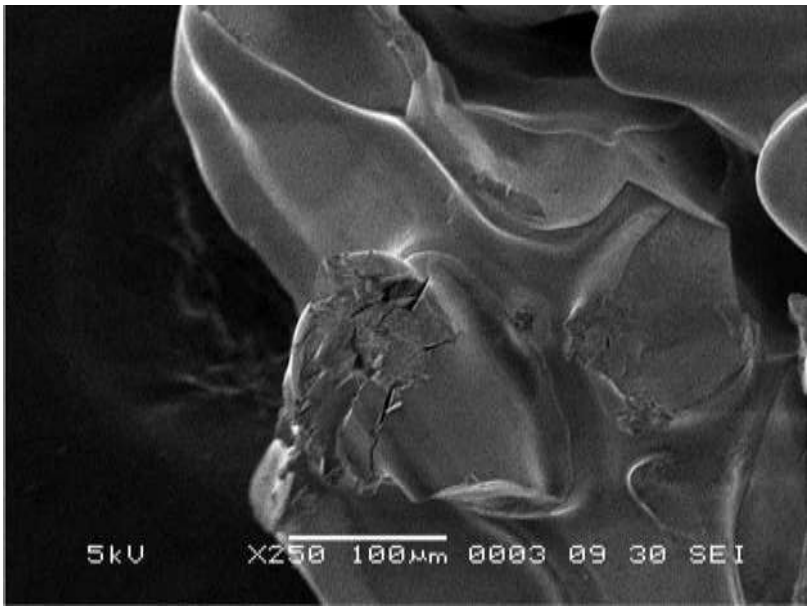

Figure 7.2: Microscopic view of crystals arrangement on SS316 tank wall at 100 rpm, concentration of 4.50 mol/dm^3, impeller diameter of 86 mm and baffled condition at different magnification: (a) magnification × 30 at exciting voltage 5 kV and different sizes (b) magnification × 100 at exciting voltage 5 kV and broken crystals spread on the scale surface

(c) magnification × 1,600 at exciting voltage 5 kV and loose crystals on the larger crystal and (d) magnification × 250 at exciting voltage 7 kV and broken crystal due to fluid shear

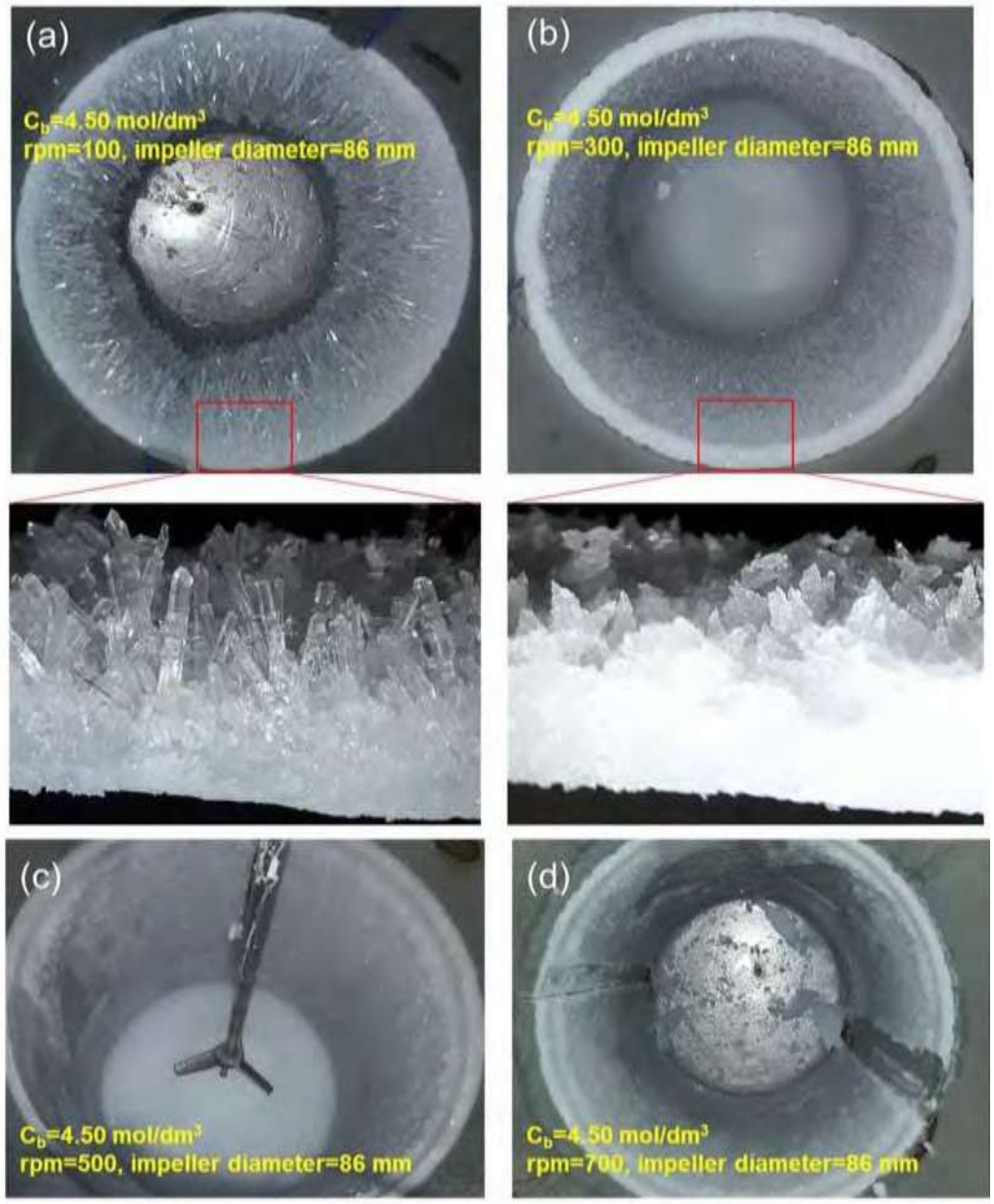

Figure 7.3: Crystal growth on SS 316 agitation tank wall surface exposed to a solution of KNO_3 at bulk temperature 48°C, ΔT=51.75°C, C_b=4.50 mol/dm^3, impeller diameter of 86 mm and unbaffled tank condition

Figure 7.3 shows the different crystal deposits on SS316 agitation tank wall after completing experiment at various agitation rates, for the concentration of 4.50 mol/dm^3 and the unbaffled

condition. Figure 7.3 (a) shows various sizes of the protruding crystals at low agitation, Figure **7.3** (b) shows the less protruding crystals at moderate agitation and Figure 7.3 (c), (d) show the crystal deposit at high agitation with almost no protruding portion.

(a)

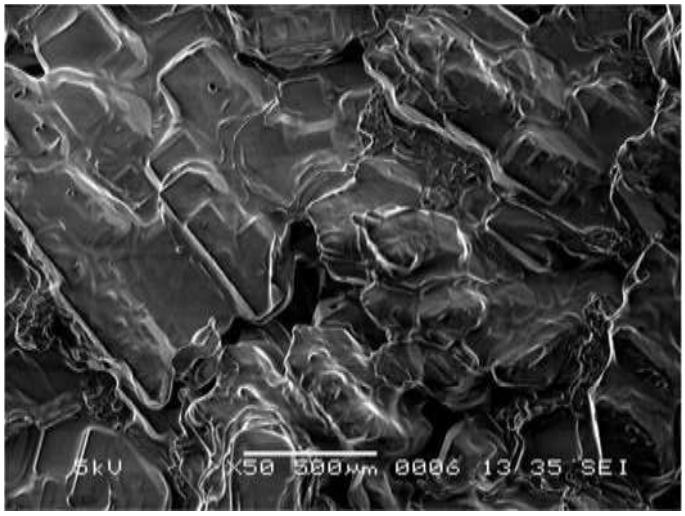

(b)

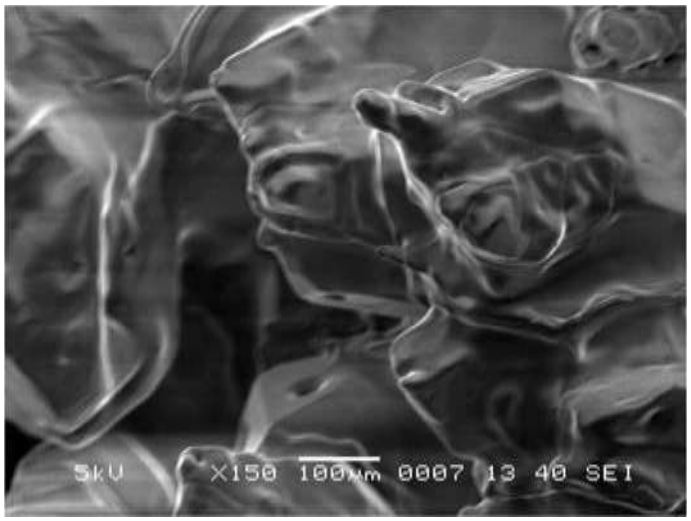

Figure 7.4: Microscopic view of crystals arrangement on SS316 tank wall at 300 rpm, concentration of 4.50 mol/dm^3, impeller diameter of 86 mm and baffled condition at different magnification: (a) magnification × 50 at exciting voltage 5 kV and different sizes (b) magnification × 150 at exciting voltage 5 kV

(a)

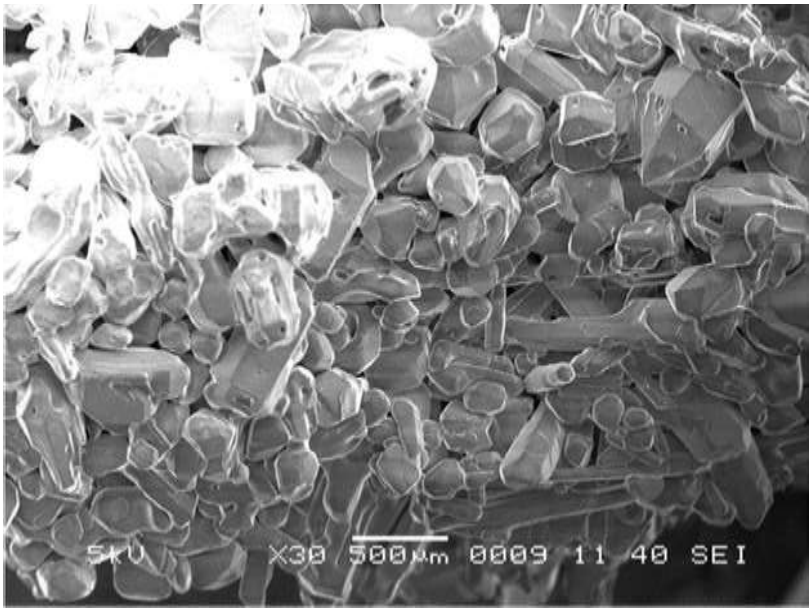

(b)

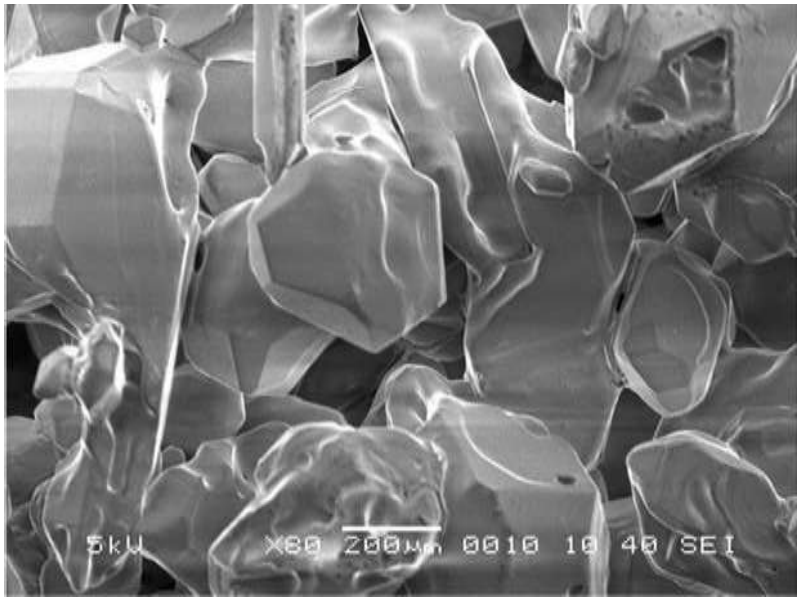

Figure 7.5: Microscopic view of crystals arrangement on SS316 tank wall at 500 rpm, concentration of 4.50 mol/dm^3, impeller diameter of 86 mm and baffled condition at different

magnification: (a) magnification × 30 at exciting voltage 5 kV and different sizes (b) magnification × 80 at exciting voltage 5 kV

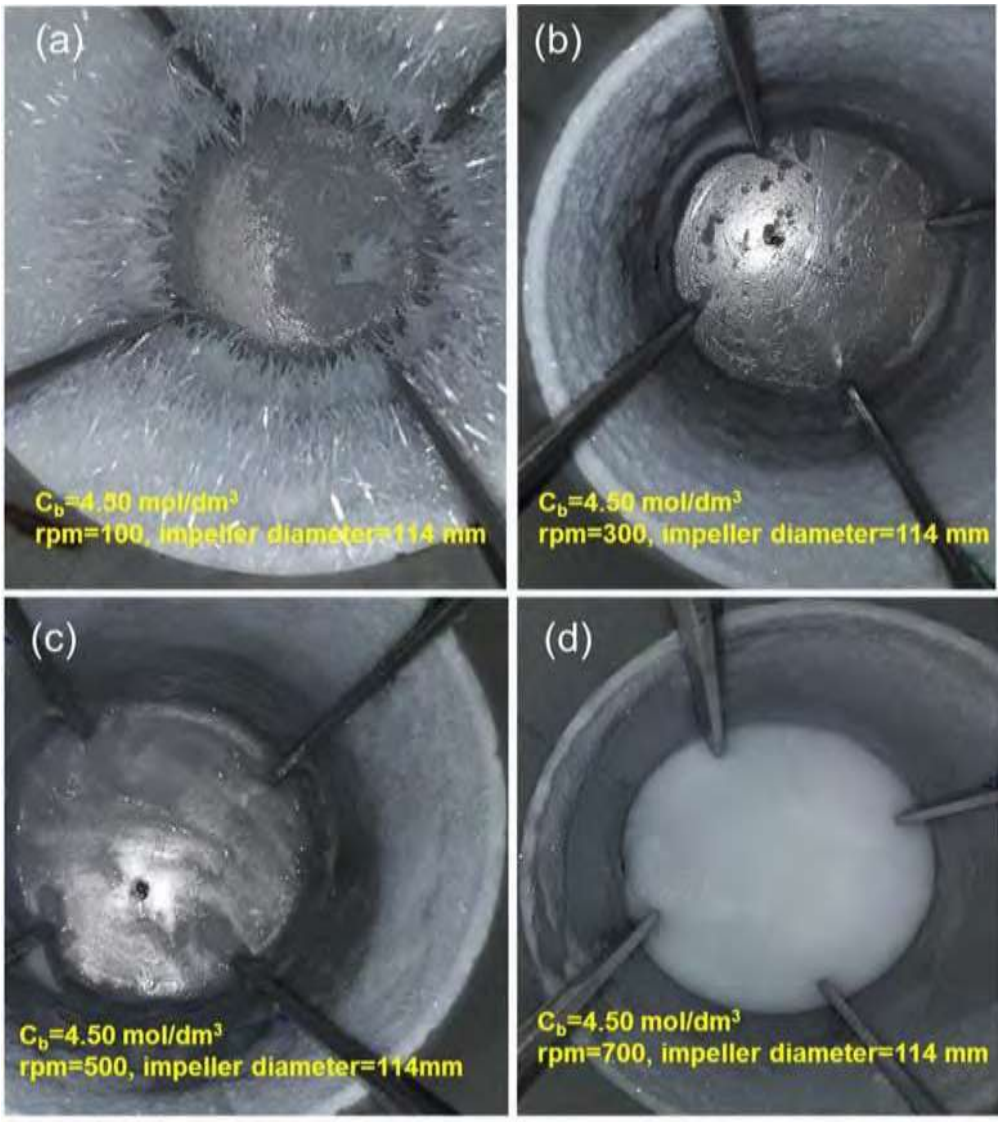

Figure 7.6: Crystal growth on SS 316 agitation tank wall surface exposed to a solution of KNO_3 at bulk temperature 48°C, ΔT=51.75°C, C_b=4.50 mol/m^3, impeller diameter of 114 mm and baffled tank condition

Figures 7.4 and 7.5 show the microscopic view of crystal morphology at different experimental conditions at agitation speed of 300 and 500 rpm, respectively. At moderate agitation intensity of 300 rpm, different sizes of crystals orientated in a regular pattern with the protruding crystals from the wall as shown in Figure 7.4. On the other hand, at high agitation intensity of 500 rpm,

crystal morphology shows a large number of different size crystals spread over the layer scale deposits. The likely explanation for a large number of the tiny crystals are that they occurred due to intense bulk crystallisation at high agitation rate. From the bulk crystallisation, many tiny crystals glued with the scale layer deposits.

Figure 7.6 shows the scale deposits on agitation tank wall at different agitation rates, for the concentration of 4.50 mol/dm^3, impeller diameter of 114 mm and the baffled condition. The scale layer, due to crystallisation at higher agitation rate with larger impeller size, decreases scale layer thickness which is attributable to the effect of high fluid erosion. At higher agitation rate, the tank wall is almost uncovered and some lighter spots are created on upper part of the agitationtank.

Figure 7.7 shows the comparison between crystal deposits for two different concentrations of 4.75 mol/dm^3 and 5.25 mol/dm^3, respectively, and different agitation rates with impeller diameter of 86 mm. It is seen from the photographs, that the thick scale layer occurred at higher concentration as compared with the lower concentration with the same agitation intensity. This result indicates that the scale deposition depends on the surface reaction control not the diffusion control. The likely explanation is that the supersaturation (concentration difference between the bulk solution and the interface of the wall) is the main driving force of crystallisation scale deposition. At the same wall temperature (maintaining constant coolant temperature for all experiments), more supersaturation occurred for higher concentrated solution at the same agitation rate. Therefore, it can be stated that the higher concentrated solution leads to more scale deposition in case of crystallisation scaling of normal soluble salts.

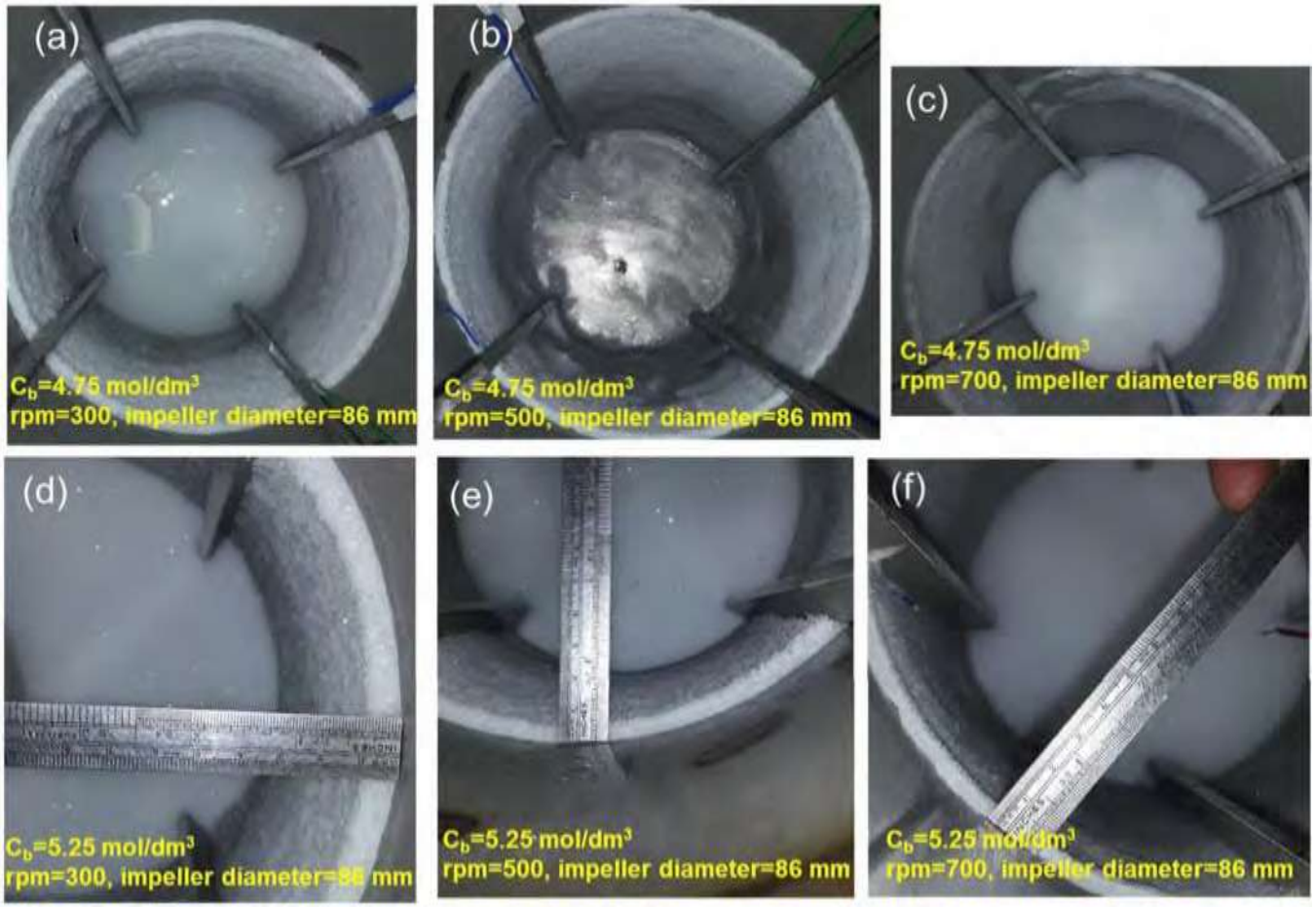

Figure 7.7: Crystal growth on SS 316 agitation tank wall surface exposed to a solution of KNO_3 at bulk temperature 48°C, ΔT=51.75°C, compared the concentration $C_b = 4.75\ \text{mol/dm}^3$ and $C_b = 5.25\ \text{mol/dm}^3$, and baffled tank conditio

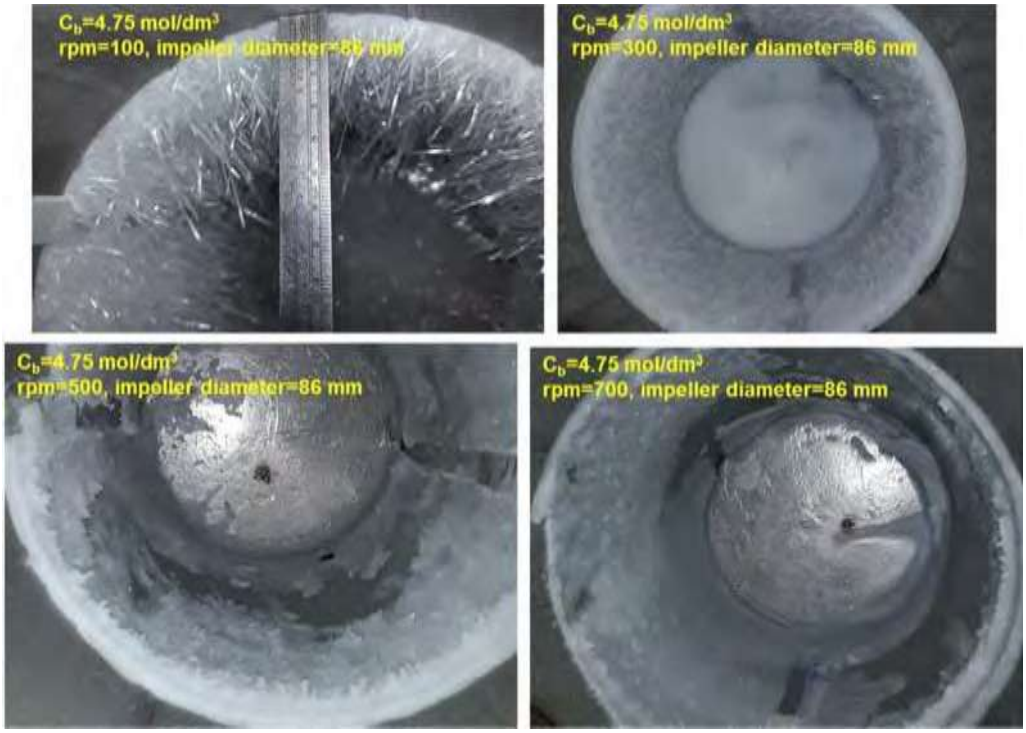

Figure 7.8: Crystal growth on SS 316 agitation tank wall surface exposed to a solution of KNO_3 at bulk temperature 48°C, ΔT=51.75°C, $C_b = 4.75\ \text{mol/dm}^3$, impeller diameter of 86 mm and unbaffled tank condition

Figure 7.8 shows the scale deposit layers in the unbaffled condition with the impeller diameter of 86 mm at different agitation rates of 100, 300, 500 and 700 rpm, respectively. The scale deposit layer thickness is seen less thicker compared to that for the baffled tank condition. In the unbaffled tank condition, the scale removal rate is higher because of the swirling flow over the wall and subsequent uniform fluid erosion effect over the scale deposits layer.

Figure 7.9 shows the scale deposition over the SS316 tank wall for the unbaffled condition with the larger impeller size diameter of 114 mm. The unbaffled tank with larger impeller shows reduced scale formation in the form of wall growth scale deposition because of the larger impeller with no baffles condition which created the higher and uniform fluid erosion effect due to severe swirl flow action.

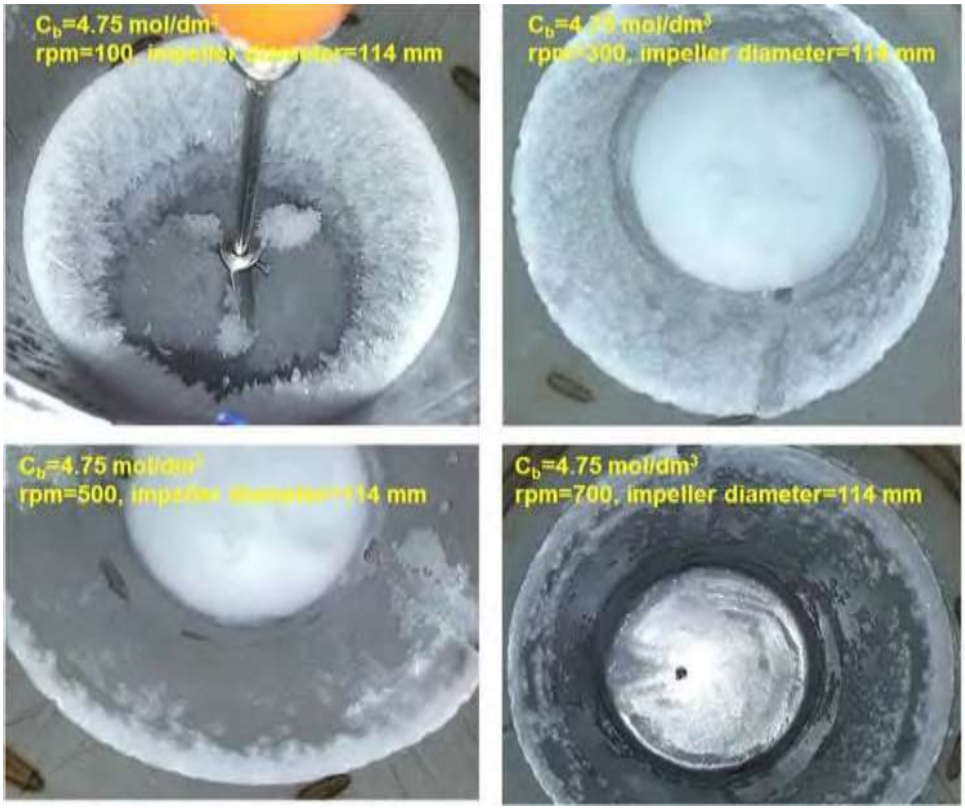

Figure 7.9: Crystal growth on SS 316 agitation tank wall surface exposed to a solution of KNO_3 at bulk temperature 48°C, ΔT=51.75°C, C_b=4.75 mol/dm^3, impeller diameter of 86 mm and unbaffled tank condition

The photographic observation reveals that more heavy deposit encrustations of KNO_3 scale formed on the agitation tank wall at a lower agitation speed than that of a higher agitation speed. Also, visual inspection of the surface shows a discontinuous scale formation on the tank wall at the higher agitation speed. It may depend on the local fluid erosion (minor eccentricity of the impeller axis from the centre of the tank) and surface characterisation (for example, distribution of the surface energy) of SS 316 tank wall (Kazi et al., 2015a; Kazi et al., 2012; Mwaba et al., 2006b; Weigand et al., 1997). It should be stated that after a careful inspection no stain on scaling surface was observed indicating no chemical attack on the surface and formation of only KNO_3 crystallisation scale was observed.

7.3 Summary

The analysis of the crystal structure (shape, size and orientation) and crystal morphology is of great importance to elucidate the crystalline scale formation and suppression mechanism. Evidently, the structure of crystal deposit is noticeably influenced by the rate of agitation, concentration and flow conditions (swirl or non-swirl). In the crystal structure, the size and alignment are distinguishably noticeable. Specifically, larger needle like shape, porous, regular pattern and perpendicular to the substrate surface orientated deposits are the main features of low agitation flow condition (such as, 100 rpm) and thicker, compact, harder and randomly orientated crystal deposits are distinctive characteristics at moderate flow condition (ranging from 200 to 400 rpm). In general, the crystal deposits are compact, harder and more adherent at low to moderate agitation condition than the violent agitation condition. The crystallisation of normal salt is a replica of scale mechanism of the Bayer liquor. Significant scale suppression could occur at high agitation hydrodynamic condition (more scale reduction occurred at high agitation with swirl flow condition) leading to thinner layer of scale which is easier and cheaper to clean.

CHAPTER 8
SCALING ON VARIOUS MATERIAL SURFACES

Material properties of the substrate surface have great influence on the crystallisation scale deposition controlled by the surface reaction rather than the mass transfer mechanism. It has been observed that more scale deposition occurs at higher thermal conductivity (Gill and Nancollas, 1980; Kazi et al., 2015a; Kazi et al., 2010;). This chapter presents the scaling behaviour on various heat exchange pipe materials during the convective heat transfer mechanism in the agitation tank. In this experimental setup, the test pipes from various materials were installed vertically at the centre of the agitation tank to provide constant and uniform flow conditions around the test pipe surface. A series of experiments were conducted using laboratory-made KNO_3 solution under varying experimental conditions, such as varied crystalline solute concentration in the process solution, varied surface temperature and properties of pipe materials. The freezing crystallisation scalings of normal soluble salt on different pipe material surfaces, such as copper (Cu), aluminium (Al), stainless steel (SS316), mild steel (MS) and polycarbonate were investigated. The results show that the crystallisation scaling deposition increases with time and is augmented with higher thermal conductivity of the pipe materials. In addition, the potential of gum arabic additive to mitigate the freezing crystallisation scaling on different materials during convective heat transfer condition was investigated. This experimental investigation also reported on the variation of overall heat transfer coefficient (OHTC) and thermal resistance (TR) that depends upon thermal conductivity.

8.1 Previous Work Review

Experimental investigation of $CaSO_4$ crystallisation fouling or scaling on different heat exchanger materials was reported by several authors (Gill and Nancollas, 1980; Kazi et al., 2012; Kazi et al., 2010). They found that the scaling deposition increases with the increasing thermal conductivity and surface energy of substrate materials, showing a hierarchy of thermal conductivity of copper, aluminium, brass and stainless steel. They also reported that the scale deposition on the surface increases with the surface roughness irrespective of types of metal and bleached kraft softwood pulp fibres promote to retard the scaling and can reduce it more

with the increase of fibre concentration (Kazi et al., 2013; Kazi et al., 2012; Kazi, 2012; Kazi et al., 2002; Kazi et al., 2010;). The non-metallic heat exchange surface, for example, polycarbonate surface, has a lower scale deposition due to the lower thermal conductivity than the other metal surfaces (stainless steel, copper, brass and aluminium) (Kazi et al., 2010).

Kazi et al. (2015a) investigated the environmentally benign additive as arabic gum powder, which retarded the scale deposition on the metal surface during the convective heat transfer conditions. Similar results were reported by another author as deposition increases with increasing thermal conductivity; for example in the order of higher to lower thermal conductivity, such as copper, brass and stainless steel (Amjad, 1988). Lower surface energy is capable of retarding the scale building on the metal surface; the weaker the adhesion of the deposition on a surface, the easier it is to clean (Lindner, 1992). Müller-Steinhagen et al. (2000) investigated the effect of surface properties on $CaSO_4$ scale formation during convective heat transfer and subcooled flow boiling. They reported that on reduction in surface energy by ion beam implantation, unbalanced magnetron sputtering, mixed sputtering and plasma arc treatment reduced the scale deposition significantly. Glade et al. (2015) studied the impact of heat transfer surface properties on crystallisation fouling in a falling film evaporator for artificial seawater desalination. They concluded that there is no simple correlation between the surface free energy and the scaling rate, but interfacial free energies between the heat transfer surface and deposit lead to increase the scale deposition. Gill and Nancollas (1980) studied the crystallisation scaling of calcium sulphate on different metal shell surfaces using a constant heat flux. They also found the high scale deposition with metals of the higher thermal conductivity, showing a hierarchy of copper, aluminium, brass and stainless steel 304.

Herz et al. (2008) investigated the effect of surface roughness of stainless steel (AISI 304 ba) on crystallisation fouling of aqueous $CaSO_4$ solution during convective heat transfer condition. They found that roughened surface has more deposition and tenacious calcium sulphate scale with the enhancement of the degree of surface roughness. The contact angle of the deposition surface has a more pronounced effect on deposition rate at lower values, which corresponds to a higher degree of surface roughness. It was observed that the surface roughness has shortened the induction period due to extra nucleation sites for primary heterogeneous nucleation by the protruding ridge of the rough surface. The rough surface reduces the shear rate in the valleys and reduces the removal rate of the crystals from the surfaces where roughness elements protrude out of the viscous sub-layer.

Keysar et al. (1994) investigated the effect of surface roughness on calcite crystallising scaling on mild steel pipe surfaces of a potable water supply system. They observed that the adhesion strength or stickiness of crystal deposit to steel and morphology of calcite scale layer was significantly influenced by the degree of surface roughness. They also showed that the tensile stress required to disbond the calcite scale layer from the rough surface was 30 times higher than that for a smooth surface. The rough surface produced more tenacious and compact deposit than the smooth surface by enhancing the nucleation density and orientation of calcite structure due to the formation of mechanically interlocking bonds between its crystallites.

Zhao et al. (2005b) studied the effect of the surface energy of Ni-P-PTFE coatings on reducing $CaSO_4$ scale formation. They examined the Ni-P-PTFE coatings on copper sheets, and stainless steel heater rods where surface energy ranging from 20-39 Mn/m have a significant potential to reduce the $CaSO_4$ scale on water treatment equipment. They also observed that the effect of the surface energy of Ni-Cu-P-PTFE coatings on the steel surface have potential to reduce the biofouling and mineral crystalline fouling (Zhao et al., 2005a). Al-Janabi et al. (2010) investigated the crystallisation fouling with electroless Ni-P coatings with or without boron-nitride (BN). The Ni-P coatings with boron-nitride reduce the tendency of the coatings to fouling due to an increase in the electron donor component of surface energy.

The adhesion of scale deposit depends on total surface free energy as the higher surface energy has stronger adhesion of scale (Fletcher, 1991), and the lower surface energy has strong resistance to build up scale deposit on it (Lindner, 1992). Azimi et al. (2014) investigated the effect of surface energy in reducing the crystalline scale formation in glass slides with depositing self-assembled monolayers (SAMs) of functionalised coatings (organosilanes) exposed to the saturated aqueous $CaSO_4$ solution. They showed that treated surface had remarkable potential to decrease the scale formation up to 90% due to the reduced number of nucleation sites, not because of reduced growth rate.

Several authors conducted experiments investigating the potential of natural fibres to mitigate the crystallisation scaling in heat exchangers during convective heat transfer (Kazi et al., 2012; Kazi et al., 2013; Kazi et al., 2010; Middis et al., 1998). Middis et al. (1998) have shown that the addition of wood pulp fibres reduces the fouling remarkably due to keeping away reactants from the heat transfer surface and preventing continuous physical collision with that surface. Kazi et al. performed experiments on $CaSO_4$ crystallisation scaling in stainless steel 316L pipe (Kazi et al., 2002). They investigated the potential of wood pulp fibres in $CaSO_4$ solution to

mitigate the fouling on the inner wall of steel pipe. They found that the heat transfer augmentation extended up to 11 days for fibre concentration of 0.15% and 45 days for the concentration of 0.25%. The possible explanation of fouling mitigation potential of fibre is it interrupted the crystalline structure on the surface.

Al-Janabi and Malayeri (2015) investigated the environment-benign approach to mitigate crystallisation fouling by minimising surface adhesion energies. They found that Lewis base polarity component has a strong repulsive energy, and reduced the adhesion between crystal precursor and the substrate. Al-Janabi et al. (2011) also studied the potential of solvent-based and water-based coatings to suppress the $CaSO_4$ fouling on the stainless surface during convective heat transfer. The solvent-based coatings showed strong mitigation performance characterised by longer induction period than water-based coating surface.

To date, several investigations have been undertaken for mitigation or suppression of scaling or fouling in heat exchange devices, such as altering the operating parameters, adding chemical additives, and adding particles and natural or artificial fibre to the process solution. Nowadays, several investigations have been undertaken to explore more environment-friendly chemical additives, such as carboxy methyl cellulose (CMC), cationic inulin polymer (CATINS), and poly-allylamine hydrochloride (PALM) rather than the additives that are hazardous to the environment (Harris and Marshall, 1981; Krisher, 1978). Kazi et al. (2015a) investigated the environment-friendly additive, such as gum arabic to reduce the crystallisation scaling from the inverse soluble salt of the $CaSO_4$ solution in the heat exchanger. The addition of gum arabic additive has significantly reduced the scale growth rate. The following sections described the scale experiment set up, materials and data acquisition in detail. The effect of scaling on different material pipes and effect of gum arabic as a scale inhibitor are also discussed in successive sections.

8.2 Experiment Setup

The second stage of experiment setup facility was specially designed to investigate the crystallisation scaling effects of normal soluble salt on various pipe materials during convective heat transfer mode by using KNO_3 solutions. The experimental apparatus consisted of one flow loop and one bulk agitation system as shown in Figure 8.1. The photograph of the experimental setup with necessary measuring apparatus is shown in Figure 8.2. The flow loop comprised of thermostatically controlled low-temperature circulation to maintain constant coolant temperature, rotameter and test pipe (different test pipes, such as Cu, Al, SS316, MS and

polycarbonate). The low-temperature coolant (50% distilled water + 50% ethylene glycol) was circulated through the test pipe which was installed at the centre of the agitation tank. The temperature of coolant was maintained between 0°C and -4°C and temperature over the test pipe surface was maintained at around -3.2°C. The scaling process solution was contained in the agitated stainless steel tank. The U-shaped PVC double wings (350 mm long and 20 mm wide) overhead impeller was used for agitation for efficient mixing. The speed of the double wings impeller was controlled by a Heidolph overhead stirrer through the variable speed drive via belt transmission.

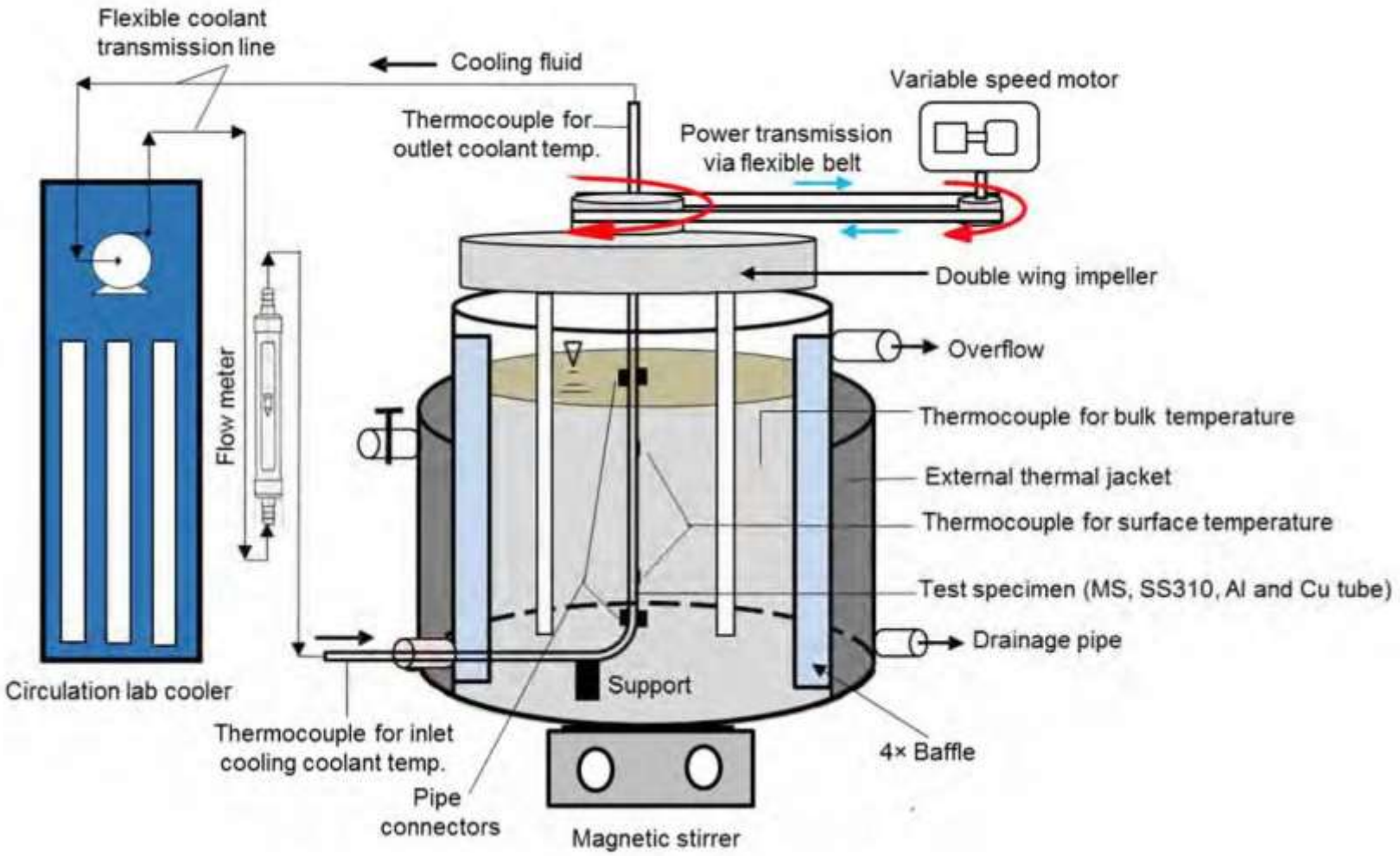

Figure 8.1: Schematic diagram of the experiment setup with necessary apparatus

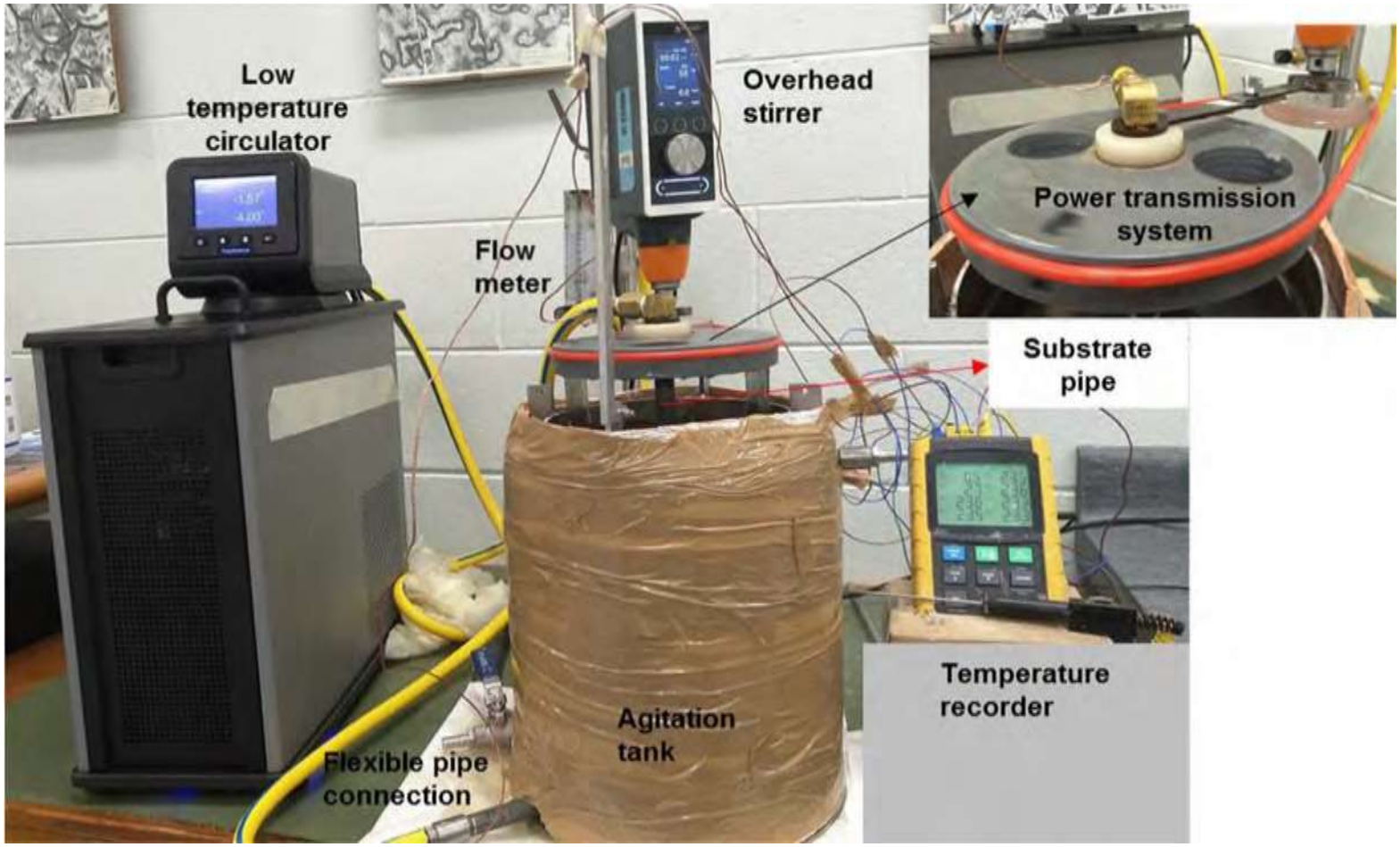

Figure 8.2: Experiment setup with necessary apparatus at open condition after experiment

8.3 Test Specimens

The effect of materials on crystalline scaling (crystallisation of normal soluble salt) was investigated using four different metal pipes, such as copper (Cu), aluminium (Al), stainless steel (SS316), mild steel (MS) and one non-metal of polycarbonate pipe as shown in Figure 8.3. All the test pipes were of 17 mm outer diameter, and 350 mm long with a wall thickness of 2 mm. Before conducting the experiment, the test pipes were cleaned by rubbing with a water-soaked cloth and flushing with hot water to remove any deposits of grease, oil, and so on.

Figure 8.3: Experimental test pipes with different materials

Table 8.1**:** Physical properties of pipe specimens

Materials	Properties at 300 K			
	ρ (kg/m^3)	C_p (J/kg.K)	k (W/m.K)	R_a (μm)
Stainless steel (SS316)	8238	468	16	1.78
Mild steel (MS)	7850	-	54	1.54
Copper (Cu)	8960	385	385	1.34
Aluminium (Al)	2702	903	250	1.25
Polycarbonate	2160	1400	0.25	0.48

8.4 Experimental Procedure

The preparation of KNO_3 scaling solution was the same as described in Chapter 4. The cooling coolant (-4°, -2° and 0°C) from lab circulator passed through the test pipe at a pre-determined flow rate in rotameter. The properly insulated steel tank was filled with heated and saturated KNO_3 solution (48±1.8°C). The average coolant flow temperature was estimated by averaging the inlet and outlet temperatures of the coolant (50% distilled water + 50% ethylene glycol) flow through the test pipe. The double wings impeller agitation speed was set at a constant 40 rpm so that the surface tangential solution velocity at the outside pipe surfaces was approximately 0.25 m/s. The heat transfer coefficients and scaling resistance were calculated on the basis of the average temperature of bulk solution and coolant. The crystallisation scaling of normal soluble salt of the KNO_3 solution accumulated on different test pipe outer surfaces due to supersaturation. After completion of each test run, the test pipe was removed, preserved in a container and then the scale was air-dried slowly for 72 hours. The scale patterns and the forms, and foreign products were examined visually as well as by scanning electronic microscope (SEM).

8.5 Data Acquisition

A 12 channel temperature recorder (BTM-4208SD) was used to record the bulk process solution temperature at two different points, inlet and outlet temperatures of coolant passing through the test pipe and the test specimen wall temperature at four different points. The K-type thermocouples were used to record the temperature, and the program was set to record the temperature at every 10 seconds. The pre-determined coolant flow rate was controlled by rotameter, and the U-shaped double wings impeller speed was controlled via belt transmission from the variable speed drive motor.

8.6 Data Reduction

The heat transfer rate (or heat flux) q through the bulk scale forming solution to coolant was calculated from the average temperature difference between the outlet and inlet of substrate pipe (Çengel, 2003).

$$q = \dot{m} C_p \Delta T = \dot{m} C_p \left(T_{coolant,out} - T_{coolant,in} \right) \tag{8.1}$$

where,

$\dot{m}$ = Coolant flow rate [m^3/sec]

C_p = Heat capacity of coolant [J/Kg.K]

$T_{coolant,out}$ = Outlet temperature of coolant [°C]

$T_{coolant,in}$ = Outlet temperature of coolant [°C]

The overall heat transfer coefficient (OHTC), U between the bulk solution and the coolant was calculated based on the heat flux and the temperature between the bulk solution and substrate wall(Çengel, 2003).

$$U = \frac{q}{T_{bulk} - T_{wall}} \tag{8.2}$$

where,

U = Overall heat transfer coefficient [W/m^2.K]

q= Heat flux [W/m^2]

T_{bulk} = Average bulk solution temperature [°C]

T_{wall} = Average wall temperature [°C]

The thermal resistance due to scale formation $R_{scale}$was determined as the inverse difference of overall heat transfer coefficient at any instant time and initial U (Çengel, 2003).

$$R_{scale} \approx \frac{x_s}{\lambda_s} = \frac{1}{U_{t=t}} - \frac{1}{U_{t=0}} \tag{8.3}$$

where,

R_{scale} = Thermal resistance due to scale deposition [m^2.K/W]

x_s = Scale thickness [mm]

λ_s = Thermal conductivity of scale deposit [W/m.K]

$U_{t=t}$ = Overall heat transfer coefficient at any instant of time [W/m^2.K]

$U_{t=0}$= Overall heat transfer coefficient at clean condition [W/m^2.K]

Alternatively, when scale deposit occurs, it leads to increase of the scale thickness around the substrate pipe due to crystallised scaling. The average scaling diameter and scaling thermal resistance were calculated by the following Eqs. (8.4) and (8.5) (Kazi et al., 2015a), respectively.

$$D_{scale} = \left\lceil \frac{4w}{L\pi\rho_s} + D_0^2 \right\rceil \quad (8.4)$$

$$R_{scale} = \frac{\ln\left(\frac{D_s}{D_0}\right)}{2\pi k_s L} \quad (8.5)$$

where,

D_{scale} = Average scaling diameter [m]

D_0 = Outer dimeter of the specimen [m]

w = Weight of the scale deposit [g]

L = Length of specimen [m]

ρ_s = Density of scaling deposit [kg/m^3]

k_s = Thermal conductivity of scaling deposit [W/m.K]

The scaling thermal resistance was based on heat transfer coefficient of the bulk solution and the coolant as follows:

$$R_{Scale} = 1/(h_i A_i) + \left(\left(\ln(r_0/r_i)\right)/2\pi k L\right) + \left(\left(\ln(r_{scale}/r_0)\right)/2\pi k L\right) + 1/(h_0 A_0) \quad (8.6)$$

where,

h_i= Convective heat transfer coefficient inside pipe specimen [W/m^2.K]

h_0= Convective heat transfer coefficient outside pipe specimen [W/m^2.K]

A_i= Heat transfer surface area inside the specimen [m^2]

A_0 = Heat transfer surface area inside the specimen [m^2]

r_i= Inside radius of specimen [m]

r_0 = Outside radius of specimen [m]

r_{scale} = Average scale radius [m]

k= Thermal conductivity of specimen material [W/m.K]

L = Solution height in the tank [m]

The following correlation for the coolant through substrate pipe can be used to estimate the heat transfer coefficient (Çengel, 2003):

$$\Rightarrow h_i = 0.027 \left(\frac{k_c}{D}\right) \left(\frac{\rho_c U D}{\mu_c}\right)^{0.8} \left(\frac{C_{pc}\mu_c}{k_c}\right)^{0.3} \left(\mu_c/\mu_{wc}\right)^{0.14} \quad (8.7)$$

where,

k_c = Thermal conductivity of coolant [W/m.K]

ρ_c = Density of coolant [kg/m^3]

$\bar{U}$ = Average velocity of coolant through the specimen pipe [m/s]

D = Inside diameter of specimen pipe [m]

μ_c = Viscosity of cooling coolant at bulk coolant temperature [Pa.s]

μ_{wc} = Viscosity of cooling coolant at wall temperature [Pa.s]

C_{pc} = Heat capacity of coolant [J/kg.K]

The values of h_i and h_o are based on the empirical equation. The inside convective heat transfer coefficient for the bulk solution in the agitated tank is estimated from the following correlation (Dream et al., 1999):

$$\Rightarrow h_0 = 0.68 \left(\frac{k_s}{D_T}\right) \left(\frac{D_A^2 N \rho}{\mu_s}\right)^{0.67} \left(\frac{C_{ps}\mu_s}{k_s}\right)^{0.33} \left(\mu_s/\mu_{ws}\right)^{0.14} \quad (8.8)$$

where,

k_s = Thermal conductivity of process solution [W/m.K]

D_T= Agitation tank diameter [m]

D_A = Agitator diameter [m]

N = Impeller speed [rev/s]

ρ = Density of process solution [kg/m^3]

μ_s = Viscosity of process solution at bulk solution temperature [Pa.s]

μ_{ws} = Viscosity of process solution at wall temperature [Pa.s]

C_{ps} = Heat capacity of process solution [J/kg.K]

8.7 Results and Discussion

The results obtained from the experimental observation of potassium nitrate crystallisation deposition on five different pipes, namely copper (Cu), aluminium (Al), stainless steel (SS316), mild steel (MS) and polycarbonate pipe are discussed below. The results include the effect of concentration, coolant temperature and agitation rate on scale deposition rate. The scaling effect on the thermal resistance and heat transfer coefficient is also discussed. The effect of gum arabic additive on the scale deposition as environmentally friendly inhibitor is also presented.

8.7.1 Scale Deposition Analysis

The scale growth characteristics on the different materials specimens during convective heat transfer condition and under various experimental conditions, such as types of material, solution concentration and coolant temperature are presented below.

8.7.2 Effect of Different Material Specimens

Scale deposition effect observed on the five different material pipe specimens (Cu, Al, SS316, MS and polycarbonate as shown in Figure 8.3) indicate the order of higher scale deposition rate on various pipes was Cu > Al > SS316 > MS > polycarbonate under the same condition of experimental parameters. The likely cause of the increase scale deposition rate is due to more reaction activity caused by the higher thermal conductivity. Referring to Table 8.1, it is seen that the cumulative scale deposition depends on types of specimen according to the hierarchy of thermal conductivity in order of Cu > Al > SS316 > MS > polycarbonate. It can also be explained by the fact that higher thermal conductivity allows a higher rate of heat transfer

across the boundary layer which augmented surface reaction activity that might increase nucleation and grain growth of scale forming crystals on the specimen surfaces.

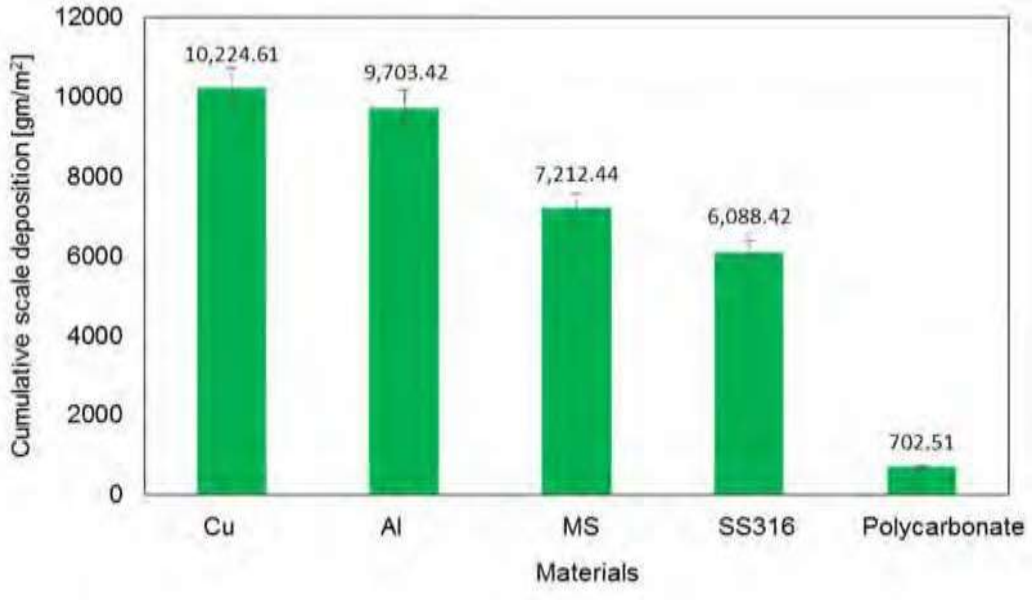

Figure 8.4: Cumulative scale deposition of potassium nitrate on different material surfaces after 170-minute

8.7.2.1 Effect of Potassium Nitrate Concentration on Scaling and Thermal Resistance

This section discussed the effect of KNO_3 concentration on scale deposition and consequential effect on scale thermal resistance. The results are shown in Figure 8.5 and they imply that more scale deposition occurred with higher solute concentration in the bulk solution. It is attributed to the higher solute concentration decreasing the initial induction period and augmenting KNO_3 scale deposition on SS316 specimen under the convective heat transfer. The increase of scale deposition on specimen leads to another adverse effect which increases the thermal resistance. Figure 8.6 shows the effect of scale deposition on the thermal resistance of specimen of SS316 and Cu. For both specimens, the thermal resistance increases with the solution concentration in bulk solution and show the quadratic line of best fit that matches the data.

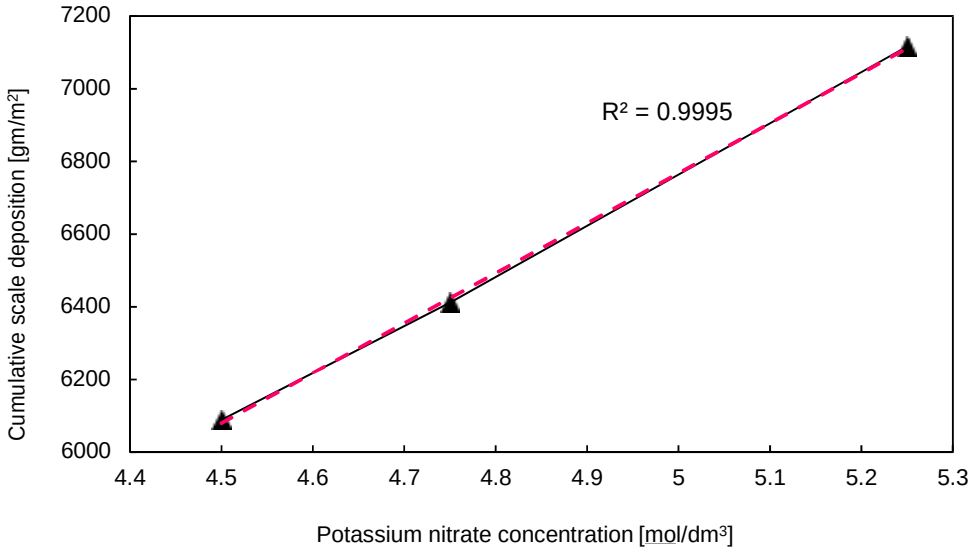

Figure 8.5: Scale deposition as a function of potassium nitrate concentration in bulk solution after 170-minute on stainless steel SS316 specimen

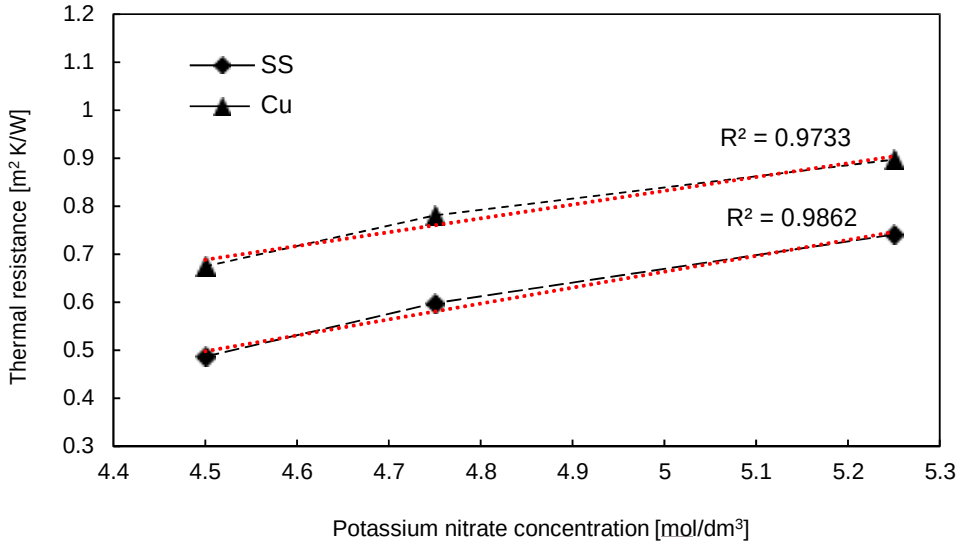

Figure 8.6: Scaling thermal resistance as a function of potassium nitrate concentration in bulk solution after 170-minute and potassium nitrate concentration of 4.50 mol/dm^3

8.7.2.2 Effect of Coolant Temperature

Figure 8.8 shows the effect of coolant temperature on cumulative scale deposition rate at -4°C, -2°C and 0°C. It is evident that the crystallisation scale deposition decreases considerably with decreasing coolant temperature through the specimen pipes. It should be noted that the lower

coolant temperature increases the OHTC due to a higher differential temperature between the bulk solution and the specimen surfaces. The lower surface temperature leads to increase of the local supersaturation on the specimen surface because of normal soluble salt of KNO_3. The increase of the lower temperature of coolant promotes to increase more solute deposition due to surface crystallisation reaction and augmented the crystalline deposition thickness.

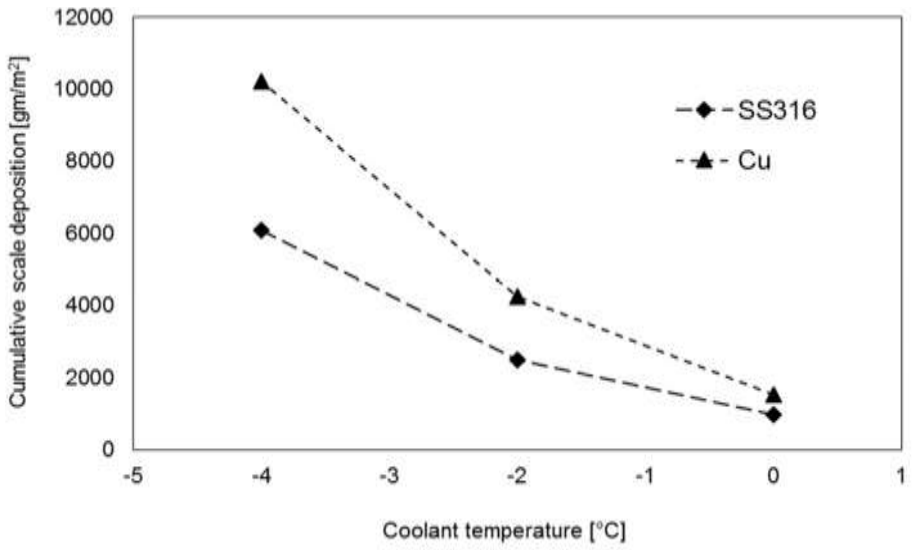

Figure 8.7: Cumulative scale deposition as a function of coolant temperature after 170-minute experimental observation

8.7.3 Scale Suppression Techniques

The scale suppression techniques during convection heat transfer condition on various material pipe specimens were investigated. Two suppression techniques based on the hydrodynamic effects and the potential of additive to reduce the crystalline scale deposition are discussed below.

8.7.3.1 Effect of Solution Agitation Rate

Figure 8.9 shows the variation of scale deposition rate as a function of bulk agitation of scale formation solution on the outside of specimen pipe surfaces. It is seen from Figure 8.9 that the scale deposition rate decreases appreciably with increasing agitation rate of U-shape PVC impeller. The increase in agitation rate has two effects. The intense agitation rate increases the heat transfer flux between the bulk solutions and coolant through the specimen pipe surfaces,

and diminishes the temperature gradient between the bulk solution and specimen pipe surfaces. This diminishing thermal gradient leads to the decrease of the local supersaturation of KNO_3 solution and as a result reduces the scale deposition on the test pipe surfaces. The higher agitation rate also created the higher fluid erosion effect on crystal layer and finally, reduced the thickness of scale deposition layer.

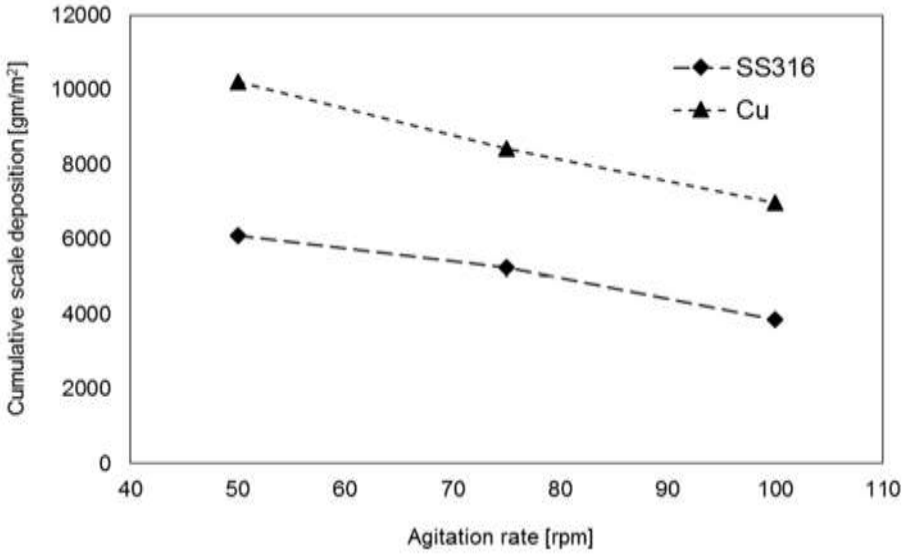

Figure 8.8: Cumulative scale deposition as a function U-shape impeller agitation rate in the bulk solution after 170-minute and potassium nitrate concentration of 4.50 mol/dm^3

8.7.3.2 Effect of Gum Arabic (Additive)

Figure 8.7 shows the effect of percentage of gum arabic additive on the crystallisation scaling deposition. The results show that the scale deposition decreases with the increase in the percentage of gum arabic in bulk scaling solution. This additive is highly soluble in water and it forms gel-like-layer. The reduction in scale deposition can be explained as the presence of gel-like-layer in the scale forming solution retards the nucleation of KNO_3 and crystal growth on the specimen surfaces. The cumulative scale deposition rate decreases asymptotically with time by 13.9%, 25.7% and 48.6% for stainless steel (SS316) specimen and 19.3%, 29.4% and 41.9% for copper (Cu) specimen due to the effect of gum arabic weight percentage (wt %) 0.5, 0.75 and 1, respectively. Therefore, this additive has great potential to be used for scale suppression.

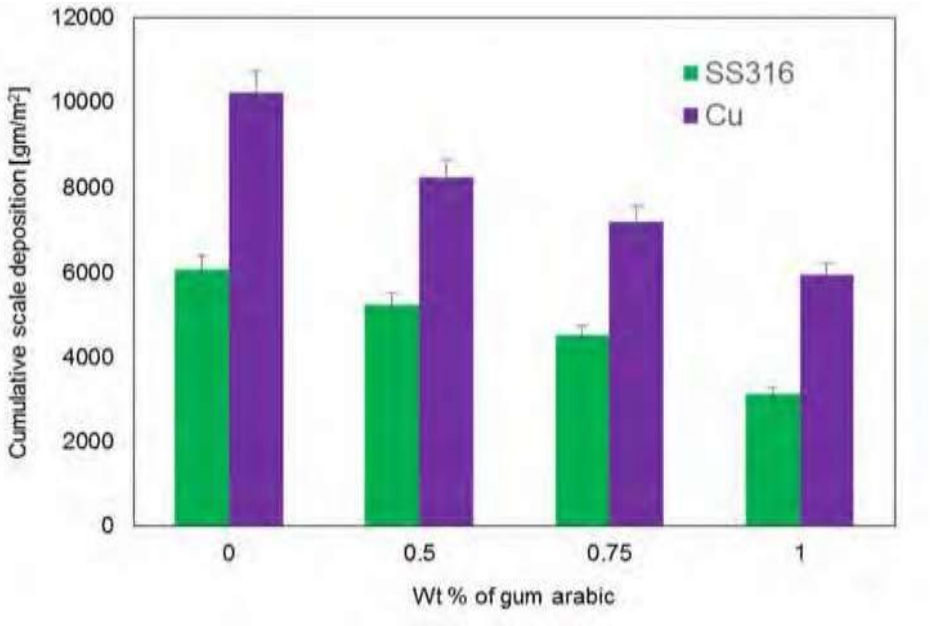

Figure 8.9: Cumulative scale deposition under the influence of wt. % of gum arabic in the bulk solution after 170-minute and potassium nitrate concentration of 4.50 mol/dm^3

8.8 Heat Transfer Analysis

This part of the analysis will reveal the effect of scale deposition on TR and OHTC as shown in Figure 8.10 for SS316 and Cu, respectively. The required data for calculation of heat transfer coefficient and thermal resistance was acquired during an experiment at every 20 sec time interval. Figure 8.10 show the OHTC and thermal resistance as a function of time. The results show that the scale thermal resistance rate increases with increasing time and finally, it becomes asymptotic around 170 minute experimental observation. At the asymptotic region, the scale deposition rate approximately equals to scale removal rate according to Kern and Seaton (1959a). The OHTC is a function of reciprocal thermal resistance. The OHTC during observation decreases with time, and finally, became an asymptotic behaviour. The scale deposition due to crystallisation of KNO_3 leads to two different consequences as an increase in thermal resistance and decrease in heat transfer coefficient because of the lower thermal conductive scale layer over the specimen pipe surfaces.

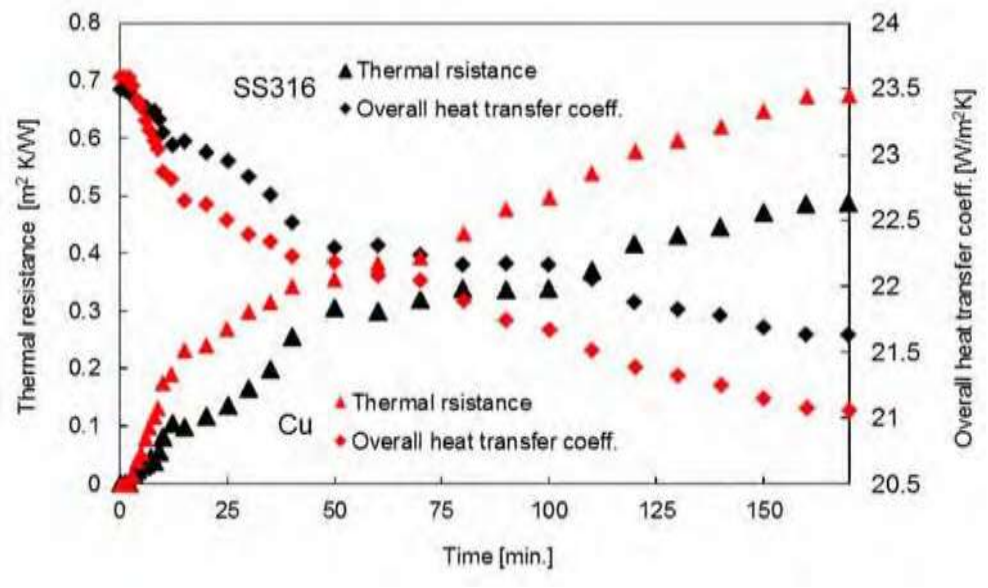

Figure 8.10: Scaling thermal resistance and overall heat transfer coefficient as a function of time on stainless steel (SS316) and copper (Cu) pipe after 170-minute and potassium nitrate concentration of 4.50 mol/dm^3

8.9 Visualisation of Crystal Structure and Crystal Morphology

This visualisation is analysed with the surface structure and morphology of the crystal structure. The photographs as presented in Figure 8.11 for Cu and Al respectively, show the scale deposition growth over the heat exchange tube during convective heat transfer between the heated KNO_3 solution and coolant (mixture ethylene glycol and water) through the tube.

Figure 8.12 shows the crystal structure of KNO_3 on the Cu and Al specimens, respectively, at the end of the experiment of 170 minutes. Figure 8.12 (a) shows the crystal structure of KNO_3 on the Cu specimen. It is observed that some granular crystal appears to compactly attach to different size KNO_3 scale crystal over Cu heat exchange tube. This compact granular crystal appears due to the agitation of bulk scale formation solution by double wing U-shape impeller and some tiny crystal also generated from the bulk crystallisation. Figure 8.12 (b) shows the crystal structure of KNO_3 on the Al specimen and very regular crystal structure was found during convective heat transfer except for any tiny crystal from bulk crystallisation and agitation effect of bulk solution.

Figure 8.11: Crystallisation scale deposition on pipe surface (a) Cu and (b) Al, concentration of 4.50 mol/dm^3, bulk temperature 48°C, surface temperature -3.6°C, coolant temperature -4°C and exposure time 170 minute

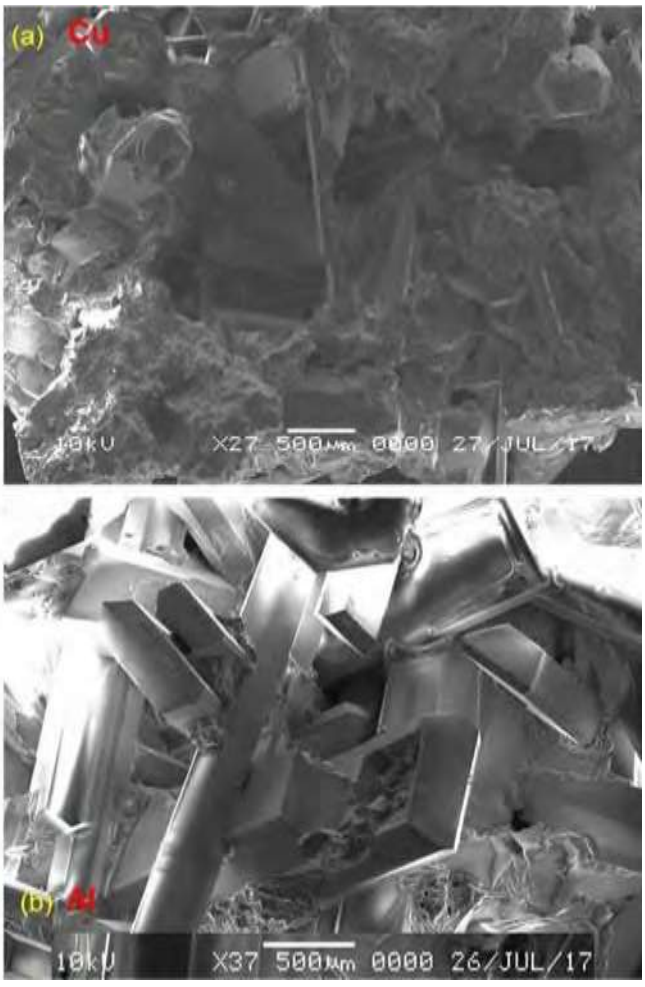

Figure 8.12: Microscopic view of crystal arrangement: (a) Cu and (b) Al

The photographs as presented in Figure 8.13 show the KNO_3 scale layer on SS316, MS and polycarbonate test specimens, respectively. The scale deposition layer thickness increases in order of hierarchy of thermal conductivity as Cu > Al > SS316 > MS > polycarbonate. It should be stated that after a careful inspection no stain on scale surface was observed indicating no chemical attack on the surface and formation of only KNO_3 crystallisation scale except mild steel specimen where reddish stains formed.

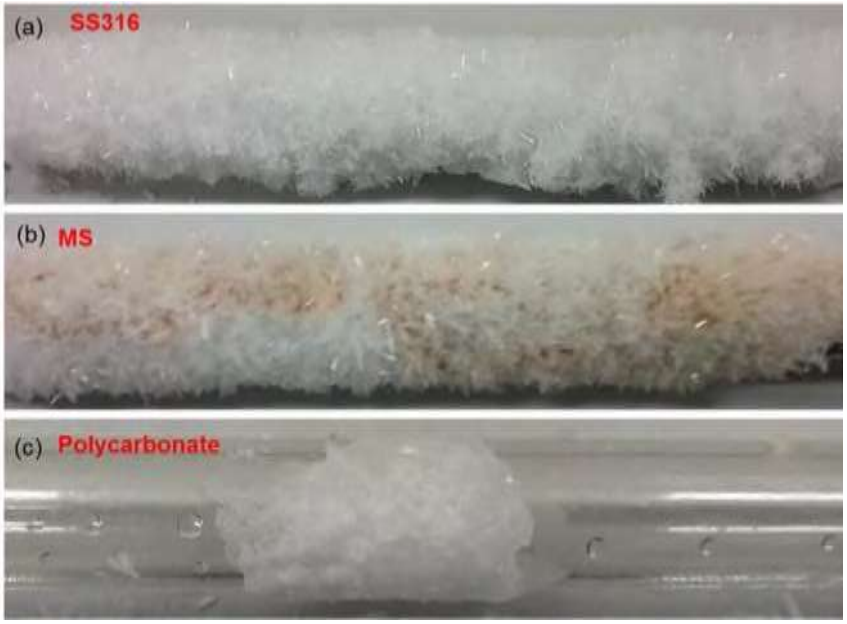

Figure 8.13: Crystallisation scale deposition on test specimen (a) SS316 (b) MS and (c) polycarbonate, concentration of 4.50 mol/dm^3, bulk temperature 48°C, surface temperature -3.6°C, coolant temperature -4°C and exposure time 170 minute

Figure 8.14 shows the microscopic view of KNO_3 crystal morphology on the SS316, MS and polycarbonate, respectively, the crystallised scale deposition during convective heat transfer between the heated bulk scale formation solution outside of the test pipe and the coolant inside the test pipe.

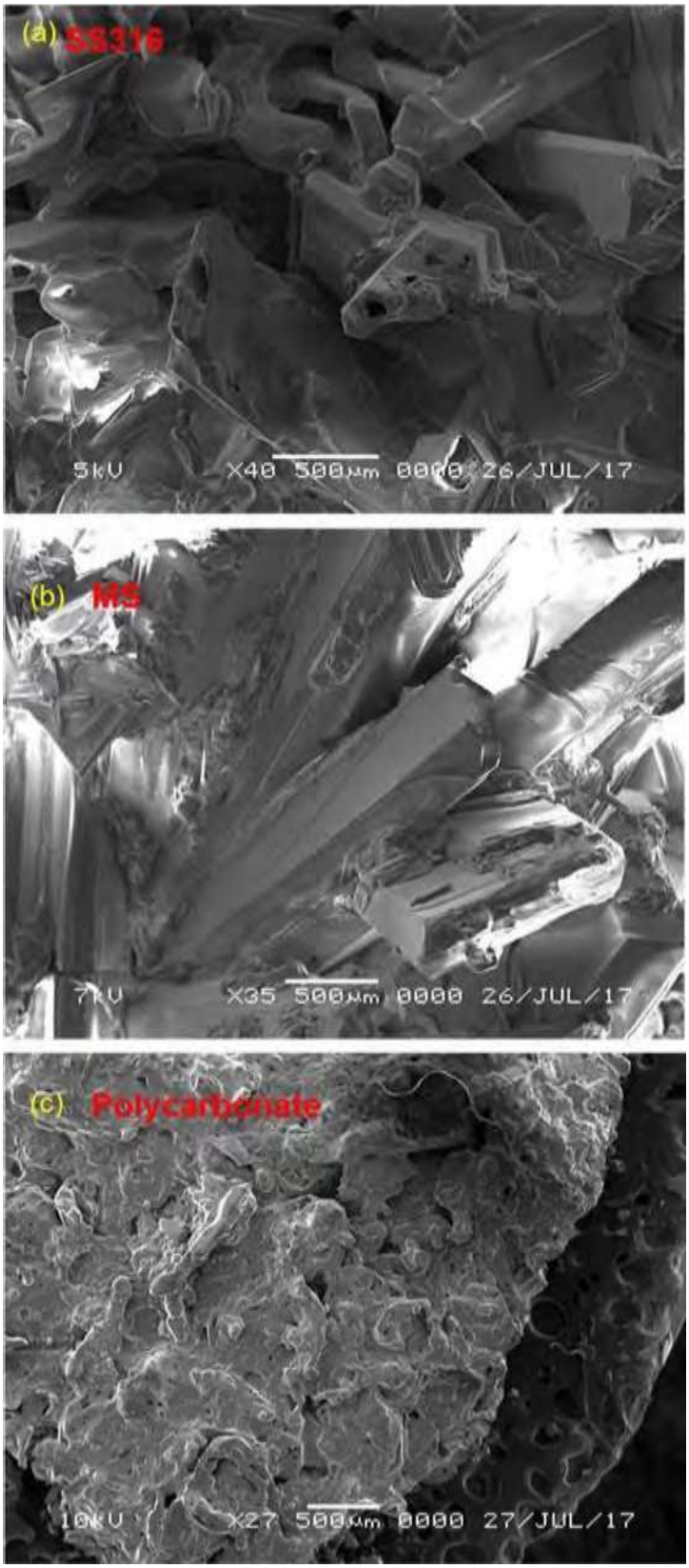

Figure 8.14: Microscopic view of crystals arrangement: (a) SS316, (B) MS and (c) Polycarbonate

The crystal structure on the SS316 and MS specimens are very regular crystal shape, and some intense to little agitation effect occurred on the crystal surface due to fluid shear. In the case of polycarbonate non-crystalline structure appears, implying that the polycarbonate pipe specimen is low conductive as no crystallisation occurs due to surface reaction method. As it is seen from Figure 8.13 (c), only a small amount of scale deposit appears on the upper part of the polycarbonate test pipe.

8.10 Summary

This chapter reveals the effects of substrate material properties on crystallisation scale deposition of normal soluble salt during the convective heat transfer condition. It was found that the scale deposition increases with increasing thermal conductivity of the substrate materials in the order of Copper (Cu) > Aluminium (Al) > Stainless steel (SS316) > Mild steel (MS) > polycarbonate. The scale deposition was also considerably affected by the solution concentration, coolant temperature and the bulk solution agitation. It is seen that the overall heat transfer coefficient (OHTC) and thermal resistance (TR) also depend on the thermal conductivity of substrate material. The OHTC decreases with the increase of thermal conductivity of substrate material and TR simultaneously increases due to the higher scale deposition. Gum arabic was also tested as an inhibitor of scale deposition on the various substrate materials and shows that it significantly retards the crystalline scale deposition during convective heattransferconditions.

CHAPTER 9
CONCLUSIONS AND FUTURE STUDY

9.1 Summary of Findings

This study has investigated and demonstrated various aspects of the hydrodynamic effects on crystallisation scale growth characteristics and their suppression in mixing or precipitation tanks using a novel experimental approach. The study involved a novel design and the development of a precipitation tank model, the formation of crystallisation scale in an experiment using laboratory made normal soluble salt solutions of potassium nitrate (KNO_3), determining the hydrodynamic effects on crystalline scale formation and the consequent adverse effects on thermal resistance and heat transfer coefficient due to scale formation. Scale growth experiments were also performed to investigate the effects of material properties on scale deposition rate, heat transfer characteristics, and also to determine the crystalline scale deposit surface characterisation and crystal morphology.

For the scale formation of KNO_3 solution, it was observed that supersaturation is the main driving force for potassium nitrate crystalline scale formation and the crystal growth occurs by the surface reaction method. Effects of the impeller agitation rates on the crystalline scale growth of the KNO_3 solutions clearly demonstrate the significant role of hydrodynamics in scale suppression. Based on the experimental investigation, results and analysis, the following findings aresummarised.

- In this study, a novel experimental set-up which consists of a model agitation tank replicating many industrial processes was designed and fabricated successfully to undertake a variety of experiments to examine the hydrodynamic effects on scaling and suppression using laboratory made solutions. The experimental rig is seen suitable to be used for further research with different conditions and other solutions.

- The scale deposition growth rate decreases with the increase in agitation rate which produces more fluid erosion effect due to increased shear force on the scale layer. Simultaneously,

the scale layer thickness also decreases with increasing agitation rate. When compared with the low agitation rate of 100 rpm, the rate of scale deposition on the agitation tank wall decreases by 1.2, 1.8, 2.4, 2.8, 3.5 and 3.9 times for impeller speeds of 200, 300, 400, 500, 600 and 700 rpm respectively, for the potassium nitrate concentration of 4.50 mol/dm^3, impeller diameter of 86 mm and the tank with baffles. For the same potassium nitrate concentration of 4.50 mol/dm^3 and the baffled tank condition, the scale deposition growth rate decreases by 1.4 to 7.9 times for the impeller diameter of 114 mm and 2.2 to 12 times for the impeller diameter of 160 mm for the corresponding increased impeller speeds (200 to 700 for the impeller diameter of 114 mm and 200 to 500 for the impeller diameter of 160 mm) when compared with 100 rpm. These results indicate that impeller agitation hydrodynamic plays a signifciant role to reduce the wall scale growth in the agitation tank.

- Decreasing scale growth with increasing velocity or agitation intensity support the scale-velocity model proposed by Jie Wu (Wu et al. 2012) for the velocity of C zone (scale suppression by erosion) as discussed in Chapter 2 and Figure 2.5.

- The scale deposition growth rate on the wall also decreases with the increase in impeller size which creates more shear force on the crystalline scale layer. The scale deposition growth on the wall decreases with the increase in impeller sizes by 1.12 to 2.23 times for the impeller diameter of 114 mm and 1.37 to 4.46 times for the impeller diameter of 160 mm when compared to impeller diameter of 86 mm for the potassium nitrate concentration of 4.50 mol/dm^3 and the baffled tank condition.

- The unbaffled tank creates a swirl flow action near the tank wall which produces a severe fluid erosion effect that is not present in the baffled tank. The unbaffled tank shows benefits because of its increased overall heat transfer coefficient and decreased thermal resistance and crystalline scale thickness which contribute to reduced scale growth. The wall scale deposition growth rate decreases for the unbaffled tank by 4.13%, 11.21%, 23.18%, 17.92%, 29.26%, 22.85% and 31% for impeller speeds of 100, 200, 300, 400, 500, 600 and 700 rpm, respectively, compared with the baffled tank for the impeller diameter of 86 mm and the potassium nitrate concentration of 4.50 mol/dm^3. The scale deposition growth rate reduces by 2.36% to 13.33% for the impeller diameter of 114 mm and 4.26% to 30.76% for the

impeller diameter of 160 mm compared with the baffled tank with the same impeller size and potassium nitrate concentration of 4.50 mol/dm^3.

- The experimental investigation of normal soluble salt potassium nitrate was controlled by the surface reaction process and supersaturation was the key driving force for crystallisation scaling. The wall scale deposition growth increases significantly with the increasing solution concentration in the bulk scaling forming solution. The wall scale deposition increases by 6.7% to 20.8% for the concentration of 4.75 mol/dm^3 and 20.4% to 31.4% for the concentration of 5.25 mol/dm^3 compared with the concentration of 4.50 mol/dm^3 with the baffled tank condition and the impeller diameter of 86 mm. This scale deposition increase for the impeller diameter of 114 mm in the baffled tank condition is 9.3% to 32% for the concentration of 4.75 mol/dm^3 and 23.3% to 46.8% for the concentration of 5.25 mol/dm^3 when compared with the 4.50 mol/dm^3 concentration. The scale deposition increases for the impeller diameter of 160 mm in the baffled tank condition by 18.5% to 37% for the concentration of 4.75 mol/dm^3 and 27.6% to 52.7% for the concentration of 5.25 mol/dm^3 respectively compared with the concentration of 4.50 mol/dm^3.

- The settled scale deposition on the tank bottom increases with the increase of agitation intensity caused the increased impeller rotation which consequently decreases the growth scale on the wall due to fluid erosion. The settled scale deposition increases with the increasing agitation rate by 5.31 to 14.81 times for the impeller diameter of 86 mm, 2.77 to 6.86 times for the impeller diameter of 114 mm and 2.37 to 4.30 times for the impeller diameter of 160 mm compared with the lower agitation rate of 100 rpm of respective impeller size for the concentration of 4.75 mol/dm^3 in the baffled tank condition. With the unbaffled tank condition and same solution concentration, the settled scale deposition increases with agitation rate by 4.85 to 12.09 times for the impeller diameter of 86 mm, 2.66 to 6.35 times for the impeller diameter of 114 mm and 2.27 to 3.69 times for the impeller diameter of 160 mm compared with the lower agitation rate of 100 rpm of respective impeller size. The settled scale deposition increases with the increasing concentration in the unbaffled tank, specifically by 7.6% to 33.3% for the concentration of 4.75 mol/dm^3 and 17.4% to 42.1% for the concentration of 5.25 mol/dm^3 compared with the concentration of 4.50 mol/dm^3 for the impeller diameter of 86 mm; 6.5% to 33.3% for the concentration of 4.75 mol/dm^3 and 23% to 45.4% for the concentration of 5.25 mol/dm^3 compared with the

concentration of 4.50 mol/dm^3 for the impeller diameter 114 mm; and 16.9% to 27.7% for the concentration of 4.75 mol/dm^3 and 16.9% to 27.7% for the concentration of 5.25 mol/dm^3 compared with concentration of 4.50 mol/dm^3 for the impeller diameter of 160 mm.

- Higher differential temperatures between the bulk scale forming solution and the heat transfer surface promote the crystalline scale growth of normal soluble salt of potassium nitrate at low agitation rate. Higher agitation rates have the favourable effect of reducing scale growth on the tank wall. Higher agitation rates also augment the heat transfer rate from the bulk scale forming solution to the coolant in the external jacket and this consequently diminishes the temperature differential between the scale forming heat transfer wall and the adjacent bulk solution to discourage the nucleation formation. The results indicate that higher agitation rates simultaneously create the effect of lowering the bulk solution temperature and increasing fluid erosion on the wall.

- Scale deposition on the heat transfer wall creates a major resistance to heat transfer. An increase in thermal resistance reduces the process equipment performance considerably. The increase of agitation rate simultaneously decreases thermal resistance (TR) and increases the overall heat transfer coefficient (OHTC). TR decreases with the agitation rate showing results of 159.37, 123.47, 112.67, 104.92, 98.58, 85.24 and 76.80 cm^{2}K/W for impeller speeds of 100, 200, 300, 400, 500, 600 and 700 rpm respectively, for the concentration of 4.50 mol/dm^3, impeller diameter of 86 mm and the baffled tank condition. With the same impeller diameter of 86 mm and the baffled tank condition, TR reduces from 185.88 to 32.59 cm^{2}K/W for the concentration of 4.75 mol/dm^3 and from 199.35 to 40.87 cm^{2}K/W for the concentration of 5.25 mol/dm^3 for the impeller speed range of 100 to 700 rpm respectively.. In the case of the unbaffled tank condition, TR decreases from 120.68 to 20.26 cm^{2}K/W for the concentration of 4.50 mol/dm^3, from 146.34 to 27.88 cm^{2}K/W for the concentration of 4.75 mol/dm^3 and from 172.55 to 34.95 cm^{2}K/W for the concentration of 5.25 mol/dm^3 for the agitation speed range of 100 to 700 rpm respectively with the impeller diameter of 86 mm. Similar results were also found for the impeller diameter of 114 mm and 160 mm at different solution concentrations.

- One of the major problems caused by scale deposition on the heat transfer surface is that it reduces the heat transfer rate because of the lower thermal conductivity of scale deposit compared with the thermal conductivity of the substrate material. The overall heat transfer

coefficient(OHTC) decreasesasymptotically by 75.9%, 60.4%, 56.1%, 54.1%, 51.4%, 44% and 38% for the concentration of 4.50 mol/dm^3, by 79.1%, 64.6%, 61.7%, 58.6%, 55.6%, 46.7%, and 40.7% for the concentration of 4.75 mol/dm^3 and by 80.4%, 70.1%, 66.4%, 63.5%, 60.3%, 57.8%, and 46.7% for the concentration of 5.25 mol/dm^3, for impeller speeds of 100, 200, 300, 400, 500, 600, and 700 rpm respectively, with impeller diameter 86 mm and the baffled tank condition. For the impeller diameter of 114 mm and baffled tank condition, OHTC decreases by 73.1% to 23.5% for the concentration of 4.50 mol/dm^3 and by 74.1% to 30.7% for the concentration of 4.75 mol/dm^3 and by 75.5% to 35.9% for the concentration of 5.25 mol/dm^3. In the case of the unbaffled tank condition, OHTC slightly improves due to the swirl flow phenomenon that is not present in the baffled tank condition.

- For the unbaffled tank condition, OHTC also decreases and for the concentration of 4.50 mol/dm^3, it decreases by 70% to 29% for the impeller diameter of 86 mm, by 64% to 19% for the impeller diameter of 114 mm and by 55% to 0.6% for the impeller diameter of 160 mm. For the concentration of 4.75 mol/dm^3, OHTC decreases by 74% to 36% for the impeller diameter of 86 mm, by 66% to 26% for the impeller diameter of 114 mm and by 63% to 2.6% for the impeller diameter of 160 mm. For the concentration of 5.25 mol/dm^3, OHTC decreases by 77% to 42% for the impeller diameter of 86 mm, by 73% to 31% for the impeller diameter of 114 mm and by 72% to 4% for the impeller diameter of 160 mm.

- The results of the experimental investigation into the effect of substrate material properties on freezing crystallisation scale deposition of normal soluble salt combined with effects of bulksolution hydrodynamics, supersaturation andcoolant temperature show that theamount of scale deposition increases with increasing thermal conductivity of the materials in the order of copper (Cu) > aluminium (Al) > stainless steel (SS316) > mild steel (MS) > polycarbonate.

- The environmentally benign inhibitor of gum arabic was tested on the various substrate materials to retard the scale deposition. The results indicated that gum arabic significantly reduced the crystallisation scale deposition during convective heat transfer conditions.

- The results obtained from this study are important in explaining and relating to the real processing fluids through relevant equations and analysis. The outcomes are significant

because they provide design guidelines for the agitation tank and selection of suitable blades that attract less or no scale deposition under hydrodynamic conditions. To the best knowledge of the author some of the blade and tank design similar to this work are being implemented in some refineries for suppressing scaling.

9.2 Recommendationsfor Further Study

The following recommendations can be made for further study:

- Scale deposition experiments should be conducted using inverse soluble salt to allow comparison with normal soluble salt. It will assist in the understanding of other chemical process scaling which act as an inverse soluble salt.
- The real industrial process solution such as Bayer liquor solution should be used for scale deposition experiment for a comparison and validation of the outcomes of this study.
- The scaling experiments should be conducted at different solution temperatures to investigate the effect on crystallisation scaling.
- The hydrodynamic effects on crystallisation scale deposition should also be checked using different sizes of radial or mixed flow impellers. There is a need to investigate the effects of boundary layer instability on scale deposition and its suppression.
- Study should be undertaken onsuppression using various materials/ methods/chemicals, and so on.

REFERENCES

Australian Government. 2017. *Department of Industry, Innovation and Science*. Available: https://www.industry.gov.au/resource/Mining/AustralianMineralCommodities/Pages/BauxiteAluminaandAluminium.aspx, [Acessed on 20th march, 2017] [Online].

AL-JANABI, A. & MALAYERI, M. R. 2015. Environmentally friendly solvent- and water-based coatings for mitigation of crystallization fouling. *Chemical Engineering & Technology,* 38**,** 147-154.

AL-JANABI, A., MALAYERI, M. R. & MÜLLER-STEINHAGEN, H. 2010. Experimental fouling investigation with electroless Ni–P coatings. *International Journal of Thermal Sciences,* 49**,** 1063-1071.

AL-JANABI, A., MALAYERI, M. R. & MÜLLER-STEINHAGEN, H. 2011. Minimization of $CaSO_4$ deposition through surface modification. *Heat Transfer Engineering,* 32**,** 291-299.

AMJAD, Z. 1988. Calcium sulfate dihydrate (gypsum) scale formation on heat exchanger surfaces: The influence of scale inhibitors. *Journal of Colloid and Interface Science,* 123**,** 523-536.

ANDRITSOS, N. & KARABELAS, A. J. 2003. Calcium carbonate scaling in a plate heat exchanger in the presence of particles. *International Journal of Heat and Mass Transfer,* 46**,** 4613-4627.

ASHLEY, M. J. 1976. The prevention of deposition on crystallizer cooling surfaces using ultrasound. *In:* MULLIN, J. W. (ed.) *Industrial Crystallization.* Boston, MA: Springer US, 437-447.

AZIMI, G., CUI, Y., SABANSKA, A. & VARANASI, K. K. 2014. Scale-resistant surfaces: Fundamental studies of the effect of surface energy on reducing scale formation. *Applied Surface Science,* 313**,** 591-599.

BANSAL, B., CHEN, X. D. & MÜLLER-STEINHAGEN, H. 2005. Deposition and removal mechanisms during calcium sulphate fouling in heat exchangers. *Int. J. Transport Phenom,* 7**,** 1-22.

BANSAL, B., CHEN, X. D. & MÜLLER-STEINHAGEN, H. 2008. Analysis of 'classical' deposition rate law for crystallisation fouling. *Chemical Engineering and Processing: Process Intensification,* 47**,** 1201-1210.

BANSAL, B., MÜLLER-STEINHAGEN, H. & CHEN, X. D. 2001. Comparison of crystallization fouling in plate and double-pipe heat exchangers. *Heat Transfer Engineering,* 22**,** 13-25.

BATHE, G. & BATHE, D. 1943. Jacob Perkins: His Inventions, His times and his contemporaries. *The Historical Society of Pennsylvania, Philadelphia*.

BEHBAHANI, R. M., MÜLLER-STEINHAGEN, H. & JAMIALAHMADI, M. 2006. Investigation of scale formation in heat exchangers of phosphoric acid evaporator plants. *The Canadian Journal of Chemical Engineering,* 84**,** 189-197.

BOHNET, M. 1987. Fouling of heat transfer surfaces. *Chemical Engineering & Technology,* 10**,** 113-125.

BOHNET, M. W. 2005. "Crystallization fouling on heat transfer surfaces – 25 years research in braunschweig" in "Heat Exchanger Fouling and Cleaning - Challenges and Opportunities", Hans Muller-Steinhagen, German Aerospace Centre, Stuttgart, Germany; M. Reza Malayeri, University of Stuttgart, Germany; A. Paul Watkinson, The University of British Columbia, Canada Eds, ECI Symposium Serie. http://dc.engconfintl.org/heatexchanger2005/43.

BORUFF, C.S. & STOLL, K.E. 1932. Intermittent Chlorination of condenser water, *Ind. Eng. Chem.*, 24, 398-400.

BOTT, T. 1996. Fouling of heat exchangers. *Fuel and Energy Abstracts,* Elsevier, 211.

BOTT, T. R. 1995. Fouling of Heat Exchangers, Elsevier.

BOTT, T. R. 1997. Aspects of crystallization fouling. *Experimental Thermaland Fluid Science,* 14**,** 356-360.

BRAHIM, F., AUGUSTIN, W. & BOHNET, M. 2003. Numerical simulation of the fouling process. *International Journal of Thermal Sciences,* 42**,** 323-334.

BRECKENRIDGE, L. P. 1899. Effects of scale on the evaporation of locomotive boilers. *Rail Gazette,* 31**,**60.

BRIANÇON, S., COLSON, D. & KLEIN, J. P. 1997. Experimental study and theoretical approach of cooling surfaces fouling in industrial crystallizers. *Chemical Engineering Research and Design,* 75**,** 147-151.

ÇENGEL, Y. A. 2004. Heat Transfer: A Practical Approach, New York, McGraw-Hill.

CHAPMAN, C. M., NIENOW, A., COOKE, M. & MIDDLETON, J. 1983. Particle-gas-liquid mixing in stirred vessels. I: Particle-liquid mixing. *Chemical engineering research and design,* 61**,** 71-81.

CHONG, T. H. & SHEIKHOLESLAMI, R. 2001. Thermodynamics and kinetics for mixed calcium carbonate and calcium sulfate precipitation. *Chemical Engineering Science,* 56**,** 5391-5400.

COLETTI, F. & MACCHIETTO, S. 2011. A dynamic, distributed model of shell-and-tube heat exchangers undergoing crude oil fouling. *Industrial & Engineering Chemistry Research,* 50**,**4515-4533.

COWAN, J. C. & WEINTRITT, D. J. 1976. Water-formed scale deposits, *Gulf Publishing Company,* Book Division.

CRITTENDEN, B. D., MENGYAN YANG, L. D., HANSON, R., JONES, J., KUNDU, K., HARRIS, J., KLOCHOK, O., ARSENYEVA, O. & KAPUSTENKO, P. 2015. Crystallizationfoulingwithenhancedheattransfersurfaces. *Heat Transfer Engineering,* 36**,** 741-749.

DAS, P., KHAN, M. M. K., RASUL, M. & SAHA, S. C. 2015. Fluid flow characteristics on scale deposition in a concentric reducer using CFD approach. *Proceedings of the 11th international conference on heat transfer, fluid mechanics and thermodynamics (HEFAT2015).* Skukuza, South Africa.

DAS, P., KHAN, M. M. K., SAHA, S. C. & RASUL, M. G. 2016. Chapter 6 - Numerical study of flow through a reducer for scale growth suppression. *Thermofluid Modeling for Energy Efficiency Applications.* Academic Press.

DEEV, A. V., RASHEED, T., WELSH, M. C., KHAN, M. M. K. & RASUL, M. G. 2009. Measurement of instantaneous flow velocities in a concentric reducer using Particle Image Velocimetry: Study of scale deposition. *Experimental Thermal and Fluid Science,* 33**,** 1003-1011.

DEMOPOULOS, G. P. 2009. Aqueous precipitation and crystallization for the production of particulate solids with desired properties. *Hydrometallurgy,* 96**,** 199-214.

DEWING, E. W. 1975. Heat capacities of liquid sodium and potassium nitrates. *Journal of Chemical & Engineering Data,* 20**,** 221-223.

DREAM, R. F., ENGINEERS, P. L. G. & CHOPEY, N. P. 1999. Heat transfer in agitated jacketed vessels. *Chemical Engineering,* 106**,** 90.

DURSTON, A. J. 1893. Transmission of Heat Through Tubes Plates. *Trans. Inst. Naval Architects,* 34.

EPSTEIN, N. 1983. Thinking about Heat Transfer Fouling: A 5 × 5 Matrix. *Heat Transfer Engineering,* 4**,** 43-56.

FAHIMINIA, F., WATKINSON, A. P. & EPSTEIN, N. 2007. Early events in the precipitation fouling of calcium sulphate dihydrate under sensible heating conditions. *The Canadian Journal of Chemical Engineering,* 85**,** 679-691.

FERNANDEZ-TORRES, M. J., FITZGERALD, A. M., PATERSON, W. R. & WILSON, D. I. 2001. A theoretical study of freezing fouling: limiting behaviour based on a heat and mass transfer analysis. *Chemical Engineering and Processing: Process Intensification,* 40**,** 335-344.

FITZGERALD, A. M., BARNES, J., SMART, I. & WILSON, D. I. 2004. A Model experimental study of coring by palm oil fats in distribution lines. *Food and Bioproducts Processing,* 82**,** 207-212.

FLETCHER, M. 1991. The physiological activity of bacteria attached to solid surfaces. *Advances in Microbial Physiology,* 32**,** 53-85.

FÖRSTER, M., AUGUSTIN, W. & BOHNET, M. 1999. Influence of the adhesion force crystal/heat exchanger surface on fouling mitigation. *Chemical Engineering and Processing: Process Intensification,* 38**,** 449-461.

FROST, V. M. & RIPPE, W. F. 1931. Experience in chlorinating condenser cooling water. *ASME Trans. ,* 53 (FSP-53-10)**,** 131-138.

GARRETT-PRICE, B. A. 1985. Fouling of heat exchangers : characteristics, costs, prevention, control, and removal, Park Ridge - N.J, Noyes Publications.

GILL, J. S. & NANCOLLAS, G. H. 1980. Kinetics of growth of calcium sulfate crystals at heated metal surfaces. *Journal of Crystal Growth,* 48**,** 34-40.

GLADE, H., STÄRK, A., KRÖMER, K., LOISEL, K., ODIOT, K. & NIED, S. 2015. Impact of tube surface properties on crystallization fouling in falling film evaporators for seawater desalination. *In:* MALAYERI, M. R., (GERMANY), T. U. D., (IRAN), S. U., MÜLLER-STEINHAGEN, H., (GERMANY), T. U. D., WATKINSON, A. P. & (CANADA), U. O. B. C., eds. Heat Exchanger Fouling and Cleaning XI - 07-12, Enfield (Dublin), Ireland.

GRAHAM, J. 1860. On the Consumption of coal in furnaces and the rtae of evaporation from engine boilers. *Memoirs Manchester Lit. & Phil. Soc.,* 20**,** 8-42.

HALL, R. E. 1925. A system of boiler water treatment based on chemical equilibrium. *Ind. Eng. Chem.,* 17**,** 283-290.

HARRIS, A. & MARSHALL, A. 1981. The evaluation of scale control additives. *Conference on Progress in the Prevention of Fouling in Industrial Plant,* University of Nottingham.

HASAN, B. O., NATHAN, G. J., ASHMAN, P. J., CRAIG, R. A. & KELSO, R. M. 2012a. The effects of temperature and hydrodynamics on the crystallization fouling under cross flow conditions. *Applied Thermal Engineering,* 36**,** 210-218.

HASAN, B. O., NATHAN, G. J., ASHMAN, P. J., CRAIG, R. A. & KELSO, R. M. 2012b. The use of turbulence generators to mitigate crystallization fouling under cross flow conditions. *Desalination,* 288**,** 108-117.

HASSON, D. 1962. Rate of decrease of heat transfer due to scale deposition. *Dechema-Monographien,* 47**,** 233-252.

HASSON, D. 1981. Precipitation fouling. *Hemisphere Pub. Crop.,* Washinton.

HASSON, D., AVRIEL, M., RESNICK, W., ROZENMAN, T. & WINDREICH, S. 1968. Mechanism of calcium carbonate scale deposition on heat-transfer surfaces. *Industrial & Engineering Chemistry Fundamentals,* 7**,** 59-65.

HASSON, D., SEMIAT, R., BRAMSON, D., BUSCH, M. & LIMONI-RELIS, B. 1998. Suppression of $CaCO_3$ scale deposition by anti-scalants. *Desalination,* 118**,** 285-296.

HASSON, D. & ZAHAVI, J. 1970. Mechanism of calcium sulfate scale deposition on heat transfer surfaces. *Industrial & Engineering Chemistry Fundamentals,* 9**,** 1-10.

HATCH, G. 1973. Evaluation of scaling tendencies. *Materials Protection and performance, vol 12, no 4, P 49-50.*

HELALIZADEH, A., MÜLLER-STEINHAGEN, H. & JAMIALAHMADI, M. 2000. Mixed salt crystallisation fouling. *Chemical Engineering and Processing: Process Intensification,* 39**,** 29-43.

HELALIZADEH, A., MÜLLER-STEINHAGEN, H. & JAMIALAHMADI, M. 2005. Mathematical modelling of mixed salt precipitation during convective heat transfer and sub-cooled flow boiling. *Chemical Engineering Science,* 60**,** 5078-5088.

HERZ, A., MALAYERI, M. R. & MÜLLER-STEINHAGEN, H. 2008. Fouling of roughened stainless steel surfaces during convective heat transfer to aqueous solutions. *Energy Conversion and Management,* 49**,** 3381-3386.

HIND, A., BHARGAVA, S. & GROCOTT, S. 1999. The surface chemistry of bayer process solids: a review. *Colloids Surf. A Physicochemical. Eng. Asp.* 146 (1–3), 359-374.

HIRSCH, J. 1891. Experiements on the overheating of steam boilers (from Bull. Soc. d'Encouragement pour L'Industrie Nationale, 1890). *Proc. Inst. Civil Eng. ,* 108**,** 464-472.

HOANG, T. A., ANG, H. M. & ROHL, A. L. 2007. Effects of temperature on the scaling of calcium sulphate in pipes. *Powder Technology,* 179**,** 31-37.

HOANG, T. A., ANG, M. & ROHL, A. L. 2011. Effects of process parameters on gypsum scale formation in pipes. *Chemical Engineering & Technology,* 34**,** 1003-1009.

HÖFLING, V., AUGUSTIN, W. & BOHNET, M. 2003. Crystallization fouling of the aqueous two-component system $CaSO_4/CaCO_3$. *In "Heat Exchanger Fouling and Cleaning: Fundamentals and Applications":* PAUL WATKINSON, U. O. B. C., CANADA; HANS MÜLLER-STEINHAGEN, GERMAN AEROSPACE CENTRE (DLR) AND UNIVERSITY OF STUTTGART; M. REZA MALAYERI, GERMAN AEROSPACE CENTRE (DLR) (eds.) *ECI Symposium Series*.

IBRAHIM, S. & NIENOW, A. 1996. Particle suspension in the turbulent regime: the effect of impeller type and impeller/vessel configuration. *Chemical engineering research & design,* 74**,** 679-688.

ISHIYAMA, E. M., PATERSON, W. R. & WILSON, D. I. 2009. Platform for Techno-economic Analysis of Fouling Mitigation Options in Refinery Preheat Trains. *Energy & Fuels,* 23**,** 1323-1337.

JAMES, M. C. 1990. Final report of the HTRI/TEMA joint committee to review the fouling section of the TEMA standards. *Heat Transfer Engineering,* 11**,** 73-107.

JAMIALAHMADI, M., BLÖCHL, R. & MÜLLER-STEINHAGEN, H. 1989. Bubble dynamics and scale formation during boiling of aqueous calcium sulphate solutions. *Chemical Engineering and Processing: Process Intensification,* 26**,** 15-26.

JAMIALAHMADI, M. & MÜLLER-STEINHAGEN, H. 2004. A new model for the effect of calcium sulfate scale formation on pool boiling heat transfer. *Transactions of the ASME-C-Journal of Heat Transfer,* 126**,** 507-517.

JAMIALAHMADI, M. & MÜLLER-STEINHAGEN, H. 2007. Heat exchanger fouling and cleaning in the dihydrate process for the production of phosphoric acid. *Chemical Engineering Research and Design,* 85**,** 245-255.

KALI, Z. 1997. The mechanism of aluminosilicate formation in alumina refining. PhD, University of South Australia.

KARABELAS, A. J. 2002. Scale formation in tubular heat exchangers—research priorities. *International Journal of Thermal Sciences,* 41**,** 682-692.

KAZI, S. 2012. Fouling and fouling mitigation on heat exchanger surfaces, *INTECH Publisher,* 507-532.

KAZI, S. N., DUFFY, G. G. & CHEN, X. D. 2002. Fiber-modified scaling in heat transfer fouling mitigation. *Chemical Engineering Communications,* 189**,** 742-758.

KAZI, S. N., DUFFY, G. G. & CHEN, X. D. 2010. Mineral scale formation and mitigation on metals and a polymeric heat exchanger surface. *Applied Thermal Engineering,* 30**,** 2236-2242.

KAZI, S. N., DUFFY, G. G. & CHEN, X. D. 2012. Fouling and fouling mitigation on heated metal surfaces. *Desalination,* 288**,** 126-134.

KAZI, S. N., DUFFY, G. G. & CHEN, X. D. 2013. Fouling mitigation of heat exchangers with natural fibres. *Applied Thermal Engineering,* 50**,** 1142-1148.

KAZI, S. N., DUFFY, G. G. & CHEN, X. D. 2015a. Study of mineral fouling mitigation on heat exchanger surface. *Applied Thermal Engineering,* 30**,** 2236-2242.

KAZI, S. N., TENG, K. H., ZAKARIA, M. S., SADEGHINEZHAD, E. & BAKAR, M. A. 2015b. Study of mineral fouling mitigation on heat exchanger surface. *Desalination,* 367**,** 248-254.

KERN, D. & SEATON, R. 1959. A theoretical analysis of thermal surface fouling. *British Chemical Engineering,* 4**,** 258-262.

KERN, D. Q. 1966, Heat Exchanger Design for Fouling Service. 3rd Int. Heat Transfer Conference, New York. AICE.

KERN, D. Q. & SEATON, R. E. 1959a. Surface fouling: how to calculate limits. *Chem. Eng. Processing,* 55**,** 71-73.

KEYSAR, S., SEMIAT, R., HASSON, D. & YAHALOM, J. 1994. Effect of surface roughness on the morphology of calcite crystallizing on mild steel. *Journal of Colloid and Interface Science,* 162**,** 311-319.

KING, W. R. 2013. Some studies in alumina trihydrate precipitation kinetics. *Essential Readings in Light Metals.* John Wiley & Sons, Inc.

KRISHER, A. S. 1978. Raw water treatment in the CPI, McGraw-Hill.

KUMAR, B. 2009. Variability of energy dissipation and shear rate with geometry in unbaffled surface aerator. *Bulletin of Chemical Reaction Engineering & Catalysis,* 4(2), 55-60.

KUMAR, B., PATEL, A. K. & RAO, A. R. 2011. Mass transfer and shear rate in baffled surface aerator. *Korean Journal of Chemical Engineering,* 28**,** 502-506.

LEIDENFROST, J. G. 1966. De Aquae Communis Nonnullis Qualitatives Tractatus, 1756 (the relevant material has been translated and published as Leidenfrost, J. G., Fixation of Water in Diverse Fire). *Int. J. Heat Mass Transfer,* 9**,** 1153-1166.

LINDNER, E. 1992. A low surface free energy approach in the control of marine biofouling. *Biofouling,* 6**,** 193-205.

LIU, Y., ZOU, Y., ZHAO, L., LIU, W. & CHENG, L. 2011. Investigation of adhesion of $CaCO_3$ crystalline fouling on stainless steel surfaces with different roughness. *International Communications in Heat and Mass Transfer,* 38**,** 730-733.

LOAN, M., KLAUBER, C. & VERNON, C. 2008. A fundamental study of gibbsite scale nucleation on mild steel. *Proceedings of the 8th International Alumina Quality Workshop,* Darwin, Australia, 334-339.

MALAYERI, M. R. & MÜLLER-STEINHAGEN, H. 2003. Analysis of Fouling Data Based on Prior Knowledge. *In "Heat Exchanger Fouling and Cleaning: Fundamentals and Applications":* PAUL WATKINSON, U. O. B. C., CANADA; HANS MÜLLER-STEINHAGEN, GERMAN AEROSPACE CENTRE (DLR) AND UNIVERSITY OF STUTTGART; M. REZA MALAYERI, GERMAN AEROSPACE CENTRE (DLR) (eds.) *ECI Symposium Series*.

MARSHALL, A. D., MUNRO, P. A. & TRÄGÅRDH, G. 2003. Influence of ionic calcium concentration on fouling during the cross-flow microfiltration of β-lactoglobulin solutions. *Journal of Membrane Science,* 217**,** 131-140.

MCADAMS, W. H., SHERWOOD, T. K. & TURNER, R. L. 1926. Heat transmission from condensing steam to water in surface condensers and feedwater heaters. *ASME Trans.,* 48**,** 1233-1268.

MEIKLE, R. A. 1973. The effect of silica in the Bayer process. *J. Geol. Soc. Jamaica* 30.

MELO, L. F., BOTT, T. R. & BEMARDO, C. A. 1987. Fouling Science and Technology, *Kluwer Academic Publishers.*

MIDDIS, J., PAUL, S. T., MÜLLER-STEINHAGEN, H. M. & DUFFY, G. G. 1998. Reduction of heat transfer fouling by the addition of wood pulp fibers. *Heat Transfer Engineering,* 19**,** 36-44.

MOFFAT, R. J. 1988. Describing the uncertainties in experimental results. *Experimental Thermal and Fluid Science,* 1**,** 3-17.

MÜLLER-STEINHAGEN, H. 1993. Fouling: the ultimate challenge for heat exchanger design. *Sixth International Symposium on Transport Phenomena in Thermal Engineering*, Seoul, Korea. 811-823.

MÜLLER-STEINHAGEN, H. 1998. Mitigation of process heat exchanger fouling: an integral approach. *Chemical Engineering Research and Design,* 76**,** 97-107.

MÜLLER-STEINHAGEN, H. 2010. Fouling of heat exchanger surfaces. *VDI Heat Atlas, VDI-Gesellschaft Verfahrenstechnik und Chemieingenieurwesen. (VDI-GVC), Springer-Verlag Berlin Heidelberg,* Section C4.

MÜLLER-STEINHAGEN, H. 2011. Heat transfer fouling: 50 years after the Kern and Seaton model. *Heat Transfer Engineering,* 32**,** 1-13.

MÜLLER-STEINHAGEN, H., JAMIALAHMADI, M. & ROBSON, B. 1994. Understanding and mitigating heat exchanger fouling in bauxite refineries. *Journal of the Minerals, Metals and Materials Society,* 46**,** 36-41.

MÜLLER-STEINHAGEN, H., MALAYERI, M. & WATKINSON, A. 2011. Heat exchanger fouling: mitigation and cleaning strategies. *Heat Transfer Engineering,* 32 (3-4), 189-196.

MÜLLER-STEINHAGEN, H., MALAYERI, M. R. & WATKINSON, A. P. 2009. Heat exchanger fouling: environmental impacts. *Heat Transfer Engineering,* 30**,** 773-776.

MÜLLER-STEINHAGEN, H., ZHAO, Q., HELALI-ZADEH, A. & REN, X.-G. 2000. The effect of surface properties on $CaSO_4$ scale formation during convective heat transfer and subcooled flow boiling. *The Canadian Journal of Chemical Engineering,* 78**,** 12-20.

MÜLLER-STEINHAGEN, H. M. & BRANCH, C. A. 1988. Influence of thermal boundary conditions on calcium carbonate fouling in double pipe heat exchangers. *Chemical Engineering and Processing: Process Intensification,* 24**,** 65-73.

MULLIN, J. 2001. Crystallization, Oxford, Butterworth-Heinemann.

MWABA, M. G., GOLRIZ, M. R. & GU, J. 2006a. A semi-empirical correlation for crystallization fouling on heat exchange surfaces. *Applied Thermal Engineering,* 26**,** 440-447.

MWABA, M. G., RINDT, C. C. M., STEENHOVEN, A. A. V. & VORSTMAN, M. A. G. 2006b. Experimental investigation of $caso_4$ crystallization on a flat plate. *Heat Transfer Engineering,* 27**,** 42-54.

NAJIBI, S. H., MÜLLER-STEINHAGEN, H. & JAMIALAHMADI, M. 1997. Calcium sulphatescaleformationduringsubcooledflowboiling. *Chemical Engineering Science,* 52**,** 1265-1284.

NAWRATH, S. J., KHAN, M. M. K. & WELSH, M. C. 2006. An experimental study of scale growth rate and flow velocity of a super-saturated caustic–aluminate solution. *International Journal of Mineral Processing,* 80**,** 116-125.

NELSON, W. L. 1934. Fouling of heat exchngers. *Refiner Nat. Gas Manuf.* 13, 271-276.

NEOFOTISTOU, E. & DEMADIS, K. D. 2004. Use of antiscalants for mitigation of silica (SiO2) fouling and deposition: fundamentals and applications in desalination systems. *Desalination,* 167**,** 257-272.

NIENOW, A. 1997. The suspension of solid particles. Mixing in the process industries, *Butterworth-Heinemann Publisher*.

NÝVLT, J. & VEVERKA, F. 1997. Scale formation on cooling surfaces in crystallizers. *Crystal Research and Technology,* 32**,** 773-781.

PÄÄKKÖNEN, T. M., RIIHIMÄKI, M., SIMONSON, C. J., MUURINEN, E. & KEISKI, R. L. 2015. Modeling $CaCO_3$ crystallization fouling on a heat exchanger surface – Definition of fouling layer properties and model parameters. *International Journal of Heat and Mass Transfer,* 83**,** 84-98.

PARFIT, M. 2005. Future Power: Where will the world get its next energy fix? *National Geographic,* 208**,** 2-31.

PARTRIDGE, E. P. 1930. Formation and Properties of Boiler Scale. *University of Michigan Engineering Research Bull. No. 15*.

PRITCHARD, A. M. 1988. The Economics of Fouling. *In:* MELO, L. F., BOTT, T. R. & BERNARDO, C. A. (eds.) *Fouling Science and Technology*. Dordrecht: Springer Netherlands.

PUHAKKA, E., RIIHIMÄKI, M. & KEISKI, R. L. 2007. Molecular modeling approach on fouling of the plate heat exchanger: titanium hydroxyls, silanols, and sulphates on TiO_2 surfaces. *Heat Transfer Engineering,* 28**,** 248-254.

RANKIN, B. H. & ADAMSON, W. L. 1973. Scale formation as related to evaporator surface conditions. *Desalination,* 13**,** 63-87.

ROSMANINHO, R., RIZZO, G., MÜLLER-STEINHAGEN, H. & MELO, L. F. 2008. Deposition from a milk mineral solution on novel heat transfer surfaces under turbulent flow conditions. *Journal of Food Engineering,* 85**,** 29-41.

ROSMANINHO, R., ROCHA, F., RIZZO, G., MÜLLER-STEINHAGEN, H. & MELO, L. F. 2007. Calcium phosphate fouling on TiN-coated stainless steel surfaces: Role of ions and particles. *Chemical Engineering Science,* 62**,** 3821-3831.

SÁNCHEZ PÉREZ, J. A., RODRÍGUEZ PORCEL, E. M., CASAS LÓPEZ, J. L., FERNÁNDEZ SEVILLA, J. M. & CHISTI, Y. 2006. Shear rate in stirred tank and bubble column bioreactors. *Chemical Engineering Journal,* 124**,** 1-5.

SEIDELL, W. F. L. A. 1942. Solubilities of inorganic and metal organic compounds. *The Journal Physical Chemistry*, 46(2).

SHEIKH, A. K., RAZA, M. K., ZUBAIR, S. M. & BUDAIR, M. 1999. Predicting level of fouling using neural network approach. *UEF Conference on Mitigation of Heat Exchanger Fouling and its Economic and Environmental Implications,* 11-16.

SIEDER, E. N. 1935. Application of fouling factors in the design of heat exchangers. *Heat Transfer, ASME***,** 82-86.

SILCOCK, H. L. 1979. Solubilities of inorganic and organic compounds. *Oxford, Pergamon Press*.

SOMERSCALES, E. F. C. 1990. Fouling of heat transfer surfaces: an historical review. *Heat Transfer Engineering,* 11**,** 19-36.

STEINHAGEN, R., MÜLLER-STEINHAGEN, H. & MAANI, K. 1993. Problems and costs due to heat exchanger fouling in New Zealand industries. *Heat Transfer Engineering,* 14**,** 19-30.

TABOREK, J., AOKI, T., RITTER, R. B., PALEN, J. W. & KNUDSEN, J. G. 1972. Fouling-the major unresolved problem in heat transfer-Part II. *Chem. Eng. Processing,* 68**,** 69-78.

TAI, C. Y. & CHEN, F. B. 1998. Polymorphism of $CaCO_3$, precipitated in a constant-composition environment. *AIChE Journal,* 44**,** 1790-1798.

TEMA 1936. Standard of thetubularexchanger manufacturersassociation. New York: *Tubular Exchanger Manufacturers Association*.

TEMA 1999. Standard of the tubular exchanger manufacturers association. 8th ed. New York: *Tubular Exchanger Manufacturers Association*.

TIJING, L. D., KIM, H. Y., LEE, D. H., KIM, C. S. & CHO, Y. I. 2009. Use of an oscillating electric field to mitigate mineral fouling in a heat exchanger. *Experimental Heat Transfer,* 22**,** 257-270.

TUFEU, R., PETITET, J. P., DENIELOU, L. & LE NEINDRE, B. 1985. Experimental determination of the thermal conductivity of molten pure salts and salt mixtures. *International Journal of Thermophysics,* 6**,** 315-330.

VEESLER, S. & BOISTELLE, R. 1993. About supersaturation and growth rates of hydrargillite $Al(OH)_3$ in alumina caustic solutions. *Journal of crystal growth,* 130**,** 411-415.

WANG, G., ZHU, L., LIU, H. & LI, W. 2011. Zinc-graphite composite coating for anti-fouling application. *Materials Letters,* 65**,** 3095-3097.

WATSON, J., GERSON, A., R ., ADDAI-MENSAH, J. & SOAR, T. 1998. The nucleation mechanism of gibbsite from bayer liquors. *Light Metals***,** 167-172.

WEBB, R. L. & LI, W. 2000. Fouling in enhanced tubes using cooling tower water: Part I: long-term fouling data. *International Journal of Heat and Mass Transfer,* 43**,** 3567-3578.

WEIGAND, B., BRAUN, J., NEUMANN, S. O. & RINCK, K. J. 1997. Freezing in forced convection flows inside ducts: A review. *Heat and Mass Transfer,* 32**,** 341-351.

WILSON, E. C. 1915. A basis for rational design of heat transfer apparatus. *ASME Trans.,* 37**,** 47-82.

WOODS, D. R., ANDERSON, S. J. & NORMAN, S. L. 1976. Evaluation of capital cost data: Heat exchangers. *The Canadian Journal of Chemical Engineering,* 54**,** 469-488.

WU, J., GRAHAM, L. J. & MEHIDI, N. N. 2006a. Estimation of agitator flow shear rate. *AIChE Journal,* 52**,** 2323-2332.

WU, J., GRAHAM, L. J., NGUYEN, B. & NABIL NOUI MEHIDI, M. 2006b. Energy efficiency study on axial flow impellers. *Chemical Engineering and Processing: Process Intensification,* 45**,** 625-632.

WU, J., GRAHAM, L. J. & NOUI-MEHIDI, N. 2007. Intensification of mixing. *Journal of Chemical Engineering of Japan,* 40**,** 890-895.

WU, J., GRAHAM, L. J. & NOUI MEHIDI, N. 2006c. Estimation of agitator flow shear rate. *AIChE journal,* 52**,** 2323-2332.

WU, J., LANE, G., LIVK, I., NGUYEN, B., GRAHAM, L., STEGINK, D. & DAVIS, T. 2012. Swirlflowagitationforscalesuppression. *International Journalof Mineral Processing,* 112–113**,** 19-29.

WU, J., NGUYEN, B. & GRAHAM, L. 2010. Energy efficient high solids loading agitation for the mineral industry. *The Canadian Journal of Chemical Engineering,* 88**,** 287-294.

WU, J., WANG, S., GRAHAM, L., PARTHASARATHY, R. & NGUYEN, B. 2011. High solids concentration agitation for minerals process intensification. *AIChE Journal,* 57**,** 2316-2324.

WU, J., ZHU, Y. & PULLUM, L. 2001. Impeller geometry effect on velocity and solids suspension. *Chemical Engineering Research and Design,* 79**,** 989-997.

WU, J., ZHU, Y. G. & PULLUM, L. 2002. Suspension of high concentration slurry. *AIChE Journal,* 48**,** 1349-1352.

XING, X., MA, C. & CHEN, Y. 2005. Mechanism of calcium carbonate scale deposition under subcooled flow boiling conditions. *Chinese Journal of Chemical Engineering,* 13**,** 464-470.

YEAP, B. L., WILSON, D. I., POLLEY, G. T. & PUGH, S. J. 2004. Mitigation of crude oil refinery heat exchanger fouling through retrofits based on thermo-hydraulic fouling models. *Chemical Engineering Research and Design,* 82**,** 53-71.

YOUNG, A., VENDITTI, S., BERRUECO, C., YANG, M., WATERS, A., DAVIES, H., HILL, S., MILLAN, M. & CRITTENDEN, B. 2011. Characterization of crude oils and their fouling deposits using a batch stirred cell system. *Heat Transfer Engineering,* 32**,** 216-227.

YU, H., SHEIKHOLESLAMI, R. & DOHERTY, W. O. S. 2002. Mechanisms, thermodynamics and kinetics of composite fouling of calcium oxalate and amorphous silica in sugar mill evaporators—A preliminary study. *Chemical Engineering Science,* 57**,** 1969-1978.

YU, H., SHEIKHOLESLAMI, R. & DOHERTY, W. O. S. 2005. Effect of thermohydraulic conditions on fouling of calcium oxalate and silica. *AIChE Journal,* 51**,** 641-648.

ZETTLER, H. U., WEI, M., ZHAO, Q. & MÜLLER-STEINHAGEN, H. 2005. Influence of surface properties and characteristics on fouling in plate heat exchangers. *Heat Transfer Engineering,* 26**,** 3-17.

ZHAO, Q., LIU, Y., WANG, C., WANG, S. & MÜLLER-STEINHAGEN, H. 2005a. Effect of surface free energy on the adhesion of biofouling and crystalline fouling. *Chemical Engineering Science,* 60**,** 4858-4865.

ZHAO, Q., LIU, Y. & WANG, S. 2005b. Surface modification of water treatment equipment for reducing CaSO4 scale formation. *Desalination,* 180**,** 133-138.

ZHAO, X. & CHEN, X. D. 2013. A critical review of basic crystallography to salt crystallization fouling in heat exchangers. *Heat Transfer Engineering,* 34**,** 719-732.

APPENDICES

Appendix A

Properties of Potassium Nitrate (KNO_3)

Thermal conductivity: (Tufeu et al., 1985)

The following equations were using to calculate the thermal conductivity of KNO_3.

White and Davis

$$\lambda = 0.2627 + 4.98 \times 10^{-4} t \qquad \text{for } 340 < t < 430°C$$

McDonald and Davis

$$\lambda = 0.337 + 3.641 \times 10^{-4} t \qquad \text{for } 330 < t < 460°C$$

Santini

$$\lambda = 0.29 + 4.04 \times 10^{-4} t \qquad \text{for } 350 < t < 500°C$$

Heat Capacity: (Dewing, 1975)

The heat capacity of KNO_3 as a function of the temperature minus the melting temperature. The results are in fair agreement with Sokolov and Shmidt, especially close to the melting point.

$$C_p = 33.9 - 0.0156(T - T_{melting}) calK^{-1} mol^{-1}$$

Properties of Ethylene Glycol-Water Mixtures

Thermal Conductivity:

The experimental data of the pure liquids can be represented by quadratic equations, for water

$$\lambda_w = 0.56276 + 1.874 \times 10^{-3} t - 6.8 \times 10^{-8} t^2 \qquad (1)$$

and for ethylene glycol

$$\lambda_{eg} = 0.24511 + 1.755 \times 10^{-4} t - 8.52 \times 10^{-7} t^2 \qquad (2)$$

where t is the temperature in °C and the thermal conductivity in W/mK.

Filippov gave the following equation to calculate thermal conductivity of mixtures from the values of the pure liquids:

$$\lambda_m = (1-x).\lambda_w + x.\lambda_{eg} - k.(\lambda_w - \lambda_{eg}).(1-x).x \quad (3)$$

In Equ. (3) x denotes the mass fraction of ethylene glycol in the mixture. The factor k, which is given by Filippov as a constant, should be described as:

$$k = 0.6635 - 0.3698.x - 8.85\times10^{-4}t \quad (4)$$

Using Equs. (1) to (4) the measured thermal conductivities can be represented with an accuracy of ±1%.

Density:

The following equation can use to calculate the density of the ethylene-glycol mixture.

$$\rho = \sum_{i=1}^{3}\sum_{j=1}^{3} A_{i,j} . x^{j-1}.t^{j-1}$$

Viscosity:

The viscosity of ethylene-glycol mixture to calculate by the fellow equation.

$$In\eta = \sum_{i=1}^{2}\sum_{j=1}^{3} A_{i,j}.x^{j-1}.t^{j-1} + \left|\sum_{j=1}^{3} A_{3,j}.x_{j-1}\right|^{1/4}.t^2$$

Appendix B

Table B.1**:** Bottom settled scale rate at various agitation rate with baffles (KNO_3 concentration 4.5 mol/dm^3)

Experiment. No	rpm	Impeller diameter 86 mm (a)		Impeller diameter 114 mm (b)		Impeller diameter 160 mm (c)	
		Total scale weight (g)	Scale rate (g/cm^2/hr.	Total scale weight (g)	Scale rate (g/cm^2/hr.	Total scale weight (g)	Scale rate (g/cm^2/hr.)
Expt. 1(a,b,c)	100	80	0.231	202	0.584	345	0.996
Expt. 2(a,b,c)	200	425	1.228	560	1.618	821	2.371
Expt. 3(a,b,c)	300	690	1.993	1010	2.918	1285	3.711
Expt. 4(a,b,c)	400	815	2.354	1165	3.365	1425	4.116
Expt. 5(a,b,c)	500	910	2.629	1254	3.622	1485	4.289
Expt. 6(a,b)	600	1050	3.033	1320	3.813	-	-
Expt. 7(a,b)	700	1185	3.423	1386	4.004	-	-

Table B.2: Wall scale growth rate at various agitation rate without baffles (KNO_3 concentration 4.5 mol/dm^3)

Experiment. No	rpm	Impeller diameter 86 mm (a)		Impeller diameter 114 mm (b)		Impeller diameter 160 mm (c)	
		Total scale weight (g)	Scale rate ($g/cm^2/hr.$)	Total scale weight (g)	Scale rate ($g/cm^2/hr.$	Total scale weight (g)	Scale rate ($g/cm^2/hr.$)
Expt. 1(a,b,c)	100	1450	1.047	1309	0.945	1055	0.762
Expt. 2(a,b,c)	200	1070	0.773	880	0.635	480	0.347
Expt. 3(a,b,c)	300	690	0.498	415	0.300	205	0.148
Expt. 4(a,b,c)	400	530	0.383	310	0.224	115	0.083
Expt. 5(a,b,c)	500	410	0.296	215	0.155	65	0.047
Expt. 6(a,b)	600	350	0.253	165	0.119	-	-
Expt. 7(a,b)	700	290	0.209	150	0.108	-	-

Table B.3: Bottom settled scale rate at various agitation rate without baffles (KNO_3 concentration 4.5 mol/dm^3)

Experiment. No	rpm	Impeller diameter 86 mm (a)		Impeller diameter 114 mm (b)		Impeller diameter 160 mm (c)	
		Total scale weight (g)	Scale rate (g/cm^2/hr.	Total scale weight (g)	Scale rate (g/cm^2/hr.	Total scale weight (g)	Scale rate (g/cm^2/hr.)
Expt. 1(a,b,c)	100	100	0.289	225	0.650	385	1.112
Expt. 2(a,b,c)	200	485	1.401	600	1.733	875	2.527
Expt. 3(a,b,c)	300	725	2.094	1085	3.134	1345	3.885
Expt. 4(a,b,c)	400	860	2.484	1215	3.510	1465	4.231
Expt. 5(a,b,c)	500	940	2.715	1310	3.784	1525	4.405
Expt. 6(a,b)	600	1105	3.192	1405	4.059	-	-
Expt. 7(a,b)	700	1209	3.492	1430	4.131	-	-

Table B.4: Wall scale growth rate at various agitation rate with baffles (KNO_3 concentration 4.75 mol/dm^3)

Experiment. No	rpm	Impeller diameter 86 mm (a)		Impeller diameter 114 mm (b)		Impeller diameter 160 mm (c)	
		Total scale weight (g)	Scale rate (g/cm^2/hr.	Total scale weight (g)	Scale rate (g/cm^2/hr.	Total scale weight (g)	Scale rate (g/cm^2/hr.)
Expt. 1(a,b,c)	100	1620	1.170	1478	1.067	1350	0.975
Expt. 2(a,b,c)	200	1320	0.953	1090	0.787	870	0.628
Expt. 3(a,b,c)	300	950	0.686	550	0.397	350	0.253
Expt. 4(a,b,c)	400	820	0.592	400	0.289	220	0.159
Expt. 5(a,b,c)	500	650	0.469	320	0.231	135	0.097
Expt. 6(a,b)	600	550	0.397	265	0.191	-	-
Expt. 7(a,b)	700	480	0.347	250	0.181	-	-

Table B.5: Bottom settled scale rate at various agitation rate with baffles (KNO_3 concentration 4.75 mol/dm^3)

Experiment. No	rpm	Impeller diameter 86 mm (a)		Impeller diameter 114 mm (b)		Impeller diameter 160 mm (c)	
		Total scale weight (g)	Scale rate ($g/cm^2/hr.$)	Total scale weight (g)	Scale rate ($g/cm^2/hr.$)	Total scale weight (g)	Scale rate ($g/cm^2/hr.$)
Expt. 1(a,b,c)	100	135	0.390	250	0.722	405	1.170
Expt. 2(a,b,c)	200	525	1.517	630	1.820	895	2.585
Expt. 3(a,b,c)	300	755	2.181	1108	3.201	1401	4.047
Expt. 4(a,b,c)	400	884	2.554	1250	3.611	1490	4.304
Expt. 5(a,b,c)	500	990	2.860	1360	3.929	1550	4.477
Expt. 6(a,b)	600	1170	3.380	1430	4.131	-	-
Expt. 7(a,b)	700	1280	3.697	1480	4.275	-	-

Table B.6: Wall scale growth rate at various agitation rate without baffles (KNO_3 concentration 4.75 mol/dm^3)

Experiment. No	rpm	Impeller diameter 86 mm (a)		Impeller diameter 114 mm (b)		Impeller diameter 160 mm (c)	
		Total scale weight (g)	Scale rate ($g/cm^2/hr.$)	Total scale weight (g)	Scale rate ($g/cm^2/hr.$	Total scale weight (g)	Scale rate ($g/cm^2/hr.$)
Expt. 1(a,b,c)	100	1570	1.134	305	0.881	425	1.228
Expt. 2(a,b,c)	200	1250	0.903	750	2.166	985	2.845
Expt. 3(a,b,c)	300	910	0.657	1230	3.553	1505	4.347
Expt. 4(a,b,c)	400	690	0.498	1360	3.929	1535	4.434
Expt. 5(a,b,c)	500	580	0.419	1410	4.073	1610	4.651
Expt. 6(a,b)	600	480	0.347	1495	4.319	-	-
Expt. 7(a,b)	700	435	0.314	1578	4.558	-	-

Table B.7: Bottom settled scale rate at various agitation rate without baffles (KNO_3 concentration 4.75 mol/dm^3)

Experiment. No	rpm	Impeller diameter 86 mm (a)		Impeller diameter 114 mm (b)		Impeller diameter 160 mm (c)	
		Total scale weight (g)	Scale rate ($g/cm^2/hr.$)	Total scale weight (g)	Scale rate ($g/cm^2/hr.$	Total scale weight (g)	Scale rate ($g/cm^2/hr.$)
Expt. 1(a,b,c)	100	180	0.520	305	0.881	425	1.228
Expt. 2(a,b,c)	200	610	1.762	750	2.166	985	2.845
Expt. 3(a,b,c)	300	850	2.455	1230	3.553	1505	4.347
Expt. 4(a,b,c)	400	1005	2.903	1360	3.929	1535	4.434
Expt. 5(a,b,c)	500	1125	3.250	1410	4.073	1610	4.651
Expt. 6(a,b)	600	1275	3.683	1495	4.319	-	-
Expt. 7(a,b)	700	1355	3.914	1578	4.558	-	-

Table B.8: Wall scale growth rate at various agitation rate with baffles (KNO_3 concentration 5.25 mol/dm^3)

Experiment. No	rpm	Impeller diameter 86 mm (a)		Impeller diameter 114 mm (b)		Impeller diameter 160 mm (c)	
		Total scale weight (g)	Scale rate ($g/cm^2/hr.$)	Total scale weight (g)	Scale rate ($g/cm^2/hr.$	Total scale weight (g)	Scale rate ($g/cm^2/hr.$)
Expt. 1(a,b,c)	100	1898	1.371	1748	1.262	1520	1.098
Expt. 2(a,b,c)	200	1620	1.170	1210	0.874	1005	0.726
Expt. 3(a,b,c)	300	1290	0.932	650	0.469	470	0.339
Expt. 4(a,b,c)	400	1060	0.765	500	0.361	310	0.224
Expt. 5(a,b,c)	500	870	0.628	421	0.304	180	0.130
Expt. 6(a,b)	600	705	0.509	380	0.274	-	-
Expt. 7(a,b)	700	554	0.400	320	0.231	-	-

Table B.9: Bottom settled scale rate at various agitation rate with baffles (KNO_3 concentration 5.25 mol/dm^3)

Experiment. No	rpm	Impeller diameter 86 mm (a)		Impeller diameter 114 mm (b)		Impeller diameter 160 mm (c)	
		Total scale weight (g)	Scale rate ($g/cm^2/hr.$)	Total scale weight (g)	Scale rate ($g/cm^2/hr.$	Total scale weight (g)	Scale rate ($g/cm^2/hr.$)
Expt. 1(a,b,c)	100	415	1.199	501	1.447	800	2.311
Expt. 2(a,b,c)	200	760	2.195	1200	3.466	1225	3.539
Expt. 3(a,b,c)	300	1015	2.932	1600	4.622	1805	5.214
Expt. 4(a,b,c)	400	1290	3.726	1810	5.228	2010	5.806
Expt. 5(a,b,c)	500	1440	4.160	1856	5.361	2130	6.153
Expt. 6(a,b)	600	1610	4.651	1910	5.517	-	-
Expt. 7(a,b)	700	1735	5.012	1940	5.604	-	-

Table B.10: Wall scale growth rate at various agitation rate without baffles (KNO_3 concentration 5.25 mol/dm^3)

Experiment. No	rpm	Impeller diameter 86 mm (a)		Impeller diameter 114 mm (b)		Impeller diameter 160 mm (c)	
		Total scale weight (g)	Scale rate ($g/cm^2/hr.$)	Total scale weight (g)	Scale rate ($g/cm^2/hr.$	Total scale weight (g)	Scale rate ($g/cm^2/hr.$)
Expt. 1(a,b,c)	100	1756	1.268	1700	1.228	1450	1.047
Expt. 2(a,b,c)	200	1410	1.018	1120	0.809	925	0.668
Expt. 3(a,b,c)	300	1065	0.769	590	0.426	405	0.292
Expt. 4(a,b,c)	400	880	0.635	450	0.325	250	0.181
Expt. 5(a,b,c)	500	740	0.534	380	0.274	155	0.112
Expt. 6(a,b)	600	630	0.455	310	0.224	-	-
Expt. 7(a,b)	700	501	0.362	275	0.199	-	-

Table B.11: Bottom settled scale rate at various agitation rate without baffles (KNO_3 concentration 5.25 mol/dm^3)

Experiment. No	rpm	Impeller diameter 86 mm (a)		Impeller diameter 114 mm (b)		Impeller diameter 160 mm (c)	
		Total scale weight (g)	Scale rate (g/cm^2/hr.)	Total scale weight (g)	Scale rate (g/cm^2/hr.	Total scale weight (g)	Scale rate (g/cm^2/hr.)
Expt. 1(a,b,c)	100	523	1.511	603	1.742	835	2.412
Expt. 2(a,b,c)	200	890	2.571	1280	3.697	1255	3.625
Expt. 3(a,b,c)	300	1150	3.322	1680	4.853	1845	5.330
Expt. 4(a,b,c)	400	1370	3.957	1880	5.431	2045	5.907
Expt. 5(a,b,c)	500	1508	4.356	1920	5.546	2225	6.427
Expt. 6(a,b)	600	1680	4.853	1950	5.633	-	-
Expt. 7(a,b)	700	1813	5.237	2007	5.797	-	-

Table B.12**:** Average scale thickness on the wall (KNO_3 concentration 4.50 mol/dm^3)

Experiment. No	rpm	Impeller diameter 86 mm		Impeller diameter 114 mm		Impeller diameter 160 mm	
		With baffle (mm)	Without baffle (mm)	With baffle (mm)	Without baffle(mm)	With baffle (mm)	Without baffle (mm)
Expt. 1	100	13.00	10.00	11.00	7.50	10.00	5.00
Expt. 2	200	6.70	6.20	5.00	4.80	4.00	2.00
Expt. 3	300	5.50	5.00	3.90	3.75	0.60	0.50
Expt. 4	400	4.80	4.20	3.50	3.00	0.40	0.20
Expt. 5	500	4.30	3.80	3.10	2.80	0.10	0.05
Expt. 6	600	3.20	2.20	2.50	1.60	-	-
Expt. 7	700	2.50	1.75	1.25	1.00	-	-

Table B.13: Average scale thickness on the wall (KNO_3 concentration 4.75 mol/dm^3)

Experiment. No	rpm	Impeller diameter 86 mm		Impeller diameter 114 mm		Impeller diameter 160 mm	
		With baffle (mm)	Without baffle (mm)	With baffle (mm)	Without baffle(mm)	With baffle (mm)	Without baffle (mm)
Expt. 1	100	15.00	12.00	11.50	8.00	10.50	7.00
Expt. 2	200	7.50	7.50	5.50	5.10	4.50	3.50
Expt. 3	300	6.45	5.50	4.85	4.30	0.75	0.6
Expt. 4	400	5.80	4.90	4.10	3.50	0.45	0.4
Expt. 5	500	5.00	4.20	3.50	3.10	0.15	0.1
Expt. 6	600	3.50	3.00	3.00	2.20	-	-
Expt. 7	700	2.80	2.40	1.80	1.50	-	-

Table B.14: Average scale thickness on the wall (KNO_3 concentration 5.25 mol/dm^3)

Experiment. No	rpm	Impeller diameter 86 mm		Impeller diameter 114 mm		Impeller diameter 160 mm	
		With baffle (mm)	Without baffle (mm)	With baffle (mm)	Without baffle(mm)	With baffle (mm)	Without baffle (mm)
Expt. 1	100	16.00	14.00	12.00	11.00	11.50	10.00
Expt. 2	200	9.50	8.50	6.50	6.00	5.00	4.50
Expt. 3	300	7.90	7.20	5.50	5.00	1.00	0.70
Expt. 4	400	7.00	6.30	5.00	4.00	0.80	0.50
Expt. 5	500	6.00	5.20	4.30	3.70	0.60	0.20
Expt. 6	600	4.30	4.10	3.50	2.50	-	-
Expt. 7	700	3.50	3.00	2.25	1.88	-	-

Appendix C

Relationship between Reynolds number and impeller rpm:

(a)

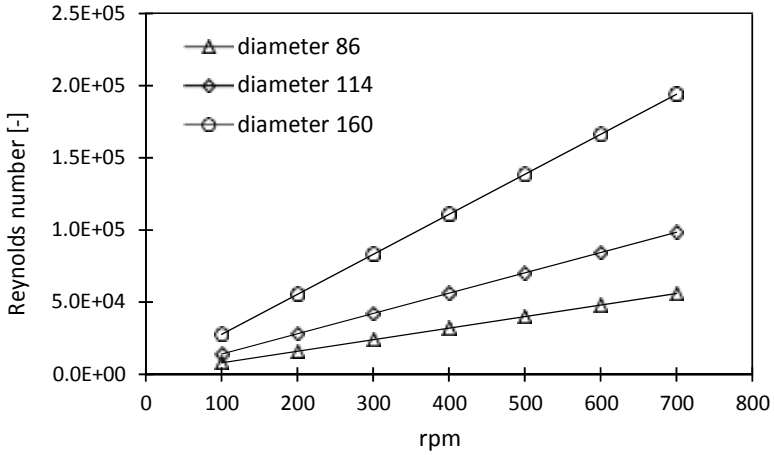

(b)

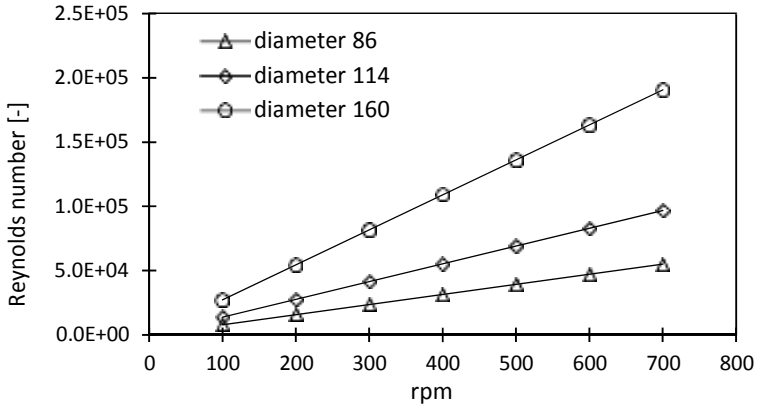

(c)

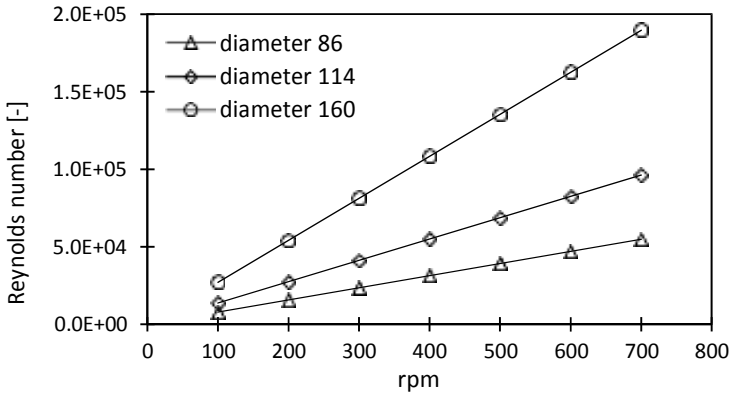

Figure C1: Reynolds number as a function of impeller speed at different KNO_3 concentration: (a) 4.50 mol/dm^3, (b) 4.75 mol/dm^3 and (c) 5.25 mol/dm^3

Relationship between Reynolds number and scale growth rate:

(a)

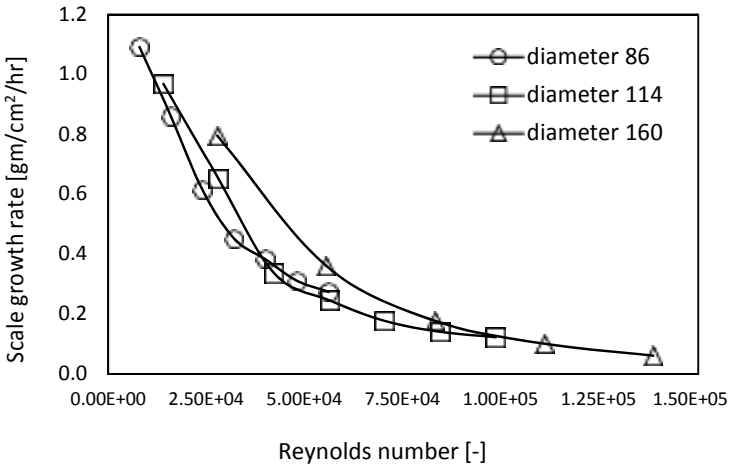

(b)

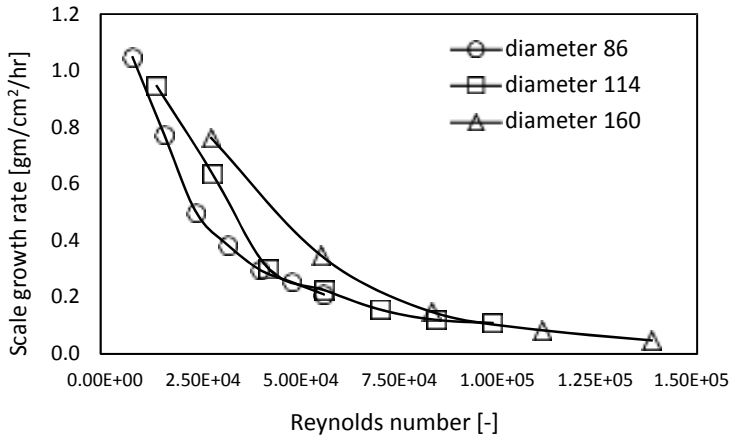

Figure C2: Relationship between Reynolds number and scale growth rate at KNO_3 concentration 4.50 mol/dm^3: (a) with baffled condition and (b) without baffled condition

(a)

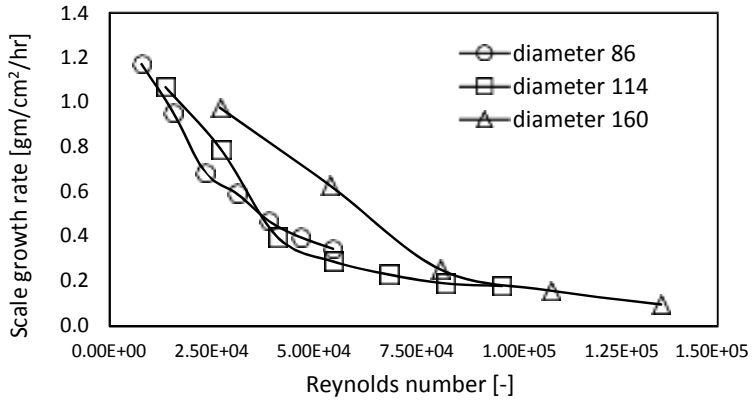

(b)

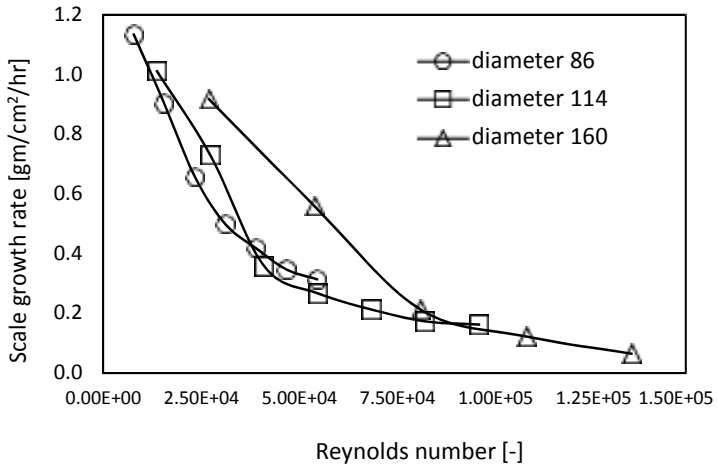

Figure C3: Relationship between Reynolds number and scale growth rate at KNO_3 concentration 4.75 mol/dm^3: (a) with baffled condition and (b) without baffled condition

(a)

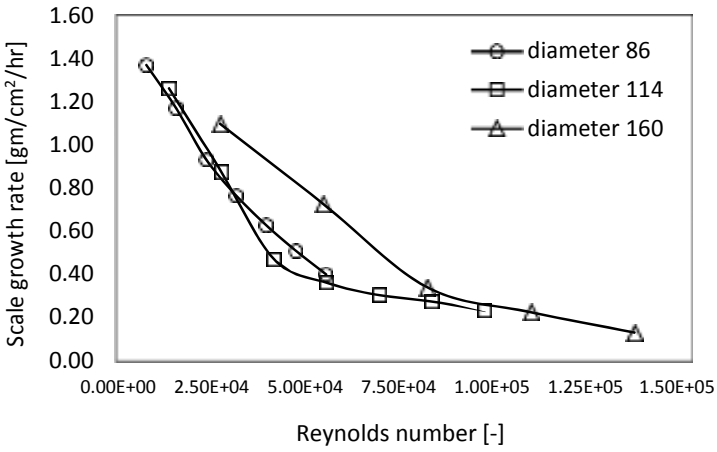

(b)

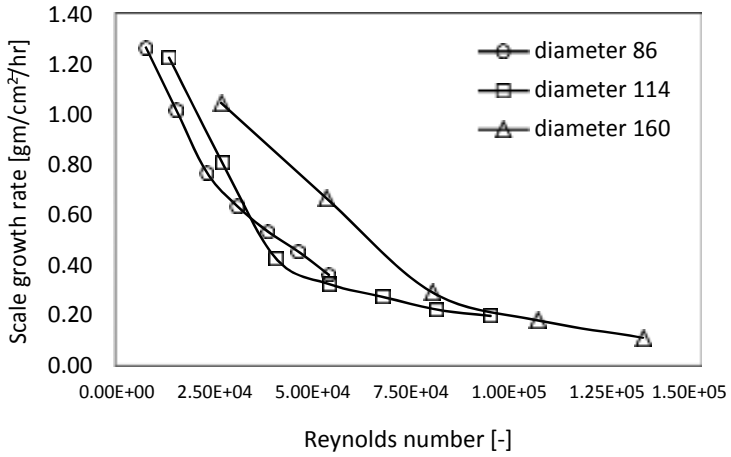

Figure C4: Relationship between Reynolds number and scale growth rate at KNO_3 concentration 5.25 mol/dm^3: (a) with baffled condition and (b) without baffled condition

Calculation of OHTC and TR:

Table C.1: Values of $U_{Overall-Scale}$[W/m^2.K] and $R_{Overall-Scale}$[m^2.K/W] at KNO_3 concentration 5.25 mol/dm^3, impeller diameter 86 mm, rpm 100 and with baffled tank condition

Time [Sec]	Scale thickness [mm]	R_{scale} [m^2.K/W]	$R_{Overall-Scale}$ [m^2.K/W]	$U_{Overall-Scale}$ [W/m^2.K]
0	0	0	0.050465585	143.0988
1	0	0	0.050465585	143.0988
2	0	0	0.050465585	143.0988
3	0.05	0.000574344	0.051039929	141.4885
4	1.066	0.012304676	0.062770261	115.0476
5	2.132	0.024736208	0.075201793	96.02918
6	3.198	0.037297238	0.087762823	82.28504
7	4.264	0.049990494	0.100456079	71.88781
8	5.33	0.062818788	0.113284373	63.74726
9	6.396	0.075785025	0.12625061	57.20027
10	7.462	0.088892204	0.139357789	51.82035
12	8.528	0.102143421	0.152609006	47.32073
15	9.594	0.115541879	0.166007464	43.50148
20	10.66	0.129090887	0.179556472	40.21893
25	11.726	0.142793865	0.19325945	37.36723
30	12.792	0.156654354	0.207119939	34.86661
35	13.858	0.170676016	0.221141601	32.65586
40	14.924	0.184862645	0.23532823	30.68723
45	15.6	0.193946302	0.244411887	29.54672
50	15.7	0.195295867	0.245761452	29.38447
55	16	0.199353648	0.249819233	28.90718
60	16	0.199353648	0.249819233	28.90718
70	16	0.199353648	0.249819233	28.90718
80	16	0.199353648	0.249819233	28.90718

Table C.2: Values of $U_{Overall-Scale}$[W/m^2.K] and $R_{Overall-Scale}$[m^2.K/W] at KNO_3 concentration 5.25 mol/dm^3, impeller diameter 86 mm, rpm 200 and with baffled tank condition

Time [Sec]	Scale thickness [mm]	R_{scale} [m^2.K/W]	$R_{Overall-Scale}$ [m^2.K/W]	$U_{Overall-Scale}$ [W/m^2.K]
0	0	0	0.048846325	147.8425
1	0	0	0.048846325	147.8425
2	0	0	0.048846325	147.8425
3	0	0	0.048846325	147.8425
4	0.3	0.003450178	0.052296503	138.0888
5	0.633	0.007291471	0.056137796	128.64
6	1.266	0.0146273	0.063473625	113.7727
7	1.899	0.022008031	0.070854356	101.9213
8	2.532	0.029434216	0.078280541	92.25238
9	3.165	0.03690642	0.085752745	84.21383
10	3.798	0.044425215	0.09327154	77.4252
12	4.431	0.051991187	0.100837512	71.61588
15	5.064	0.059604931	0.108451256	66.58815
20	5.697	0.067267054	0.116113379	62.19411
25	6.33	0.074978176	0.123824501	58.321
30	6.963	0.082738926	0.131585251	54.88129
35	7.596	0.090549949	0.139396274	51.80604
40	8.229	0.098411899	0.147258224	49.04018
45	8.862	0.106325444	0.155171769	46.5392
50	9.35	0.112461901	0.161308226	44.76876
55	9.5	0.114354398	0.163200723	44.24962
60	9.5	0.114354398	0.163200723	44.24962
70	9.5	0.114354398	0.163200723	44.24962
80	9.5	0.114354398	0.163200723	44.24962

Table C.1: Values of $U_{Overall-Scale}$[W/m^2.K] and $R_{Overall-Scale}$[m^2.K/W] at KNO_3 concentration 5.25 mol/dm^3, impeller diameter 86 mm, rpm 300 and with baffled tank condition

Time [Sec]	Scale thickness [mm]	R_{scale} [m^2.K/W]	$R_{Overall-Scale}$ [m^2.K/W]	$U_{Overall-Scale}$ [W/m^2.K]
0	0	0	0.048189678	149.8571
1	0	0	0.048189678	149.8571
2	0	0	0.048189678	149.8571
3	0	0	0.048189678	149.8571
4	0.34	0.003910948	0.052100626	138.608
5	0.526	0.006055847	0.054245525	133.1274
6	1.052	0.01214226	0.060331938	119.6972
7	1.578	0.01825955	0.066449228	108.6779
8	2.104	0.024408032	0.07259771	99.47375
9	2.63	0.030588025	0.078777703	91.67019
10	3.156	0.036799855	0.084989533	84.97008
12	3.682	0.04304385	0.091233528	79.15475
15	4.208	0.049320346	0.097510024	74.05975
20	4.734	0.055629683	0.103819361	69.55897
25	5.26	0.061972206	0.110161884	65.55415
30	5.786	0.068348266	0.116537944	61.96753
35	6.312	0.07475822	0.122947898	58.73682
40	6.838	0.08120243	0.129392108	55.81151
45	7.364	0.087681264	0.135870942	53.15021
50	7.89	0.094195097	0.142384775	50.71869
55	7.8	0.093078064	0.141267742	51.11973
60	7.9	0.094319275	0.142508953	50.67449
70	7.9	0.094319275	0.142508953	50.67449
80	7.9	0.094319275	0.142508953	50.67449

Table C.4: Values of $U_{Overall-Scale}$[W/m^2.K] and $R_{Overall-Scale}$[m^2.K/W] at KNO_3 concentration 5.25 mol/dm^3, impeller diameter 86 mm, rpm 400 and with baffled tank condition

Time [Sec]	Scale thickness [mm]	R_{scale} [m^2.K/W]	$R_{Overall-Scale}$ [m^2.K/W]	$U_{Overall-Scale}$ [W/m^2.K]
0	0	0	0.047821342	151.0113
1	0	0	0.047821342	151.0113
2	0	0	0.047821342	151.0113
3	0.18	0.002068922	0.049890264	144.749
4	0.31	0.003565354	0.051386696	140.5337
5	0.466	0.005363527	0.053184869	135.7823
6	0.932	0.010751017	0.058572359	123.293
7	1.398	0.016162686	0.063984028	112.8651
8	1.864	0.021598751	0.069420093	104.027
9	2.33	0.027059434	0.074880776	96.44086
10	2.796	0.032544959	0.080366301	89.85815
12	3.262	0.038055552	0.085876894	84.09209
15	3.728	0.043591443	0.091412785	78.99953
20	4.194	0.049152867	0.096974209	74.46895
25	4.66	0.054740059	0.102561401	70.41214
30	5.126	0.06035326	0.108174602	66.75844
35	5.592	0.065992713	0.113814055	63.45059
40	6.058	0.071658664	0.119480006	60.44165
45	6.524	0.077351364	0.125172706	57.69284
50	6.99	0.083071067	0.130892409	55.17179
55	7	0.083194105	0.131015447	55.11998
60	7	0.083194105	0.131015447	55.11998
70	7	0.083194105	0.131015447	55.11998
80	7	0.083194105	0.131015447	55.11998

Table C.5: Values of $U_{Overall-Scale}$[W/m^2.K] and $R_{Overall-Scale}$[m^2.K/W] at KNO_3 concentration 5.25 mol/dm^3, impeller diameter 86 mm, rpm 500 and with baffled tank condition

Time [Sec]	Scale thickness [mm]	R_{scale} [m^2.K/W]	$R_{Overall-Scale}$ [m^2.K/W]	$U_{Overall-Scale}$ [W/m^2.K]
0	0	0	0.04758208	151.7706
1	0	0	0.04758208	151.7706
2	0	0	0.04758208	151.7706
3	0	0	0.04758208	151.7706
4	0.3	0.003450178	0.051032258	141.5098
5	0.4	0.004602434	0.052184514	138.3852
6	0.8	0.009222502	0.056804582	127.13
7	1.2	0.013860339	0.061442419	117.5339
8	1.6	0.018516084	0.066098164	109.2552
9	2	0.023189873	0.070771953	102.0399
10	2.4	0.027881849	0.075463929	95.6956
12	2.8	0.032592153	0.080174233	90.07341
15	3.2	0.037320929	0.084903009	85.05666
20	3.6	0.042068321	0.089650401	80.55253
25	4	0.046834479	0.094416559	76.48624
30	4.4	0.05161955	0.09920163	72.79686
35	4.8	0.056423684	0.104005764	69.4343
40	5.2	0.061247036	0.108829116	66.35695
45	5.6	0.066089758	0.113671838	63.52997
50	6	0.070952008	0.118534088	60.92398
55	6.01	0.071073816	0.118655896	60.86144
60	6.01	0.071073816	0.118655896	60.86144
70	6	0.070952008	0.118534088	60.92398
80	6	0.070952008	0.118534088	60.92398

Table C.6: Values of $U_{Overall-Scale}$[W/m^2.K] and $R_{Overall-Scale}$[m^2.K/W] at KNO_3 concentration 5.25 mol/dm^3, impeller diameter 86 mm, rpm 600 and with baffled tank condition

Time [Sec]	Scale thickness [mm]	R_{scale} [m^2.K/W]	$R_{Overall-Scale}$ [m^2.K/W]	$U_{Overall-Scale}$ [W/m^2.K]
0	0	0	0.047410374	152.3203
1	0	0	0.047410374	152.3203
2	0	0	0.047410374	152.3203
3	0	0	0.047410374	152.3203
4	0	0	0.047410374	152.3203
5	0.286	0.00328895	0.050699324	142.439
6	0.572	0.006586894	0.053997268	133.7394
7	0.858	0.009893884	0.057304258	126.0214
8	1.144	0.013209967	0.060620341	119.1277
9	1.43	0.016535195	0.063945569	112.933
10	1.716	0.019869619	0.067279993	107.336
12	2.002	0.023213288	0.070623662	102.2542
15	2.288	0.026566255	0.073976629	97.61956
20	2.574	0.029928571	0.077338945	93.37555
25	2.86	0.033300288	0.080710662	89.47475
30	3.146	0.03668146	0.084091834	85.87715
35	3.432	0.040072139	0.087482513	82.54869
40	3.718	0.04347238	0.090882754	79.46026
45	4.004	0.046882236	0.09429261	76.58678
50	4.29	0.050301761	0.097712135	73.90656
55	4.576	0.053731011	0.101141385	71.40072
60	4.862	0.057170042	0.104580416	69.05277
70	5.148	0.060618908	0.108029282	66.84825
80	5.434	0.064077667	0.111488041	64.77437

Table C.7: Values of $U_{Overall-Scale}$[W/m^2.K] and $R_{Overall-Scale}$[m^2.K/W] at KNO_3 concentration 5.25 mol/dm^3, impeller diameter 86 mm, rpm 700 and with baffled tank condition

Time [Sec]	Scale thickness [mm]	R_{scale} [m^2.K/W]	$R_{Overall-Scale}$ [m^2.K/W]	$U_{Overall-Scale}$ [W/m^2.K]
0	0	0	0.047280771	152.7378
1	0	0	0.047280771	152.7378
2	0	0	0.047280771	152.7378
3	0	0	0.047280771	152.7378
4	0	0	0.047280771	152.7378
5	0.1	0.001148963	0.048429734	149.1142
6	0.233	0.002678781	0.049959552	144.5482
7	0.466	0.005363527	0.052644298	137.1766
8	0.699	0.008054263	0.055335034	130.5062
9	0.932	0.010751017	0.058031788	124.4415
10	1.165	0.013453816	0.060734587	118.9037
12	1.398	0.016162686	0.063443457	113.8268
15	1.631	0.018877655	0.066158426	109.1556
20	1.864	0.021598751	0.068879522	104.8434
25	2.097	0.024326002	0.071606773	100.8503
30	2.33	0.027059434	0.074340205	97.14214
35	2.563	0.029799077	0.077079848	93.68942
40	2.796	0.032544959	0.07982573	90.46665
45	3.029	0.035297107	0.082577878	87.45159
50	3.262	0.038055552	0.085336323	84.62477
55	3.5	0.04087972	0.088160491	81.91387
60	3.5	0.04087972	0.088160491	81.91387
70	3.5	0.04087972	0.088160491	81.91387
80	3.5	0.04087972	0.088160491	81.91387

Table C.8: Values of $U_{Overall-Scale}$[W/m^2.K] and $R_{Overall-Scale}$[m^2.K/W] at KNO_3 concentration 5.25 mol/dm^3, impeller diameter 86 mm, rpm 100 and without baffled tank condition

Time [Sec]	Scale thickness [mm]	R_{scale} [m^2.K/W]	$R_{Overall-Scale}$ [m^2.K/W]	$U_{Overall-Scale}$ [W/m^2.K]
0	0	0	0.050465585	143.0988
1	0	0	0.050465585	143.0988
2	0	0	0.050465585	143.0988
3	0.2	0.002299021	0.052764606	136.8638
4	0.6	0.006910255	0.05737584	125.8642
5	0.933	0.010762604	0.061228189	117.9451
6	1.866	0.021622135	0.07208772	100.1775
7	2.799	0.032580354	0.083045939	86.9587
8	3.732	0.043639072	0.094104657	76.73975
9	4.665	0.054800148	0.105265733	68.60322
10	5.598	0.066065496	0.116531081	61.97118
12	6.531	0.077437082	0.127902667	56.46144
15	7.464	0.088916929	0.139382514	51.81116
20	8.397	0.100507119	0.150972704	47.83361
25	9.33	0.112209792	0.162675377	44.39252
30	10.263	0.124027154	0.174492739	41.38608
35	11.196	0.135961475	0.18642706	38.7367
40	12.129	0.148015093	0.198480678	36.38425
45	12.9	0.158067535	0.20853312	34.63033
50	13.55	0.166607953	0.217073538	33.26785
55	13.92	0.171496574	0.221962159	32.53514
60	14	0.172556184	0.223021769	32.38056
70	14	0.172556184	0.223021769	32.38056
80	14	0.172556184	0.223021769	32.38056

Table C.9: Values of $U_{Overall-Scale}$[W/m^2.K] and $R_{Overall-Scale}$[m^2.K/W] at KNO_3 concentration 5.25 mol/dm^3, impeller diameter 86 mm, rpm 200 and without baffled tank condition

Time [Sec]	Scale thickness [mm]	R_{scale} [m^2.K/W]	$R_{Overall-Scale}$ [m^2.K/W]	$U_{Overall-Scale}$ [W/m^2.K]
0	0	0	0.048846325	147.8425
1	0	0	0.048846325	147.8425
2	0	0	0.048846325	147.8425
3	0	0	0.048846325	147.8425
4	0.3	0.003450178	0.052296503	138.0888
5	0.566	0.006517614	0.055363939	130.438
6	1.132	0.013070647	0.061916972	116.633
7	1.698	0.019659488	0.068505813	105.4154
8	2.264	0.026284528	0.075130853	96.11985
9	2.83	0.032946169	0.081792494	88.29131
10	3.396	0.039644816	0.088491141	81.6078
12	3.962	0.046380883	0.095227208	75.83513
15	4.528	0.053154791	0.102001116	70.79891
20	5.094	0.059966968	0.108813293	66.3666
25	5.66	0.066817847	0.115664172	62.43565
30	6.226	0.073707872	0.122554197	58.92551
35	6.792	0.080637492	0.129483817	55.77198
40	7.358	0.087607164	0.136453489	52.9233
45	7.924	0.094617356	0.143463681	50.33726
50	8.2	0.098050592	0.146896917	49.16079
55	8	0.095561765	0.14440809	50.00806
60	8	0.095561765	0.14440809	50.00806
70	8	0.095561765	0.14440809	50.00806
80	8	0.095561765	0.14440809	50.00806

Table C.10: Values of $U_{Overall-Scale}$[W/m^2.K] and $R_{Overall-Scale}$[m^2.K/W] at KNO_3 concentration 5.25 mol/dm^3, impeller diameter 86 mm, rpm 300 and without baffled tank condition

Time [Sec]	Scale thickness [mm]	R_{scale} [m^2.K/W]	$R_{Overall-Scale}$ [m^2.K/W]	$U_{Overall-Scale}$ [W/m^2.K]
0	0	0	0.048189678	149.8571
1	0	0	0.048189678	149.8571
2	0	0	0.048189678	149.8571
3	0.2	0.002299021	0.050488699	143.0333
4	0.3	0.003450178	0.051639856	139.8448
5	0.48	0.005525033	0.053714711	134.4429
6	0.96	0.011075497	0.059265175	121.8517
7	1.44	0.016651628	0.064841306	111.3729
8	1.92	0.022253665	0.070443343	102.5159
9	2.4	0.027881849	0.076071527	94.93127
10	2.88	0.033536426	0.081726104	88.36304
12	3.36	0.039217643	0.087407321	82.61971
15	3.84	0.044925755	0.093115433	77.555
20	4.32	0.050661015	0.098850693	73.05531
25	4.8	0.056423684	0.104613362	69.03103
30	5.28	0.062214026	0.110403704	65.41056
35	5.76	0.068032306	0.116221984	62.13599
40	6.24	0.073878796	0.122068474	59.15998
45	6.72	0.079753771	0.127943449	56.44344
50	7.2	0.08565751	0.133847188	53.95383
55	7.2	0.08565751	0.133847188	53.95383
60	7.2	0.08565751	0.133847188	53.95383
70	7.2	0.08565751	0.133847188	53.95383
80	7.2	0.08565751	0.133847188	53.95383

Table C.11: Values of $U_{Overall-Scale}$[W/m^2.K] and $R_{Overall-Scale}$[m^2.K/W] at KNO_3 concentration 5.25 mol/dm^3, impeller diameter 86 mm, rpm 400 and without baffled tank condition

Time [Sec]	Scale thickness [mm]	R_{scale} [m^2.K/W]	$R_{Overall-Scale}$ [m^2.K/W]	$U_{Overall-Scale}$ [W/m^2.K]
0	0	0	0.047821342	151.0113
1	0	0	0.047821342	151.0113
2	0	0	0.047821342	151.0113
3	0	0	0.047821342	151.0113
4	0.3	0.003450178	0.05127152	140.8494
5	0.42	0.004833017	0.052654359	137.1504
6	0.84	0.009685484	0.057506826	125.5775
7	1.26	0.014557556	0.062378898	115.7694
8	1.68	0.019449393	0.067270735	107.3508
9	2.1	0.024361157	0.072182499	100.0459
10	2.52	0.029293009	0.077114351	93.6475
12	2.94	0.034245116	0.082066458	87.99657
15	3.36	0.039217643	0.087038985	82.96934
20	3.78	0.044210761	0.092032103	78.46792
25	4.2	0.049224641	0.097045983	74.41388
30	4.62	0.054259455	0.102080797	70.74365
35	5.04	0.059315379	0.107136721	67.40516
40	5.46	0.064392592	0.112213934	64.35536
45	5.88	0.069491273	0.117312615	61.55833
50	6.3	0.074611605	0.122432947	58.98387
55	6.3	0.074611605	0.122432947	58.98387
60	6.3	0.074611605	0.122432947	58.98387
70	6.3	0.074611605	0.122432947	58.98387
80	6.3	0.074611605	0.122432947	58.98387

Table C.12: Values of $U_{Overall-Scale}$ [W/m^2.K] and $R_{Overall-Scale}$ [m^2.K/W] at KNO_3 concentration 5.25 mol/dm^3, impeller diameter 86 mm, rpm 500 and without baffled tank condition

Time [Sec]	Scale thickness [mm]	R_{scale} [m^2.K/W]	$R_{Overall-Scale}$ [m^2.K/W]	$U_{Overall-Scale}$ [W/m^2.K]
0	0	0	0.04758208	151.7706
1	0	0	0.04758208	151.7706
2	0	0	0.04758208	151.7706
3	0.2	0.002299021	0.049881101	144.7755
4	0.4	0.004602434	0.052184514	138.3852
5	0.346	0.003980079	0.051562159	140.0555
6	0.692	0.007973338	0.055555418	129.9885
7	1.038	0.011979865	0.059561945	121.2446
8	1.384	0.015999749	0.063581829	113.5791
9	1.73	0.020033079	0.067615159	106.8039
10	2.076	0.024079945	0.071662025	100.7726
12	2.422	0.028140438	0.075722518	95.3688
15	2.768	0.032214651	0.079796731	90.49953
20	3.114	0.036302676	0.083884756	86.08914
25	3.46	0.040404607	0.087986687	82.07568
30	3.806	0.04452054	0.09210262	78.40784
35	4.152	0.04865057	0.09623265	75.0428
40	4.498	0.052794794	0.100376874	71.94454
45	4.844	0.05695331	0.10453539	69.08252
50	5.19	0.061126217	0.108708297	66.4307
55	5.2	0.061247036	0.108829116	66.35695
60	5.2	0.061247036	0.108829116	66.35695
70	5.2	0.061247036	0.108829116	66.35695
80	5.2	0.061247036	0.108829116	66.35695

Table C.13: Values of $U_{Overall-Scale}$[W/m^2.K] and $R_{Overall-Scale}$[m^2.K/W] at KNO_3 concentration 5.25 mol/dm^3, impeller diameter 86 mm, rpm 600 and without baffled tank condition

Time [Sec]	Scale thickness [mm]	R_{scale} [m^2.K/W]	$R_{Overall-Scale}$ [m^2.K/W]	$U_{Overall-Scale}$ [W/m^2.K]
0	0	0	0.047410374	152.3203
1	0	0	0.047410374	152.3203
2	0	0	0.047410374	152.3203
3	0	0	0.047410374	152.3203
4	0.05	0.000574344	0.047984718	150.4971
5	0.1	0.001148963	0.048559337	148.7163
6	0.273	0.003139257	0.050549631	142.8608
7	0.546	0.006286708	0.053697082	134.4871
8	0.819	0.009442396	0.05685277	127.0222
9	1.092	0.012606364	0.060016738	120.3258
10	1.365	0.015778656	0.06318903	114.2851
12	1.638	0.018959316	0.06636969	108.8082
15	1.911	0.022148387	0.069558761	103.8196
20	2.184	0.025345915	0.072756289	99.25693
25	2.457	0.028551944	0.075962318	95.06774
30	2.73	0.03176652	0.079176894	91.208
35	3.003	0.034989689	0.082400063	87.64031
40	3.276	0.038221496	0.08563187	84.3327
45	3.549	0.041461988	0.088872362	81.25774
50	3.822	0.044711212	0.092121586	78.39169
55	4.095	0.047969215	0.095379589	75.71397
60	4.1	0.048028968	0.095439342	75.66657
70	4.1	0.048028968	0.095439342	75.66657
80	4.1	0.048028968	0.095439342	75.66657

Table C.14: Values of $U_{Overall-Scale}$[W/m^2.K] and $R_{Overall-Scale}$[m^2.K/W] at KNO_3 concentration 5.25 mol/dm^3, impeller diameter 86 mm, rpm 600 and without baffled tank condition

Time [Sec]	Scale thickness [mm]	R_{scale} [m^2.K/W]	$R_{Overall-Scale}$ [m^2.K/W]	$U_{Overall-Scale}$ [W/m^2.K]
0	0	0	0.047280771	152.7378
1	0	0	0.047280771	152.7378
2	0	0	0.047280771	152.7378
3	0.03	0.000344574	0.047625345	151.6328
4	0.05	0.000574344	0.047855115	150.9047
5	0.1	0.001148963	0.048429734	149.1142
6	0.2	0.002299021	0.049579792	145.6554
7	0.4	0.004602434	0.051883205	139.1889
8	0.6	0.006910255	0.054191026	133.2613
9	0.8	0.009222502	0.056503273	127.8079
10	1	0.011539191	0.058819962	122.774
12	1.2	0.013860339	0.06114111	118.1131
15	1.4	0.016185964	0.063466735	113.785
20	1.6	0.018516084	0.065796855	109.7555
25	1.8	0.020850714	0.068131485	105.9945
30	2	0.023189873	0.070470644	102.4762
35	2.2	0.025533579	0.07281435	99.17779
40	2.4	0.027881849	0.07516262	96.07923
45	2.6	0.030234701	0.077515472	93.1629
50	2.8	0.032592153	0.079872924	90.4132
55	3	0.034954223	0.082234994	87.81623
60	3	0.034954223	0.082234994	87.81623
70	3	0.034954223	0.082234994	87.81623
80	3	0.034954223	0.082234994	87.81623

Table C.15: Values of $U_{Overall-Scale}$[W/m^2.K] and $R_{Overall-Scale}$[m^2.K/W] at KNO_3 concentration 5.25 mol/dm^3, impeller diameter 114 mm, rpm 100 and with baffled tank condition

Time [Sec]	Scale thickness [mm]	R_{scale} [m^2.K/W]	$R_{Overall-Scale}$ [m^2.K/W]	$U_{Overall-Scale}$ [W/m^2.K]
0	0	0	0.04909	147.1091
1	0	0	0.04909	147.1091
2	0	0	0.04909	147.1091
3	0	0	0.04909	147.1091
4	0.4	0.004602	0.053692	134.4991
5	0.8	0.009223	0.058312	123.8428
6	1.6	0.018516	0.067606	106.8185
7	2.4	0.027882	0.076972	93.82107
8	3.2	0.037321	0.086411	83.57253
9	4	0.046834	0.095924	75.28401
10	4.8	0.056424	0.105514	68.4421
12	5.6	0.06609	0.11518	62.69833
15	6.4	0.075834	0.124924	57.80779
20	7.2	0.085658	0.134747	53.5934
25	8	0.095562	0.144652	49.92388
30	8.8	0.105548	0.154638	46.69987
35	9.6	0.115618	0.164708	43.8448
40	10.4	0.125772	0.174862	41.29867
45	11.2	0.136013	0.185103	39.01385
50	11.7	0.142458	0.191548	37.70117
55	11.8	0.143751	0.192841	37.44836
60	12	0.146341	0.195431	36.95199
70	12.1	0.147639	0.196728	36.70831
80	12.1	0.147639	0.196728	36.70831

Table C.16: Values of $U_{Overall-Scale}$[W/m^2.K] and $R_{Overall-Scale}$[m^2.K/W] at KNO_3 concentration 5.25 mol/dm^3, impeller diameter 114 mm, rpm 200 and with baffled tank condition

Time [Sec]	Scale thickness [mm]	R_{scale} [m^2.K/W]	$R_{Overall-Scale}$ [m^2.K/W]	$U_{Overall-Scale}$ [W/m^2.K]
0	0	0	0.04798	150.5122
1	0	0	0.04798	150.5122
2	0	0	0.04798	150.5122
3	0	0	0.04798	150.5122
4	0	0	0.04798	150.5122
5	0.2	0.002299	0.050279	143.63
6	0.433	0.004983	0.052963	136.3515
7	0.866	0.009987	0.057966	124.5818
8	1.299	0.015011	0.062991	114.6446
9	1.732	0.020056	0.068036	106.1427
10	2.165	0.025123	0.073103	98.78614
12	2.598	0.030211	0.078191	92.35794
15	3.031	0.035321	0.083301	86.69277
20	3.464	0.040452	0.088432	81.66234
25	3.897	0.045605	0.093585	77.1656
30	4.33	0.050781	0.098761	73.12186
35	4.763	0.055978	0.103958	69.46592
40	5.196	0.061199	0.109179	66.14452
45	5.629	0.066442	0.114422	63.11371
50	6.062	0.071707	0.119687	60.33694
55	6.495	0.076996	0.124976	57.78353
60	6.5	0.077058	0.125037	57.75525
70	6.5	0.077058	0.125037	57.75525
80	6.5	0.077058	0.125037	57.75525

Table C.17: Values of $U_{Overall-Scale}$[W/m^2.K] and $R_{Overall-Scale}$[m^2.K/W] at KNO_3 concentration 5.25 mol/dm^3, impeller diameter 114 mm, rpm 300 and with baffled tank condition

Time [Sec]	Scale thickness [mm]	R_{scale} [m^2.K/W]	$R_{Overall-Scale}$ [m^2.K/W]	$U_{Overall-Scale}$ [W/m^2.K]
0	0	0	0.04753	151.9375
1	0	0	0.04753	151.9375
2	0	0	0.04753	151.9375
3	0	0	0.04753	151.9375
4	0	0	0.04753	151.9375
5	0.25	0.002874	0.050404	143.2728
6	0.366	0.004211	0.05174	139.5731
7	0.732	0.008436	0.055966	129.0356
8	1.098	0.012676	0.060206	119.9479
9	1.464	0.016931	0.064461	112.0301
10	1.83	0.021201	0.068731	105.0698
12	2.196	0.025487	0.073016	98.90322
15	2.562	0.029787	0.077317	93.40189
20	2.928	0.034103	0.081633	88.46363
25	3.294	0.038435	0.085965	84.00618
30	3.66	0.042782	0.090312	79.96255
35	4.026	0.047145	0.094675	76.27764
40	4.392	0.051524	0.099053	72.90574
45	4.758	0.055918	0.103448	69.80856
50	5.124	0.060329	0.107859	66.95382
55	5.49	0.064756	0.112286	64.31412
60	5.5	0.064877	0.112407	64.24478
70	5.5	0.064877	0.112407	64.24478
80	5.5	0.064877	0.112407	64.24478

Table C.18: Values of $U_{Overall-Scale}$[W/m^2.K] and $R_{Overall-Scale}$[m^2.K/W] at KNO_3 concentration 5.25 mol/dm^3, impeller diameter 114 mm, rpm 400 and with baffled tank condition

Time [Sec]	Scale thickness [mm]	R_{scale} [m^2.K/W]	$R_{Overall-Scale}$ [m^2.K/W]	$U_{Overall-Scale}$ [W/m^2.K]
0	0	0	0.047277	152.7489
1	0	0	0.047277	152.7489
2	0	0	0.047277	152.7489
3	0	0	0.047277	152.7489
4	0	0	0.047277	152.7489
5	0.18	0.002069	0.049346	146.3446
6	0.333	0.00383	0.051108	141.301
7	0.666	0.007673	0.05495	131.4203
8	0.999	0.011528	0.058805	122.8054
9	1.332	0.015395	0.062672	115.2277
10	1.665	0.019274	0.066552	108.5106
12	1.998	0.023166	0.070444	102.5153
15	2.331	0.027071	0.074349	97.13125
20	2.664	0.030989	0.078266	92.2696
25	2.997	0.034919	0.082196	87.85777
30	3.33	0.038862	0.086139	83.83607
35	3.663	0.042818	0.090095	80.15494
40	3.996	0.046787	0.094064	76.77285
45	4.329	0.050769	0.098046	73.65477
50	4.662	0.054764	0.102041	70.77093
55	4.995	0.058773	0.10605	68.09587
60	5	0.058833	0.10611	68.05718
70	5	0.058833	0.10611	68.05718
80	5	0.058833	0.10611	68.05718

Table C.19: Values of $U_{Overall-Scale}$[W/m^2.K] and $R_{Overall-Scale}$[m^2.K/W] at KNO_3 concentration 5.25 mol/dm^3, impeller diameter 114 mm, rpm 500 and with baffled tank condition

Time [Sec]	Scale thickness [mm]	R_{scale} [m^2.K/W]	$R_{Overall-Scale}$ [m^2.K/W]	$U_{Overall-Scale}$ [W/m^2.K]
0	0	0	0.047113	153.2806
1	0	0	0.047113	153.2806
2	0	0	0.047113	153.2806
3	0	0	0.047113	153.2806
4	0	0	0.047113	153.2806
5	0.15	0.001724	0.048837	147.8701
6	0.286	0.003289	0.050402	143.2784
7	0.572	0.006587	0.0537	134.4792
8	0.858	0.009894	0.057007	126.678
9	1.144	0.01321	0.060323	119.7143
10	1.43	0.016535	0.063649	113.46
12	1.716	0.01987	0.066983	107.812
15	2.002	0.023213	0.070327	102.6861
20	2.288	0.026566	0.07368	98.01309
25	2.574	0.029929	0.077042	93.73554
30	2.86	0.0333	0.080414	89.80524
35	3.146	0.036681	0.083795	86.18155
40	3.432	0.040072	0.087185	82.82992
45	3.718	0.043472	0.090586	79.7208
50	4.004	0.046882	0.093996	76.82879
55	4.29	0.050302	0.097415	74.1319
60	4.3	0.050422	0.097535	74.04089
70	4.3	0.050422	0.097535	74.04089
80	4.3	0.050422	0.097535	74.04089

Table C.20: Values of $U_{Overall-Scale}$[W/m^2.K] and $R_{Overall-Scale}$[m^2.K/W] at KNO_3 concentration 5.25 mol/dm^3, impeller diameter 114 mm, rpm 600 and with baffled tank condition

Time [Sec]	Scale thickness [mm]	R_{scale} [m^2.K/W]	$R_{Overall-Scale}$ [m^2.K/W]	$U_{Overall-Scale}$ [W/m^2.K]
0	0	0	0.046996	153.6645
1	0	0	0.046996	153.6645
2	0	0	0.046996	153.6645
3	0	0	0.046996	153.6645
4	0	0	0.046996	153.6645
5	0.12	0.001379	0.048375	149.2844
6	0.233	0.002679	0.049674	145.3779
7	0.466	0.005364	0.052359	137.9235
8	0.699	0.008054	0.05505	131.1821
9	0.932	0.010751	0.057747	125.0559
10	1.165	0.013454	0.060449	119.4645
12	1.398	0.016163	0.063158	114.3406
15	1.631	0.018878	0.065873	109.6281
20	1.864	0.021599	0.068594	105.2792
25	2.097	0.024326	0.071322	101.2535
30	2.33	0.027059	0.074055	97.51614
35	2.563	0.029799	0.076795	94.03726
40	2.796	0.032545	0.079541	90.79093
45	3.029	0.035297	0.082293	87.75458
50	3.262	0.038056	0.085051	84.90846
55	3.495	0.04082	0.087816	82.23523
60	3.5	0.04088	0.087875	82.17965
70	3.5	0.04088	0.087875	82.17965
80	3.5	0.04088	0.087875	82.17965

Table C.21: Values of $U_{Overall-Scale}$ [W/m^2.K] and $R_{Overall-Scale}$ [m^2.K/W] at KNO_3 concentration 5.25 mol/dm^3, impeller diameter 114 mm, rpm 700 and with baffled tank condition

Time [Sec]	Scale thickness [mm]	R_{scale} [m^2.K/W]	$R_{Overall-Scale}$ [m^2.K/W]	$U_{Overall-Scale}$ [W/m^2.K]
0	0	0	0.046907	153.9555
1	0	0	0.046907	153.9555
2	0	0	0.046907	153.9555
3	0	0	0.046907	153.9555
4	0	0	0.046907	153.9555
5	0.11	0.001264	0.048171	149.916
6	0.153	0.001758	0.048665	148.3928
7	0.306	0.003519	0.050426	143.2108
8	0.459	0.005283	0.05219	138.3717
9	0.612	0.007049	0.053956	133.8425
10	0.765	0.008818	0.055724	129.5944
12	0.918	0.010589	0.057496	125.602
15	1.071	0.012363	0.05927	121.8428
20	1.224	0.014139	0.061046	118.2971
25	1.377	0.015918	0.062825	114.9471
30	1.53	0.0177	0.064607	111.7771
35	1.683	0.019484	0.066391	108.7729
40	1.836	0.021271	0.068178	105.9219
45	1.989	0.023061	0.069968	103.2125
50	2.142	0.024853	0.07176	100.6346
55	2.295	0.026648	0.073555	98.1788
60	2.3	0.026707	0.073614	98.1005
70	2.3	0.026707	0.073614	98.1005
80	2.3	0.026707	0.073614	98.1005

Table C.22: Values of $U_{Overall-Scale}$ [W/m^2.K] and $R_{Overall-Scale}$ [m^2.K/W] at KNO_3 concentration 5.25 mol/dm^3, impeller diameter 114 mm, rpm 100 and without baffled tank condition

Time [Sec]	Scale thickness [mm]	R_{scale} [m^2.K/W]	$R_{Overall-Scale}$ [m^2.K/W]	$U_{Overall-Scale}$ [W/m^2.K]
0	0	0	0.04909	147.1091
1	0	0	0.04909	147.1091
2	0	0	0.04909	147.1091
3	0	0	0.04909	147.1091
4	0.5	0.005756	0.054846	131.6707
5	0.733	0.008447	0.057537	125.5111
6	1.466	0.016954	0.066044	109.3443
7	2.199	0.025522	0.074612	96.78866
8	2.932	0.034151	0.08324	86.7555
9	3.665	0.042842	0.091931	78.55388
10	4.398	0.051596	0.100685	71.72406
12	5.131	0.060414	0.109503	65.9483
15	5.864	0.069297	0.118386	60.99994
20	6.597	0.078246	0.127335	56.71296
25	7.33	0.087261	0.136351	52.96297
30	8.063	0.096345	0.145435	49.65495
35	8.796	0.105498	0.154588	46.71502
40	9.529	0.114721	0.16381	44.08491
45	10.262	0.124014	0.173104	41.71803
50	10.6	0.128324	0.177414	40.70461
55	10.9	0.132162	0.181252	39.84264
60	11	0.133445	0.182534	39.56279
70	11	0.133445	0.182534	39.56279
80	11	0.133445	0.182534	39.56279

Table C.23: Values of $U_{Overall-Scale}$ [W/m^2.K] and $R_{Overall-Scale}$ [m^2.K/W] at KNO_3 concentration 5.25 mol/dm^3, impeller diameter 114 mm, rpm 200 and without baffled tank condition

Time [Sec]	Scale thickness [mm]	R_{scale} [m^2.K/W]	$R_{Overall-Scale}$ [m^2.K/W]	$U_{Overall-Scale}$ [W/m^2.K]
0	0	0	0.04798	150.5122
1	0	0	0.04798	150.5122
2	0	0	0.04798	150.5122
3	0	0	0.04798	150.5122
4	0.3	0.00345	0.05143	140.4151
5	0.4	0.004602	0.052582	137.3381
6	0.8	0.009223	0.057202	126.2458
7	1.2	0.01386	0.06184	116.7777
8	1.6	0.018516	0.066496	108.6015
9	2	0.02319	0.07117	101.4695
10	2.4	0.027882	0.075862	95.19374
12	2.8	0.032592	0.080572	89.62865
15	3.2	0.037321	0.085301	84.65996
20	3.6	0.042068	0.090048	80.19664
25	4	0.046834	0.094814	76.1653
30	4.4	0.05162	0.099599	72.50608
35	4.8	0.056424	0.104404	69.16971
40	5.2	0.061247	0.109227	66.11525
45	5.6	0.06609	0.11407	63.30839
50	6	0.070952	0.118932	60.72018
55	6	0.070952	0.118932	60.72018
60	6	0.070952	0.118932	60.72018
70	6	0.070952	0.118932	60.72018
80	6	0.070952	0.118932	60.72018

Table C.24: Values of $U_{Overall-Scale}$ [W/m^2.K] and $R_{Overall-Scale}$ [m^2.K/W] at KNO_3 concentration 5.25 mol/dm^3, impeller diameter 114 mm, rpm 300 and without baffled tank condition

Time [Sec]	Scale thickness [mm]	R_{scale} [m^2.K/W]	$R_{Overall-Scale}$ [m^2.K/W]	$U_{Overall-Scale}$ [W/m^2.K]
0	0	0	0.04753	151.9375
1	0	0	0.04753	151.9375
2	0	0	0.04753	151.9375
3	0	0	0.04753	151.9375
4	0.25	0.002874	0.050404	143.2728
5	0.333	0.00383	0.05136	140.6064
6	0.666	0.007673	0.055203	130.8192
7	0.999	0.011528	0.059057	122.2804
8	1.332	0.015395	0.062925	114.7654
9	1.665	0.019274	0.066804	108.1005
10	1.998	0.023166	0.070696	102.1492
12	2.331	0.027071	0.074601	96.80253
15	2.664	0.030989	0.078518	91.97291
20	2.997	0.034919	0.082449	87.58873
25	3.33	0.038862	0.086392	83.59107
30	3.663	0.042818	0.090348	79.93095
35	3.996	0.046787	0.094317	76.56734
40	4.329	0.050769	0.098299	73.46559
45	4.662	0.054764	0.102294	70.59626
50	4.995	0.058773	0.106302	67.93414
55	5	0.058833	0.106363	67.89563
60	5	0.058833	0.106363	67.89563
70	5	0.058833	0.106363	67.89563
80	5	0.058833	0.106363	67.89563

Table C.25: Values of $U_{Overall-Scale}$ [W/m^2.K] and $R_{Overall-Scale}$ [m^2.K/W] at KNO_3 concentration 5.25 mol/dm^3, impeller diameter 114 mm, rpm 400 and without baffled tank condition

Time [Sec]	Scale thickness [mm]	R_{scale} [m^2.K/W]	$R_{Overall-Scale}$ [m^2.K/W]	$U_{Overall-Scale}$ [W/m^2.K]
0	0	0	0.047277	152.7489
1	0	0	0.047277	152.7489
2	0	0	0.047277	152.7489
3	0	0	0.047277	152.7489
4	0.18	0.002069	0.049346	146.3446
5	0.266	0.003059	0.050336	143.4671
6	0.532	0.006125	0.053402	135.2291
7	0.798	0.009199	0.056477	127.868
8	1.064	0.012281	0.059559	121.251
9	1.33	0.015371	0.062649	115.2705
10	1.596	0.018469	0.065747	109.8391
12	1.862	0.021575	0.068853	104.8842
15	2.128	0.024689	0.071967	100.346
20	2.394	0.027811	0.075089	96.17382
25	2.66	0.030941	0.078219	92.32519
30	2.926	0.03408	0.081357	88.76385
35	3.192	0.037226	0.084504	85.45877
40	3.458	0.040381	0.087658	82.38324
45	3.724	0.043544	0.090821	79.51414
50	3.99	0.046715	0.093992	76.83136
55	4	0.046834	0.094112	76.73389
60	4	0.046834	0.094112	76.73389
70	4	0.046834	0.094112	76.73389
80	4	0.046834	0.094112	76.73389

Table C.26: Values of $U_{Overall-Scale}$[W/m^2.K] and $R_{Overall-Scale}$[m^2.K/W] at KNO_3 concentration 5.25 mol/dm^3, impeller diameter 114 mm, rpm 500 and without baffled tank condition

Time [Sec]	Scale thickness [mm]	R_{scale} [m^2.K/W]	$R_{Overall-Scale}$ [m^2.K/W]	$U_{Overall-Scale}$ [W/m^2.K]
0	0	0	0.047113	153.2806
1	0	0	0.047113	153.2806
2	0	0	0.047113	153.2806
3	0	0	0.047113	153.2806
4	0.17	0.001954	0.049067	147.1769
5	0.246	0.002828	0.049942	144.5997
6	0.492	0.005663	0.052777	136.8321
7	0.738	0.008505	0.055619	129.8409
8	0.984	0.011354	0.058467	123.5151
9	1.23	0.014209	0.061322	117.7642
10	1.476	0.017071	0.064184	112.5131
12	1.722	0.01994	0.067053	107.6993
15	1.968	0.022815	0.069929	103.2705
20	2.214	0.025698	0.072811	99.18213
25	2.46	0.028587	0.075701	95.39645
30	2.706	0.031484	0.078597	91.88103
35	2.952	0.034387	0.0815	88.6079
40	3.198	0.037297	0.084411	85.55285
45	3.444	0.040215	0.087328	82.69478
50	3.69	0.043139	0.090252	80.01522
55	3.7	0.043258	0.090371	79.90983
60	3.7	0.043258	0.090371	79.90983
70	3.7	0.043258	0.090371	79.90983
80	3.7	0.043258	0.090371	79.90983

Table C.27: Values of $U_{Overall-Scale}$[W/m^2.K] and $R_{Overall-Scale}$[m^2.K/W] at KNO_3 concentration 5.25 mol/dm^3, impeller diameter 114 mm, rpm 600 and without baffled tank condition

Time [Sec]	Scale thickness [mm]	R_{scale} [m^2.K/W]	$R_{Overall-Scale}$ [m^2.K/W]	$U_{Overall-Scale}$ [W/m^2.K]
0	0	0	0.046996	153.6645
1	0	0	0.046996	153.6645
2	0	0	0.046996	153.6645
3	0.08	0.000919	0.047915	150.7169
4	0.12	0.001379	0.048375	149.2844
5	0.166	0.001908	0.048904	147.6696
6	0.332	0.003819	0.050814	142.1164
7	0.498	0.005733	0.052728	136.9578
8	0.664	0.00765	0.054645	132.1533
9	0.83	0.00957	0.056565	127.6676
10	0.996	0.011493	0.058488	123.4699
12	1.162	0.013419	0.060415	119.5334
15	1.328	0.015348	0.062344	115.8344
20	1.494	0.017281	0.064276	112.3521
25	1.66	0.019216	0.066212	109.0679
30	1.826	0.021155	0.06815	105.9654
35	1.992	0.023096	0.070092	103.03
40	2.158	0.025041	0.072037	100.2485
45	2.324	0.026989	0.073985	97.60902
50	2.49	0.02894	0.075936	95.10105
55	2.5	0.029058	0.076053	94.95395
60	2.5	0.029058	0.076053	94.95395
70	2.5	0.029058	0.076053	94.95395
80	2.5	0.029058	0.076053	94.95395

Table C.28: Values of $U_{Overall-Scale}$[W/m^2.K] and $R_{Overall-Scale}$[m^2.K/W] at KNO_3 concentration 5.25 mol/dm^3, impeller diameter 114 mm, rpm 700 and without baffled tank condition

Time [Sec]	Scale thickness [mm]	R_{scale} [m^2.K/W]	$R_{Overall-Scale}$ [m^2.K/W]	$U_{Overall-Scale}$ [W/m^2.K]
0	0	0	0.046907	153.9555
1	0	0	0.046907	153.9555
2	0	0	0.046907	153.9555
3	0	0	0.046907	153.9555
4	0.1	0.001149	0.048056	150.2746
5	0.125	0.001436	0.048343	149.3812
6	0.25	0.002874	0.049781	145.0658
7	0.375	0.004314	0.051221	140.9881
8	0.5	0.005756	0.052663	137.1289
9	0.625	0.007199	0.054106	133.471
10	0.75	0.008644	0.055551	129.9992
12	0.875	0.010091	0.056998	126.6995
15	1	0.011539	0.058446	123.5596
20	1.125	0.012989	0.059896	120.568
25	1.25	0.014441	0.061348	117.7145
30	1.375	0.015895	0.062802	114.9897
35	1.5	0.01735	0.064257	112.3852
40	1.625	0.018808	0.065714	109.8931
45	1.75	0.020267	0.067173	107.5063
50	1.875	0.021727	0.068634	105.2182
55	1.88	0.021786	0.068693	105.1287
60	1.88	0.021786	0.068693	105.1287
70	1.88	0.021786	0.068693	105.1287
80	1.88	0.021786	0.068693	105.1287

Table C.29: Values of $U_{Overall-Scale}$[W/m^2.K] and $R_{Overall-Scale}$[m^2.K/W] at KNO_3 concentration 5.25 mol/dm^3, impeller diameter 160 mm, rpm 100 and with baffled tank condition

Time [Sec]	Scale thickness [mm]	R_{scale} [m^2.K/W]	$R_{Overall-Scale}$ [m^2.K/W]	$U_{Overall-Scale}$ [W/m^2.K]
0	0	0	0.047995	150.4636
1	0	0	0.047995	150.4636
2	0	0	0.047995	150.4636
3	0	0	0.047995	150.4636
4	0.5	0.005756	0.053751	134.3517
5	0.766	0.008829	0.056825	127.0853
6	1.532	0.017723	0.065719	109.8859
7	2.298	0.026684	0.074679	96.70133
8	3.064	0.035711	0.083706	86.2725
9	3.83	0.044807	0.092802	77.81696
10	4.596	0.053971	0.101967	70.82288
12	5.362	0.063206	0.111201	64.94134
15	6.128	0.072512	0.120507	59.9263
20	6.894	0.081891	0.129886	55.5993
25	7.66	0.091343	0.139338	51.82773
30	8.426	0.100869	0.148865	48.511
35	9.192	0.110472	0.158467	45.57141
40	9.958	0.120151	0.168147	42.94803
45	10.724	0.129909	0.177905	40.59237
50	11.2	0.136013	0.184008	39.24589
55	11.3	0.137299	0.185295	38.97346
60	11.5	0.139876	0.187871	38.43896
70	11.5	0.139876	0.187871	38.43896
80	11.5	0.139876	0.187871	38.43896

Table C.20: Values of $U_{Overall-Scale}$[W/m^2.K] and $R_{Overall-Scale}$[m^2.K/W] at KNO_3 concentration 5.25 mol/dm^3, impeller diameter 160 mm, rpm 200 and with baffled tank condition

Time [Sec]	Scale thickness [mm]	R_{scale} [m^2.K/W]	$R_{Overall-Scale}$ [m^2.K/W]	$U_{Overall-Scale}$ [W/m^2.K]
0	0	0	0.047291	152.7058
1	0	0	0.047291	152.7058
2	0	0	0.047291	152.7058
3	0	0	0.047291	152.7058
4	0.2	0.002299	0.04959	145.6263
5	0.3	0.00345	0.050741	142.3224
6	0.333	0.00383	0.051121	141.2642
7	0.666	0.007673	0.054963	131.3884
8	0.999	0.011528	0.058818	122.7776
9	1.332	0.015395	0.062685	115.2032
10	1.665	0.019274	0.066565	108.4889
12	1.998	0.023166	0.070457	102.4959
15	2.331	0.027071	0.074362	97.11384
20	2.664	0.030989	0.078279	92.25388
25	2.997	0.034919	0.082209	87.84352
30	3.33	0.038862	0.086152	83.8231
35	3.663	0.042818	0.090108	80.14308
40	3.996	0.046787	0.094077	76.76197
45	4.329	0.050769	0.098059	73.64476
50	4.662	0.054764	0.102055	70.76168
55	4.995	0.058773	0.106063	68.08731
60	5	0.058833	0.106124	68.04863
70	5	0.058833	0.106124	68.04863
80	5	0.058833	0.106124	68.04863

Table C.31: Values of $U_{Overall-Scale}$[W/m^2.K] and $R_{Overall-Scale}$[m^2.K/W] at KNO_3 concentration 5.25 mol/dm^3, impeller diameter 160 mm, rpm 300 and with baffled tank condition

Time [Sec]	Scale thickness [mm]	R_{scale} [m^2.K/W]	$R_{Overall-Scale}$ [m^2.K/W]	$U_{Overall-Scale}$ [W/m^2.K]
0	0	0	0.047005	153.6342
1	0	0	0.047005	153.6342
2	0	0	0.047005	153.6342
3	0	0	0.047005	153.6342
4	0	0	0.047005	153.6342
5	0.03	0.000345	0.047349	152.5162
6	0.066	0.000758	0.047763	151.1954
7	0.132	0.001517	0.048522	148.8314
8	0.198	0.002276	0.049281	146.5387
9	0.264	0.003036	0.050041	144.3143
10	0.33	0.003796	0.050801	142.155
12	0.396	0.004556	0.051561	140.058
15	0.462	0.005317	0.052322	138.0208
20	0.528	0.006079	0.053084	136.0407
25	0.594	0.006841	0.053846	134.1155
30	0.66	0.007603	0.054608	132.2428
35	0.726	0.008366	0.055371	130.4206
40	0.792	0.00913	0.056135	128.6468
45	0.858	0.009894	0.056899	126.9195
50	0.924	0.010658	0.057663	125.2369
55	0.99	0.011423	0.058428	123.5973
60	1	0.011539	0.058544	123.3526
70	1	0.011539	0.058544	123.3526
80	1	0.011539	0.058544	123.3526

Table C.32: Values of $U_{Overall-Scale}$[W/m^2.K] and $R_{Overall-Scale}$[m^2.K/W] at KNO_3 concentration 5.25 mol/dm^3, impeller diameter 160 mm, rpm 400 and with baffled tank condition

Time [Sec]	Scale thickness [mm]	R_{scale} [m^2.K/W]	$R_{Overall-Scale}$ [m^2.K/W]	$U_{Overall-Scale}$ [W/m^2.K]
0	0	0	0.046845	154.16
1	0	0	0.046845	154.16
2	0	0	0.046845	154.16
3	0	0	0.046845	154.16
4	0	0	0.046845	154.16
5	0	0	0.046845	154.16
6	0.025	0.000287	0.047132	153.2208
7	0.053	0.000609	0.047453	152.1822
8	0.106	0.001218	0.048063	150.2535
9	0.159	0.001827	0.048672	148.3721
10	0.212	0.002437	0.049282	146.5364
12	0.265	0.003047	0.049892	144.7447
15	0.318	0.003658	0.050502	142.9953
20	0.371	0.004268	0.051113	141.2869
25	0.424	0.004879	0.051724	139.618
30	0.477	0.00549	0.052335	137.9872
35	0.53	0.006102	0.052947	136.3933
40	0.583	0.006714	0.053559	134.835
45	0.636	0.007326	0.054171	133.3112
50	0.689	0.007939	0.054783	131.8207
55	0.742	0.008551	0.055396	130.3623
60	0.8	0.009223	0.056067	128.8022
70	0.8	0.009223	0.056067	128.8022
80	0.8	0.009223	0.056067	128.8022

Table C.33: Values of $U_{Overall-Scale}$[W/m^2.K] and $R_{Overall-Scale}$[m^2.K/W] at KNO_3 concentration 5.25 mol/dm^3, impeller diameter 160 mm, rpm 500 and with baffled tank condition

Time [Sec]	Scale thickness [mm]	R_{scale} [m^2.K/W]	$R_{Overall-Scale}$ [m^2.K/W]	$U_{Overall-Scale}$ [W/m^2.K]
0	0	0	0.04674	154.5034
1	0	0	0.04674	154.5034
2	0	0	0.04674	154.5034
3	0	0	0.04674	154.5034
4	0	0	0.04674	154.5034
5	0	0	0.04674	154.5034
6	0	0	0.04674	154.5034
7	0.02	0.00023	0.04697	153.7479
8	0.04	0.000459	0.0472	152.9995
9	0.08	0.000919	0.04766	151.5239
10	0.12	0.001379	0.048119	150.0761
12	0.16	0.001839	0.048579	148.6551
15	0.2	0.002299	0.049039	147.2602
20	0.24	0.002759	0.0495	145.8907
25	0.28	0.00322	0.04996	144.546
30	0.32	0.003681	0.050421	143.2253
35	0.36	0.004141	0.050882	141.928
40	0.4	0.004602	0.051343	140.6536
45	0.44	0.005064	0.051804	139.4014
50	0.48	0.005525	0.052265	138.1708
55	0.52	0.005987	0.052727	136.9612
60	0.56	0.006448	0.053189	135.7723
70	0.6	0.00691	0.053651	134.6033
80	0.6	0.00691	0.053651	134.6033

Table C.34: Values of $U_{Overall-Scale}$[W/m^2.K] and $R_{Overall-Scale}$[m^2.K/W] at KNO_3 concentration 5.25 mol/dm^3, impeller diameter 160 mm, rpm 100 and without baffled tank condition

Time [Sec]	Scale thickness [mm]	R_{scale} [m^2.K/W]	$R_{Overall-Scale}$ [m^2.K/W]	$U_{Overall-Scale}$ [W/m^2.K]
0	0	0	0.047995	150.4636
1	0	0	0.047995	150.4636
2	0	0	0.047995	150.4636
3	0.4	0.004602	0.052598	137.2977
4	0.5	0.005756	0.053751	134.3517
5	0.666	0.007673	0.055668	129.7251
6	1.332	0.015395	0.06339	113.9225
7	1.998	0.023166	0.071162	101.4808
8	2.664	0.030989	0.078984	91.43075
9	3.33	0.038862	0.086857	83.14299
10	3.996	0.046787	0.094782	76.19123
12	4.5	0.052819	0.100814	71.63244
15	5.2	0.061247	0.109242	66.10588
20	5.866	0.069321	0.117316	61.55635
25	6.532	0.077449	0.125445	57.56773
30	7.198	0.085633	0.133628	54.04222
35	7.864	0.093872	0.141868	50.90354
40	8.53	0.102168	0.150164	48.09127
45	9.196	0.110522	0.158517	45.55694
50	9.6	0.115618	0.163613	44.13808
55	9.9	0.119416	0.167411	43.13676
60	10	0.120684	0.16868	42.81233
70	10	0.120684	0.16868	42.81233
80	10	0.120684	0.16868	42.81233

Table C.35: Values of $U_{Overall-Scale}$[W/m^2.K] and $R_{Overall-Scale}$[m^2.K/W] at KNO_3 concentration 5.25 mol/dm^3, impeller diameter 160 mm, rpm 200 and without baffled tank condition

Time [Sec]	Scale thickness [mm]	R_{scale} [m^2.K/W]	$R_{Overall-Scale}$ [m^2.K/W]	$U_{Overall-Scale}$ [W/m^2.K]
0	0	0	0.047291	152.7058
1	0	0	0.047291	152.7058
2	0	0	0.047291	152.7058
3	0	0	0.047291	152.7058
4	0.1	0.001149	0.04844	149.0837
5	0.2	0.002299	0.04959	145.6263
6	0.3	0.00345	0.050741	142.3224
7	0.6	0.00691	0.054201	133.2369
8	0.9	0.01038	0.057671	125.2201
9	1.2	0.01386	0.061151	118.0939
10	1.5	0.01735	0.064641	111.7178
12	1.8	0.020851	0.068141	105.9791
15	2.1	0.024361	0.071652	100.7869
20	2.4	0.027882	0.075173	96.06655
25	2.7	0.031413	0.078704	91.75657
30	3	0.034954	0.082245	87.80564
35	3.3	0.038506	0.085797	84.17067
40	3.6	0.042068	0.089359	80.81521
45	3.9	0.045641	0.092932	77.7082
50	4.2	0.049225	0.096515	74.82301
55	4.5	0.052819	0.100109	72.13671
60	4.5	0.052819	0.100109	72.13671
70	4.5	0.052819	0.100109	72.13671
80	4.5	0.052819	0.100109	72.13671

Table C.36: Values of $U_{Overall-Scale}$[W/m^2.K] and $R_{Overall-Scale}$[m^2.K/W] at KNO_3 concentration 5.25 mol/dm^3, impeller diameter 160 mm, rpm 300 and without baffled tank condition

Time [Sec]	Scale thickness [mm]	R_{scale} [m^2.K/W]	$R_{Overall-Scale}$ [m^2.K/W]	$U_{Overall-Scale}$ [W/m^2.K]
0	0	0	0.047005	153.6342
1	0	0	0.047005	153.6342
2	0	0	0.047005	153.6342
3	0	0	0.047005	153.6342
4	0	0	0.047005	153.6342
5	0.02	0.00023	0.047235	152.8871
6	0.03	0.000345	0.047349	152.5162
7	0.0466	0.000535	0.04754	151.9044
8	0.0932	0.001071	0.048076	150.2123
9	0.1398	0.001607	0.048611	148.5568
10	0.1864	0.002143	0.049147	146.9367
12	0.233	0.002679	0.049684	145.3508
15	0.2796	0.003215	0.05022	143.7981
20	0.3262	0.003752	0.050757	142.2776
25	0.3728	0.004289	0.051294	140.7882
30	0.4194	0.004826	0.051831	139.329
35	0.466	0.005364	0.052368	137.8992
40	0.5126	0.005901	0.052906	136.4978
45	0.5592	0.006439	0.053444	135.1239
50	0.6058	0.006977	0.053982	133.7769
55	0.6524	0.007516	0.054521	132.4558
60	0.699	0.008054	0.055059	131.1601
70	0.7	0.008066	0.055071	131.1325
80	0.7	0.008066	0.055071	131.1325

Table C.37: Values of $U_{Overall-Scale}$[W/m^2.K] and $R_{Overall-Scale}$[m^2.K/W] at KNO_3 concentration 5.25 mol/dm^3, impeller diameter 160 mm, rpm 400 and without baffled tank condition

Time [Sec]	Scale thickness [mm]	R_{scale} [m^2.K/W]	$R_{Overall-Scale}$ [m^2.K/W]	$U_{Overall-Scale}$ [W/m^2.K]
0	0	0	0.046845	154.16
1	0	0	0.046845	154.16
2	0	0	0.046845	154.16
3	0	0	0.046845	154.16
4	0	0	0.046845	154.16
5	0.02	0.00023	0.047074	153.4078
6	0.0333	0.000382	0.047227	152.9115
7	0.0666	0.000765	0.04761	151.6827
8	0.0999	0.001148	0.047992	150.473
9	0.1332	0.001531	0.048375	149.2822
10	0.1665	0.001914	0.048758	148.1096
12	0.1998	0.002297	0.049141	146.955
15	0.2331	0.00268	0.049525	145.8179
20	0.2664	0.003063	0.049908	144.6979
25	0.2997	0.003447	0.050291	143.5946
30	0.333	0.00383	0.050675	142.5077
35	0.3663	0.004214	0.051059	141.4368
40	0.3996	0.004598	0.051442	140.3815
45	0.4329	0.004982	0.051826	139.3415
50	0.4662	0.005366	0.05221	138.3165
55	0.4995	0.00575	0.052595	137.3061
60	0.5	0.005756	0.0526	137.2911
70	0.5	0.005756	0.0526	137.2911
80	0.5	0.005756	0.0526	137.2911

Table C.38: Values of $U_{Overall-Scale}$[W/m^2.K] and $R_{Overall-Scale}$[m^2.K/W] at KNO_3 concentration 5.25 mol/dm^3, impeller diameter 160 mm, rpm 500 and without baffled tank condition

Time [Sec]	Scale thickness [mm]	R_{scale} [m^2.K/W]	$R_{Overall-Scale}$ [m^2.K/W]	$U_{Overall-Scale}$ [W/m^2.K]
0	0	0	0.04674	154.5034
1	0	0	0.04674	154.5034
2	0	0	0.04674	154.5034
3	0	0	0.04674	154.5034
4	0	0	0.04674	154.5034
5	0	0	0.04674	154.5034
6	0.005	5.74E-05	0.046798	154.3139
7	0.0133	0.000153	0.046893	154.0002
8	0.0266	0.000306	0.047046	153.5001
9	0.0399	0.000458	0.047199	153.0032
10	0.0532	0.000611	0.047352	152.5094
12	0.0665	0.000764	0.047504	152.0188
15	0.0798	0.000917	0.047657	151.5313
20	0.0931	0.00107	0.04781	151.0468
25	0.1064	0.001223	0.047963	150.5653
30	0.1197	0.001375	0.048116	150.0868
35	0.133	0.001528	0.048269	149.6113
40	0.1463	0.001681	0.048422	149.1388
45	0.1596	0.001834	0.048575	148.6691
50	0.1729	0.001987	0.048728	148.2024
55	0.1862	0.00214	0.048881	147.7385
60	0.1995	0.002293	0.049034	147.2774
70	0.2	0.002299	0.049039	147.2602
80	0.2	0.002299	0.049039	147.2602

Table D1: Properties of QAL Caustic-Aluminate slurry (Pullum and Kilpatrick, 1995)

Fluid Description		Post-Interstate Cooling Precipitation Tank
Solids	Density [kg/m^3]	2420
	Concentration [g/L]	326
	Size Fraction d_{50} [µm]	77.5
Liquid	Density [kg/m^3]	1280
Combined Liquor/Solids Density [kg/m^3]		1433
Temperature [°C]		61
Rheological Model		

Table D2: Measure parameter, instrumentation and errors

Instrumentation	Parameter	Error
Overhead stirrer, value/precision 100, Heidolph, Germany	Impeller rpm, torque	-
Advanced programmable temperature controller circulator model AP07R-20 (Poly Science Inc., USA)	Coolant temperature	-
ARES (Advanced Rheometric Expansion System)	Viscosity	-
Rotameter, FR2000 (Brooks Instruments, USA)	Flow rate	± 5% Full scale
Thermocouple (k-type thermocouple) and Temperature Recorder (BTM-4208SD model 12 channels)	Temperature	± 0.1% of total saved data max. (BTM-4208SD model 12 channels)
	Scale weight	
Hot Plate Magnetic Stirrer	Solution heating temperature	± 0.1%
SEM (JEOL-JSM-6360LA)	Crystal microstructure	-